Technical Report No. AE-76-2

University of Maryland, College Park
Department of Aerospace Engineering

(NASA-CR-153244) AN EXPERIMENTAL INVESTIGATION OF A TWO AND A THREE-DIMENSIONAL LOW SPEED TURBULENT BOUNDARY LAYER (Maryland Univ.) 189 p HC A09/MF A01 CSCL 01A G3/02

N77-25087

Unclas 30390

AN EXPERIMENTAL INVESTIGATION OF A TWO AND A THREE-DIMENSIONAL LOW SPEED TURBULENT BOUNDARY LAYER

A. E. WINKELMANN and W. L. MELNIK

Department of Aerospace Engineering

Prepared for

National Aeronautics and Space Administration
NGR-21-002-303

and

Office of Naval Research
Contract N00014-75-C-0613

DECEMBER, 1976

ABSTRACT

Experimental studies of a two and a three-dimensional low speed turbulent boundary layer were conducted on the side wall of the University of Maryland Boundary Layer Wind Tunnel. The 20 ft. long test section, with a rectangular cross section measuring 17.5 in. x 46 in., produced a 3.5 in. thick turbulent boundary layer at a free stream Reynolds number of 3.15 x 10^5/ft. The three-dimensional turbulent boundary layer was produced by a 30^o swept wing-like model faired into the side wall of the test section.

Preliminary studies in the two-dimensional boundary layer indicated that the flow was nonuniform on the 46 in. wide test wall. The nonuniform boundary layer is characterized by transverse variations in the wall shear stress and is primarily caused by nonuniformities in the inlet damping screens.

Over the 15 in. span of a special transverse device, the local skin friction coefficient varied (at discrete locations) $\pm 9\%$ about a mean. Transverse variations in the flow velocity, yaw, pitch and turbulence intensity were also measured in the boundary layer at set distances above the wall. Measurements with a pitch probe revealed the presence of a vortex-like flow to exist above the edge of the boundary layer at two locations along the 15 in. traverse line. This structure occurred above both test walls and appeared to be symmetrical about the center plane of the test section. The apparent origin of the vortex-like flow was traced to imperfections in the next to the last of five inlet damping screens where the weave was very slightly closer together. These imperfections existed in two small "bands", each about 0.4 in. wide, that extended across the entire width of the inlet screen. An analysis of the data suggests that the wakes produced by these imperfections

"bands" tend to roll up into trailing vortices which occur on both sides of the center plane of the test section.

A second traverse device was used to make surveys through the boundary layer at select stations along the transverse survey line. Surveys made with a yaw probe and pitch probe indicated the presence of a definite type of directional structure in the nonuniform turbulent boundary layer.

The transverse traverse device was also used to survey the three-dimensional flow field downstream of the wing-like model. These measurements indicated that the presence of the wing model tended to amplify the nonuniformities in the boundary layer.

Only one representative set of boundary layer surveys were made in the three-dimensional flow at a station 0.5 in. behind the trailing edge of the wing model. Surveys with a yaw probe indicated a maximum cross flow of 22.4^{o} to occur in the nominally 4.0 in. thick boundary layer. Measurements with the pitch probe showed the flow to be pitched toward the wall by over 4.7^{o} in the boundary layer at about 1 in. above the wall. Static pressure measurements indicated a decrease in the static pressure of 5.5% of the free stream dynamic pressure in going from the surface to a point 6 in. off the wall.

Acknowledgements

This work was performed at the University of Maryland while the first author was a Minta Martin fellow and later a graduate research assistant on leave from the Naval Surface Weapons Center, Silver Spring, MD 20910.

The authors wish to thank Dr. K. S. Hebbar, Mr. James Deveney, and the staff of the Wind Tunnel Operations Department for their efforts in completing these experiments.

This research was funded partially by the Minta Martin Fund for Aeronautical Research, by NASA under Grant NGR-21-002-303 and by the Office of Naval Research under Contracts N00014-67-A-0239-0029 and N00014-75-C-0613. Computer time for this investigation was supported in full through the facilities of the Computer Science Center of the University of Maryland.

TABLE OF CONTENTS

LIST OF TABLES

LIST OF FIGURES

Page

Page

NOMENCLATURE

B	= barometric pressure in mm Hg, constant in King's law
C_a	= calibration constant for angular response of pitch and 3-tube probes
C_f	= skin friction coefficient
C_k	= calibration constant for static disk probe
C_p	= $\frac{P_s - P_{ref}}{q_{ref}}$ = static pressure coefficient
C_{Re}	= Reynolds number correction coefficient
D	= external diameter
e	= external width of rectangular pitot tube
H	= external height of rectangular pitot probe
h	= speed setting in inches of DC-200 silicon oil, internal height of rectangular pitot probe
K	= correction factor to dynamic pressure measured by side tubes of pitch probe ($K = 0.54$)
ℓ	= distance measured along tunnel $\mathbb{C}_L$ from start of test section
P	= pressure
ΔP	= differential pressure
ΔP_{sides}	= differential pressure measured across the side tubes of the 3-tube probes or pitch probes
$\Delta P_{uncorrected}$	= pressure differential of pitot probe uncorrected for viscous effects
P_d	= pressure measured by static disk probe
P_{ref}	= reference static pressure
P_s	= static pressure
P_T	= total pressure
q	= $\frac{1}{2}\rho U^2$ = dynamic pressure

q_{ref}	= reference dynamic pressure
q_∞	= local free stream dynamic pressure
$\frac{dq}{dy}$	= gradient of q through boundary layer
Re	= unit Reynolds number (ft^{-1})
s.g.	= specific gravity
T_d	= dry bulb temperature
T_m	= temperature of monometer fluid
T_W	= wet bulb temperature
U	= total velocity
U_e	= velocity at edge of boundary layer
U_{ref}	= reference velocity measured by reference pitot-static probe
U_s	= streamwise component of velocity in the 3-DTBL
U_∞	= local free stream velocity
u^+	= U/u_τ = velocity in wall coordinates
u_τ	= $\sqrt{\rho/\tau_W}$ = friction velocity
Δu	= wall proximity correction
W	= cross flow velocity component, specific humidity
x	= longitudinal (streamwise) coordinate, coordinate parallel to centerline of test wall, distance measured (parallel to test wall centerline) from diagonal line passing through pressure taps no. 22 and 5 on aluminum wall
y	= coordinate normal to test wall, distance measured from test wall outward through boundary layer
y_c	= effective center of pitot tube
y^+	= $\frac{y\,u_\tau}{\nu}$ = distance in wall coordinates
z	= transverse coordinate normal to x-y plane, distance measured from center line of test wall
z_e	= distance measured from centerline of test wall along a line parallel to the trailing (leading) edge of wing model

$\frac{\sqrt{\bar{u}^2}}{Ue}$	= longitudinal turbulence intensity
α	= cross flow angle measured relative to centerline of test wall
β	= pitch angle
δ	= boundary layer thickness
μ	= viscosity of dry air
ν	= Kinematic viscosity
ρ	= ρ_e density of (humid) air
ρ_f	= density of DC-200 silicon oil used in micromanometers
τ_w	= local wall shear stress
Ω	= resistance in ohms

I. INTRODUCTION

This report presents the results of an experimental study of a two and a three-dimensional low speed turbulent boundary layer. In the way of introduction, a short description of the three-dimensional turbulent boundary layer (3-DTBL) will first be given. Following this, a brief review of past studies of 3-DTBLs will be made. Finally the scope of the present study will be indicated.

A. The Three-Dimensional Turbulent Boundary Layer

The three-dimensional turbulent boundary layer represents a general class of viscous flows that include the two-dimensional turbulent boundary layer (2-DTBL) as a special case. The 2-DTBL has been studied in far greater detail than the general 3-DTBL because of the reduced number of variables required for the 2-D case. Fortunately, many practical engineering problems can be solved by applying the well developed 2-D techniques. However, many problems remain which must be treated by a 3-D analysis. Some of the techniques recently developed for 3-D flows will be noted in the next section. First, however, the 3-DTBL will be described in more detail.

The 3-DTBL is characterized as a boundary layer flow which has both streamwise and cross-flow mean velocity components. Three-dimensional boundary layers can either be skewed or collateral. The direction of flow varies through the skewed boundary layer and the velocity profile is contained in a twisted plane (fig. 1b). By contrast, the velocity profile of the 3-D collateral boundary layer lies in a plane normal to the surface. This type of boundary layer occurs for example in the diverging flow on a cone at zero angle of attack.

The two-dimensional boundary layer is at times also referred to as a collateral flow, but the velocity components in this case are aligned in the streamwise direction (fig. 1a).

B. Past Studies of the 3-DTBL

In recent years, a number of computational and experimental studies of three-dimensional turbulent boundary layers have been completed. Computational methods for 3-DTBLs have in general been extensions of the well developed techniques for 2-D flows. As in the two-dimensional methods, two basic techniques exist: i.) momentum integral techniques and ii.) differential techniques. A review of these methods as well as the derivations of the basic equations can be found in references 1 - 5.

Common to both the momentum integral technique and the differential technique is the need for experimental data to help develop closure schemes. Integral techniques require data on mean quantities such as velocity profiles and wall shear stress. The differential techniques require additional information on the turbulence structure of the boundary layer. A proper evaluation of the various computational techniques depends in part on the type of 3-DTBL under consideration.

The majority of experimental studies of 3-DTBLs have been conducted in low speed flows. Classified according to flow geometry (as done in ref. 6), these include: i.) curved channel flows (e.g. ref. 6 - 11, ref. 12 (supersonic)), ii) flows on swept wings or plates (e.g. ref. 13 - 25), iii). stagnation point flows in 2-DTBLs (e.g. ref. 26 - 31), iv). flows on rotating bodies (e.g. ref. 32 - 40), v.) corner flows (e.g. ref. 41 - 43), vi.) (supersonic) flows on yawed cones (e. g. ref. 44) and vii.) two-dimensional diffuser flows (e.g. ref. 45). The first six geometries produce skewed boundary layers while the last geometry produces a collateral boundary layer. For a review of past experimental work in 3-DTBLs, the reader is referred to survey articles by Johnston (ref. 46), Horlock, et. al. (ref. 47), Fernholz (ref. 48), Nash and Patel (ref. 5) and Joubert, et. al. (ref. 3).

The experimental studies to date have largely concentrated on obtaining mean velocity profiles and wall shear stress data. Only a few recent studies (e.g. ref. 20, 21, 31 and 37) have obtained turbulence data suitable for use in checking the assumptions made in the differential techniques. With this in mind, an experimental study of 3-DTBLs was initiated at the University of Maryland. In the next section, the scope of the first stage of this study will be indicated.

C. Scope of the Present Study

The motivation for the experimental study presented in this report was to obtain data for use in evaluating the various closure schemes used in 3-DTBL computational techniques. In selecting a flow geometry to produce the 3-DTBL, it was desired that: i.) the boundary layer should be relatively thick to assure spatial resolution of the measurements and ii.) the boundary layer should be predominately shear driven in order to be a good test case for evaluating the various closure schemes. The geometry which was selected consisted of a 30° swept wing-like model faired into the side wall of a boundary layer wind tunnel. The relatively thick two-dimensional turbulent boundary layer which developed on the wall upstream of the medel was pressure driven (by the model) into a 3-D flow. Downstream of the model, the 3-DTBL relaxed under a small pressure gradient and eventually returned to a 2-D flow. The relaxing boundary layer was considered to be influenced by both shear and pressure forces. In the present study, the 3-D boundary layer measurments were made in this relaxing region.

While conducting preliminary studies of the 3-DTBL produced by a prototype of the wing model, the boundary layer in the wind tunnel was discovered to be nonuniform. The nonuniform boundary layer is characterized by transverse variations in the wall shear stress and is primarily caused by nonuniformities in the inlet damping screens. An effort was made to improve the flow, but this was not successful. Following this, an extensive study of the nonuniform turbulent boundary layer (both two and three-dimensional) was conducted.

To study the nonuniformities, a special traverse device was developed that allowed one to survey the boundary layer in a direction transverse to the mean flow at at set distances off the wall. Transverse surveys were made using several different probes which included a 3-tube probe (combined total pressure and yaw probe), Preston tubes, a pitch probe and a hot-wire probe. A second traverse device was developed to make surveys through the boundary layer at select stations using the same types of probes. A number of boundary layer surveys were conducted in the 2-DTBL (on the side wall without the model installed) to gather data on the nonuniformities as well as to check out the probes and measuring techniques. However, because of time limitations, only one representative boundary layer survey was completed in the 3-D flow field downstream of the wing model.

In the following chapter a detailed description is given of the boundary layer wind tunnel and the wing-like model, followed by a description of the instrumentation used in the study. Next, an outline of the test procedure and data reduction is presented. The third chapter contains a discussion of the results. Finally the conclusions of the study and recommendations for further work are given in the last two chapters. A more extensive discussion of the work completed for this report is presented in a Ph.D. dissertation by the senior author (ref. 49).

II. EXPERIMENTAL PROGRAM

The experimental program carried out in this study will be outlined below. A detailed description of the test facility and the instrumentation will be given first, followed by a discussion of the experimental procedure and data reduction. Finally an assessment of the accuracy of the measurements will be made.

A. Test Facility

The description of the test facility will be presented in two parts: general description of wind tunnel; 3-D model and instrumented wall.

1. General Description of Wind Tunnel

The experimental studies carried out for this report were conducted in the low speed indraft boundary layer tunnel of the University of Maryland (figs. 2 and 3). The original facility, from which the boundary layer tunnel evolved, had a 4 ft. long test section. In order to convert the facility to a boundary layer tunnel, the length of the test section was extended to 20 ft.

During a series of preliminary studies (to select a model for producing the 3-DTBL) (see reference 49) it was discovered that the two-dimensional turbulent boundary layer which developed on the side wall of the test section was nonuniform in nature. This meant that there were transverse variations in the wall shear stress at any given station along the test section. According to the available literature (e.g. ref. 50, 51), the problem is caused primarily by intake damping screens that have an open-area ratio of less than about 0.57. The two screens that were in the original inlet had an open-area ratio of only 0.44. Hence, it was decided to try to improve the boundary layer flow by making a number of alterations to the wind tunnel. Details of these alterations, as well as a description of each component of the wind tunnel system, are given below.

The filter system shown in figures 2 and 3 was added to the existing facility in order to reduce the intake of dust. After the air has been drawn through the filter, it enters the rectangular inlet (60 in. wide, 88.5 in. high) to the tunnel and passes through a honeycomb and damping screen assembly. At the start of the present study it was thought that a more effective honeycomb might help to reduce the nonuniformity problems observed in the boundary layer. Hence the original honeycomb (1.50 in. O.D. x 1.38 in. I.D. paper tubes, 7.5 in. long) was replaced (upon the advise of references 52 and 53) by ordinary plastic drinking straws (0.234 in. O.D., 0.007 in. wall, 8.25 in. long).

As noted earlier, the original facility had two stainless steel screens with an open-area ratio of 0.436 (20 mesh, 0.017 in. diam wire). Based on recommendations of the available literature, it was decided to replace the old screens with a set of new ones with an open-area ratio of 0.57 or more. Since it was not possible to purchase "off the shelf" stainless steel screens of sufficient width (67 in. with frames), a polyester screening with an open-area ration of 0.59 (15 mesh, 0.0157 in. diam filament) and 80 in. width was selected (manufactured by TET/Kressilk). Four screen assemblies were made by nailing the tightly stretched screen to frames of 2 x 4's glued together. A remnant piece of stainless steel screening with an open-area ratio of 0.64 (20 mesh, 0.010 in. diam wire) was later obtained and a fifth screen assembly was constructed. The stainless steel screen was located directly behind the honeycomb in order to withstand the large loads that were expected from the straws (since a large pressure drop was calculated to occur across the honeycomb). In the final assembly, the screens were 3 in. apart, whereas the two screens in the original inlet were only 1.5 in. apart.

The design of the original inlet contraction section was based on calculations of an axisymmetric contraction cone (ref. 54). Contours for the side walls of the three-dimensional rectangular contraction section were selected by fairing in curves to the plotted results of these calculations. The original shape (18 in. x 46.5 in. at the exit plane) was modified slightly to match in with the inlet of the new test section (17 in. x 45.5 in.). With an entrance of 60 in. x 88.5 in., the 69 in. long contraction section had a contraction ratio of 6.9.

In order to obtain a nominally zero pressure gradient along the test section, all four walls were diverged 0.5 in.. The new test section had a cross section measuring 17 in. x 45.5 in. at the entrance and 18 in. x 46.5 in. at the exit. To assure that the turbulent boundary layer developed from the same location in every test, a tripping device consisting of a 0.065 in. thick, 0.25 in. wide aluminum strip was epoxied to all four sides of the test section at the entrance.

The test section was constructed in three parts; one 4 ft. long section and two 8 ft. long sections. The sections were bolted together and a wide plastic tape was used to seal the joints and blend in the surfaces. The wall sections could be adjusted in or out and could be removed completely for modification. Access to the test section was through three doors on one side of the test section and three doors in the floor. A special segmented access door for use with the boundary layer traverse device was constructed in several interchangeable parts that allowed the traverse to be located any place over the area of the door. No doors or openings were put on the test wall in order to avoid flow disturbances from any door-wall mismatches.

The test section was originally supported on 2 x 6 planks which were extensions of the wall reinforcements. However, additional heavy bracing off an adjacent concrete wall was needed to hold the test section steady and to reduce the vibrations of the walls.

The test wall was instrumented with a series of 0.047 in. diameter static taps located nominally every 16 in. along the entire length. The location of these taps is given in table 1.

To monitor the speed of the wind tunnel, a United Sensors pitot-static probe (PAC-12-KL) was mounted on the side wall (with the access doors) at a station 60 in. downstream of the entrance to the test section. The tip of the probe was located 6.25 in. off the wall and 9.38 in. above the centerline of the tunnel in order to keep the wake of the probe well clear of the area to be studied downstream. A micromanometer described in a later section was used to measure the pressure differential of the probe.

The diffuser, which was constructed of 0.25 in. thick steel, provided a transition from the rectangular test section to the 48 in. diameter circular inlet of the blower. To reduce the mechanical transmission of vibration, the diffuser was physically separated from the test section and the blower. The 0.13 in. wide gap at the end of the test section was sealed over with a wide plastic tape to prevent leakage.

Pitot rake surveys made in the original test section indicated that the variations of free stream velocity distribution were within 0.5% of the mean. Similar results were obtained in the present study with surveys taken in the new test section. The operating speed could generally be set to well within 0.2% at speeds between 45 ft/sec and 55 ft/sec. Judging from the random variations of the miniscus in the micromanometer, the operating speed fluctuated on the order of ± 0.1% about the mean. For wind tunnel tests lasting several hours, the mean position of the miniscus remained virtually fixed, although the ambient test conditions (and hence the operating speed) generally varied slightly during this time. The free stream turbulence level of the tunnel was measured as 0.2% at a free stream velocity of 50 ft/sec.

2. 3-D Model and Instrumented Wall

The three-dimensional turbulent boundary layer that was studied for this report was produced by a 30^{o} swept wing-like model that was faired into the side wall of the test section (figs. 3-4). The model produces the 3-D flow by pressure driving the relatively thick two-dimensional turbulent boundary layer that develops over the first 11 ft. of the test wall. Downstream of the model the boundary layer relaxes under a small pressure gradient and eventually returns to a two-dimensional state. It was in this downstream region where the 3-D boundary layer measurements for this report were made.

A 0.250 in. thick aluminum plate was laminated (epoxied) onto the rear 8 ft. section of the test wall to provide a smooth working surface and to assure the accurate location of static taps. The aluminum plate also allowed the wall contact of boundary layer probes to be monitored with an ohmmeter. The plate was given a mirror-like finish so that a special technique (to be described later) could be used to align the probe tips. A total of 67 static taps (0.029 in. diameter, depth of 0.125 in.) were drilled in the aluminum plate (prior to lamination) downstream of the intended location of the 3-D model (fig. 4). In addition, ten 0.750 in. dimater instrumentation ports (used in ref. 55) were also located on the plate. When not in use, each port was closed with a flush fitting dummy plug which had a 0.029 in. diameter static tap located on the center. The location of the static taps and ports is given in table 2.

The model configuration shown in figure 4 was selected after a long series of prototype studies summarized in reference 49. The model itself consisted of a frame work of wooden ribs over which 0.125 in. thick masonite sheet was glued. The location of the 35 static pressure taps (0.047 in. dia.) installed on the model is given in table 3. After the model was secured to the test wall, an epoxy filler material was used to make a 20 in. radius fairing at both the leading and trailing edges. With special care, it was possible to "feather in" the trailing edge to the aluminum wall with a step of less than 0.001 inch.

B. Instrumentation

Two traverse devices were used to survey the flow field in the boundary layer tunnel; a transverse traverse device and a boundary layer traverse device. Most of the measurements were made using pressure probes together with manometers and pressure transducers. Some limited surveys were also made using a hot-wire anemometer system.

1. Transverse Traverse Device

A special transverse traverse device was designed and constructed to obtain surveys of the wind tunnel boundary layer in a direction transverse to the mean flow and at set distances above the wall (figs. 5 and 6). In order to reduce disturbance effects on the flow field, the device was mounted on the wall opposite the test wall (fig. 6). Various probes could be mounted in the probe holder that extended across to the test wall.

The traverse device consists essentially of a carriage that rides on two 0.438 in. diameter steel drill rods. A small variable speed reversible dc motor is used to drive the carriage by means of a threaded rod. With this combination, surveys could be conducted with sweep rates ranging from 0.4 in./min to 2.7 in./min. The motion of the carriage was monitored by a 10 turn potentiometer (1KΩ) which was connected to the carriage by a pulley-spool-fishing line combination. The transverse distance was limited to 15 in. so that the surveys could be recorded full scale on a Hewlett-Packard Moseley 7004A X-Y recorder.

A second carriage-drill rod combination (fig. 5) was mounted on the main traverse carriage and allowed the height of the probe to be adjusted at the end of each pass. This was done by inserting a screw driver through a hole in the wall and turning on a 40 threads per inch threaded rod that moved the probe carriage in or out. From initial wall contact the probes could be adjusted up to 6 in. off the surface. Further distances off the wall could be obtained by changing the probe holder.

To help reduce the effects of flow field interference caused by the traverse device, the probe tips were located 4.5 in. ahead of the probe holder (3.5 in. ahead of the projection of the traverse device). This appeared to be about the practical limit from the standpoint of probe vibration and deflection due to aerodynamic loading. Mechanical deflections of the probes, which occurred when the carriages were traversed back and forth, were generally small. For the main transverse carriage, the variation in yaw (yaw defined in a plane parallel to the test wall) over the 15 in. travel was within 2 minutes (as determined by a small precision bubble level). Over this same distance, the probe underwent a pitching motion (pitch defined in a plane normal to the wall and parallel to the mean flow direction) of about 10 minutes. The smaller probe carriage indicated a change of 0.4° in yaw when traversed over its 6 in. span. The variation of pitch over this distance was on the order of 15 minutes. The relative change in height of the probe off the wall to a slight bow in the main traverse drill rods was about 0.003 in. for the 15 in. travel of the main carriage (as determined by a set-up on a milling machine). Finally, with the combination of wall vibrations, probe vibrations and variations in the wall flatness itself, the accuracy of the lcoation of the probe above the wall was estimated to be between 0.005 in. and 0.010 in..

2. Boundary Layer Traverse Device

A second traverse device was designed and constructed for use in making accurate surveys through a three-dimensional turbulent boundary layer (fig. 7). In addition to a translational motion, the traverse device also provided a yawing motion so that the probe could be aligned with the local flow direction throughout the boundary layer (fig. 8). The traverse device was mounted on a heavy theodolite camera stand and made no direct contact with the tunnel walls in order to avoid the transmission of wall vibrations to the probe.

The translational motion of the traverse was provided by a carriage riding on two 1 in. diameter stainless steel guide rods and moved in and out by means of a brass lead screw. A 6 in. Brown and Sharpe dial indicator calipers accurate to 0.001 in. was used to directly measure the relative location of the carriage. A Starrett dial indicator with a range of 0.5 in. and 0.0005 in./division was temporarily clamped to the base of the traverse device and provided increased accuracy for measurements made very close to the test wall.

Yawing motion to the probes was provided by a rotating assembly mounted on the carriage (fig. 7). A graduated angle ring and vernier accurate to 1 min., was used to measure the relative angular position of the probe. A combination magnifying glass and prism assembly was used to conveniently read the scale.

A 0.375 in. O.D. x 0.250 in. I.D. stainless steel traverse shaft was mounted in the rotation assembly and extended into the test section to serve as a mounting for the boundary layer probes (figs. 8 and 9). Additional support for the traverse shaft was provided by a 0.375 in. thick aluminum plate that extended about 3 in. into the flow (fig. 9). The opening in the wall for the aluminum extension was sealed over using plastic food wrap that provided an air tight seal but transmitted a negligible amount of wall vibration.

A Clineometer placed on the carriage indicated an angular run out of about 3 minutes over the 6 in. motion. Possible twisting of the traverse shaft due to drag in the oilite bushings was estimated to be less than 1 minute. Machine blocks and a 0.0001 in./division dial indicator were used to check the motion of the carriage and found it accurate to the smallest division of the 6 in. calipers (0.001 in.) and the 0.5 in. dial indicator (0.0005 in.).

3. Pressure Probes

Five different types of pressure probes were used in the present study: i) pitot tubes (circular and rectangular), ii) yaw probes (Conrad and 3-tube), iii) pitch probe, iv.) static pressure probes (static tube and static disk), v.) Preston tubes. A photograph of the boundary layer pitot probe is shown in figure 10. The offset stem design of this probe was required for measurements made in the 3-DTBL. With the probe mounted in the traverse device as sketched in figure 8, the probe tip could be aligned with the local flow direction in the boundary layer while remaining fixed in location (coincident with the axis of the traverse probe shift). Since the remaining boundary layer probes were all of similar design, only the bottom portion of each probe is shown in figure 11, along with some details of the probe tip. Similar types of probes were constructed for use with the transverse traverse device and are shown in figure 12. Details on the design and construction of the pressure probes are given in reference 49.

Two pitot tubes were used to measure the total pressure profiles through the boundary layer (which were used to determine the velocity profiles when combined with the local static pressure). The overall profiles were obtained using the circular flat faced probe shown in figures 10 and 11a. In order to obtain data closer to the wall than was possible with the circular tube, a rectangular pitot probe shown in figure 11b was constructed. At wall contact, the center of the probe tip was 0.0043 in. off the wall compared to 0.014 in. for the circular tube probe. A microphoto of the rectangular probe tip is shown in figure 11c.

The yaw probe (generally called a Conrad probe) and the pitch probe differ only in the orientation of the plane passing through the probe tips. The Conrad probe (fig. 11d) was used to measure flow angularity (yaw) in a plane parallel to the wall by nulling the probe at each location through the boundary layer (i.e. aligning the probe in yaw so that the pressure difference between the two sides of the probe is zero). The flow angle profile determined with the Conrad probe was used to align all other boundary layer probes with the local flow direction. The pitch probe (fig. 11e) was fixed in position (although aligned in yaw) and the differential pressure measured between the tubes was used together with a calibration to the determine the pitch.

Some boundary layer measurements were made using a 3-tube probe consisting of a total tube and a tube to each side beveled off at 55° -- essentially a combined pitot and Conrad probe. However, because of the very poor response time of the particular probe constructed here, its use was discontinued in favor of the two individual probes. For surveys made with the transverse traverse device, the 3-tube probe was required since no nulling capability existed and a simulataneous measurement of the total tube pressure and the side tube differential pressure was needed.

Static pressure surveys were made using a conventional static tube (United Sensors probe PSB-12) and a static pressure disk suggested in reference 56 (fig. 11f). The static tube is rather sensitive to flow angularity while the static disk (according to reference 56) is virtually insensitive to $\pm 20^{\circ}$ of yaw (defined in the plane of the disk) and $\pm 5^{\circ}$ in pitch. The static tube was mounted in a holder such that the static holes were in line with the axis of the traverse shaft. The static disk does not read the static pressure directly and a small correction of about 0.08 times the local dynamic pressure is required.

Four Preston tubes (fig. 11g) with dimensions:

O.D. inches		I.D. inches
0.0591	x	0.041
0.0426	x	0.027
0.0283	x	0.016
0.0183	x	0.010

were used to measure the local skin friction (using a calibration for each probe) at each boundary layer survey station. These probes had a common probe body and had to be interchanged and aligned at each station. The four sizes of probes were used to check on the existence of near wall similarity in the 3-DTBL.

The tips used on the pressure probes for the transverse traverse device (fig. 12) were similar to the tips used with the boundary layer probes and only the dimensions will be summarized here:

3-tube	tubing used:	0.032 in. O.D. x 0.020 in. I.D.
pitch	tubing used:	0.0283 in. O.D. x 0.016 in. I.D.
3-tube Preston	tubing used:	0.0283 in. O.D. x 0.016 in. I.D.
Preston	tubing used:	0.0591 in. O.D. x 0.041 in. I.D.
static disk	same as fig. 11f	

4. Pressure Measuring Systems

The primary pressure measuring instrument and standard used in this study was the differential liquid manometer. In addition, pressure transducers were used with the transverse traverse probes.

Two micromanometers were designed and constructed based on a paper by Smith and Murphy (ref. 57). The calibration micromanometer (fig. 13a) was used as a pressure standard for calibration purposes and to measure pressures from the various boundary layer probes. The second micromanometer was used mainly to set the wind tunnel operating speed.

The calibration micromanometer consisted of a small volume brass reservoir mounted on the adjustable arm of a 6 in. vernier calipers and connected by a flexible polyurethane tube to a fixed glass tube inclined at 10^{o}. A Dow Corning, 1 centistoke DC-200 silicon oil was used as the manometer fluid. Mounting a dial indicator under the reservoir (fig. 13a) gave added accuracy and reading convenience over a limited range (0.5 in. by 0.0001 in./division).

The miniscus was viewed with the aid of a homemade microscope that gave about a 65X magnification. A mirror mounted under the glass tube was used to reflect light from the overhead flourescent lamps and provided adequate illumination. Initially a cross-hair reticle was used in the mircoscope eyepiece to serve as a reference line for the miniscus. However, a considerable amount of time was required to obtain a single reading because the reservior had to be adjusted several times in order to return the mean position of the miniscus to the hair line (reference position). The cross-hair reticle was later replaced with a second reticle which had a 10 mm scale divided into 100 parts. A calibration of the reticle scale against the vertical motion of the reservoir was found to be linear, with each division of the scale being equivalent to 0.000187 vertical inches of manometer fluid. The use of this reticle greatly reduced the time required to obtain a reading because it was no longer necessary to return the miniscus to the zero position. Instead, once the miniscus was in the field of view and had stablized, the number of divisions between the zero line and the miniscus could be counted and a correction made to the reading on the dial indicator or calipers to obtain the true reading.

The manometer fluid (DC-200 silicon oil) was calibrated in a water bath against temperature using two different precision hydrometers (accurate to specific gravity of 0.001) and a precision thermometer (accuare to $0.1^{\circ}C$). As shown in figure 14, the calibrations varied from the least squares fit by about 0.00065 slugs/ft.^{3} at 34° C (variation in s.g. of 0.0005), but agreed quite well at the lower temperatures.

The micromanometers were found to be quite sensitive to temperature variations since a temperature change of $1^{\circ}C$ would cause a shift in the zero reading of over 0.001 in.. After trying a number of ways to pack insulation around the manometer tubes, the best thermal protection was provided by placing a paste-board box over the entire instrument. A precision thermometer (accurate to $0.1^{\circ}C$) was mounted inside the box to monitor the temperature. With the use of the paste-board box and by checking the zero repeatedly throughout a test, the zero shift was generally within 0.0002 in. of DC-200 silicon oil.

In addition to the two micromanometers described above, a second type of micromanometer was constructed specifically for use with the boundary layer yaw probes (fig. 13b). The manometer was used only in nulling the yaw probes and could not be used to measure pressure differentials. It consisted simply of a U-tube mounted on an aluminum plate inclined at 7.5° to the horizon (fig. 13b). A microscope was used to sight the miniscus in one of the tubes. In use, the yaw probe was rotated until the miniscus returned to the initial zero - i.e. zero pressure differential existed between the two tubes of the probe and the probe was then aligned with the local flow direction.

The differential pressures from the probes used with the transverse traverse device was monitored by pressure transducers (Pace Wiancko model P90D $\pm$ 0.03PSID together with a Dynasciences Corp. transducer indicator model CD25). The output from the transducer indicators were recorded on X-Y plotters. The transducers were calibrated against the calibration micromanometer.

5. Hot-Wire Probe and Equipment

Hot-wire anemometer measurements were made using a DISA model 55F31 single wire probe mounted in a 55A21 probe holder (fig. 12). With the probe mounted on a special stem, it was used with the boundary layer traverse device to measure the free stream turbulence level of the wind tunnel. The probe was also used with the transverse traverse device to obtain surveys in the boundary layer.

The constant temperature hot-wire anemometer system used with the transverse traverse device is shown in figure 15. The hot-wire probe was powered by a DISA 55D05 CTA which was run off a 12 volt car battery. The nonlinear signal of the CTA was linearized using a DISA 55D10 linearizer and the output was filtered at 10K Hz using TSI model 1057 unit. The signal was then fed to a DISA 55D35 rms voltmeter, a DISA 55D30 dc voltmeter and a TSI model 1047 averging circuit. Finally the output from the rms voltmeter and the averaging circuit were recorded on X-Y plotters. The hot-wire probe was calibrated in a small free-jet facility before and after each test.

C. Experimental Procedure

The experimental procedure followed in the present study will be described in this section under the headings of: static pressure measurements, transverse traverse surveys and boundary layer surveys. The procedures used for the 2-D studies (i.e. without the wing model in the test section) and the 3-D studies (with the wing model in the test section) were basically the same.

All wind tunnel tests were conducted at a constant reference free stream Reynolds number Re = 3.15E + 05* ft^{-1} (Re = 3.00E + 05 ft^{-1} for an early series of measurements). Because of daily changes in ambient conditions, the reference free stream velocity U_{ref} (measured by the reference pitot-static probe) varied over a range of 50 ft/sec $\leq U_{ref} \leq$ 55 ft/sec. Tests were only conducted when moderate temperatures ($15^{o}C \leq T \leq 30^{o}C$) and relatively dust free conditions existed in the laboratory building. The usual proceudre in conducting a test was to first run the tunnel about 45 minutes to assure proper air circulation and temperature stabilization before the speed was set. The proper speed setting in inches of DC-200 manometer fluid (for a constant Re) was calculated with the use of several computer generated tables and the values of the test conditions consisting of the dry bulb temperature T_d, the wet bulb temperature T_w, the barometric pressure P and the temperature of the speed micromanometer T_m (usually $T_d = T_m$). A further description of the procedure for calculating the speed setting is given in reference 49. The test conditions were taken

---

*E + 05 is conventional computer notation for 1 x 10^5.

every hour during a long run and the speed was reset when conditions had drifted too far from the original readings (typically if T_d had changed more than 1.5^{o}C).

1. Static Pressure Measurements

Static pressure measurements were made on the wind tunnel test wall and on the 3-D wing model. The location and description of the static taps has been given in the previous section together with tables 1-3. Prior to any measurements, each tap was cleaned with high pressure air and reinspected with a hand held 50X microscope.

The static pressure measurements made in a series of 2-D studies were referenced to static tap no. 5 (table 2) located on the aluminum insert. This tap was chosen since it was found to be sufficiently far away from the intended location of the transverse traverse and boundary layer surveys to be free of any significant interference problems. For the 3-D studies, a reference tap was installed upstream of the wing model (table 3). The pressure differential between a given static tap and the reference tap was measured with the calibration micromanometer.

Early tests indicated that the reading precision of the manometer system was limited because of small oscillations in the static pressure distribution. To improve the readability of the system, damping lines consisting of lengths of 0.027 in. I.D. stainless steel tubing were added to the plastic tubing that was used to connect the static taps to the manometer. The length of the damping lines varied between 9 in. and 18 in.. With damping lines, the unsteadiness of the miniscus was generally reduced to ± 1 division ($\pm$ 0.0002 in. DC-200) and these variations were slow enough to permit an averaging by eye to be done.

In making the actual static pressure measurements, more than sufficient time was given for each pressure tap to fully respond. The zero reading was recorded after each pressure tap measurement in order to assure the greatest accuracy and to minimize errors due to the temperature drifting problem of the manometer noted in a previous section.

2. Transverse Traverse Surveys

The location of transverse traverse surveys made in this study are shown in figure 16. Two stations at ℓ = 34 in. and ℓ = 18 ft (ℓ = distance measured from the start of the test section) were selected for the 2-D studies. Both stations were centered on the centerline of the test wall. Three survey stations were chosen for the tests downstream of the wing model; one being the "old" 18 ft. 2-D station, a second along a line which was nominally 0.5 in. behind the trailing edge and passed through pressure taps 5-19 (table 2)(also centered on the side wall centerline), a third was on the centerline and ran from the trailing edge, 15 in. downstream.

As previously noted, the transverse traverse device was mounted on the wall opposite the test wall to reduce aerodynamic disturbances (fig. 6). Because the walls of the test section were not exactly parallel, small shims had to be placed under one end of the traverse base to assure that a probe would remain at a fixed distance above the wall over the 15 in. survey line. To accurately locate a probe in the probe stem, a sheet of graph paper (tracing paper quality) was first taped to the aluminum wall, over the region to be surveyed. Several lights were placed on the outside of the test wall such that the light shining through the pressure taps created a "star field" on the paper. By using this "star field", the paper was positioned so that one axis of the graph was parallel to the centerline of the test wall (essentially parallel to the horizon). A fine point Rapidograph pen was used to mark the location of each tap under the paper and to draw in the location of the survey line. A probe was then installed such that its tip extended to the survey line (approximately 4.5 in. ahead of the probem stem), and was parallel to lines on the graph sheet (hence parallel to the centerline of the test wall). With careful adjustments, the probe tip could be located to within 0.025 in. of the intended survey line.

Because each probe was interchangeable with a common probe stem, it was necessary to check the alignment of the probe tip each time a different probe was installed. To accomplish this, a special probe sighting device (fig. 17), based on a technique in use at NBS (ref. 58), was designed and constructed. In principle, the technique involves using a microscope - mirror combination to sight along the surface of the wall and view the approach of the probe tip to the wall. With a polished aluminum surface, the probe tip and its mirror image can be seen in the microscope, hence effectively doubling the magnification power of the microscope. The 5mm, 100 divisions reticle was calibrated against a second 0.1 in., 100 division reticle. Each division of the microscope reticle corresponded to 0.00063 in.. Since the sighting device was hand held and focused, the magnification of the microscope used here ($\sim$ 50X) appeared to be about the maximum practical.

Using the probe sighting device, each probe was aligned everytime it was reinstalled in the probe stem. The 3-tube probe (fig. 12) was adjusted so that the side tubes were at the same distance off the walls (the best adjustment possible resulted in one side being at most 0.00030 in. further off the wall than the other). This was critical to reduce errors in flow angularity measurements which are introduced because of gradients in the total pressure through the boundary layer. Similar techniques were used to align the Preston probe, the 3-tube Preston probe, the static disk probe, the pitch probe and the hot-wire probe. The initial distance off the wall of the hot-wire element (electrical contact made with the probe holder) was also determined with the probe sighting device. The Preston probes were "driven into the wall" (i.e. the probe tips were slightly "spring loaded" against the wall) several counts ($\sim$0.0075 in.) beyond initial electrical contact to assure that the tips remained on the surface over the 15 in. traverse. The axis of the Preston probe was brought in at about 2° to the wall in order to prevent the tip from lifting off due to a possible bending effect if the probe body made contact at a point behind the tip.

The pressure probes were connected to pressure transducers by lengths of plastic tubing and damping lines (typically 30 in. lengths of 0.020 in. I.D. stainless steel tubing). The side tubes of the 3-tube probe and the pitch probe were connected to opposite sides of a single transducer which monitored the differential pressures of the probes. The total tube of the 3-tube and Preston probes and the static disk probe were connected to one side of a transducer while the other side was connected to a reference static pressure tap.

The procedures followed in making surveys with the transverse traverse device were similar for all probes and will only be briefly outlined here. At the start of each test, the x-axis of the X-Y plotter was carefully adjusted to match the 15 in. span of the traverse carriage. When the operating speed was properly set, the probe was advanced to the wall until electrical contact was made. The probe (and the walls) were noted to deflect with wind on such that contact was about 0.010 in. earlier than noted with wind off. For the

3-tube probe, after wall contact was established, the probe tip was traversed (always in the same direction to reduce backlash) to the first survey line above the wall. The transverse traverse was then made at a slow rate ($\sim$1 in./min) to assure proper probe response when surveying through regions in which relatively large transverse gradients occurred. A reverse scan was made to average out any hysteresis effects due to probe lag or backlash in the carriage-potentiometer connection. At the end of a survey, the distance of the probe off the wall was readjusted and another transverse scan was made. In this way surveys at 0.063, 0.125, 0.250, 0.50, 1, 2, 3, 6 in. off the wall were made in a typical test with the 3-tube probe to obtain transverse measurements of the total pressure and flow angularity (yaw). Similar surveys were made using the pitch probe, the static disk probe and the hot-wire probe (to obtain transverse measurements of pitch, static pressure, velocity and longitudinal turbulence intensity respectively). The Preston tubes (for transverse measurements of the skin friction) were traversed at a slower rate (0.75 in./min) and wall contact was continuously monitored on an ohmmeter. The pressure transducers were calibrated after each test using the calibration micromanometer. The hot-wire probe was calibrated (mean voltage output versus mean velocity) before and after each test.

3. Boundary Layer Surveys

The location of boundary layer surveys made in this study are shown in figure 16. These stations were selected on the basis of data obtained with the transverse traverse device. For the 2-D studies, a number of surveys were made along the ℓ = 18 ft. station to assess the variations produced by the nonuniform boundary layer. Because of time limitations, only one representative boundary layer survey made in the 3-D flow (on the centerline of the test wall, 0.5 in. downstream of the trailing edge of the wing model).

The first step in setting up the boundary layer traverse device was to adjust the various sections of the segmented access door, so that a 6.75 in. wide vertical opening was provided for insertion of the traverse stem and shaft (figs. 7-9). Once the traverse was positioned and the theodolite stand lowered onto wooden blocks and braced, the 6.75 in. wide opening was filled with plexiglas window inserts. The remaining small gap that remained between the door and the traverse stem was sealed using masking tape and plastic food wrapping (fig. 9). Final alignment of the traverse device, as outlined below, was provided by adjustment screws on the mounting base (fig. 7).

By placing a sheet of accurate graph paper on the test wall (as done for the transverse traverse surveys) the location of a survey station relative to the adjacent static taps could easily be determined. With careful adjustments, the probe tip could be positioned to within 0.01 in. of the intended survey station. Alignment of the traverse shaft normal to the test wall was estimated to be within 2 minutes of 90°.

Each time a boundary layer probe was mounted in the traverse shaft, the probe sighting device was used to check on the alignment of the probe tip relative to the test wall. The probe tip was "leveled" to the horizon by placing a small line level on the upper part of the probe (i.e. on the portion of the 0.250 in. diameter tubing that is essentially parallel to the bottom of the probe (fig. 10)) and adjusting the rotating assembly of the traverse device. In this way, the probe tips were always positioned paralled to the centerline of the test wall at the start of each test. To assure greater leveling accuracy for the Conrad probe, a small precision bubble level was made by epoxying two sensitive viles (75 sec viles available from a surveying equipment repair shop) onto a glass microscope slide. With the precision level, the relative "leveling" of the Conrad probe was considered to be within 2 minutes from one station to another. The remaining boundary layer probes were leveled with the line level to within 0.25°.

Pressure connections to the micrometers were made with plastic tubing that was taken out through the hollow traverse shaft. Damping lines (9 in. to 18 in. lengths of 0.027 in. I.D. stainless steel tubing) were selected to give a relatively steady manometer response with a reasonably fast time response. The Conrad probe was nulled (i.e. aligned to the local flow direction) at each point through the boundary layer by using the nulling micromanometer (fig. 13b). The outputs from the pitot probes, Preston tubes and static disk probe were monitored on the calibration micromanometer along with a reference static pressure. The differential pressure from the pitch probe was also monitored on the calibration micromanometer.

Electrical contact (using a ohmmeter set at R x 10 KΩ) between the probe and the aluminum wall was used to "locate" the probe tip relative to the surface. Because of the combination of wall and probe vibration, this techinque was limited in accuracy to about 0.001 in.. Although the wall could be "located" quite accurately, the actual location of the wall relative to the traverse device (and hence the probe) was noted to change slightly (typically $\leq$ 0.001 in.) during the course of a run. A machinist's dial indicator (0.0005 in./div) was mounted on a heavy stand and used to monitor the wall motion. The shifting of the side wall (which was braced to the side of the lab building) was apparently associated with thermal expansion/contraction of the building and the side wall braces. The wall motion (dial indicator reading) was recorded throughout a run and the probes were brought back to "relocate" the wall several times during the test.

After the wall was located, a typical boundary layer survey consisted of taking data at a series of points starting from wall contact to 6 in. off the surface. Data points through the boundary layer (i.e. a series of y values, where y is distance above the surface) were selected to be approximately equal distances apart on a plot of $\log_{10} y/\delta$ vs U/U_∞ (where U_∞ = local free stream velocity).

At each station, a boundary layer survey using the Conrad probe (fig. 11d) was completed first to provide a profile of the flow angularity (yaw) through the boundary layer. This yaw profile was later used to align the other boundary layer probe tips parallel to the local flow direction through the boundary layer. The two tubes of the Conrad probe were monitored on the nulling manometer, and the probe was rotated by trial and error at each point until the tip was aligned to the local flow direction. For locations very near to the wall, this procedure required nearly 10 minutes per point because of slow probe response. In this region, the sensitivity of the probe-manometer system was estimated to be on the order of 0.10°. At points above y = 2 in., the sensitivity was on the order of 1 minute and proper alignment took less than 5 minutes per data point. The zero of the null manometer was repeatedily checked and reset throughout a run to assure the greatest accuracy.

Following the Conrad probe survey, the circular pitot probe (figs. 10 and 11a) was used to obtain the total pressure profile through the boundary layer. A technique was developed to more accurately locate the probe tip relative to the wall: The probe was first traversed to the wall and then "driven into the surface" about 0.002 in. beyond the point where electrical contact was first established. After the probe-calibration micromanometer system had responded, the probe was advanced away from the wall in steps of 0.0005 in., each time allowing 30 sec for the manometer system to react to any changes in pressure. When the probe tip just left the surface, a change in the manometer reading (on the order of 0.003 in. of DC-200 for the 2-D studies) was readily apparent.

The rectangular pitot probe (figs. 11b and 11c) was used to obtain total pressure measurements in the region 0.0043 in. $\leq y \leq$ 0.5 in.. For a limited region (0.050 in. $\leq y$) near the wall, the probe tip was located to within 0.00025 in. by a more careful application of the above technique - together with repeated checks of the wall location throughout a test.

Preston tube surveys, to obtain the local skin friction coefficient, were made using four sizes of probe tips (fig. 11g). The probe tips were located using the graph sheet and checked using the sighting device. To assure that the tips made continuous contact with the wall during a test, the probe was "driven in" about 0.005 in. beyond electrical contact.

Surveys with the pitch probe (fig. 11e) were taken at each station to measure the relative change in pitch through the boundary layer. As noted earlier, the pressure differential between the two tubes of the probe (produced by pitch and/or total pressure gradient) were monitored on the calibration micromanometer. The alignment (pitch) of the probe relative to the wall was noted for each test by using the probe sighting device.

A static disk probe (fig. 11f) was used to survey the boundary layer for the static pressure profile. The distance off the wall of the center plane of the static disk was determined using the probe sighting device. Additional measurements of the static pressure through the boundary layer were made using the static tube probe (United Sensors PSB-12).

D. Data Reduction

The procedures used to reduce the data obtained from the static pressure measurements, the transverse traverse surveys and the boundary layer surveys will be outlined in this section. As noted in the previous section on test procedures, the test conditions tended to drift slightly during the course of a long run. Using the input data (T_d, W, etc.) taken at the start and finish of each run (a long run was broken into two or three shorter runs), the averaged values of the test variables were calculated for use in reducing the data obtained during that run. A discussion of typical variations in the test variables is presented in the next section on the accuracy of the measurements. The various corrections and calibrations required in reducing the data are described in detail in reference 49.

1. Static Pressure Measurements

The data obtained from the static pressure measurements on the test wall and wing model were reduced to a static pressure coefficient

$$C_p = \frac{P_s - P_{ref}}{q_{ref}} \qquad (1)$$

The reference static pressure tap for the 2-D studies was tap no. 5 on the aluminum insert (table 2), while a special reference tap upstream of the wing model (table 1) was used in the 3-D studies.

2. Transverse Traverse Surveys

Most of the surveys obtained with the transverse traverse device have been presented as Xerox reproductions of the original X-Y plotter graph sheets. Information on test variables, calibrations, etc., pertaining to these tests have been included on these sheets or in separate tables. Only a portion of the data obtained in these surveys was reduced for this report.

The data which was reduced was first read off the graph sheets using a special machine which produced punched computer cards. These cards, together with additional information on test conditions and calibrations were run in a computer program to obtain the final results.

Surveys obtained using the 3-tube probe were reduced to the form of U/U_e vs z and α vs z, where U_e (essentially U_∞) is the velocity at y = 6 in. above the test wall, z is the transverse location relative to the center line of the test wall and α is the flow angle relative to the centerline. Since the local static pressure was slightly different from that at the reference tap used for the surveys, a small correction ($\Delta C_p \approx$ 0.22E - 02, based on the wall static pressure measurements) was applied to the data obtained with the center (total) tube of the probe. As will be noted later, this correction also allowed for a small interference effect that the transverse traverse device had on the upstream reference tap. The required pressure differential for the calculation of the local velocity U (using Bernoulli's equation) is given by:

$$\Delta P = P_T - P_{ref} - \Delta C_p \, q_{ref} \tag{2}$$

The local flow angle α measured by the 3-tube probe was calculated as follows:

$$\alpha = C_a \frac{\Delta P_{sides}}{q} \quad \text{degrees} \tag{3}$$

C_a = calibration constant for the angular response of the probe (C_a = 18.69 for the data reduced in this report)

Data obtained with the 0.0591 in. O.D. Preston tube were reduced to obtain a local skin friction coefficient C_f. The pressure differential measured by the Preston tube was corrected for ΔC_p as given by equation (2) and then used in a calibration of the tube (see reference 49) to determine τ_w.

Additional calculations were made to determine the velocity at the effective center of the Preston tube. Because the tube was resting on the wall, three corrections were applied to the data to account for shear displacement, Reynolds number effects and wall proximity effects.

The procedures used to reduce the data obtained with the 3-tube Preston probe are similar to those described for the 3-tube probe and the single tube (0.0591 in. O.D.) Preston probe. The local skin friction τ_w was calculated using a calibration obtained for a single tube Preston probe with D = 0.0283 in.. A value of 23.05 was used as the calibration constant C_a for the side tubes in equation (3). Corrections for shear displacement, Reynolds number effects and wall proximity effects (based on the corrections for a circular pitot tube) were also made.

The data obtained with the hot-wire probe was reduced to obtain U/U_e vs. z and $\sqrt{\overline{u^2}}/U_e$ vs z, where $\sqrt{\overline{u^2}}/U_e$ is the longitudinal turbulence intensity. Data from the X-Y plotter traces, along with calibrations of the hot-wire probe and before and after each test were fed into the computer. The program was written to least squares fit the calibration data, interpolate between the calibrations to allow for a small drift during a test, and calculate the values listed above.

None of the data obtained with the pitch probe was reduced for this report. However, a scale has been included on each graph sheet showing the approximate pitch measured during the test. A few early trial tests using the static disk probe indicated that the transverse traverse device was producing relatively large disturbance effects on the measured static pressure distribution (to be discussed in the next chapter). Further work with this probe was discontinued.

3. Boundary Layer Surveys

The procedures followed in reducing the data obtained from the boundary layer surveys were similar to those used for the transverse traverse surveys. The velocity U at each point through the boundary layer was calculated by using Bernoulli's equation. Although the probe was aligned in yaw to the local flow throughout the 3-D boundary layer, it was subject to over 4.0^{o} of pitched flow in the outer region of the boundary layer. Since a calibration of the pitot probe showed less than 0.25% change in the measured dynamic pressure at a yaw angle of 4.0^{o}, no corrections (calibrations) were made for the pitched flow.

Three corrections were applied to the pitot tube data to account for shear displacement, Reynolds number effects and wall proximity effects. The shear displacement correction suggested by MacMillan (ref. 59) was applied to the present data. This correction locates the effective center of the probe at 0.15D further away from the wall than the geometric center, where D is the external diameter of the circular pitot tube. This correction was applied to all data points obtained in the boundary layer.

The Reynolds number correction applied to the present data was also due to MacMillan (ref. 60). His results were expressed as a correction coefficient C_{Re}:

$$C_{Re} = \frac{\Delta P_{uncorrected}}{q} \tag{4}$$

The largest correction coefficient C_{Re} for the present data (when the pitot probe was resting on the wall) was on the order of 1.006. This produces a 0.3% decrease in the uncorrected velocity (i.e. the velocity which would otherwise be calculated using $\Delta P_{uncorrected}$).

Pitot tube data obtained very close to the wall requires a further correction (the wall proximity correction) to account for the effects of the probe-wall flow field interaction. MacMillan (ref. 59) gives this correction as a small increase in the velocity Δu for data obtained in the range $0.5 \leq y/D \leq 2.0$, where y is the distance from the wall to the geometric center of the pitot tube. The maximum value of Δu equals 0.015 U when the probe is resting on the wall ($y = 0.5D$).

The procedures used to reduce the data obtained with the rectangular pitot tube were identical to those for the circular pitot. However, the values used for the corrections were different (because of the differences in geometry). The shear displacement correction of Quarmby and Das (ref. 61) was applied to the present data. This correction locates the effective center of the probe at 0.19H further from the wall than the geometric center plane of the probe tip, where H is the external height of the probe tip. As for the circular pitot tube, this correction was applied for all data points in the boundary layer. The Reynolds number correction was based on a study of the viscous effects on rectangular pitots by MacMillan (ref. 62). The largest correction coefficient C_{Re} was on the order of 1.01 (producing a 0.5% decrease of the "uncorrected" velocity). The wall proximity correction was based on MacMillan's results for circular pitots (ref. 61), but with the external pitot tube diameter D replaced with the external width e of the rectangular probe tip. This was suggested by Quarmby and Das (ref. 61) who also found the wall proximity correction to be function of the Reynolds number. No corrections were available for data obtained in the range $0.12 < y/e \leq 0.5$ (the aspect ratio of the probe used in this study was $e/H = 4.0$, fig. (11c)). However, an estimate of the wall proximity effect at $y/e = 0.12$ (when the probe tip is on the wall) was obtained from the position of effective centers of flat surface tubes given in reference 63 (for the present data this gave $\Delta u \approx 0.19U$ at $y/e = 0.12$). Using this, together with MacMillan's results, a wall proximity correction curve for the range $0.12 \leq y/e < 2.0$ was constructed. Further details have been given in reference 49.

Since no detailed boundary layer surveys were made to obtain the turbulence distribution, no corrections for turbulence have been made in the pitot tube data.

Data from the pitot surveys were plotted on an enlarged graph to locate the boundary layer edge where $U = 0.995\ U_\infty$. The local free stream velocity (dynamic pressure) measured by the pitot tube was fed into these programs as U_∞/U_{ref} (q_∞/q_{ref}). The skin friction coefficient C_f (from Preston tube surveys to be described below) was used in the pitot tube program to calculate the variables for the universal velocity plots, u^+ vs y^+.

The data obtained from the Conrad probe surveys were reduced to the yaw angle α vs y and α vs y^+ (using C_f from the Preston tube surveys). A correction for shear displacement of 0.15D (where D = diameter of one of the Conrad side tubes) was applied to the data. However, this correction may not be appropriate because of the difference in geometry between the Conrad probe tip and the circular pitot tube. No corrections for Reynolds number effects, wall proximity effects, turbulence or pitched flow (in the 3-D boundary layer survey) have been made to the data.

Measurements obtained with the four different sizes of Preston tubes were reduced to obtain an average skin friction coefficient C_f.

The pressure differentials measured by the Preston tubes were corrected for ΔC_p as given by equation (2) and then used in a calibration (one calibration for each tube) to determine the skin friction τ_w. The calibrations, given in reference 49 were fed into the computer program as a third order polynomial.

The data taken with the pitch probe were reduced to obtain the variation of the pitch angle β through the boundary layer. Since the probe was fixed in orientation with respect to pitch, the differential pressure ΔP_{sides} measured across the two sides of the probe was used with a calibration to determine β. The account for the effects of a velocity gradient across the probe tip (since one side of the probe is closer to the wall than the other), a correction must be made to ΔP_{sides} before β can be calculated. The equation used to determine β has been derived in reference 49 as:

$$\beta = C_a \left[\frac{\Delta P_{sides}}{q} - \frac{KD}{q}\frac{dq}{dy}\right] \tag{5}$$

where

K = correction factor which accounts for the fact that each tube (Beveled off at 55°) reads a smaller pressure than the total pressure (K = 0.54, see reference 49).

The calibration constant C_a was found to vary with velocity (see reference 49):

$$C_a = 24.48 - 0.015U \tag{6}$$

This was used to calculate C_a, with the velocity being determined from q.

The dynamic pressure q vs y and the gradient dq/dy vs y were obtained from the pitot tube surveys. The gradient was determined by hand after plotting an enlarged graph of q vs y. Both quantities were fed into the pitch tube program on computer cards.

The effective center of the probe was assumed to be 0.15D further away from the wall than the geometric center. This "correction for shear" was made as a matter of convenience so that direct use of computer generated cards (q vs y) from the pitot tube program could be made. This "correction" may not be appropriate here because of the difference in geometry between the pitch probe and circular pitot tube.

Measurements of the static pressure distribution through the boundary layer were reduced to a static pressure coefficient C_p vs y. The pressure coefficient was given previously as:

$$C_p = \frac{p_s - p_{ref}}{q_{ref}} \qquad (1)$$

In the present case, p_s is the local static pressure at a given point in the boundary layer. For surveys conducted in the 2-DTBL, the static pressure was assumed constant through the boundary layer and equal to the value measured on the wall. Surveys conducted in the 2-D flow were used to calibrate the static pressure probes for use in the 3-DTBL.

Static tube data obtained in the 2-D flow indicated that the probe was reading a slightly different pressure than the wall static pressure. Since these differences generally amounted to a variation in C_p of less than ± 0.001, no corrections were made when using the probe in the 3-DTBL. The static tube was aligned in pitch to within 1.7^o over most of the 3-D flow (where pitch angles of over 4.7^o were measured). Hence no corrections for the small amount of pitch were made to the static tube data.

The static disk probe requires a calibration which relates the pressures measured by the disk to the local static pressure. This is expressed by:

$$P_s - P_d = C_k\, q \qquad (7)$$

From the surveys conducted in the 2-DTBL, values of C_k ranged from 0.08 at the edge of the boundary layer to 0.094 at y = 0.5 in. above the wall. This variation (C_k vs y) was used in the data reduction program for the 3-DTBL (see reference 49 for details). For the present case, the variation of C_p vs y was used in the pitot tube program to calculate U vs y. Using this profile as a starting point, a profile of q vs y was fed into the data reduction program for the static disk probe.

In the 3-DTBL, the static disk probe was subject to over 4.7^o of pitched flow. No corrections were made for this since calibrations indicated that the probe was nearly insentive to pitch over a $\pm$ 4.0^o range (changes to C_k were less than 0.005).

E. Accurary of Measurements

In this section, an assessment will be made of the errors involved in the various types of measurements obtained for this report. For convenience, these have been listed in Tables 4a-4c.

Table 4a lists the variations of test conditions and test variables during a typical boundary layer survey. The variations given in the table were based on the average of variations noted in sixteen pitot tube runs.

The estimated errors involved in the static pressure measurements and the transverse traverse surveys are given in table 4b. For the transverse traverse data, the estimated errors have been given at several locations through the boundary layer. The measurements on the wall of U/Ue and α contain the maximum errors while those at $y \approx \delta$, the minimum errors. The errors in the transverse traverse data are associated largely with the inability to accurately read the somewhat scratchy output traces that were recorded on the X-Y plotters. A further discussion of the determination of these errors is given in the next chapter.

Table 4c contains an estimate of the errors associated with the data obtained from the boundary layer surveys. As for the transverse traverse data, the errors for several locations in the boundary layer have been given. Further details on the calculation of these errors are given in the next chapter.

III. RESULTS AND DISCUSSION

The results of this study have been divided into two parts; two--dimensional studies (i.e. without the wing model in the tunnel) and three-dimensional studies (with the wing model in the tunnel). Some early 2-D studies, concerned with the general operating characteristics of the tunnel and some attempts at improving the nonuniform 2-DTBL, are discussed in reference 49. In addition, reference 49 contains the results of a series of prototype studies which were made in selecting a model to produce the 3-DTBL.

A. Two-Dimensional Studies

The results of the two-dimensional studies will be discussed under the headings of: static pressure measurements, transverse traverse surveys and boundary layer surveys.

1. Static Pressure Measurements

The results of the static pressure surveys completed during the 2-D studies are presented in figures 18-20. The static pressure coefficient C_p is based on measurements relative to a reference pressure P_{ref}, monitored at tap no. 5 of the aluminum insert (table 2). The reference dynamic pressure q_{ref} is calculated from the wind tunnel operating speed as measured by the reference pitot-static probe in the upstream portion of the test section.

The pressure distribution measured along the length of the test section is shown in Figure 18. Results from three separate runs are shown: i) an early test made before the boundary layer trip was installed, at a free stream Reynolds number of Re = 3.00E + 05, ii.) a later test made at Re = 3.15E + 05 (and with the trip) and iii.) a partial survey made with the transverse traverse device installed at the 18 ft. station (see fig. 16). The general trend of the data indicates that a weak favorable pressure gradient was present along the test wall. In comparing the data taken with and without the boundary layer trip, it is noted that the C_p for the untripped boundary layer is larger (except for the first point) than the C_p for the tripped flow over the first 5 ft of the test wall, but is consistently lower between ℓ = 6 ft and ℓ = 11 ft.

Results from the third test indicate the disturbance effect produced by the presence of the transverse traverse device mounted at the 18 ft station. Although the traverse was mounted on the wall opposite the test wall (see fig. 6) and about 2 ft downstream of reference tap no. 5, a slight disturbance effect was still noted at tap no. 5. This can be seen in figure 18 as a slight (constant) upward shift in the data between $\ell \approx 8.5$ and $\ell \approx 11.3$ ft. The static taps at ℓ = 12.6 ft and ℓ = 14.5 ft. are increasingly influenced by the presence of the traverse device. The upward shift in the data is caused when tap no. 5 experiences a small drop in pressure ($\sim$ 0.002 vertical inches of DC-200 silicon oil) due to an accelerated flow past the traverse device. Since the upstream pressures P remain unaffected, a small decrease in P_{ref}. produces a small increase in C_p. The static pressure at tap no. 32 (ℓ = 17.9 ft, about 6 in. upstream of the traverse device) undergoes a relatively large drop off due to the accelerated flow.

The pressure distribution on the aluminum insert (ℓ > 15 ft) has been presented in more detail in figures 19 and 20. The expanded C_p scale (fig. 19) shows the degree to which the data can be repeated in a single run and how repeatable the data is from one run to another (solid symbols) (repeatability within 0.0005 in. DC-200 during a single run and within 0.001 in. DC-200 from one run to another). In figure 19, all of the data has been plotted relative to a transverse line passing through tap no. 5. Data from taps no. 5-17 and no. 22-23 agree quite well and indicate a relatively fast drop in pressure at $x \approx 3$ in.. Following a relatively flat region, the pressure increases until abour $x \approx 23$ in. and then falls off on approach to the exit of the test section. The data from taps no. 60-71 is shifted upward from the other two rows, but it follows the same general trend. The decreasing static pressure gradient would generally be expected. The exact cause of the favorable pressure gradient over the last portion of the test wall was not readily apparent. Presumably, because of the particular geometry involved and the development of the boundary layer, the flow experiences an acceleration over the last portion ($x \geq 36$ in.) of the test section. A general trend towards decreasing pressure appears to already start with the drop off from $\ell \approx 14.5$ ft. to the first pressure taps on the aluminum insert (fig. 18).

In figure 20, the static pressure along several diagonal rows of static taps has been plotted versus z_e, the distance measured along the diagonal (see tables 2 and 3). The data along diagonal rows of taps nos. 1-76 and nos. 5-60 indicates a relatively flat pressure distribution. However, data along the row with taps no. 2-77 indicate an increase of pressure in going to the bottom portion of the test wall. A comparison of data taken along taps no. 16-71 and taps no. 17-72 shows the effect of the diffuser on the static pressure distribution. The data plotted in this manner was used to obtain (by interpolation) the static pressures at the location of boundary layer survyes made on the test wall (see fig. 16).

2. Transverse Traverse Surveys

The surveys made with the transverse traverse device were primarily conducted to give a qualitative indication of the flow field in the 2-D and 3-D boundary layers. For this reason, most of the results obtained in these surveys will be presented as Xerox reproductions of the original X-Y plotter traces. Information on test variables, calibrations, etc. for the tests shown in the reproductions have been included on the figures or in a separate table. Since some of the traces did not reproduce well, they have been enhanced with a broken line in several of the figures. Only a portion of the surveys obtained in the 2-D studies have been reduced.

The results of a number of preliminary studies using the transverse traverse device have been summarized in reference 49. These tests were mostly concerned with attempts to reduce the nonuniformities in the boundary layer by the use of various thicknesses of tripping devices, corner fillets, etc. These "preliminary" studies were concluded when it was realized that further inprovements in the boundary layer flow could only be obtained by still further modifictions of the inlet of the wind tunnel. It was then decided to go ahead with the planned 3-D studies under the assumption (as stated in reference 50) that the slight nonuniformities in the boundary layer would not cause serious problems in the interpretation of the data. Prior to the 3-D studies, a number of transverse traverse surveys were conducted in the 2-D test section (i.e. without the wing model installed) to obtain further data on the nonuniform boundary layer. The results of these tests will be presented below.

Transverse surveys in the 2-D test section were obtained at two streamwise locations; the first at ℓ = 34 in. (where ℓ = distance measured from the start of the test section) and a second at ℓ = 18 ft. (see fig. 16). Both stations were nominally centered on the centerline of the test wall. The bulk of the surveys were made at the 18 ft. station, while tests at the 34 in. station were made near the conclusion of the 2-D studies in order to trace the origins of a peculiar flow pattern observed at ℓ = 18 ft.

Surveys obtained at the 18 ft. station using the 3-tube probe are shown in figures 21a and 21b. This test was conducted at a reference free stream Reynolds number Re = 3.15E + 05 ft^{-1} and with the boundary layer trip in place. The vertical scale in figure 21a is the output from the pressure transducer used to monitor the center (total) tube of the 3-tube probe. With one side of the transducer connected to the reference static tap, the output is essentially $P_T - P_{ref}$. The calibration for the transducer has been listed in table 5, along with the test variables (U_{ref}, Re, etc.) for the run. Because of a problem with reversed polarity when hooking up the X-Y plotters, the calibrations were slightly nonlinear in some of the runs. Hence, the calibration has been given in the tables in two or three parts, each for a given range of the plotter output. The distances above the wall at which surveys were obtained are listed on the right side of the figures. The x axis of the graph is the transverse location (in true scale) of the 15 in. survey. Because of the large number of graphs to be presented, only the centerline of the test wall will be shown in each figure along with an indication of the scale. In addition, some transverse locations (z locations) that are commonly referred to in the text will be indicated on the various graph sheets. The numbered arrows at the top edge of some of the figures refer to boundary layer surveys to be discussed in the next section. As shown in the sketch on figure 21a, the portion of the graph to the left of centerline shows the survey obtained below the centerline of the test wall, while +z refers to the portion obtained above centerline. The orientation of all other transverse traverse surveys shown in this report is the same. The centerline of the test section indicated on the graphs is generally shifted to one side of the centerline of the graph sheet. This occurs because it was difficult to center the 15 in- span of the traverse device exactly on the centerline of the test wall. Instead, care was taken to adjust the limits of the traverse device to within 0.05 in. of the 15 in. span so that the trace on the plotter was full (true) scale.

The output in figure 21a clearly indicates the existence of nonuniformities in the 2-D turbulent boundary layer on the test wall. For example, the variation in velocity U (the output $P_T - P_{ref}$ is proportional to U^2) at $y = 0.5$ in.is on the order of 9% (where y is the distance above the wall in inches). The survey taken at $y = 3$ in. indicates the variation of the boundary layer thickness δ over the 15 in. span. At $z = -4.5$ in., the boundary layer is relatively thick while at $z = +6.5$ in. the thickness is near the minimum over the survey. Boundary layer surveys (to be discussed in the next section) indicated that δ varied from 3.1 to 3.9 in. over the 15 in. span at select stations. The transverse variations in figure 21a appear to have a "wave-like" structure. The "wave length" of the variations is on the order of 2δ.

Similar data showing the variations of velocity (dynamic pressure) have been obtained in a number of other wind tunnel facilities. Most notable are reports by Fernholz (ref. 64), Bradshaw (ref. 50) and de Bray (ref. 51). Perkins (ref. 43) has suggested that the nonuniform 2-D turbulent boundary layer may contain weak longitudinal vortices which alternatirely "pump" fluid into and out of the inner portion of the boundary layer. In figure 22, a sketch of Perkin's model is given for the transverse variations seen in the present $P_T - P_{ref}$ data. The regions of low $P_T - P_{ref}$ output correspond to those areas where low momentum flow from the inner portion of the boundary layer is transferred outward. Also shown in figure 22 are the expected outputs of probes used to measure the transverse variations in total pressure, yaw and pitch through the lower portion of the imbedded vortices. Surveys through the outer portions of the vortices would have the sign of the yaw angle α reversed.

The differential output of the sides tubes of the 3-tube probe ΔP_{sides} are shown in figure 21b. As for the 3-tube total tube, the calibration for the transducer has been given in table 5. The output shown here is indicative of the apparent yaw angle α of the flow and can be calculated using equation (3) (p. 31). In order to separate the traces taken at different values of y, the zeroes of each trace (i.e. where the plotter pen was located when there was no pressure differential across the transducer) have been shifted on the graph. These have been given as "zeroes" along the right side of the sheet. An output that is above the "zero" indicated a yawed flow that is directed towards the floor of the test section ($\alpha > 0$) while an output below zero is a flow towards the test section roof ($\alpha < 0$). The sign convention on α was chosen so that the flow angle observed behind the 3-D wing model (where the yawed flow was directed towards the floor) was considered as positive. In the data obtained with the 3-tube probe, the actual (absolute) flow angle depends on the original alignment of the probe. Hence, the output on the X-Y plotter must be interpreted as a relative change in α. The variations in ΔP_{sides} through the boundary layer is in part due to the variations in $P_T - P_{ref}$ seen in figure 21a, since the calibration of the side tubes is dependent on the local dynamic pressure. The trace at y = 6 1/8 in. was first thought to indicate swirl in the test section. A honeycomb was placed in the diffuser in an attempt to remove this "swirl" (see fig. 3). The honeycomb had no apparent effect on the trace at 6 1/8 in. Later studies of the possible disturbance effects of the traverse device suggested that the "swirl" was due to the disturbing effect of the traverse itself. As sketch below, the flow which approaches the traverse device must diverge off to either side of the centerline.

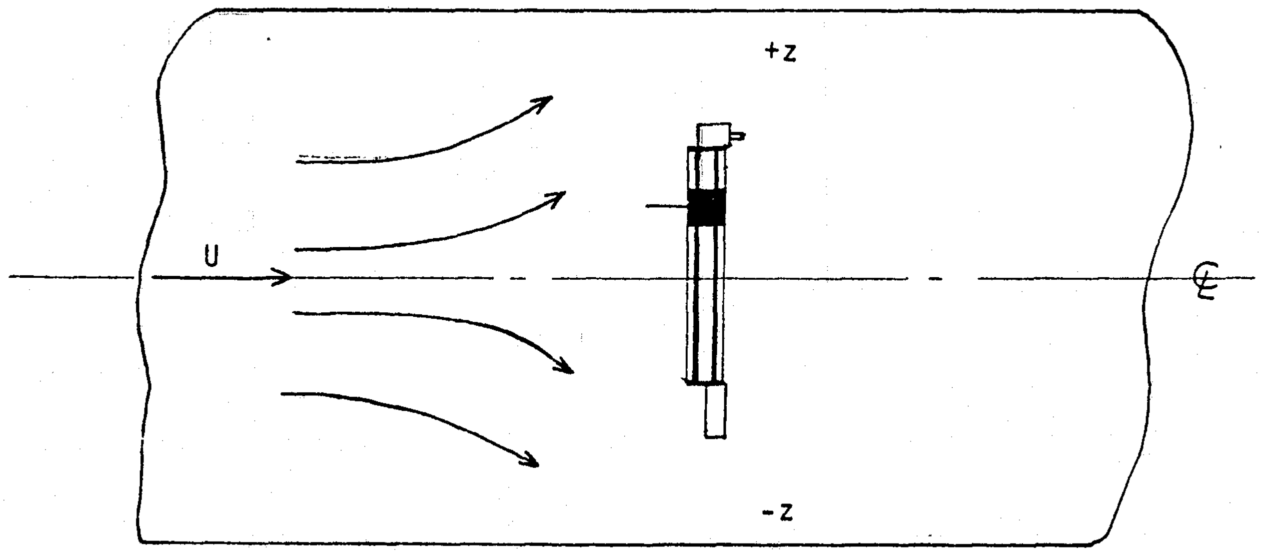

This affect is most pronounced on the wall upon which the traverse is mounted. However, the effects will still be felt at points across the test section and above the test wall. The data in figure 21b at y = 6 1/8 in. shows that the relative flow angle goes from $\alpha > 0$ at $z = -7.5$ in. to $\alpha < 0$ at $z = +7.5$ in.. This change is also suggested by the flow deflections in the sketch above. The total variation in α at y = 6 1/8 in. was less than 1^{o} over the 15 in. span.

A comparison of the yaw data in figure 21b with the flow model in figure 22 is not directly possible because ΔP_{sides} in figure 21b undergoes variations due to the variations in $P_T - P_{ref}$ shown in figure 21a.

The accuracy of the measurements obtained with the 3-tube probe (as well as the other transverse traverse probes to be discussed below) is mainly dependent on the accuracy with which the somewhat scratchy traces can be read. For the data obtained with the 3-tube probe, the accuracies were estimated as follows: for U/U_e, $\pm 4\%$ on the wall (i.e. survey completed with the single

Preston tube), $\pm 1.5\%$ at $y = .5$ in. and $\pm 0.5\%$ at $y = \delta$, for α, 0.2° on the wall (3-tube Preston), 0.1° at $y = 5$ in. and 0.05° at $y = \delta$.

About a year before the tests in figure 21 were conducted, an earlier series of transverse traverse surveys were completed at the 18 ft station. These tests were conducted at Re = 3.00E + 05 ft^{-1} and with the boundary layer trip installed (the Reynolds number was increased to Re = 3.15E + 05 ft^{-1} in the second series of tests (fig. 21) in order to get more response from the pressure probes). The surveys obtained in the first series of tests were reduced and are plotted in figures 23a and 23b. The vertical axis in figure 23a gives U/U_e, where U_e is the velocity at $y = 6$ in.. The traces are shifted slightly because the 15 in. span of the traverse was not quite centered on the test wall. Also shown in figure 23a are the results of a hot-wire anemometer survey. The data from both tests agree to within 2% over most of the 15 in. span. In comparing the traces obtained in the two series of tests, some variations in the nonuniformities were apparent. The wave like pattern in figure 21a appears to be shifted about 1 in. to the left of the original traces shown in figure 23a. These changes might occur if the inlet damping screens and honeycomb had changed slightly during the year (i.e. the polyester screens may have sagged due to long term creep effects or the screens may have become slightly dirty).

Measurements obtained from four boundary layer surveys (to be discussed in the next section) are also shown in figure 23a. The agreement between the boundary layer and transverse surveys is good (within 2%) over most of the boundary layer.

Figure 23b shows the variations in the yaw angle α measured by the side tubes of the 3-tube probe. An additional trace obtained by the 3-tube Preston survey on the wall is also included (effective center of Preston probe is at $y = 0.018$ in.). As noted earlier, $\alpha > 0$ implies a downward flow directed toward the floor of the test section. Portions of the data might appear to be in agreement with the flow model shown in figure 22. For example, at the far left of figure 23b ($z = -7$ in.), the yaw angle is seen to be decreasing to a minimum point (in traversing to the right) in the same way as the idealized trace in figure 22. Returning to figures 21a and 21b, a similar behavior can be seen in the original X-Y plotter output. In traversing to the right, the minimum point in ΔP_{sides} (at $z = -6.5$ in.) occurs before the minimum in $P_T - P_{ref}$ at $z = -4.5$ in. (the same way that the minimum in the idealized α curve occurs before the minimum in $P_T - P_{ref}$ of the same area in figure 22). Another portion of the output showing some agreement with the model occurs at $z = +4.5$ in. in figure 23b. In this region the maximum in α occurs before the maximum in U/U_e when traversing to the right (which is in agreement with the patterns shown in figure 22). Four data points from boundary layer surveys (to be discussed in the next section) are shown on the left half of figure 23b. The free stream flow angles measured by these probes showed no apparent "swirl" in the flow.

The longitudinal turbulence intensity measured by the hot-wire probe is shown in figure 24. The accuracy of these measurements were estimated to be: 6% at $y = 0.5$ in. and 8% at $y = \delta$. Data from reference 65 is shown for comparison at the boundary layer survey stations completed in the first series of tests. The agreement is generally good for points closer to the wall (within 3% at $y = 0.25$ in.) and in the freestream. However, the present surveys are consistently higher than the results of reference 65 for the surveys in between (at $y = 3$ in., the present results are over 50% higher). The large variations in the outer part of the flow represent variations of the intermittancy of the turbulence in the boundary layer. Similar variations in the intermittancy of a turbulent boundary layer (in the transverse direction) were observed by Kiben and Kovasnay (ref. 66). Extensive (transverse) measurements of the turbulence structure in a nonuniform boundary layer are presented in reference 67.

The transverse variations in the skin friction along the 15 in. span are shown in figure 25. The X-Y plotter trace obtained with the single tube (0.0591 in. O.D.) Preston tube is shown at the top of the figure. The data obtained in the two surveys separated by about one year, show an apparent change in the flow structure as previously noted in the 3-tube probe data. These variations were presumably caused by changes in the inlet damping screens and honeycomb. The small change in Reynolds number between the two series of tests would be expected to produce a small decrease in C_f for the second series of tests (Re = 3.15E + 05 ft^{-1}). For example, based on a 1/7th power law velocity profile, the change in C_f at ℓ = 18 ft would be on the order of 1%. This decrease for the C_f in the second series of tests may explain some of the changes on the left side of figure 25, but cannot account for the large difference on the right of the figure. The data taken with the 3-tube Preston probe are on the order of 8% lower than the single tube data over the 15 in. span. The variations are believed to be caused by the use of a somewhat inappropriate calibration (the 3-tube Preston probe was not itself calibrated - the calibration of an 0.0283 in. O.D. circular Preston probe was used). A comparison with data obtained in the boundary layer surveys has also been included and shows agreement to within 7% for all points. The accuracy of the Preston tube measurements was estimated to be on the order of 5% (based on the reading accuracy of the traces).

Transverse surveys using the pitch probe were only obtained during the second series (Re = 3.15E + 05 ft^{-1}) of tests. The differential pressures measured by the side tubes of the pitch probe at ℓ = 18 ft are shown in figure 26. An output which is above the zero for a given trace indicated a flow which is pitched away from the wall (relative to the surrounding flow). For the present tests, the accuracies of the measurements were estimated to be: 0.2° at $y = 1$ in. and 0.05° at $y = \delta$. The interpretation of the results in the boundary layer are complicated by the fact that the pressure differenital for a given pitch angle β is a function of the local dynamic pressure and is affected by the variation in dynamic pressure through the boundary layer. The local pitch angle β could be calculated using equation (9) if the required information (q and dq/dy) were obtained from the data. For the present tests, the accuracies of the measurements were estimated to be: 0.2° at $y = 1$ in. and 0.05° at $y = \delta$. The following discussion will be limited to the results obtained at the outer portions of the boundary layer and above, where $q \approx$ constant and $dq/dy \approx 0$. Of particular interest are the relatively large variations in pitch noted at $z \approx -4.0$ in. and $z \approx +5.5$ in.. According to the scale (which applies only for freestream data), these variations are as large as 0.4° and indicate a local flow that is pitched away from the wall relative to the flow to either side. Moreover, the variations at $z = -4.0$ in. indicate that the flow goes through a type of reversal in pitch with a small dip downward at $z = -4.75$ in. followed by a large upward shift at $z = -4.0$ in.. The traces at $z = -4.0$ in. appear to skew slightly to the right in going from $y = 4$. to $y = 9$, whereas the traces at $z = +5.5$ in. show a definite shift to the right in going away from the wall. In addition, the maximum variations in the pitch decrease in going towards the centerplane of the test section (at $y = 8.95$ in.). The surveys at $y = 8$ in. and 9 in. show that these variations change sign in crossing over the centerplane of the tunnel. Returning to figure 21b, there are also indications in the output from the side tubes of the 3-tube probe that small variations in yaw occur at $z = -4.0$ in. and $z = +5.0$ in.. In particular, the trace taken at $y = 4$ in. (in figure 21b) shows small variations ($<0.2^{\circ}$) at $z = -4.0$ in. and $z = +5.0$ in., suggesting a small local upwardly yawed flow.

When the nonuniformities in the pitch probe output were observed, a careful check of the inlet damping screens and honeycomb were made. The expected location of the origins of these variations were estimated by scaling the distance on the X-Y plotter traces relative to the centerline of the test section (i.e. with the test section height = 46 in. and the inlet height = 88.5 in., the nonuniformities would then appear to possibly come from the screens at z = -7.7 in. and z = +10.6 in. above the centerline of the inlet wall). A marking pen was used to mark these locations on the inlet wall. When the screens were inspected from inside the inlet using a flashlite, no apparent cause for the nonuniformities could be seen. To inspect the honeycomb, several lights were placed outside in front of the inlet and the honeycomb was viewed from the inside of the (now dark) inlet contraction section. The photograph in figure 27a shows the light diffraction patterns (Moiré patterns) that were produced by the honeycomb and screens. Running across these patterns were two narrow interference bands which lined up closely with the locations of the pen marks (the pen mark for the variation in pitch at z = -4.0 in. was within 1. in. of the bottom band while the mark for the variation at z = +5.5 in. was about 2 in. higher than the topband). A closer inspection with a flashlite showed that the second to the last screen had a slightly closer weave in the region of the light diffraction band. The photograph in figure 27b shows that this nonuniform weave was limited to only about 6 openings of the screen (approximately 0.4 in. in width). Apparently, the flow field (wake) developed by this nonuniform weave traveled down the test section and affected the pitch probe output at ℓ = 18 ft (nearly 24 ft. from the last screen).

After the wing model was installed in the test section, a further study of the developing 2-D boundary layer at an upstream station was made. These surveys were made at ℓ = 34 in. and were primarily conducted to obtain more information on the nonuniformities coming off the screens in the location of the nonuniform weave. The surveys taken with the 3-tube probe are shown in figures 28a and 28b. The surveys in figure 28a indicate the boundary layer was about 1 in. thick. The traces obtained with the side tubes above the edge of the boundary layer show an interesting local variation in the yaw angle at z = +4.50 in. and y = 2 in. amounting to nearly 0.4° of upwardly yawed flow (i.e. to the top of the test section). Similar changes (though smaller and shifted in z) can be seen at y = 1 in. and y = 3 in. The variation also appears to skew off to the upper right corner of the graph sheet.

A comparison of the Preston tube (0.0591 in. O.D.) surveys at ℓ = 34 in. and ℓ= 18 ft is shown in figure 29. The variations in C_f at ℓ = 34 in. were on the order of $\pm 5\%$ compared to the variations of $\pm 9\%$ at ℓ = 18 ft. Moreover, the patterns of nonuniformites are different for the two stations. Although the wing model was in the tunnel for the surveys conducted at ℓ = 34 in., this was not thought to significantly affect the Preston tube measurements.

Figure 30 shows the pitch probe surveys conducted at ℓ = 34 in.. In comparing with the results from figure 26 for the survey at ℓ = 18 ft, it is seen that the relatively large changes in pitch above the edge of the boundary layer occur in the same z locations for both tests. The plotter gain on the survey in figure 26 was set at twice the gain of figure 30, so the scales for the approximate pitch angle are different in the two cases. The regions of non-uniform pitch appear to occur at and above the edges of the boundary layer for both stations. Although the variations in pitch are accompanied by variations in yaw at y = 2 in. and z = +4.50 in. (comparing figs. 28b and 30), no apparent variations in yaw occur at y = 2 in. and z = -3.5 in. in figure 28b.

The pitch probe was next mounted on an extended bent probe holder that allowed surveys to be made 10 in. ahead of the surveys shown in figure 30 and also allowed surveys to be made across the centerline and above the wall on which the traverse was mounted. The probe was extended forward to reduce disturbance effects from the traverse device. Pitch probe surveys obtained with this arrangement are shown in figure 31. The probe was traversed along two y locations to each side of the centerline. These results show that the maximum variations in pitch decrease to zero on the centerplane of the test section and then show a reversed sign above the opposite wall. The pitch probe survey at y = 2 in. above the transverse traverse wall shows a relatively large pitch away from the wall at z = -3.5 in., flanked on both sides with small pitch towards the wall. The same extended probe holder was used to make several surveys above the traverse wall using the 3-tube probe. The traces shown in figure 32 now show variations in yaw at z = -3.5 in. (y = 1.17 in., the closest the probe could get to the wall) and a variation in yaw at y = 2 in. and z = +5.0 in. that was smaller but similar (i.e. indicating upward flow) to the variation seen at y = 2 in. and z = +5.0 in. above the test wall. These tests indicated that the flow structure coming from the bands of nonuniform weave was symmetric to both sides of the centerplane of the test section.

The results of the transverse surveys at ℓ = 34 in. and ℓ = 18 ft suggest that a type of vortex like flow may be produced by the bands of nonuniform weave. The wake flow that these bands produce develops into a vortex structure that extends down the length of the test section and occurs to both sides of the centerplane of the tunnel. The flow structure that one of the bands may produce is sketched in figure 33. The cross sectional rear view shows a vortex pair occuring to each side of the vertical centerplane of the tunnel. Both pairs of vortices are producing a flow component that is directed away from the wall. Consideration was also given to only one vortex existing to each side of the centerplane. In figure 34, the expected outputs from the pitch probe and the 3-tube probe are given for the two possible vortex models: the first in which only one vortex is present on each side of the centerplane and a second (already shown in fig. 33) where there is a vortex pair on each side. The output from a total tube would be unaffected to the resolution of the present measurements because of the weak vortices involved. Surveys conducted through various regions of the vortex flows (numbered as 1, 2, 3) would produce the output traces shown as 1, 2 and 3. The data from the pitch probe, in particular, the survey made at 2 in. above the traverse wall (see fig. 30), appears to support the vortex pair model. On the other hand, the surveys obtained using the 3-tube probe indicated little or no evidence of any comparable yawed flow (associated with the possible vortex flow). The output that was noted in figure 21b (at y = 2 in., z = +5.0 in. and z = -4.0 in.) and in figure 28b (y = 2 in. and z = +4.50 in.) could appear to support either vortex model. The 3-tube yaw survey shown at z = +4.5 in. and y = 1, 2 and 3 in. in figure 28b suggested that one may simply be missing the large components of yawed flow at z = -3.5 in. (where the large peaks in pitch were noted) by making surveys in 1 in. intervals in y. Hence an additional test using the 3-tube probe was made to survey the flow field over the range of -7.5 in.< z < -1.5 in. in increments of y = 0.25 in. The results of this test are shown in figure 35 where surveys from y = 0.5 in. to y = 4 in. were completed. No evidence could be found for any large component of yawed flow in the same location (z = -4 in.) as the relatively large variations of pitch. However, some small variations in yaw were noted at z = -3.75 in. and y = 2 3/8 in. to y = 2 3/4 in. Several surveys were extended to z = +7.5 in. to show the variations of yaw above and below the maximum variation at z = +4.5 in., y = 2 in.. Finally, the 3-tube probe was rolled by 90^{o} to serve as a pitch probe. The survey shown at the top of figure 35 shows that both the pitch probe and 3-tube probe were nearly equal in sensitivity and both indicated a relatively large change in pitch at z = -3.75 in..

To stimulate a wake flow coming from the screens, a piece of plastic tape 0.05 in. wide was placed across the entire screen. The tape was located nominally on the horizontal centerplane of the tunnel and was located approximately midway between the two bands of the nonuniform weave. The results of several different surveys are shown in figure 36. The output of the Preston probe at $\ell = 34$ in. were virtually unaffected by the presence of the tape on the screen. A similar result was obtained at $\ell = 18$ ft. The 3-tube (total) output at $y = 2$ in. was also unaffected to the accuracy of the X-Y plotter. However, the output of the side tubes of the probe (i.e. yaw) show a sharp change slightly to one side of the centerline. In addition, the output signal was quite noisy through this region as is apparent in figure 36. The pitch probe at both $\ell = 34$ in. and $\ell = 18$ ft showed a large change in pitch (indicating pitch away from the wall) due to the tape, although the pitch at $\ell = 34$ in. is again shifted slightly to one side of the centerline. The output from both the yaw and pitch probes at $\ell = 34$ in. appears to support the vortex pair model shown in fig. 34b. Unfortunately, no additional surveys with the tape on the screens were conducted to further help clarify the flow field structure and to confirm the model in figure 34b.

The exact affect that the two vortex flows have on the boundary layer is not clear from the present data. Certainly the interaction between these vortices and the weak longitudinal vortices shown in figure 22 is quite complex.

3. Boundary Layer Surveys

As noted in the previous section, the transverse traverse surveys were conducted primarily to obtain a qualitative understanding of the boundary layer flow on the test wall. Based on these studies, a number of boundary layer surveys were completed at select stations along the transverse traverse survey line. Two series of boundary layer surveys (accompanying the two series of transverse traverse surveys) separated by about a years time were made: The first at Re = 3.00E + 05 ft^{-1} and the second at Re = 3.15E + 05 ft^{-1}. The Reynolds number was increased for the second series of tests (as previously noted) in order to get a larger output (pressure differential) from the various pressure probes that were used.

For the first series of tests, boundary layer surveys were conducted at four stations along the transverse traverse line. These are shown in figure 16 as stations 1-4. Surveys at the remaining stations 5-7 were completed during the second series of tests. The location of these stations have been indicated by small arrows on the upper edge of several of the figures showing the transverse traverse data (figs. 21-29). These particular stations were selected in hopes of measuring the pitch and yaw of the weak longitudinal vortices that may exist in the nonuniform boundary layer (see figure 22).

The 3-tube probe was used during the first series of tests to obtain profiles of both the velocity and yaw variations through the boundary layer. Because of the poor time response of this probe, it was replaced during the second series of tests by separate pitot tubes (circular and rectangular) and a Conrad probe. Preston tube and pitch probe measurements were obtained during both series of tests. The static tube and static pressure disk were used only during the second series of tests. A listing of the data obtained in both series of boundary layer surveys is given in table 6. The average values of the test variables for each survey is also included in the same tables.

The velocity profiles obtained in these tests are shown in figures 37-39. The results from each series of tests were plotted separately since the Reynolds number was slightly changed and there appeared to have been changes in the nonuniform boundary layer over the one year interval. Figures 37a and 37b show the velocity ratio U/U_∞ vs y, where y has been plotted on a logarithmic scale to expand (in y) the inner portion of the boundary layer. This was done to show the variations due to the nonuniformities that occur near to the wall. In figure 37a, the variations are largest between stations 1 and 3 (5% at y = 0.05 in., 6% at y = 0.5 in.). As shown in figure 23a station 3 corresponds to a "dip" in the output of $P_T - P_{ref}$ recorded from the 3-tube probe of the transverse traverse device. As previously noted, the transverse traverse surveys agree to within 2% of the boundary layer surveys (fig. 23a). The surveys from the second series of tests (fig. 37b) show large variations to occur between a maximum and minimum point on the transverse output shown in figure 21a. The variations between stations 5 and 7 (where 7 is at a minimum point) are: 9% at y = 0.05 in. and 7% at y = 0.5 in. The survey taken at station 6 shows an even lower value of U/U_∞ at a given y location than station 7. On the otherhand, the transverse traverse survey in figure 21a shows the velocity to be slightly higher at station 6 than at station 7. The reason for this discrepancy was not apparent from the present data. When the two sets of profiles are compared, the data from the first series of tests is seen to fall entirely within the spread of data shown in figure 37b.

Data obtained with the rectangular pitot tube has also been plotted in figure 37b as the solid symbols. The agreement with the circular pitot data is very close (within 0.5%) over most of the profile, with a number of the points coinciding. Slight deviations were apparent in the range of 0.0184 in. $\leq y \leq 0.030$. These differences were attributed to near wall effects on the output from the circular pitot tube. This would suggest that the corrections applied to the circular pitot tube data were not entirely adequate.

The velocity data has been replotted as U/U_∞ vs y/δ in figures 38a and 38b. The boundary layer thickness δ (defined here as the point where $U = 0.995\ U_\infty$) was determined by plotting U vs y on an enlarged graph. Based on the scatter in the data, δ could be determined to within 0.025 in.. The values of δ at each station are listed in table 6. The variations between stations for the data in figures 38a and 38b are still quite apparent even for the normalized data. The $1/7^{th}$ power law velocity profile has been shown in each figure and is not in good agreement for the surveys obtained on or below the centerline of the test wall (no. 1, 2, 3, 4, 6 and 7). The power law does appear in good agreement with the survey at station 5. Assuming that the turbulent boundary layer starts at the boundary layer trip ($\ell = 0$), the boundary layer thickness at $\ell = 18$ ft (for Re = 3.15E + 05 ft^{-1}) was $\delta = 3.56$ in.. The boundary layer thicknesses measured at stations 5, 6, 7 (with Re = 3.15E + 05 ft^{-1}) were 3.14 in., 3.85 in. and 3.72 in. respectively. For clarity, none of the rectangular pitot tube data has been shown in these plots.

Figures 39a and 39b show the velocity plotted in the wall coordinates u^+ and y^+. The data are now seen to collapse very closely along a single curve over most of the profile. The data over the range $30 \leq y^+ \leq 500$ is seen to fall along a straight line given by:

$$u^+ = 5.58 \log y^+ + 5.5 \tag{12}$$

In the literature, other values for the two constants (5.58, 5.5) have been given. These include: (5.6, 4.9) according to Clauser (ref. 68), (5.57, 5.10) from Coles (ref. 69) and (5.5, 5.45) from Patel (ref. 70). Below $y^+ = 30$, the data from the 3-tube probe deviates further from the straight line than the circular pitot tube. This may be due to the use of the circular pitot tube corrections for the 3-tube probe. As noted earlier, the use of the circular pitot corrections for the 3-tube probe may not be entirely appropriate.

The rectangular pitot tube data in figure 39b is seen to follow the surve $u^+ = y^+$ over a limited range and then deviates below $y^+ = 7$. Figure 40 shows the data replotted as U vs y. The straight lines are the slopes of the velocity profile determined from the measured skin friction on the wall (in the linear sublayer $\tau_w = \mu dU/dy$). In the linear sublayer (below approximately y = 0.005 in. in the present case) the data for each survey should fall along its straight line. Above y = 0.005 in., the data should approach the line from above (i.e. the velocity gradient is steadily increasing up to the value in the sublayer). The results in figure 40 show this to be the case for points beyond about y = 0.010 in.. However, the data below this level is seen to indicate velocities that are too high. This shows that the corrections for shear and wall proximity were not appropriate in the region close to the surface. The present data indicates that the effective center of the probe y_c when resting on the surface is at $y_c/H = 0.67$, where H is the external height of the probe.

Based on the reading accuracies of the micromanometer probe systems, an estimate of the accuracy of the circular pitot tube data was calculated at three points in the boundary layer. These were: $\pm 0.25\%$ at $y = \delta$, $\pm 0.6\%$ at y = 0.5 in. and $\pm 3\%$ for the probe on the wall with effective center at y_c = 0.0184 in.. It should be noted, however, that the data obtained near the wall is subject to several corrections whose accuracy determines the final accuracy of the plotted results. This is particularly true for the rectangular pitot tube data.

The data obtained with the Preston tubes were used in the pitot tube data reduction to obtain u^+ and y^+. The values of the skin friction coefficient C_f at each measuring station have been listed in table 6. The measurements have also been compared to the transverse traverse measurements (fig. 25) and were seen to agree to within 6%. An estimate of the accuracy of the Preston tube measurements was based on the scatter seen in the data obtained with four different sized tubes. For the present data, all measurements at a given station agreed to within 3%.

Figures 41a and 41b show the measured profiles of the yaw angle α vs y through the boundary layer. The data must be compared on a relative basis since the absolute yaw angle relative to the horizon is not known. In the present case, $\alpha = 0^{\circ}$ is the angular position at which the probe was initially "leveled" (as described in a previous section). The geometric axis of both the 3-tube probe and the Conrad probe were within 10 minutes (0.17°) of alignment to this "leveled" position. For the purposes of discussion, a positive α denotes a flow directed (relative) upwards towards the roof of the test section. The data taken at station 4 in figure 41a appears to agree qualitatively with the trend seen in the transverse traverse data shown in figure 23b (i.e. the yaw angle becomes less negative with increasing y). The survey taken at station 1 appaears to pass close to a region of downswelling since in figure 23a it is located near the center of the top of the "wave". As noted in the previous section, the pattern of the nonuniformities appears to have shifted about 1 in. to the left on the graph sheet during the one year interval between the tests. Hence, one must shift the same distance in comparing the survey at station 1 with the model. The survey indicates a relative upward yawing of the flow with increasing y whereas the model predicts the opposite trend. A comparison of the data at station 5 in figure 41b with the model in figure 22 appears to show the correct trend. The variation in yaw at station 6 is very small over most of the bouundary layer and would seem to suggest that the survey was obtained in a region between two vortices - i.e. along the adjacent upswelling shown in the model in figure 22. The survey at station 7, which was originally selected to be in a region of upswelling (based on the proposed model) would then be shifted to the right in figure 22. The trend of the data would then agree with the model.

The accuracy of the yaw probe measurements were estimated on the basis of the sensitivity of the nulling manometer system during an actual survey. These were: 0.025° at $y = \delta$, 0.06° at $y = 0.5$ in. and 0.1° at points very near to the surface. The alignment from one survey station to another was considered to be within 2 minutes (0.03°). For the second series of tests, the alignment of the Conrad probe was checked between runs at a location in the upstream portion of the test section. The mounting device used for the hot-wire calibrations was located on the test wall 3 ft. from the inlet. The Conrad probe was installed, leveled and then aerodynamically aligned with the local flow during a short test. For every test completed, the aerodynamic alignment of the probe agreed to within 1 minute (0.017°) of the first test that preceeded the first Conrad probe survey.

Surveys obtained with the pitch probe are shown in figures 42a and 42b. As in the case of the 3-tube and Conrad probe measurements, the pitch angle β must be compared on a relative basis from one station to another. In the present figures, the results from the data reduction have been plotted directly and $\beta = 0^{\circ}$ has no special (absolute) meaning. The geometric axis of the probe was estimated to be pitched downward toward the wall by less than 0.5°. This angle was checked before each test (using the probe sighting device) and found to vary less than 0.1° from one station to another. The scatter in the data is very large below $y = 0.25$ in. with a number of the points lying well off the graphs. This was caused by inaccuracies in determining the gradient of dynamic pressure near the surface. The gradient of q is used in equation (9) to correct for the effects of the dynamic pressure gradient over the tip of the probe.

A comparison of the pitch probe surveys and the model in figure 22 is more difficult than for the yaw probe surveys because at any given station the pitch will always generally be in the same direction (according to the model). The survey taken at station 1 (which is near to a downswell according to the proposed model) shows a pitching toward the wall with decreasing y. The survey at station 3 was located near an upswelling and appears to indicate a pitching toward the wall with decreasing y. The survey at station 3 was located near an upswelling and appears to indicate a pitching away from the wall with decreasing y. However, the survey at station 4, also located near to an upswell shows a relative pitching towards the wall with decreasing y. Obviously, any interpretation of these surveys in regards to the model in figure 22 depends on the relative location of $\beta = 0^{\circ}$ in figures 42a and 42b.

The surveys in figure 42b are of interest in connection with the vortex--like flow patterns that were caused by the bands of nonuniform weave in the inlet screens. In particular, the survey at station 6 was selected to pass through the location of a local peak in the pitch probe data obtained with the transverse traverse device (see fig. 26). This survey indicates an area at y = 4.75 in. where the flow is shown to locally pitch away from the wall relative to the rest of the survey. In regards to the vortex pair model, this location may be taken as the center of the vortex pair. The survey at station 7 also indicates a similar pattern with the maximum pitch occurring at y = 3.5 in.. However, according to the vortex model, station 7 should have been in a region of flow pitched toward the wall (see fig. 26).

The accuracy of the pitch probe surveys depends on the accuracy of the calibration for the probe and also on the accuracy of the corrections for the gradient in dynamic pressure. As shown in figure 42b, the correction for the dynamic pressure gradient is quite large for y < 1 in. Based on the accuracies of the calibration and the determination of dq/dy, the estimated accuracies of the data are: 0.1° at y = 1 in., 0.05° at $y = \delta$.

The attempts to compare the yaw probe and pitch probe surveys with the proposed model in figure 22 have been somewhat speculative. The interpretations depend in a number of cases by what is meant by yawing downward or upward and what is meant by pitching away from or toward the wall. Moreover, the flow field structure may be more complex than the simple side by side vortex model shown in figure 22. For example, in a study of the flow on a concave wall (where Gortler type vortices are produced) So and Mellor (ref. 71) speculated that a double system of longitudinal vortices may exist. Further comparisons of the present data with other models is certainly required. The pitch and yaw probe data do appear to show some type of directional structure in the nonuniform boundary layer. However, more detailed and closely spaced surveys are required to further understand the flow field.

Static tube measurements in the 2-D turbulent boundary layer were limited to "spot checks" through the flow. The static tube reading indicated a slightly higher pressure than the local wall static for points taken over the outer half of the boundary layer and above. The differences in C_p were on the order of 0.0007. Closer to the wall the static tube read increasingly lower pressures relative to the measurements in the outer half of the boundary layer. At y = 0.25 in., the static tube was reading a lower pressure than the local wall static, with the difference in C_p's amounting to 0.0013. The decrease in the static tube reading was presumably caused by wall interference problems which would produce an accelerated flow around the static tube. The result of these tests showed that the static tube could be used to measure the static pressure through most of the boundary layer with an error in C_p of about +0.001.

Three static disk probe surveys were completed during the second series of tests. Two of the surveys were made at stations 5 and 7 while the third was located above static tap no. 32 on the aluminum insert (see table 2). A partial velocity survey (not discussed above) was also obtained at the station above tap no. 32. Assuming a constant static pressure through the 2-D turbulent boundary layer, the calibration coefficient C_k for the static disk probe was calculated using equation (11) from a previous section. In figure 43, C_k has been plotted vs y. At the edge of the boundary layer and above, C_k has a constant value of about 0.0805. The value for C_k increases nearly linearly to the wall where $C_k = 0.095$. Similar variations were noted by Johnston (ref. 21) for a static disk used in a 3-D turbulent boundary layer. According to a calibration presented in reference 56, the value of C_k does not vary greatly with velocity. Hence, in the present case, the data would suggest that the variations are caused by the effects of wall interference. This does not appear to be entirely correct because the variations noted here are seen to occur first at $y = \delta$ ($y = 3.5$ in.) and are virtually constant for $y > \delta$. Unfortunately no separate calibration for the present probe vs. velocity was completed.

B. Three-Dimensional Studies

As for the 2-D studies, the results of the three-dimensional studies will be discussed under the headings of: static pressure measurements, transverse traverse surveys and boundary layer surveys.

1. Static Pressure Measurements

The static pressure measurements that were obtained on the test wall and 3-D wing-like model will be presented in this section. All of these measurements were referenced to a reference static tap located about 16 in. upstream of the wing model (table 3). Only a limited set of measurements were obtained downstream of the model on the aluminum wall. These were primarily intended for use in reducing the data obtained with the transverse traverse and boundary layer probes. A complete set of static pressure measurements on the aluminum wall were completed by Hebbar and are reported in reference 55.

The pressure distribution measured along the test wall and wing model is shown in figure 44. The measurements along the first 11 ft of the test wall were made using taps no. 1-8 (table 1) that were 6 in. above the centerline of the plywood wall. The pressure distribution shown on the wing was measured by wing taps no. 7-29 (table 3) and on the aluminum wall by taps 22-34 (table 2). The line of taps on the wing model and aluminum wall were 1.125 in. above the centerline of the test wall. The wing model is seen to produce a pressure coefficient of over 1.0 at its point of maximum thickness. The pressure distribution over the first 8 ft of the test wall is virtually unaffected by the presence of the wing model (compare figure 44 with figure 18). Beyond ℓ = 8 ft (where ℓ is the distance from the start of the test section) the pressure gradient is slightly adverse up to the start of the wing. The pressures measured at the first two taps nearest the leading edge of the model (taps no. 7 and 8 in table 3) were noticeably unsteady compared to the measurements at taps no. 9 and 10 further downstream on the model. This was apparent in the micromanometer as a very jittery miniscus for measurements at taps no. 7 and 8. Together with the adverse pressure gradient noted between ℓ = 8 ft and the L. E., this behavior may suggest that an early stage of a separation bubble existed at the very start of the wing.

The pressure distribution over the wing appears quite symmetric except for points approaching the leading and trailing edges. Figure 45 shows the pressure distribution over the wing in more detail where x is measured relative to the first diagonal row of static taps behind the wing (in this case to tap no. 22). The pressure distribution downstream of the wing model (on the aluminum wall) is seen to be weakly favorable. On approach to the diffuser, the pressure distribution again shows a drop off as was seen in the 2-D measurements (figs. 18 and 19). In figure 46, the pressures measured at taps no. 43-47 and taps no. 35-36 are shown for comparison with pressures along taps 22-34. This grouping of taps near the trailing edge was used to obtain (by interpolation) the static pressure coefficient at the location of the 3-D boundary layer survey discussed in a latter section.

Figures 47a shows the static pressure distribution along the two diagonal lines of static taps on the foreward and rearward surfaces of the wing model (see sketch in fig. 47b). The coordinate z_e is measured from the centerline of the test wall along a line that is parallel to the trailing (or leading) edge of the wing. The pressure distributions on the wing are virtually linear for both the foreward and rearward surfaces. Data obtained along pressure taps no. 1-76 on the aluminum wall are also shown in figure 47a. This line of taps is 0.50 in. downstream of the trailing edge of the wing or at x = 0.375 in., where, as before, x is the distance measured from the first diagonal row of pressure taps behind the trailing edge (taps no. 5-60 in table 2). The distribution along this line of taps is also nearly linear. The scatter about the straight line through the data is several times larger than the reading accuracy of the micromanometer (a C_p equivalent to 0.004 in. of DC-200 manometer fluid is shown in figure 47a - the reading accuracy of the manometer for the static pressure measurements was on the order of 0.0004 in. DC-200). Between z_e = -4 in. and z_e = -24 in., the distribution appears to have a slight curvature. Pressure distributions further downstream of the trailing edge of the wing are shown in figure 47b. The data along the line at x = 0.375 in. (from figure 47a) has also been replotted for comparison with the other data. The remaining surveys at x = 0.000 in. 12 in., 16 in. and 26 in. were used to map out the pressure disbribution for the transverse traverse surveys made in the 3-D flow at the original (2-D) ℓ = 18 ft station.

2. Transverse Traverse Surveys

Transverse traverse surveys were conducted at three stations behind the wing model (as shown in fig. 16): i.) the first was at the original ℓ = 18 ft station used in the 2-D studies, ii.) the second was along a line that was parallel to the trailing edge of the model, 0.5 in. downstream of the trailing edge and centered on the side wall centerline, and iii). a third station that was along and parallel to the test wall centerline and which extended 15 in. downstream of the trailing edge. At each station, surveys were completed using the 3-tube probe, the single tube Preston probe, the 3-tube Preston probe and the pitch probe. Xerox reproductions of the data obtained at all three stations are presented in reference 49. For the present report, only the 3-tube survey taken along the T.E. of the wing model will be discussed.

The 3-tube surveys obtained along the trailing edge of the wing model are shown in figure 48. The distanced measured along the 15 in. survey line are designated as z_e, where z_e is measured along a line parallel to the trailing edge of the model. The 3-tube total surveys in figure 48a show an apparent amplification of the nonuniformities and a slight shift to the right when compared with figure 21a. When comparing the 2-D surveys with the surveys in figure 48 it must be remembered that the surveys at the T.E. are along a diagonal line. The surveys made at y = 1/16, 1/8, 1/4 and 1/2 in. indicates that the boundary layer velocity profiles immediately behind the trailing edge lack "fullness" (i.e. low velocities exist for some distance off the wall whereas in the zero pressure gradient boundary layer, the velocities increase very quickly just above the surface). As noted earlier, these "retarded" velocity profiles are the result of the region of adverse pressure gradient on the rearward side of the wing model. The yaw probe surveys at $y = 5$ in. and 6 in. in figure 48b now show the output due to the non-uniformities at $z = -3.5$ in. to have the same shape as the expected output for the vortex pair model in figure 34b (trace 1 for the survey at $y = 5$ in., trace 2 for the survey at $y = 6$ in.).

3. Boundary Layer Surveys

Boundary layer surveys were made at only one station behind the 3-D wing model. This station was located on the centerline of the test wall, 0.5 in. downstream of the trailing edge of the model. The results of these surveys will be presented in this section.

Surveys were first completed using the Conrad probe to obtain the profile of the cross flow angle α vs. y. This data was then used to align the remaining probes to the local flow direction at each point in the boundary layer. Figure 49 shows the variation of α from the wall ($y = 0.0148$ in.) to $y = 6$ in.. An enlargement of the near wall region shows that the maximum cross flow angle does not occur at the wall, but rather at about $y = 0.070$ in. A similar type of behavior was observed by Hebbar (ref. 55) who conducted hot-wire anemometry studies at the adjacent instrumentation ports (see fig. 4). By performing a sublayer analysis on his data, he was able to relate the decrease in flow angle in going from the maximum α point to the wall, to the pressure gradient existing at the T.E. of the wing model. In figure 49, the crossflow angle at $y = 6$ in. is about 0.69° and appears to be decreasing to $\alpha = 0^{\circ}$ at $y = 9$ in. (the center plane of the test section at this station was at $y = 8.92$ in.). The boundary layer on the wall opposite the wing model is also weakly three-dimensional and this flow will have a small influence on the free stream flow angle above the test wall.

The cross flow angle α has been replotted in wall coordinates in figure 50. The maximum angle α is not apparent at $y^+ = 45$. The last few points from $y^+ = 11.6$ to $y^+ = 13.6$ appear to indicate a constant crossflow angle of $\alpha = 22.05^{\circ}$. Measurements obtained by Hebbar (ref. 55) for points as close to the surface as $y^+ = 3.2$, showed that the flow angle remained constant for all points less than $y^+ = 10$. In the literature, the region near the wall where the crossflow angle is constant is generally referred to as a region of near wall collateral flow. This effect has been observed in a number of other studies which include work by Johnston (ref. 72), Lewkowicz (ref. 7), Francis and Pierce (ref. 8) and Hornung and Joubert (ref. 26). On the other hand, a numerical study by Pierce and East (ref. 73) suggested that the flow angle through the linear sublayer continues to change right down to the wall and no region of collateral flow actually exists. Instead, the flow merely appears to be collateral flow actually exists. Instead, the flow merely appears to be collateral because of low probe sensitivity close to the wall - in particular for directionally sensitive pressure probes such as the Conrad probe or 3-tube probe (in the present experiment the sensitivity of the Conrad probe near the wall was on the order of 0.1°). An experimental study by Rogers and Head (ref. 74), using a special near-wall traverse device with a hot-wire probe, has shown that the crossflow angle in a 3-DTBL can change continuous right down to the wall. The existence of collateral or noncollateral flow in the near wall region of a 3-DTBL may well depend on the type of 3-DTBL which is being studied. The experimental measurement of the changes in the flow angles through the sublayer depends finally on the sensitivity of the probe being used.

Since the calculation of the velocity through the boundary layer requires the value of the local static pressure, the results of the static tube and static disk surveys will be presented next. The pressure coefficient C_p vs y for both surveys is shown in figure 51. The static pressure coefficient for the disk probe was calculated using equation (7) (p. 37) together with the local dynamic pressure (which was calculated using the local static pressure as measured by the static tube). For points beyond y = 2 in. the agreement in C_p between the two surveys is generally within 0.00075. Moreover, the pressure distribution above y = 2.0 in. varies linearly out to y = 6.0 in.. Below y = 2.0 in. both surveys indicate widely differing pressures. While the static tube indicates a nearly constant C_p between y = 1.75 in. and y = 1.0 in., the C_p from the disk probe continues to change. The extrapolation of both sets of data to the surface appear to be in good agreement with the wall static pressure coefficient (C_p = +0.001 on the wall at this station). This result may be somewhat fortuitous since both probes are subject to interference problems when used close to the surface. The extrapolation to the wall of the linear variation noted above y = 2.0 in., would give a wall static pressure coefficient of C_p = +0.008. Hence the variations in C_p below y = 2.0 in. do appear to be real. Since a greater confidence was placed in the C_p's measured by the static tube (the disk probe used a correction C_k which could easily vary ± 0.005 in the inner region of the boundary layer), the velocity profile through the boundary layer was calculated by using the C_p profile determined by the static tube. Moreover, as will be seen in the discussion of the pitch probe results, the static disk probe may have been in error for points below y + 2.0 in. because of the effects of pitched flow.

As shown in figure 1, the total velocity U in a 3-D velocity profile can be projected onto orthogonal planes to form a streamwise velocity component U_s and a crossflow component W. For the present survey, the direction of the streamline at y + 5.0 in. was used as the "streamwise direction". As seen in figure 49, the flow angle above the edge of the boundary layer is continuously changing and the correct choice for the streamwise direction is not entirely clear. Hence with U_∞ = velocity at y = 5.0 in., the normalized streamwise and crossflow velocities U_s/U_∞ and W/U_∞ are plotted vs y in figure 52. Again the choice of a free stream velocity is not clear since in Figure 52, the velocity is seen to vary continuously even up to y + 6.0 in.. Because of this varying "free stream" velocity, a definable boundary layer thickness δ (e.g. where U = 0.995 U) cannot be determined. If the velocity at y + 5.0 in. were assumed to be the "free stream velocity", then the boundary layer thickness would be on the order of δ = 4.0 in..

The streamwise velocity profiel U_s/U_∞ in figure 52 shows the effects of the extended adverse pressure gradient that exists over the rearward surface of the wing model. The adverse pressure gradient tends to make the velocity profile less "full", with low speeds ($U_s/U_\infty < 0.5$) existing nearly up to y = 0.7 in.. In comparison, the 2-D velocity profile U/U_∞ in figure 38a shows $U/U_\infty < 0.5$ for $y \leq 0.2$ in..

The total velocity U for the 3-D flow has been plotted in wall coordinates in figure 53 (where $u^+ = U/U_\tau$). For a limited range of $25 < y^+ < 170$, the data can be fit to a straight line given by:

$$u^+ = 5.07 \log y^+ + 5.76 \qquad (13)$$

The constants (5.07, 5.76) differ from the set determined for the 2-D velocity surveys (from equation (12), the constants for the 2-D flow were (5.58, 5.5)). In the literature (e.g. ref. 21 and 28), the velocity profiles obtained in 3-DTBLs do tend to show agreement with the 2-D log laws such as given by equation (12). In the present case, the line from equation (12) was shifted above the data. This difference may be associated in part with an error in the skin friction coefficient C_f. As discussed below, the four sizes of Preston tubes used in the surveys gave values of C_f which differed by 10%. The data obtained with the rectangular pitot probe is seen to agree poorly with the curve $u^+ = y^+$. This suggests that the corrections used for the 2-DTBL are not appropriate for use in the 3-DTBL of the present study. Since the corrections are likely to be a function of C_f, then the factor of two difference in C_f between the 2-D and 3-D tests probably explains why the 2-D corrections cannot be applied to the present 3-D data.

Figure 54 shows the crossflow velocity W/U_∞ plotted against U_s/U_∞. This plot is generally referred to as the "polar plot" and was first extensively used by Johnston (ref. 72) to analyze data obtained in a 3-DTBL. When straight lines are faired through the data, a characteristic triangular outline is formed. For the present data, the vertex of the triangle occurs at about $U_s/U_\infty = 0.345$. The line running off to the lower left has been drawn in at an angle equal to the angle measured by the Conrad probe at the last few points above the wall (from fig. 49, the limiting angle $\alpha_o = 22.05^o$). The data (mainly from the rectangular pitot probe) is seen to fall slightly below this line. The location of the vertex of the triangle is of interest in certain analysis of the data. In the present case, the vertex is located at $y^+ = 88$. Hornung and Joubert (ref. 26), working with a 3-D flow produced by a right circular cylinder mounted on a flat plate, measured the vertex to be as high as $y^+ = 150$. On the otherhand, Johnston (ref. 72), working in a 3-DTBL developed by flow impinging on a back wall, measured y^+ no higher than $y^+ = 16$.

The data obtained with the four sizes of Preston tubes is plotted in figure 55 as skin friction coefficient vs D, where D is the external diameter of the Preston tube. In addition, the data obtained at stations 5, 6 and 7 in the 2-D tests have been included. A scale indicating the variation of the measured C_f at a given station is shown along the right of the graph. A line is drawn through each set of data to designate the average value for all four Preston tubes. For the 2-D tests, the variations in the data obtained with the four sizes of Preston tubes are well within 3%. The 0.0183 in. O.D. Preston tube appears to read high for two of the three tests in the 2-D flow. The data from the 3-D flow show an increase in C_f with decreasing diameter D (the total variations are now about 10%). In data obtained by Prahlad (ref. 28), a similar trend was noted. He concluded from his results that the larger diameter Preston tubes were outside of the region of wall similarity. On the other hand, smaller diameter Preston tubes were seen to measure the same values of C_f, hence indicating that the smaller tubes were within the region of wall similarity. In the data shown in figure 55, the C_f measured by the 0.0183 in. O.D. tube in the 3-D flow is reading higher than the C_f from the 0.0283 in. O.D. tube. However, this trend was also noted in the 2-D surveys at stations 5 and 6. Hence, the C_f's measured by the two smaller tubes may be in the same relative agreement in the 3-D flow as they were in the 2-D flow. For the purposes of reducing the data taken in the 3-D flow, the C_f measured by the 0.0283 in. O.D. Preston tube was used.

The results of the pitch probe survey conducted in the 3-D flow are shown in figure 56. A negative pitch angle β indicates flow that is pitched towards the wall. The pitch angle β is seen to increase as one goes from y = 6 in. down to y = 1.0 in.. The pitch angle then decreases in going from y = 1.0 in. to the wall. The presence of the wall apparently reduces the pitch over the inner 1 in. of the boundary layer. Returning to figure 51, the deviations in C_p below y = 2 in. are seen to occur in the same region where the pitch angle exceeds -4.0^o. Since the static tube was already pitched at -3^o to the wall, the maximum relative pitch angle over the probe was 1.75^o. No corrections for the effects of this relative pitched flow were made to the static tube data (as noted in reference 75 a static tube aligned to within 4^o of the local flow has an error of less than 0.5% of the local dynamic pressure). The disk probe was aligned to be parallel to the wall and hence was subject to a pitched flow of $\beta = -4.75^o$ at y = 1.0 in.. Although a check calibration showed that the static disk output (or equivalently the calibration constant C_k) was nearly unaffected when pitched to 4^o, this may not be the case at 4.75^o (unfortunately no angles larger than 4^o were checked in the present tests). As shown in a calibration of a static disk probe given in reference 56, the calibration constant C_k was unaffected ($C_k = 0.12$) up to flows angles of 5^o. At 7^o the value of the calibration constant had risen to $C_k = 0.23$. In the present case, a similar error may have occurred in the value of C_k used to reduce the static disk data. The static disk probe in this tests should have been rolled by 90^o so that it would have been insensitive to the pitch. Alignment in yaw would have been provided by the boundary layer traverse device. Or alternately, the plane of the disk could have been pitched down by 3^o so that the pitch angles would not have exceeded 1.75^o.

IV. SUMMARY AND CONCLUSIONS

Experimental studies of a two and a three-dimensional low speed turbulent boundary layer were conducted on the side wall of the University of Maryland Boundary Layer Wind Tunnel. The 20 ft. test section, with a rectangular cross section measuring 17.5 in. x 46 in., produced a 3.5 in. thick turbulent boundary layer at a free stream Reynolds number of 3.15 x 10^5/ft. The three-dimensional turbulent boundary layer was produced by a 30° swept wing-like model faired into the side wall of the test section.

Preliminary studies in the two-dimensional boundary layer indicated that the flow was nonuniform on the 46 in. wide test wall. The nonuniform boundary layer is characterized by transverse variations in the wall shear stress and is primarily caused by nonuniformities in the inlet damping screens. An effort was made to improve the flow by changing the existing screens, but this was not successful. Following this, an extensive study of the nonuniform boundary layer was conducted.

To study the nonuniformities, a special tranverse device was developed to allow one to survey the boundary layer in a direction transverse to the mean flow and at set distances off the wall. Transverse surveys were made using several different probes which included a 3-tube probe (combined yaw and pitot probe), Preston tubes, a pitch probe and a hot-wire probe. Over the 15 in. span of the transverse device, the local skin friction coefficient varied (at discrete locations) $\pm$ 9% about a mean. Transverse variations in the flow velocity, yaw, pitch and turbulence intensity were also measured in the boundary layer at set distances above the wall. The transverse surveys were compared to a possible model for the nonuniform turbulent boundary layer proposed by Perkins (ref. 43). In this model, a series of counter-rotating longitudinal vortices are thought to exist in the boundary layer. Although some regions of the surveys indicated general agreement with the model, comparisons in other regions were inconclusive.

Measurements with the pitch probe revealed the presence of a vortex-like flow to exist above the edge of the boundary layer at two locations along the 15 in. traverse line. This structure occurred above both test walls and appeared to be symmetrical about the center plane of the test section. The apparent origin of the vortex-like flow was traced to imperfections in the next to the last of five inlet damping screens where the weave was very slightly closer together. These imperfections existed in two small "bands", each about 0.4 in. wide, that extended across the entire width of the inlet screen. An analysis of the data suggests that the wakes produced by these imperfections "bands" tend to roll up into trailing vortices which occur on both sides of the center plane of the test section. Comparisons were made with two possible models for the vortex flow: The first in which only one vortex occurs to each side of the center plane of the test section and a second where a vortex pair occurs to each side. The pitch probe data appeared to support the second model. Measurements with the 3-tube yaw probe in regions of the vortex-like flow failed to consistently indicate any substantial yaw in the flow which would be expected to accompany the relatively large variations in pitch.

A second traverse device was also developed to make surveys through the boundary layer at select stations along the transverse survey line. The probes used with this traverse device included pitot probes (circular and rectangular), yaw probes (3-tube and Conrad), a pitch probe, Preston tubes and static probes (static tube and static disk). Velocity profiles plotted as U/U_∞ vs y/δ showed relatively large variations in going from one survey station to another because of the nonuniformities. However, when the data was replotted as u^+ vs log y^+, all of data showed very close agreement with a logarithmic universal velocity distribution (in the form of $u^+ = A \log y^+ + B$). The velocity profile obtained with the rectangular pitot probe very close to the wall showed poor agreement with the sublayer velocity law ($u^+ = y^+$). The discrepancies were primarily due to the effects of the near wall corrections applied to the data. These results point out the need for more accurate near wall corrections for the rectangular pitot probe. Surveys made with the yaw probes and pitch probes indicated the presence of a definite type of directionaly structure in the nonuniform turbulent boundary layer (i.e. the yaw and pitch angles of the flow varied through the boundary layer). As for the transverse traverse surveys, some of the boundary layer surveys appeared to agree with the longitudinal vortex model while others suggested a more complex flow structure. A survey using the pitch probe at the station where the vortex-like flow occurred (due to the imperfections in the inlet screen) showed a region above the edge of the boundary layer where the local flow was pitched away from the wall as was indicated by the transverse traverse surveys.

The transverse traverse device was also used to survey the three-dimensional flow field developed downstream of the wing-like model. These measurements suggested that the presence of the wing model tended to amplify the nonuniformities in the boundary layer.

Only one representative set of boundary layer surveys were made in the three-dimensional flow at a station 0.5 in. behind the trailing edge of the wing model. Surveys with a yaw probe indicated a maximum cross flow of 22^o to occur at 0.07 in. above the wall in the nominally 4.0 in. thick turbulent boundary layer. Data from the pitot tube surveys, plotted as u^+ vs log y^+ (where u^+ = total velocity/u_τ) showed a limited range over which a logarithmic universal velocity distribution (in the form of $u^+ = A \log y^+ + B$) could be fitted to the data. The range in y^+ was smaller than for the 2-D boundary layer and the constants (A,B) were slightly different. The measurements obtained with the rectangular pitot probe very close to the wall showed very poor agreement with the sublayer velocity law ($u^+ = y^+$). These results suggest that the near wall corrections used for the 2-D flow (where the skin friction was over twice as large as in the 3-D flow) are not appropriate for the present survey. Measurements with the pitch probe showed the flow to be pitched toward the wall by over 4.7^o in the boundary layer at about 1 in. above the wall. Static pressure measurements indicated a decrease in the static pressure of 5.5% of the free stream dynamic pressure in going from the surface to a point 6 in. off the wall. Moreover, the variation in the static pressure coefficient C_p was linear from 2 in. above the wall to 6 in. above the wall. Below 2 in. the distribution of C_p deviated from the linear variation. Measurements with the Preston tubes showed variations of 10% between the data obtained with the smallest (0.0183 in. O.D.) and largest (0.0591 in. O.D.) probes. Since the variations in the 2-D flow were well within 3% this suggests that the calibrations for the 2-D flow cannot be accurately used (for all four Preston tubes) in the 3-D turbulent boundary layer in this study.

V. RECOMMENDATIONS FOR FUTURE WORK

Experimental work in three-dimensional turbulent boundary layers will continue for many years before sufficient information is obtained to calculate the variety of 3-DTBLs that occur on a number of different kinds of geometry. Recommendations for further experimental work in 3-DTBLs have been well documented in the literature. The greatest need at the present time is for turbulence data for use in the differential calculation schemes (which appear to have the greatest chance of eventually predicting the more general 3-D flows).

In regards to the present study, a number of recommendations for future work can be given:

i.) A further a more detailed study should be made of the peculiar vortex-like flow patterns which were formed by the impefection "bands" on the inlet screen. Additional probes such as a hot-wire X-probe or a four-wire vortex probe may help to obtain further insight into the flow structure. Complete surveys should be completed with a narrow piece of tape on the last inlet damping screen to see if the wake flow from the tape produces the same flow patterns as the imperfection "bands" in the screen.

ii.) Before any additional three-dimensional measurements are made behind the wing model, further attempts should be made to reduce the nonuniformities in the boundary layer. The first step would be to remove the second to the last damping screen (which had the imperfection bands) and see what affect this had on the boundary layer flow. Before any further modifictions were made to the inlet honeycomb and screens, it would be desirable to study the nonuniform turbulent boundary layer in a smaller, more manageable facility. The effects of honeycomb and screen combinations as well as the shape of the contraction inlet should be investigated. In addition, the effects of a wall or floor located very close to the inlet cowling should be considered (in the present tests the bottom of the inlet was located close to the floor.) To improve the flow in the present wind tunnel, the 0.59 open area ratio polyester screens will probably have to be replaced by high quality stainless steel screens with an open area ratio of about 0.67. Obviously, the screens should be very carefully checked for manufacturing imperfections before permanent installation. The plastic drinking straw honeycomb should be discarded and a honeycomb of approximately 3/8 in. diameter cells by 8 in. length should be used.

iii.) A hot-wire probe should be used to make any future velocity measurements through the 3-D flow behind the wing model. The use of the hot-wire probe would eliminate the errors caused by the uncertainty of the static pressure distribution through the boundary layer. Pitch probe and yaw probe measurements could also be made by using an X-probe.

iv.) Further studies should be made to determine the correct calibrations of Preston tubes to be used in 3-D turbulent boundary layers.

v.) Additional data is required to help develop more accurate near wall corrections for the rectangular pitot tube. These tests might be done in conjunction with a hot-wire probe which could be used to accurately measure the velocity very close to the wall.

vi.) Future studies of the 3-DTBL developed behind the wing should include the measurement of the turbulence structure through the boundary layer.

REFERENCES

1. Mager, A., "Generalization of Boundary-Layer Momentum Integral Equations to Three-Dimensional Flows Including Those of Rotating Systems," NACA TR 1067, 1952.

2. Cooke, J.C. and Hall, M.G., "Boundary Layers in Three Dimensions," Progress in Aeronautical Sciences, Pergamon Press, Inc., New York, 1962, Vol. 2, pp. 221-282.

3. Joubert, P.N., et.al., "Critical Review and Current Developments in Three-Dimensional Turbulent Boundary Layers," Fluid Mech. of Internal Flows, Elsevier, 1967.

4. Sherman, F.S., "Introduction to Three-Dimensional Boundary Layers," Rand Corp. RM-4843-PR, 1968.

5. Nash, J.F. and Patel, V.C., Three-Dimensional Turbulent Boundary Layers, SBC Technical Books, Atlanta, 1972.

6. Vermeulen, A.J., "Measurements of Three-Dimensional Turbulent Boundary Layers," Doctoral Dissertation, University of Cambridge, England, 1971.

7. Lewkowicz, A., "Two and Three Dimensional Incompressible Turbulent Boundary Layers," Doctoral Dissertation, University of Liverpool, England, 1965.

8. Francis, G.P. and Pierce, F.J., "An Experimental Study of Skewed Turbulent Boundary Layers in Low Speed Flows," Journal of Basic Engineering, Trans. ASME, Series D, Vol. 89, No. 3, Sept. 1967, pp. 597-608.

9. Klinksiek, W.F. and Pierce, F.J., "Simultaneous Lateral Skewing in a Three-Dimensional Turbulent Boundary Layer Flow," Journal of Basic Engineering, Trans. ASME, Series D, Vol. 92, No. 1, Mar. 1970, pp. 83-92.

10. Smith, M.D., "Incompressible Skewed Trubulent Boundary Layer on an End Wall of a Curved Two-Dimensional Diffuser," Doctoral Dissertation, Iowa State Univ., 1970.

11. Power, J.L., "Wall Shear Stress and Mean Velocity Measurements in a Three-Dimensional Turbulent Boundary Layer," NSRDC Rept. 4056, 1973.

12. Hall, M.G., "Experimental Measurements in a Three-Dimensional Turbulent Boundary Layer in Supersonic Flow," AGARDograph 97, May 1965, pp. 829-853.

13. Kuethe, A.M., McKee, P.B. and Curry, W.H., "Measurements in the Boundary Layer of a Yawed Wing," NACA TN 1946, 1949.

14. Altman, J.M. and Hayter, N.L.F., "A Comparison of the Turbulent Boundary Layer Growth on an Unswept and a Swept Wing," NACA TN 2500, 1951.

15. Ashkenas, H. and Riddell, F.R., "Investigation of the Turbulent Boundary Layer on a Yawed Flat Plate," NACA TN 3383, 1955.

16. Cumpsty, N.A. and Head, M.R., "The Calculation of Three-Dimensional Turbulent Boundary Layers. Part I: Flow Over the Rear of an Infinite Swept Wing," Aeronautical Quarterly, Vol. 18, 1967, pp. 55-84.

17. Cumpsty, N.A. and Head, M.R., "The Calculation of Three-Dimensional Turbulent Boundary Layers. Part II: Attachment-Line Flow on an Infinite Swept Wing," Aeronautical Quarterly, Vol. 18, 1967, pp. 150-164.

18. Compsty, N.A. and Head, M.R., "The Calculation of the Three Dimensional Trubulent Boundary Layer. Part III: Comparison of Attachment-Line Calculations With Experiment," The Aeronautical Quarterly, Vol. 20, 1969, pp. 99-113.

19. Cumpsty, N.A. and Head, M.R., "The Calculation of Three-Dimensional Turbulent Boundary Layers. Part IV: Comparison with Measurements on the Rear of a Swept Wing," The Aeronautical Quart., Vol. 21, 1970, pp. 121-132.

20. Bradshaw, P. and Terrell, M.G., "The Response of a Turbulent Boundary Layer on an Infinite Swept Wing to the Sudden Removal of Pressure Gradient," NPL Aero Report 1305, 1969.

21. Johnston, J.P., "Measurements in a Three-Dimensional Turbulent Boundary Layer Induced by a Swept Forward Facing Step," J. Fluid Mech. (1970), Vol. 42, part 4, pp. 823-844.

22. Etheridge, D.W., "Three-Dimensional Turbulent Boundary Layers on 45° Swept Plate and Drag Calculation for a Series of Bodies of Revolution," Doctoral Dissertation, University of London, England, 1972.

23. Swamy, N.V.C., "Turbulent Boundary Layer on a Yawed Flat Plate," Z. Flugwiss. 19, (1971), Heft 12, pp. 496-502.

24. Swamy, N.V.C., "Turbulent Boundary Layer on a Yawed Wing," Z. Flugwiss, 21, (1973), Heft 5, pp. 163-166.

25. Van Den Berg, B., et. al., "Measurements in an Incompressible Three-Dimensional Turbulent Boundary Layer, Under Infinite Swept-Wing Conditions, and Comparison with Theory," Journal Fl. Mech. (1975), Vol. 70, part 1, pp. 127-148.

26. Hornung, H.G. and Joubert, P.N., "The Mean Velocity Profile in Three-Dimensional Turbulent Boundary Layers," J. Fluid Mech. (1963), Vol. 15, pp. 368-384.

27. Perry, A.E. and Joubert, P.N., "A Three-Dimensional Turbulent Boundary Layer," J. Fluid Mech. (1965), Vol. 22, part 2, pp. 285-304.

28. Prahlad, T.S., "Wall Similarity in Three-Dimensional Turbulent Boundary Layers," AIAA Journal, Vol. 6, No. 9, Sept. 1968, pp. 1772-1774.

29. East, L.F. and Hoxey, R.P., "Low-Speed Three-Dimensional Turbulent Boundary Layer Data," Parts 1 and 2, A.R.C. R&M 3653, 1971.

30. Prahlad, T.S., "Mean Velocity Profiles in Three-Dimensional Incompressible Turbulent Boundary Layers," AIAA Journal, Vol. 11, No. 3, Mar. 1973, pp. 359-365.

31. Ezekwe, C.I., "Turbulent Shear Stress Tensors in a Three-Dimensional Boundary Layer," Doctoral Dissertation, Virginia Polytechnic Institute and State University, 1975.

32. Moore, R.W., Jr. and Richardson, D.L., "Skewed Boundary Layer Flow Near the End Walls of a Compresor Cascade," Trans. ASME, Vol. 79, Nov. 1957, pp. 1789-1800.

33. Furvya, Y., Nakamura, I. and Kawachi, H., "The Experiment on the Skewed Boundary Layer on a Rotating Body," Bulletin of JSME, Vol. 9, No. 36, 1966, pp. 702-710.

34. Kawoguchi, T. and Furvya, Y., "The Rotating Flows in a Vaneless Diffuser Having Two Parallel Discs," Bulletin of JSME, Vol. 9, No. 36, pp. 711-718.

35. Cham, T.S. and Head, M.R., "Turbulent Boundary Layer Flow on a Rotating Disk," J. Fluid Mech. (1969), Vol. 37, part 1, pp. 129-137.

36. Lakshminarayana, B., Jabbari, A. and Yamaoka, H., "Turbulent Boundary Layer on a Rotating Helical Blade," J. Fluid Mech. (1972), Vol. 51, pt. 3, pp. 545-569.

37. Bissonnette, L. R. and Mellor, G.L., "Experiments on the Behavior of an Axisymmetric Turbulent Boundary Layer with a Sudden Circumferential Strain," J. Fluid Mech. (1974), Vol. 63, pt. 2, pp. 369-413. See also: Bissonnette, L. R., Doctoral Dissertation, Princeton University, 1970.

38. Lohmann, R.P., "The Response of a Developed Turbulent Boundary Layer to Local Transverse Surface Motion," Doctoral Dissertation, University of Conn., 1974.

39. Cebeci, T. and Abbott, D.E., "Boundary Layers on a Rotating Disk," AIAA Journal, Vol. 13, No. 6, June 1975, pp. 829-832.

40. Anand, A.K. and Lakshminarayana, B., "Three-Dimensional Turbulent Boundary Layer in a Rotating Helical Channel," J. of Fluids Engr., Trans. ASME, Series I, Vol. 97, No. 2, June 1975, pp. 197-210.

C-2

41. Brundrett, E. and Baines, W.D., "The Production and Diffusion of Vorticity in Duct Flow," J. Fluid Mech. (1964), Vol. 19, part 3, pp. 375-394.

42. Gessner, F.B. and Jones, J.B., "On Some Aspects of Fully-Developed Turbulent Flow in Rectangular Channels," J. Fluid Mech. (1965), Vol. 23, part 4, pp. 689-713.

43. Perkins, H.J., "The Formation of Streamwise Vorticity in Turbulent Flow," J. Fluid Mech. (1970), Vol. 44, part 4, pp. 721-740.

44. Rainbird, W.J., "Turbulent Boundary Layer Growth and Separation on a Yawed Cone," AIAA Journal, Vol. 6, No. 12, Dec. 1968, pp. 2410-2416.

45. Pierce, F.J., "The Turbulent Flow at the Plane of Symmetry of a Collateral Three-Dimensional Boundary Layer," Journal of Basic Engineering, Trans. ASME, Series D, Vol. 86, No. 2, June 1964, pp. 227-233.

46. Johnston, J.P., "Three-Dimensional Turbulent Boundary Layers," presented at Symposium on Experimental Turbulent Boundary Layers, Purdue University, 1970.

47. Horlock, J.H., et.al., "Three-Dimensional Boundary Layers: A Report on Euromech 2," J. Fluid Mech. (1967), Vol. 27, part 2, pp. 369-380.

48. Fernholz, H., "Three-Deimensional Turbulent Boundary Layers: A Report on Euromech 33," J. Fluid Mech. (1973), Vol. 58, part 1, pp. 177-186.

49. Winkelmann, A.E., "Experimental Studies of a Two and Three-Dimensional Low Speed Turbulent Boundary Layer, Doctoral Dissertation, University of Maryland, 1976.

50. Bradshaw, P., "The Effect of Wind-Tunnel Screens on Nominally Two-Dimensional Boundary Layers," J. Fluid Mech. (1965), Vol. 22, part 4, pp. 679-687.

51. de Bray, B.G., "Some Investigations into the Spanwise Non-uniformity of Nominally Two-Dimensional Incompressible Boundary Layers Downstream of Gauze Screens," A.R.C. R&M 3578, 1969.

52. Loehrke, R.I., "Experiments on Management of Free-Stream Turbulence", AGARD Rept. No. 598, 1972.

53. Nagib, H., Personal Communication, Illinois Inst. of Tech., Chicago, Ill.

54. Tsien, H.S., "On the Design of the Contraction Cone for a Wind Tunnel," J. of Aero. Sciences, 1943, pp. 68-70.

55. Hebbar, K.S., "An Experimental Investigation of the Near-Wall Region of a Three-Dimensional Incompressible Turbulent Boundary Layer Relaxing in a Zero Pressure Gradient", Doctoral Dissertation, University of Maryland, 1976.

56. Bryer, D.W., Walshe, D.E. and Garner, H.C., "Pressure Probes Selected for Three-Dimensional Flow Measurements," ARC R&M 3037, 1968.

57. Smith, A.M.O. and Murphy, J.S., 'Micromanometer for Measuring Boundary Layer Profiles,: The Review of Scientific Instruments, Vol. 26, No. 8, 1955, pp. 775-781

58. Tidstrom, K., National Bureau of Standards, Gaithersburg, Md., Personal communication.

59. MacMillan, F.A., "Experiments on Pitot-Tubes in Shear Flow," A.R.C. R&M 3028, 1957.

60. MacMillan, F.A., "Viscous Effects on Pitot Tubes at Low Speeds," Journal of the Royal Aero. Soc., Vol. 58, 1955, pp. 570-572.

61. Quarmby, A. and Das, H.K., "Displacement Effects on Pitot Tubes with Rectangular Mouths," The Aero. Quarterly, May 1969, p. 129-139.

62. MacMillan, F.A., 'Viscous Effects on Flattened Pitot Tubes at Low Speeds," Journal of Royal Aero. Soc., Vol. 58, 1954, pp. 837-839.

63. Bradshaw, P. and Gregory, N., "The Determination of Local Turbulent Skin Friction From Observations in the Viscous Sub-Layer," A.R.C. R&M 3202, 1961.

64. Fernholz, H., "Three-Dimensional Disturbances in a Two-Dimensional Incompressible Turbulent Boundary Layer," A.R.C. R&M 3368, 1962.

65. Klebanoff, P.S., "Characteristics of Turbulence in a Boundary Layer with Zero Pressure Gradient," NACA Rept. 1247, 1955.

66. Kiben, V. and Kovasnay, L.S.G., "The Intermittent Region of a Turbulent Boundary Layer," Interim Tech. Rept. No. 1, U.S. Army Office - Durham Contract No. DA-31-124-ARO-D-313, Dept. of Mech. Engr., The John Hopkins Univ., Jan. 1969.

67. Favre, A. and Gaviglio, J., "Turbulence Et Perturbations Dans La Couche Limte D'Une Plaque Plane," AGARD Rept. 278, April 1960.

68. Clauser, F.H.,"Turbulent Boundary Layers in Adverse Pressure Gradients," J. of Aero. Sciences, Vol. 21, No. 1, 1954, pp. 91-108.

69. Coles, D., "The Law of the Wake in the Turbulent Boundary Layer," J. Fl. Mech. (1956), Vol. 1, part 2, pp. 191-226.

70. Patel, V.C., "Calibration of the Preston Tube and Limitations on its Use in Pressure Gradients," J. Fl. Mech (1965), Vol. 23, part 1, pp. 185-208.

71. So, R.M.C. and Mellor, G.L., "An Experimental Investigation of Turbulent Boundary Layers Along Curved Surfaces," NASA CR-1940, 1972.

72. Johnston, J.P., "On the Three-Dimensional Turbulent Boundary Layer Generated by Secondary flow," J. of Basic Engr., Trans, ASME Series D, Vol. 82, 1960, pp. 233-248.

73. Pierce, F.J. and East, J.L., Jr., "Near-Wall Collateral Flow in Three-Dimensional Turbulent Boundary Layers," AIAA Journal, Vol. 10, No. 3, Mar. 1972, pp. 334-336.

74. Rogers, B.K. and Head, M.R., "Measurements of Three-Dimensional Boundary Layers," The Aero. Journal of the Royal Aero. Soc., Vol. 73, Sept. 1969, pp. 796-798.

75. Thompson, J.S. and Holder, D.W., "Notes on Wind Tunnel Pressure Measurements From Operator's Point of View", AGARD Rept. 164, Mar. 1958.

Table 1 Location of Static Pressure Taps on Test Wall (2-D)

tap no.	ℓ in.	z in.
1	7.00	6.00
2	23.00	6.00
3	39.00	4.50
4	55.00	6.00
5	71.00	
6	87.00	
7	103.00	
8	119.00	
9	135.00	
10	151.75	
11	173.25	
ref.	119.00	-4.00

ℓ is measured from start of test section

z is measured from test wall centerline

static taps over last 5 ft of test wall (i.e. the aluminum insert) are given in table 2.

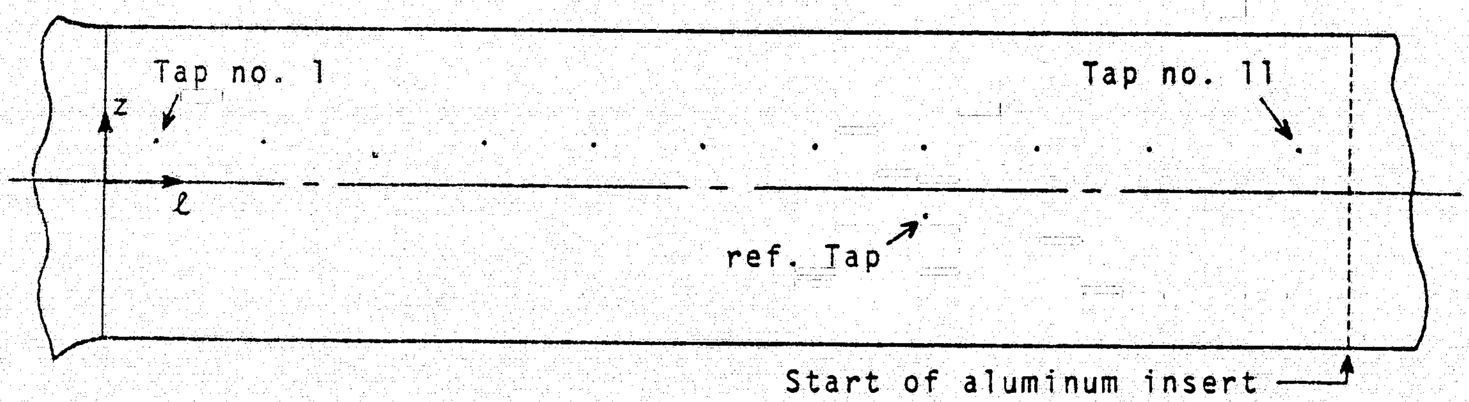

Table 2 Location of Static Pressure Taps on Aluminum Wall

tap no.	x in.	z in.	tap no.	x in.	z in.
1	0.375	18.00	40	15.625	-1.000
2	12.000	18.00	41	23.625	
3	0.375	11.94	42	34.625	
4	12.000	11.94	43	0.000	-3.125
5	0.000	5.875	44	0.375	
6	0.375		45	0.875	
7	0.875		46	1.625	
8	1.625		47	2.500	
9	2.500		48	3.500	
10	3.500		49	5.000	
11	5.000		50	7.000	
12	7.000		51	9.000	
13	9.000		52	12.000	
14	12.000		53	16.000	
15	16.000		54	26.000	
16	26.000		55	36.000	
17	36.000		56	0.625	-4.500
18	0.625	5.000	57	0.375	-5.500
19	0.375	3.500	58	5.000	
20	5.000		59	12.000	
21	12.000		60	0.000	-7.125
22	0.000	1.125	61	0.375	
23	0.375		62	0.875	
24	0.875		63	1.625	
25	1.625		64	2.500	
26	2.500		65	3.500	
27	3.500		66	5.000	
28	5.000		67	7.000	
29	7.000		68	9.000	
30	9.000		69	12.000	
31	12.000		70	16.000	
32	16.000		71	26.000	
33	26.000		72	36.000	
34	36.000		73	0.625	-8.000
35	0.625	-1.000	74	0.375	13.19
36	2.625		75	12.000	13.19
37	5.625		76	0.375	19.25
38	9.625		77	12.000	19.25
39	12.000				

x is measured relative to a line parallel to T.E. and passing through tap no. 22 (see sketch in table 3)

z is measured relative to centerline of test wall

Table 3 Location of Static Taps on Wing Model

tap no.	x in.	z in.	tap no.	x in.	z_e in.
7	-60.78	1.13	1	-53.29	22.30
8	-59.78		3		15.30
9	-58.28		5		8.30
10	-56.29		11		1.30
11	-53.29		30		- 5.70
12	-49.30		32		-12.70
13	-44.86		34		-19.70
14	-40.86				
15	-37.84		2	-12.45	22.30
16	-35.84		4		15.30
17	-34.34		6		8.30
18	-32.84		25		1.30
19	-31.35		31		- 5.70
20	-29.86		33		-12.70
21	-27.84		35		-19.70
22	-24.84				
23	-20.83				
24	-16.43				
25	-12.45				
26	- 9.46				
27	- 7.45				
28	- 5.96				
29	- 4.94				

x is measured on surface of model

z_e is measured from test wall centerline, parallel to T.E.

taps (1-34) are on a line through tap 11, parallel to L.E.
taps (2-35) are on a line through tap 25, parallel to T.E.

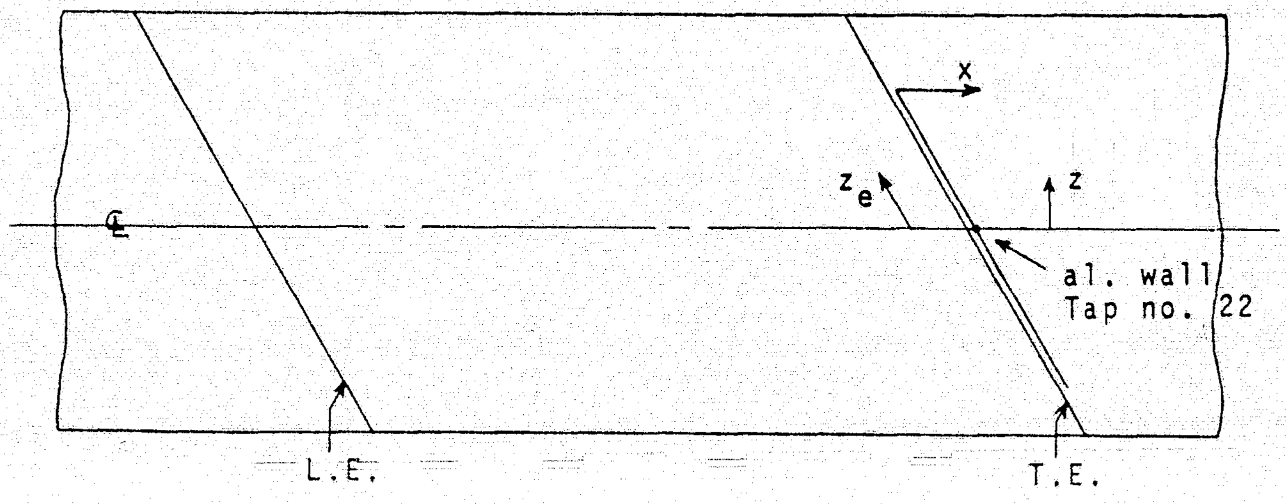

Table 4a Typical Variation of Test Conditions and Test Variables

Quantity	Reading Accuracy	Typical Value	Typical Variation	% Variation
T_d °C	0.2	26.5	± 0.5	$\pm 0.17\%$
W	0.0001	0.0122	± 0.0004	$\pm 3.3\%$
B mm Hg	0.1	760.5	± 0.8	$\pm 0.11\%$
T_m °C	0.1	26.4	± 0.5	$\pm 0.17\%$
h in. DC-200	0.001	0.761	± 0.0014	$\pm 0.18\%$
Re ft^{-1}		3.15E+05	$\pm$0.08E+05	$\pm 2.5\%$
U ft/sec		53.42	± 0.085	$\pm 0.16\%$
q lbf/ft^2		3.238	± 0.004	$\pm 0.12\%$
ρ $slugs/ft^3$		2.269E-03	$\pm$0.005E-03	$\pm 0.22\%$
μ slugs/ft-sec		3.852E-07	$\pm$0.005E-06	$\pm 0.13\%$

Table 4b Estimated Errors for Static Pressure Measurements and Transverse Traverse Surveys

Quantity	Location	Estimated Error
C_p	all	± 0.0005
y	all	± 0.005 in.
$\frac{U}{U_e}$	on wall	$\pm 4\%$
	$y = 0.5$ in.	$\pm 1.5\%$
	$y = \delta$	$\pm 0.5\%$
α	on wall	$0.2°$
	$y = 0.5$ in.	$0.1°$
	$y = \delta$	$0.05°$
β	$y = 1.0$ in.	$0.2°$
	$y = \delta$	$0.05°$
C_f	all	5%
$\frac{\sqrt{\bar{u}^2}}{U_e}$	$y = 0.5$	6%
	$y = \delta$	8%

Table 4c Estimated Errors for Boundary Layer Surveys

Quantity	Location	Estimated Error
y	$y < 0.5$ in.	0.0005 in.
	$y > 0.5$ in.	0.001 in.
δ	all	0.025 in.
U/U_∞	on wall	$\pm 2\%$
	$y = 0.5$ in.	$\pm 0.6\%$
	$y = \delta$	$\pm 0.25\%$
α	on wall	0.1°
	$y = 0.5$ in.	0.05°
	$y = \delta$	0.025°
β	$y = 1.0$ in.	0.1°
	$y = \delta$	0.03°
C_f	all	2.5%
C_p	$y = 0.5$ in.	.002
	$y = \delta$	.001

Table 5 Test Variables For Transverse Traverse Surveys

Fig.	$Re \times 10^5$	U	q	$\rho \times 10^6$	$\mu \times 10^6$	Calibrations range	C1	C2
21a	3.16	52.44	3.162	.2300	.3813	$6 \leq Y \leq 10$	.0813	-.0530
						$0 \leq Y \leq 6$	.0746	-.0130
21b	3.16	52.44	3.162	.2300	.3813	all	.0200	.0000
26	3.15	52.71	3.183	.2291	.3840	all	.0086	.0000
28a	3.16	54.25	3.318	.2255	.3872	all	.0725	.0000
28b	3.16	54.25	3.318	.2255	.3872	all	.0236	.0000
30	3.15	53.76	3.265	.2260	.3854	all	.0236	.0000
48a	3.15	53.65	3.258	.2263	.3857	$7 \leq Y \leq 10$	.0858	-.0770
						$3 \leq Y \leq 7$	.0764	-.0135
						$0 \leq Y \leq 3$	.0721	-.0035
48b	3.15	53.65	3.258	.2263	.3857	y = 4,5,6 in.	.0242	.0000
						all others	.0483	.0000

units:
Re[ft^{-1}] q[lbf/ft^2] μ[slugs/ft.sec]
U[ft/sec] μ[$slugs/ft^3$]

Calibrations are in the form of YY = C1*Y+C2, where YY is inches of DC-200 silicon oil at 25°C and Y refers to inches on the graph measured from the zero of each trace.

Table 6a Boundary Layer Survey Measurements - Station 1

R_e = 3.00E+05 ρ = .2251E-02 δ = 3.070

U_{ref} = 51.55 μ = .3871E-06 C_f = .2579E-02

q = 2.991

y	U	α	β	y	U	α	β
.021	21.47	1.05		.634	38.81	.68	-.40
.024	22.87	1.07		.754	39.81	.70	
.028	24.04	1.05		.904	40.88	.70	-.34
.032	25.16	1.05		1.054	42.01	.67	
.037	26.01	1.05	+2.16	1.254	43.29	.63	-.26
.044	26.91	1.05	- .63	1.504	44.86	.62	
.052	27.58	.97		1.804	46.46	.62	-.12
.060	28.12	.90	- .81	2.104	47.93	.58	
.071	28.91	.90		2.504	49.59	.53	-.01
.084	29.62	.90	- .89	2.754	50.33	.53	
.099	30.18	.87		3.004	50.82	.43	-.09
.116	30.98	.87	- .62	3.129	50.95	.43	
.139	31.70	.82		3.254	51.06	.43	
.164	32.41	.85	- .52	3.504	51.12	.37	-.13
.194	32.99	.87		4.004	51.16	.30	-.13
.229	33.10	.82	- .37	5.004	51.05	.22	-.10
.269	33.94	.82		5.971	51.02	.18	-.10
.324	35.62	.82	- .39				
.384	36.35	.77					
.454	37.13	.82	- .35				
.534	37.88	.75					

Table 6b Boundary Layer Survey Measurements - Station 2

$Re = 3.00E+05$ $\rho = .2255E-02$ $\delta = 3.250$

$U_{ref} = 51.45$ $\mu = .3872E-06$ $C_f^* =$

$q = 2.984$

y	U	α	β*	y	U	α	β*
.021	20.89	.50		.634	38.24	.67	
.024	22.07	.50		.754	39.47	.65	
.028	23.45	.45		.904	40.55	.67	
.032	24.35	.52		1.054	41.40	.63	
.037	25.15	.48		1.254	42.89	.58	
.044	26.15	.48		1.504	44.29	.58	
.052	26.99	.43		1.804	46.06	.50	
.060	27.46	.53		2.104	47.32	.48	
.071	28.41	.43		2.504	49.18	.43	
.084	28.79	.48		3.004	50.39	.40	
.099	29.56	.47		3.129	50.59	.38	
.116	30.19	.50		3.254	50.77	.37	
.139	31.18	.48		3.504	50.95	.37	
.164	31.70	.53		4.004	51.03	.30	
.194	32.71	.48		5.004	51.29	.22	
.229	33.15	.55		5.997	50.99	.18	
.269	34.22	.52					
.324	34.80	.57					
.384	35.88	.55					
.454	36.49	.62					
.534	37.47	.63					

*No surveys were completed at this station with the Preston tubes or the pitch probe.

Table 6c Boundary Layer Profile Measurements - Station 3

Re = 3.00E+05 ρ = .2301E-02 δ = 3.550

U_{ref} = 49.72 μ = .3818E-06 C_f = .2320E-02

q = 2.843

y	U	α	β	y	U	α	β
.021	19.25	.03		.904	37.34	.48	+.07
.024	20.88	.12		1.054	38.31	.50	
.028	21.88	.22		1.254	39.60	.50	+.00
.032	22.77	.10	+2.47	1.504	41.15	.52	
.037	23.38	.03		1.804	42.88	.53	-.01
.044	24.52	.15	- .17	2.104	44.41	.52	
.052	25.17	.13		2.504	46.21	.52	+.03
.060	25.75	.13	- .12	3.004	48.06	.50	-.03
.071	26.32	.13		3.254	48.63	.47	
.084	26.94	.07	- .21	3.504	49.05	.48	-.14
.099	27.42	.13		3.604	49.13	.47	-.09
.116	28.02	.20	- .16	3.704	49.24	.45	
.139	28.74	.17.		4.004	49.35	.48	-.14
.165	29.44	.15	- .22	5.004	49.35	.43	-.11
.194	30.06	.15		5.979	49.35	.33	-.07
.229	30.73	.18	- .01				
.269	31.56	.22					
.324	32.37	.27	+ .06				
.384	33.08	.30					
.454	33.80	.33	+ .14				
.534	34.50	.37					
.634	35.30	.38	+ .16				
.754	36.38	.43					

Table 6d Boundary Layer Survey Measurements - Station 4

$Re = 3.00E+05$ $\rho = .2308E-02$ $\delta = 3.250$

$U_{ref} = 49.40$ $\mu = .3809E-06$ $C_f = .2429E-02$

$q = 2.816$

y	U	α	β	y	U	α	β
.021	19.74	-.23		.634	36.24	.00	+.06
.024	20.80	-.25		.754	37.20	.05	
.028	21.98	-.30		.904	38.32	.07	+.09
.032	23.02	-.30	+2.61	1.054	39.42	.10	
.037	23.86	-.32		1.254	40.76	.15	+.02
.044	24.75	-.32	- .83	1.504	42.36	.20	
.052	25.62	-.32		1.804	44.03	.22	+.05
.060	26.18	-.28	- .78	2.104	45.56	.25	
.071	26.81	-.30		2.504	47.23	.28	+.10
.084	27.49	-.30	- .77	3.004	48.74	.32	+.17
.099	28.09	-.30		3.129	48.93	.33	
.116	28.61	-.30	- .55	3.254	49.00	.32	
.139	29.44	-.30		3.379	49.08	.32	
.164	30.12	-.25	- .44	3.504	49.19	.32	+.17
.194	30.73	-.25		4.004	49.23	.35	+.17
.229	31.57	-.25	- .33	5.004	49.23	.33	+.14
.269	32.03	-.22		5.975	49.19	.33	+.14
.324	32.77	-.17	- .23				
.384	33.94	-.12					
.454	34.53	-.10	- .12				
.534	35.42	-.08					

Table 6e Boundary Layer Profile Measurements - Station 5

Re = 3.15E+05 ρ = .2259E-02 δ = 3.140

U_{ref} = 53.79 μ = .3863E-06 C_f = .2640E-02

q = 3.268

y	U	α	β	y	U	α	β
.018	23.29	.75		3.004	53.43	-.07	.22
.019	24.00	.70		3.204	53.59		.
.021	24.64	.70		3.254	53.63	-.13	.19
.024	25.63	.70		3.304	53.69		
.028	26.69	.73		3.354	53.75		
.032	27.45	.75	-2.46	3.404	53.77		.
.037	28.16	.77	- .16	3.454	53.82		
.044	28.96	.77	- .98	3.504	53.83	-.22	.21
.052	29.75	.75	-1.21	3.554	53.83		
.060	30.35	.77	-1.10	3.604	53.83	-.	.
.071	31.10	.77	- .90	3.654	53.83	-.	.
.084	31.72	.75	- .85	3.704	53.87	-.	.
.099	32.46	.77	- .71	3.754	53.85		
.116	33.24	.77	- .81	3.804	53.87		
.139	34.06	.75	- .75	4.004	53.86	-.25	.28
.164	34.84	.73	- .72	5.004	53.84	-.35	.23
.194	35.70	.73	- .68	5.976	53.82	-.45	.27
.229	36.62	.75	- .65				
.269	37.39	.73	- .66				
.324	38.28	.72	- .65				
.384	39.17	.72	- .66				
.454	40.11	.72	- .67				
.534	40.88	.68	- .68				
.634	41.91	.65	- .71				
.754	42.96	.63	- .72				
.904	44.13	.62	- .73				
1.054	45.11	.58	- .71				
1.254	46.39	.53	- .68				
1.454	47.63	.48	- .63				
1.654	48.66	.35	- .57				
1.904	49.79	.28	- .52				
2.154	50.88		- .45				
2.454	51.96	.18	- .36				
2.754	52.93	.03	- .28				

Table 6f Boundary Layer Profile Measurements - Station 6

Re = 3.15E+05 ρ = .2275E-02 δ = 3.850

U_{ref} = 53.36 μ = .3848E-06 C_f = .2225E-02

q = 3.238

y	U	α	β	y	U	α	β
.018	20.43	-.07		.634	37.54	-.12	-.10
.019	21.15	-.07		.754	38.49	-.12	-.10
.021	21.87	-.07		.904	39.53	-.12	-.08
.024	22.83	-.07		1.054	40.60	-.10	-.06
.028	23.82	-.08		1.254	41.88	-.12	-.02
.032	24.55	-.08	+2.67	1.454	43.07	-.12	-.03
.037	25.23	-.05	- .11	1.654	44.33	-.10	-.01
.044	26.04	-.05	-1.07	1.904	45.73	-.10	-.03
.052	26.66	-.05	- .95	2.154	47.03	-.10	-.04
.060	27.22	-.05	- .75	2.454	48.44	-.10	-.06
.071	27.91	-.05	- .62	2.754	49.83	-.12	-.06
.084	28.64	-.08	- .57	3.004	50.79	-.12	-.07
.099	29.30	-.12	- .65	3.254	51.69	-.13	-.06
.115	29.92	-.13	- .65	3.504	52.38	-.20	-.03
.139	30.67	-.13	- .59	4.004	53.12	-.28	+.04
.164	31.37	-.18	- .48	4.504			+.12
.194	32.09	-.18	- .43	5.004	53.34	-.27	+.13
.229	32.80	-.17	- .38	5.504			+.06
.269	33.60	-.18	- .33	5.989	53.32	-.22	-.03
.324	34.45	-.18	- .27				
.384	35.32	-.18	- .24				
.454	36.14	-.18	- .21				
.534	36.99	-.15	- .15				

Table 6g Boundary Layer Profile Measurements - Station 7

Re = 3.15E+05 ρ = .2232E-02 δ = 3.720

U_{ref} = 54.86 μ = .3876E-06 C_f = .2340E-02

q = 3.359

y	U	α	β	y	U	α	β
.018	21.64	- .28		.634	39.53	-.27	.44
.019	22.31	- .28		.754	40.50	-.27	.41
.021	23.07	- .27		.904	41.62	-.22	.37
.024	24.15	- .28		1.054	42.65	-.18	.32
.028	26.14	- .30		1.254	43.97	-.15	.30
.032	25.91	- .30	+2.32	1.454	45.23	-.12	.25
.037	26.55	- .33	+ .01	1.654	46.31	-.08	.23
.044	27.40	- .32	- .81	1.904	47.71	-.07	.17
.052	28.12	- .32	- .77	2.154	49.00	-.03	.14
.060	28.75	- .32	- .67	2.454	50.48	-.02	.12
.071	29.36	- .32	- .57	2.754	51.74	-.02	.10
.084	30.14	- .33	- .54	3.004	52.76	-.03	.07
.099	30.78	- .33	- .67	3.254	53.54	-.07	.05
.116	31.50	- .33	- .67	3.504	54.20	-.12	.03
.139	32.22	- .33	- .62	3.704	54.50		
.164	32.96	- .33	- .52	3.804	54.61		
.194	33.68	- .33	- .51	3.904	54.70		
.229	34.50	- .33	- .49	4.004	54.77	-.18	.05
.269	35.29	- .33	- .49	4.129	54.82		
.324	36.17	- .32	- .47	4.254	54.84		
.384	37.04	- .35	- .49	4.504	54.84		
.454	37.81	- .33	- .45	5.004	54.81	-.20	.14
.534	38.66	- .30	- .43	5.992	54.78	-.18	.19

Table 6h Boundary Layer Profile Measurements
3-DTBL Survey

Re = 3.15E+05 ρ = .2321E-02 δ^* =

U_{ref} = 51.95 μ = .3829E-06 C_f = .1108E-02

q = 3.132

y	U	α	β	y	U	α	β
.018	12.38	22.05		.754	28.80	11.43	-4.58
.019	12.80	22.02		.904	31.28	9.50	-4.74
.021	13.26	22.02		1.054	33.70	7.83	-4.75
.024	14.14	22.05		1.254	37.09	6.02	-4.69
.028	14.84	22.13		1.454	40.16	4.65	-4.54
.032	15.52	22.30	+4.45	1.654	42.91	3.67	-4.29
.037	16.17	22.27	+ .84	1.904	45.48	2.87	-4.10
.044	16.82	22.30	- .98	2.154	47.26	2.43	-3.96
.052	17.32	22.27	-1.36	2.454	48.69	2.08	-3.85
.060	17.79	22.40	-1.36	2.754	49.97	1.83	-3.77
.071	18.18	22.40	-1.36	3.004	50.89	1.65	-3.70
.084	18.63	22.40	-1.26	3.254	51.58	1.48	-3.63
.099	18.92	22.30	-1.35	3.404	52.02		
.116	19.33	22.13	-1.54	3.504	52.18	1.37	-3.58
.139	19.84	21.90	-1.65	3.604	52.34		
.164	20.34	21.47	-1.81	3.704	52.48		
.194	20.79	20.98	-2.13	3.804	52.60		
.229	21.24	20.42	-2.32	3.904	52.72		
.269	21.80	19.72	-2.62	4.004	52.75	1.15	-3.49
.324	22.66	18.78	-2.88	4.504	52.95		-3.41
.384	23.51	17.60	-3.31	5.004	53.08	.93	-3.35
.454	24.54	16.33	-3.61	5.504	53.17		-3.31
.534	25.59	15.77	-3.96	5.994	53.31	.72	-3.20
.634	26.88	13.27	-4.25				

*No definable boundary layer thickness was determined from the data

Table 6i Boundary Layer Survey Measurements
Rectangular Pitot Probe Data

Station 5

Re = 3.15E+05 ρ = .2283E-02 δ = 3.140

U_{ref} = 53.02 μ = .3845E-06 C_f = .2640E-02

q = 3.209

y	U	y	U	y	U
.0059	12.31	.0214	24.46	.2514	36.10
.0064	12.58	.0254	25.55	.3214	37.34
.0069	13.18	.0294	26.23	.4514	39.05
.0079	14.46	.0344	27.17	.6316	41.00
.0089	15.91	.0414	28.00	.9016	43.01
.0099	17.28	.0494	28.75	1.2516	45.38
.0109	18.78	.0579	29.41	1.6516	47.68
.0127	20.03	.0684	30.16	2.1516	49.99
.0142	21.15	.0814	30.93	2.7516	51.93
.0157	22.08	.0964	31.68	3.2516	52.79
.0169	22.84	.1134	32.32	4.9556	52.96
.0187	23.52	.1614	34.00		

Station 6

Re = 3.15E+05 ρ = .2258E-02 δ = 3.850

U_{ref} = 54.01 μ = .3869E-06 C_f = .2225E-02

q = 3.293

y	U	y	U	y	U
.0059	10.71	.0267	23.11	.4509	35.35
.0064	11.41	.0309	24.06	3.4016	52.94
.0069	11.62	.0359	24.84	3.5016	53.17
.0079	12.91	.0417	25.45	3.6016	53.40
.0089	14.50	.0499	26.10	3.7016	53.59
.0099	15.79	.0579	26.81	3.8016	53.76
.0109	16.80	.0689	27.45	3.9016	53.96
.0126	18.02	.0819	28.09	4.0016	54.01
.0142	18.98	.0967	28.78	4.1016	54.08
.0159	19.59	.1137	29.49	4.2016	54.14
.0177	20.40	.1617	30.93	3.8516	53.88
.0194	21.07	.2514	32.80	5.0016	54.18
.0224	22.08	.3212	33.83	5.9646	54.15

Table 6i Boundary Layer Survey Measurements
Rectangular Pitot Probe Data (Cont'd)

Station 7

Re = 3,15E+06 ρ = .2242E-02 δ = 3,720

U_{ref} = 54,31 μ = ,3867E-06 C_f = .2340E-02

q = 3.306

y	U	y	U	y	U
.0059	11.56	.0154	20.51	.0964	30.50
.0064	11.89	.0169	21.38	.1134	31.22
.0069	12.39	.0184	22.01	.1614	32.75
.0079	13.53	.0214	23.19	.2514	34.80
.0090	15.21	.0254	24.39	.3214	35.92
.0098	16.20	.0294	25.25	.4514	37.60
.0101	16.45	.0344	26.10	3.501	53.86
.0107	17.28	.0414	26.97	3.601	54.04
.0111	17.62	.0494	27.70	3.701	54.17
.0122	18.70	.0574	28.31	3.801	54.27
.0127	18.75	.0684	29.02	3.901	54.35
.0137	19.67	.0814	29.77	4.973	54.45

3-DTBL Survey

Re = 3,15E+05 ρ = .2304E-02 δ = 3.175

U_{ref} = 52.49 μ .3836E-06 C_f = 0.1108E-02

q = 3.174

y	U	y	U	y	U
.0059	7.26	.0154	12.04	.0684	17.95
.0061	7.33	.0166	12.66	.0814	18.35
.0064	7.41	.0184	13.07	.0961	18.75
.0067	7.63	.0210	13.94	.1131	19.18
.0079	8.10	.0254	14.75	.1611	20.02
.0087	8.59	.0289	15.49	.2511	21.36
.0099	9.25	.0342	16.06	.3211	22.35
.0107	9.82	.0410	16.75	.4511	24.14
.0124	10.62	.0489	17.14	.5311	25.33
.0137	11.38	.0574	17.58	5.0059	53.28

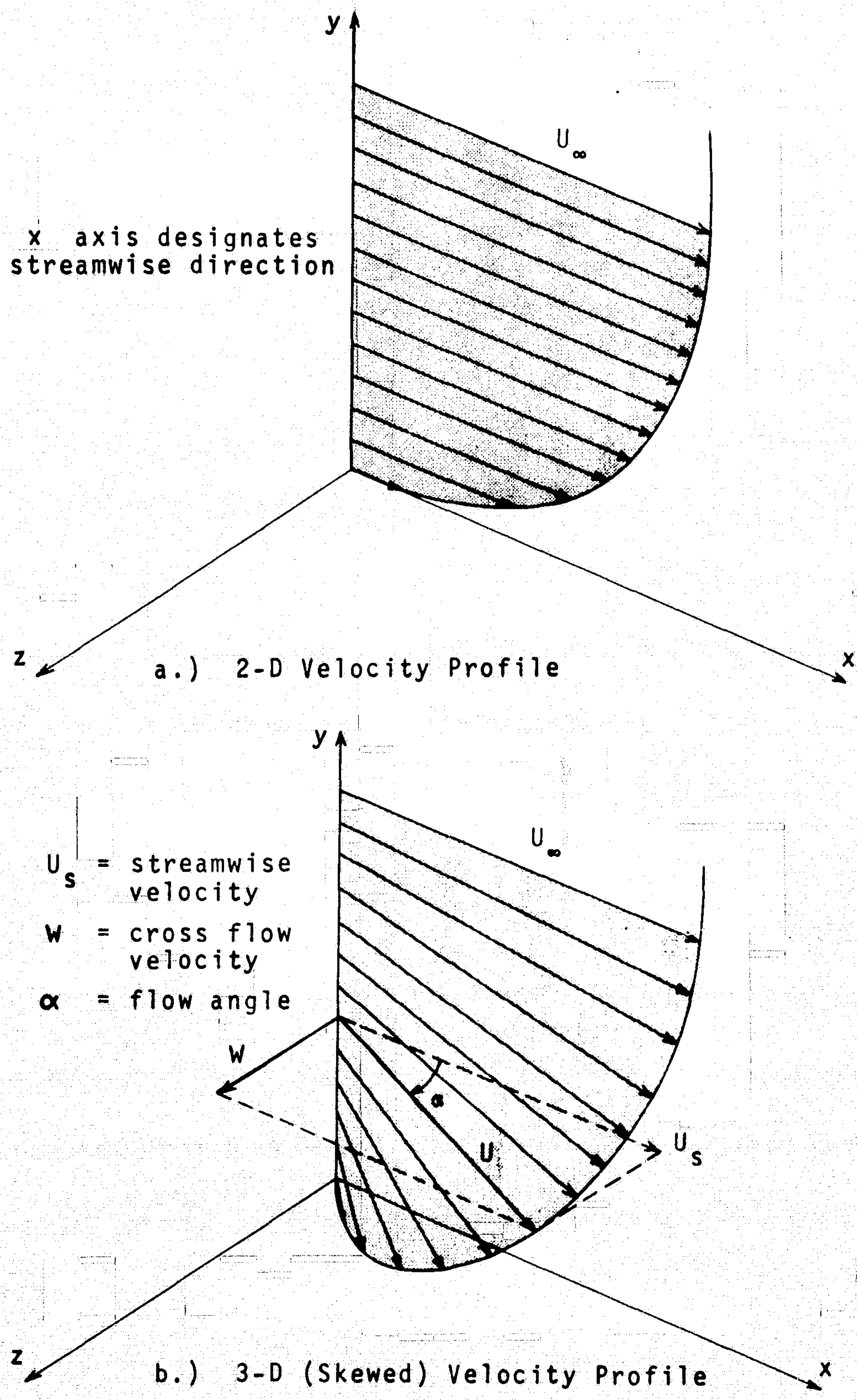

Fig. 1 The Two and Three-Dimensional Boundary Layer

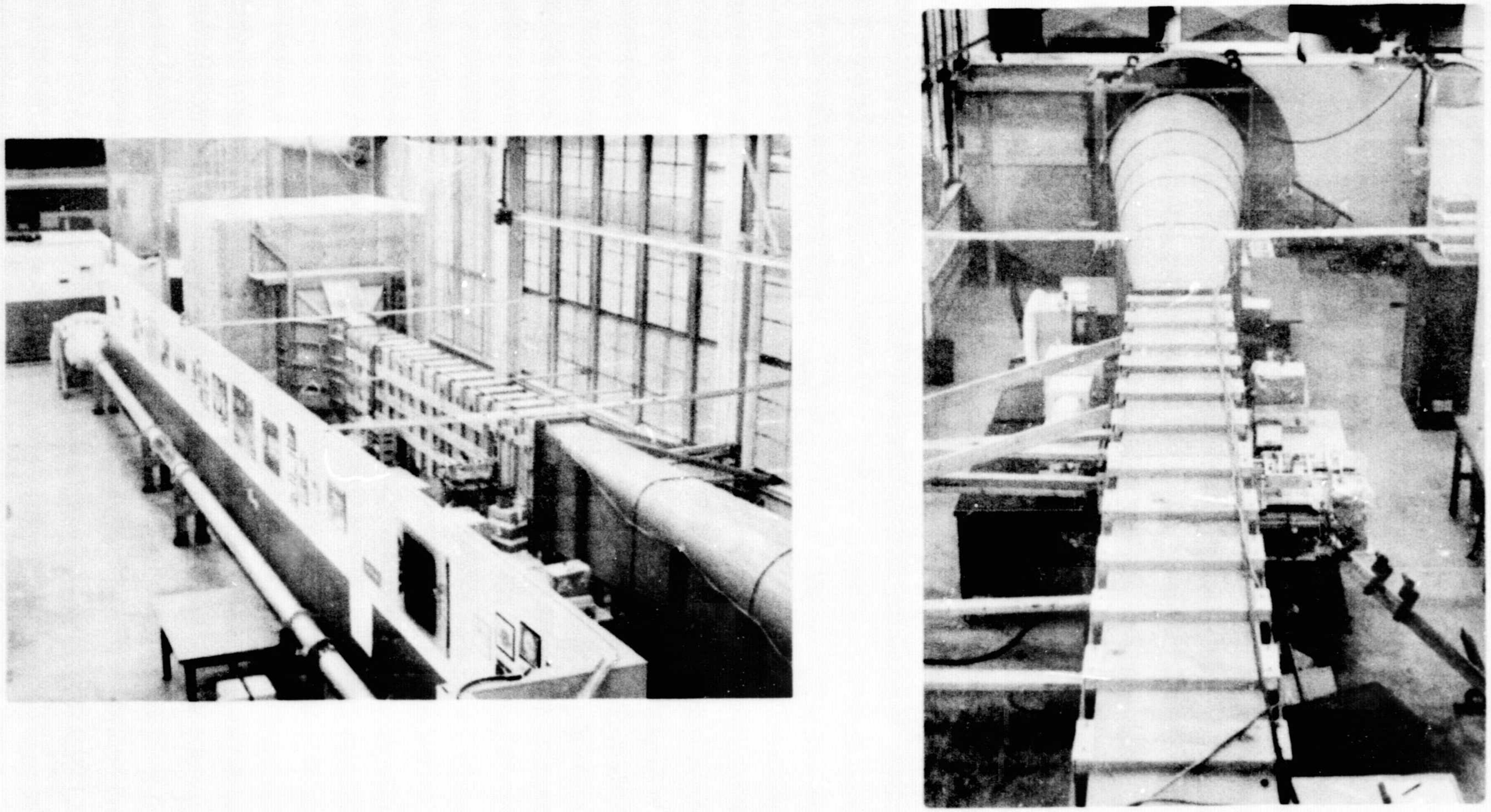

Fig. 2 The University of Maryland Boundary Layer Wind Tunnel

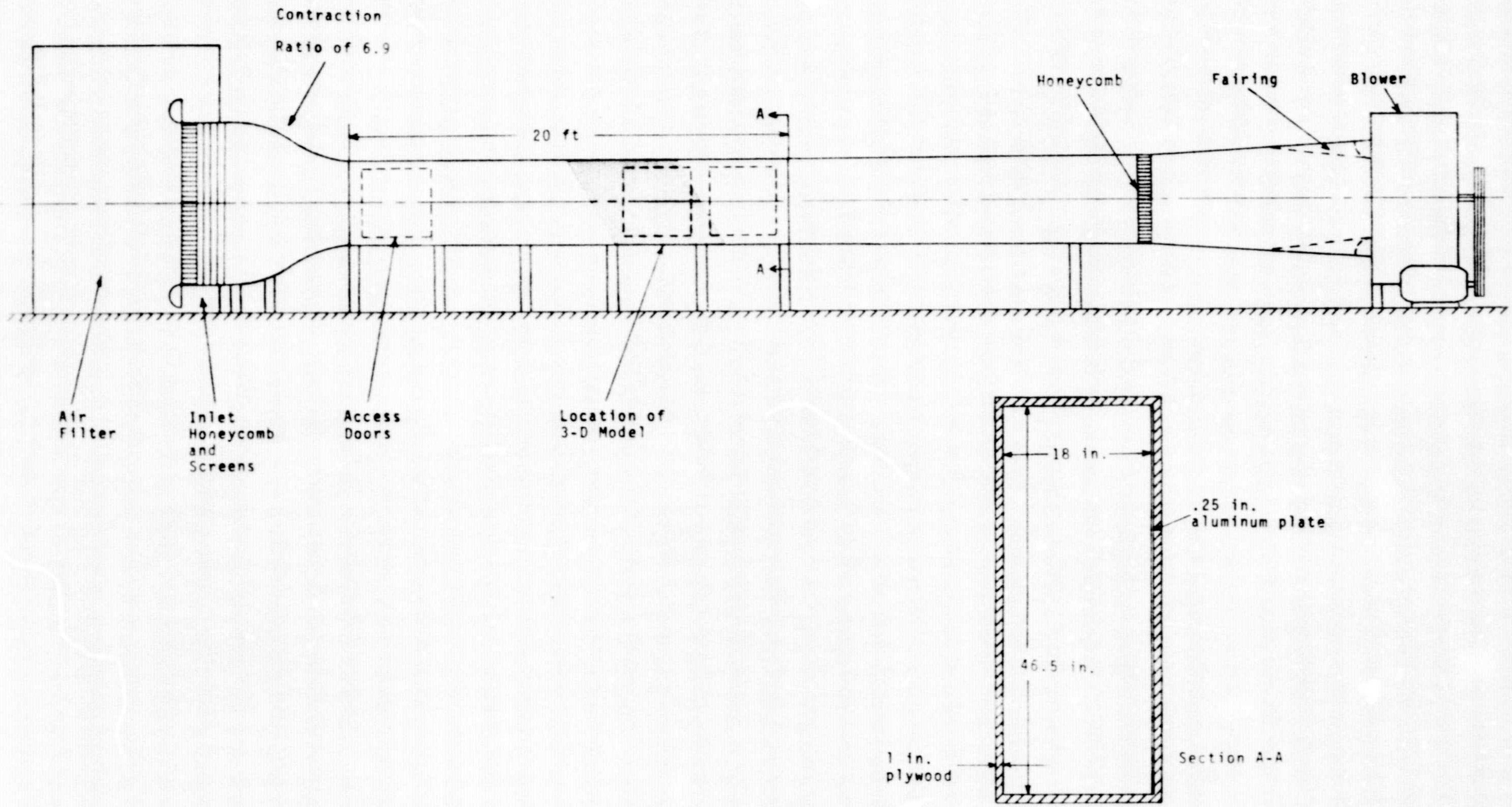

Fig. 3 Side View of Boundary Layer Wind Tunnel

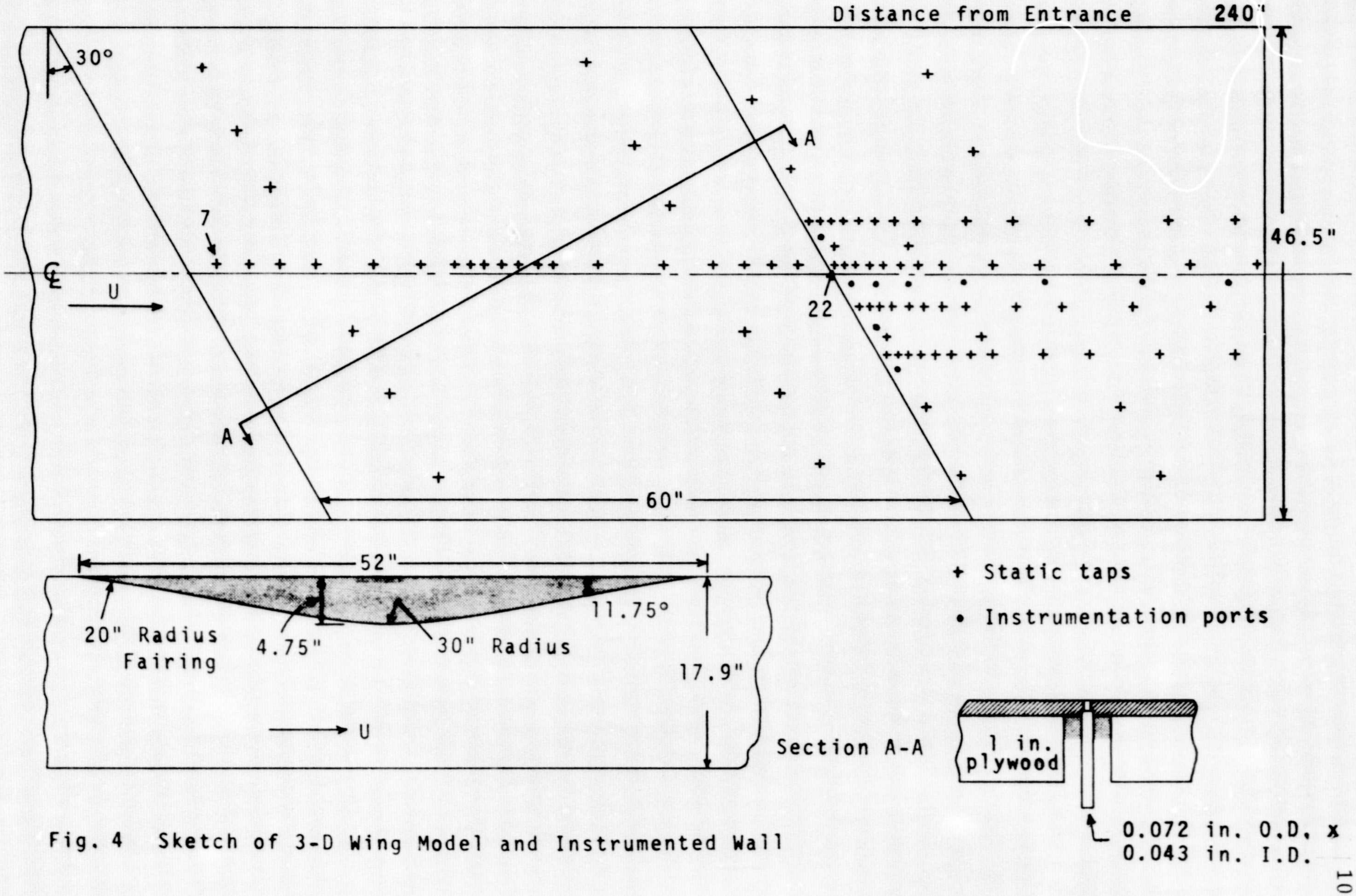

Fig. 4 Sketch of 3-D Wing Model and Instrumented Wall

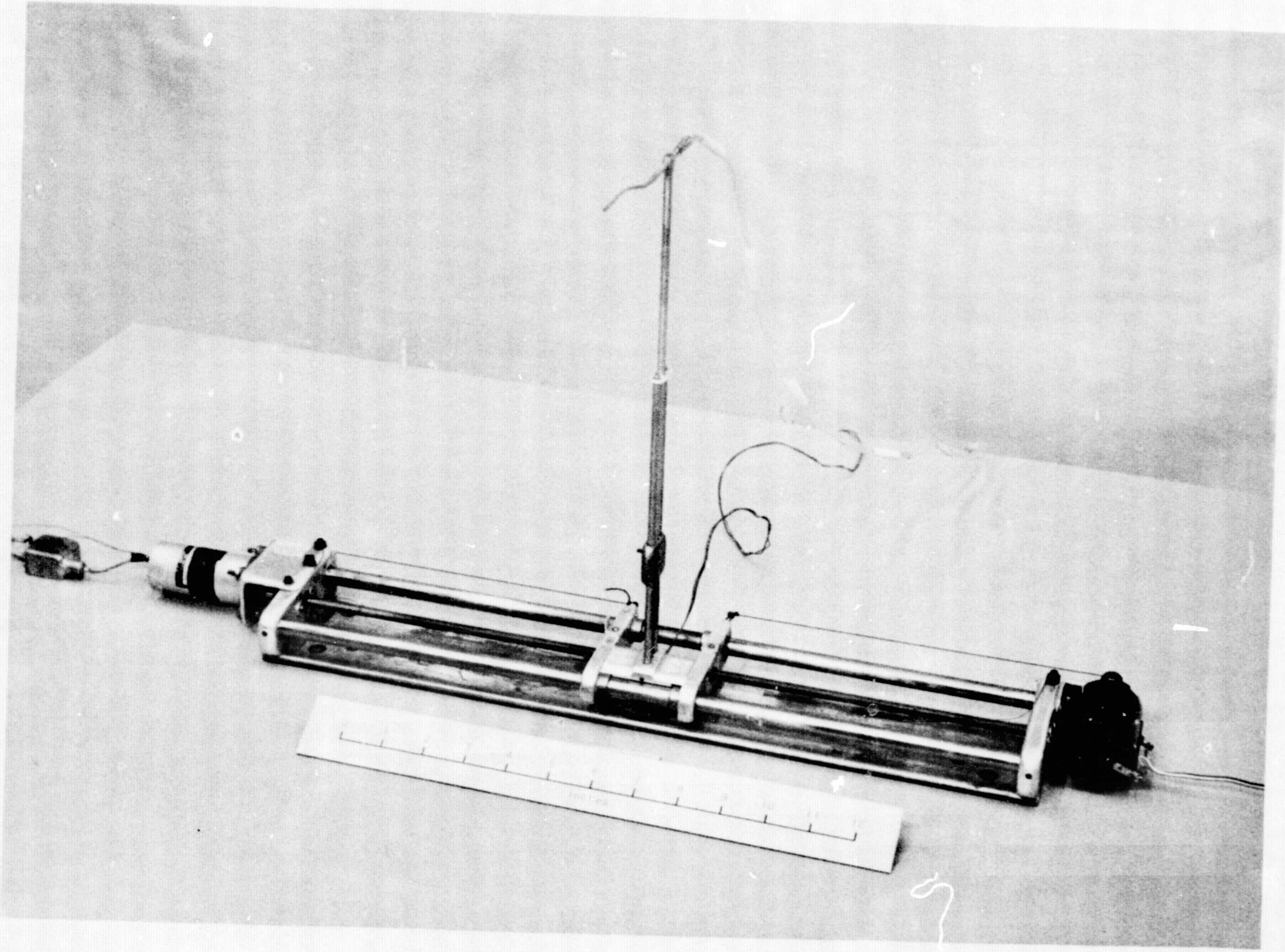

Fig. 5 Transverse Traverse Device

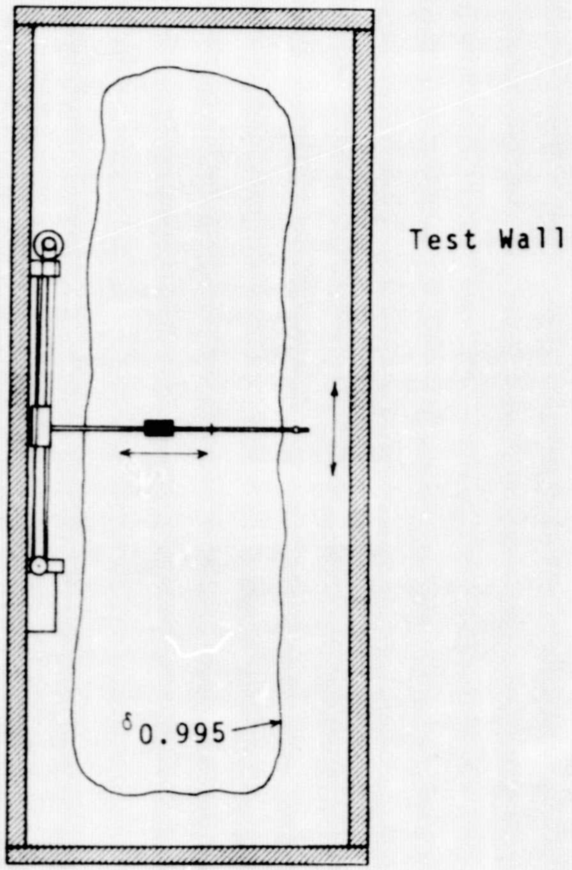

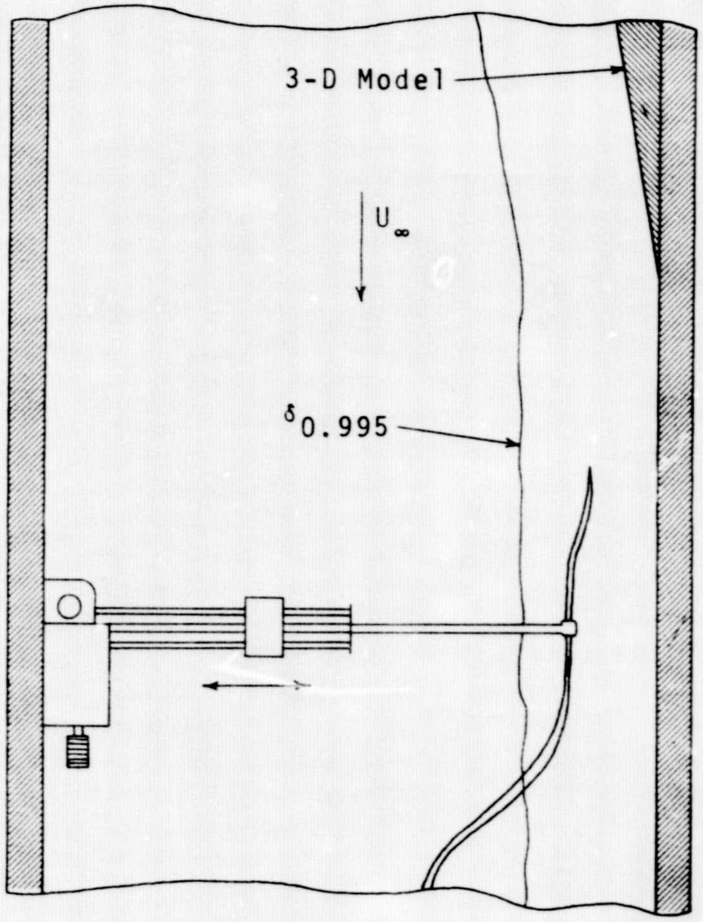

Fig. 6 Transverse Traverse Device Mounted In Tunnel

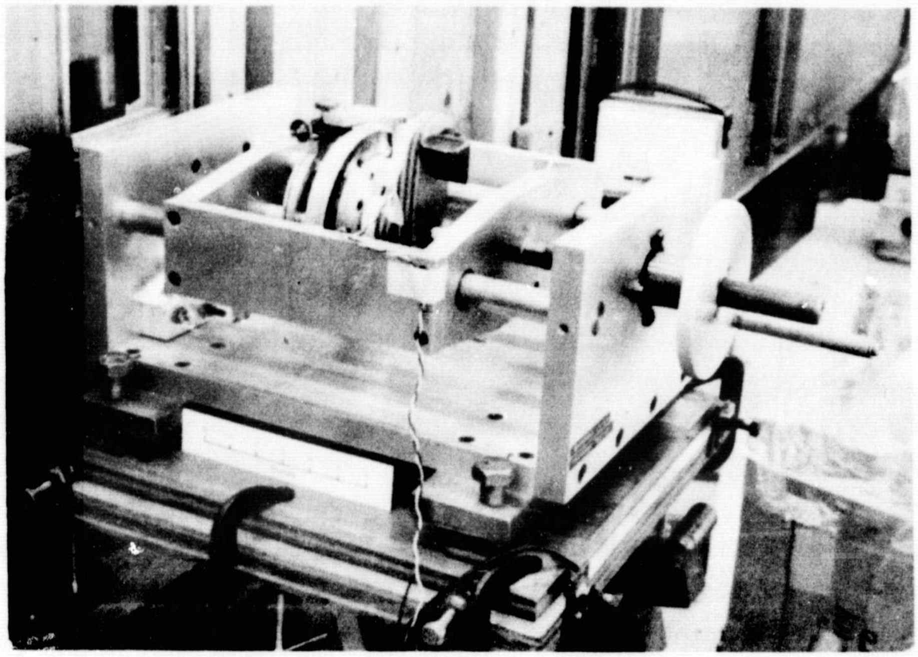

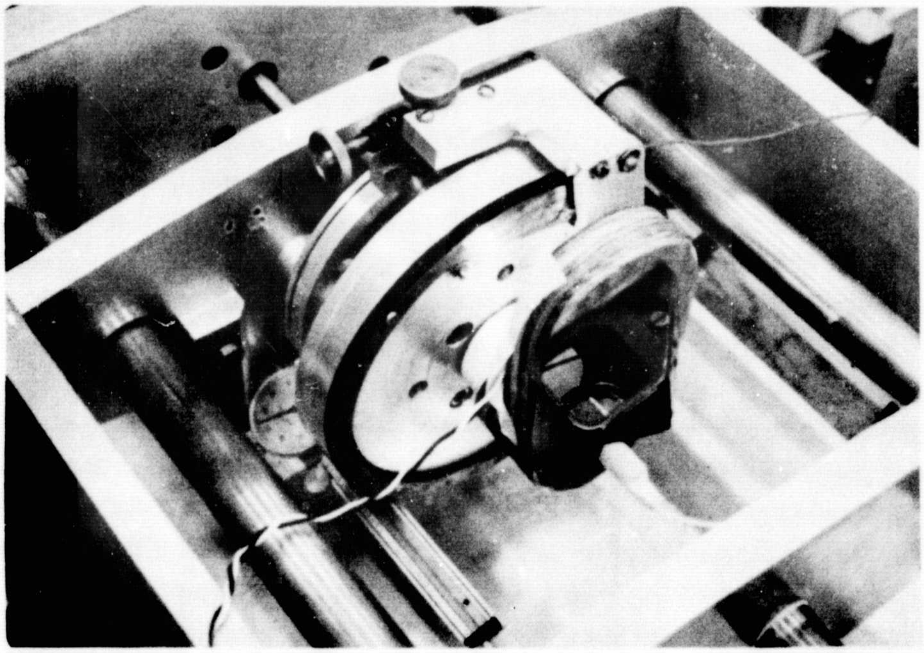

Fig. 7 Boundary Layer Traverse Device

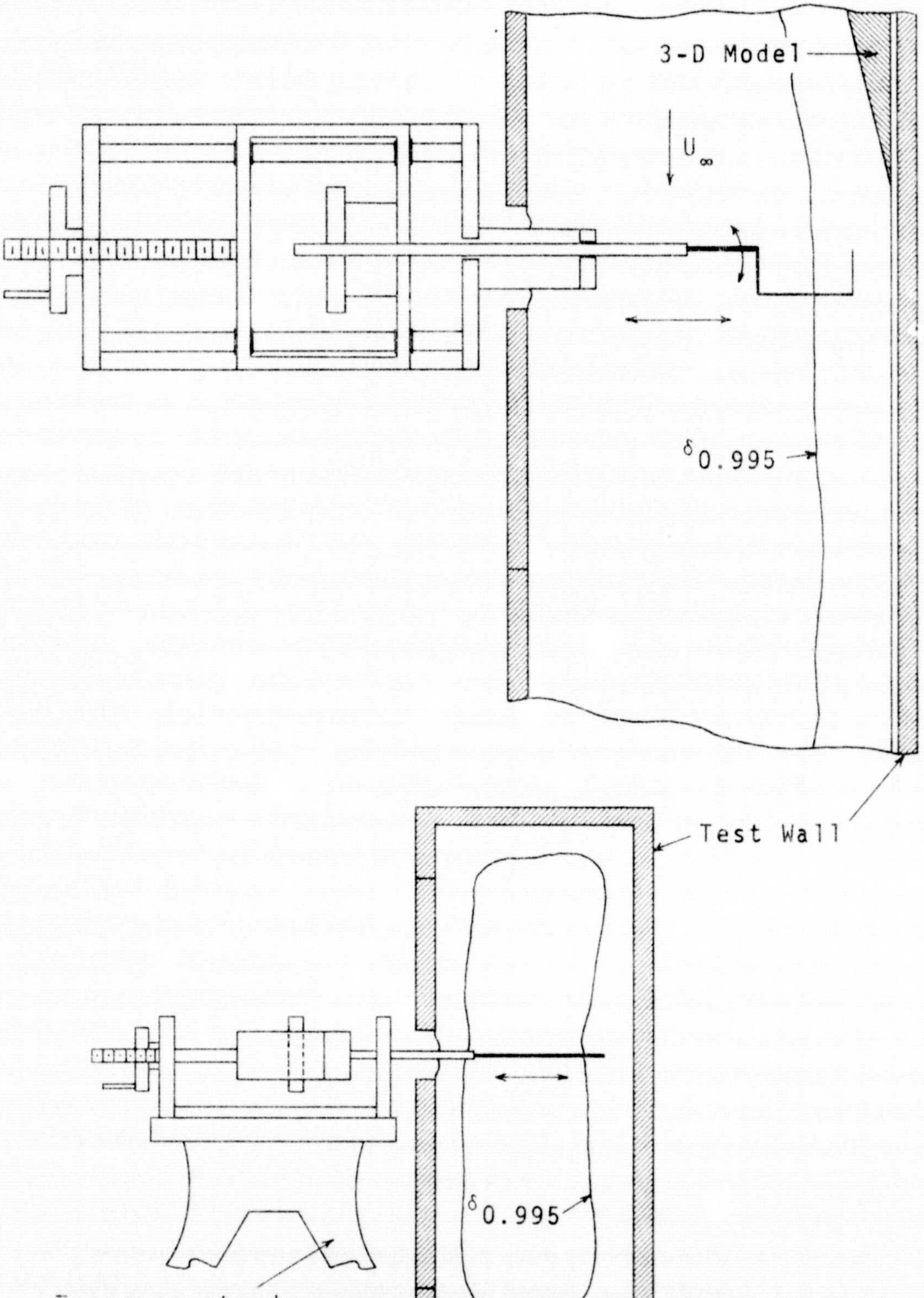

Fig. 8 Boundary Layer Traverse Device In Tunnel

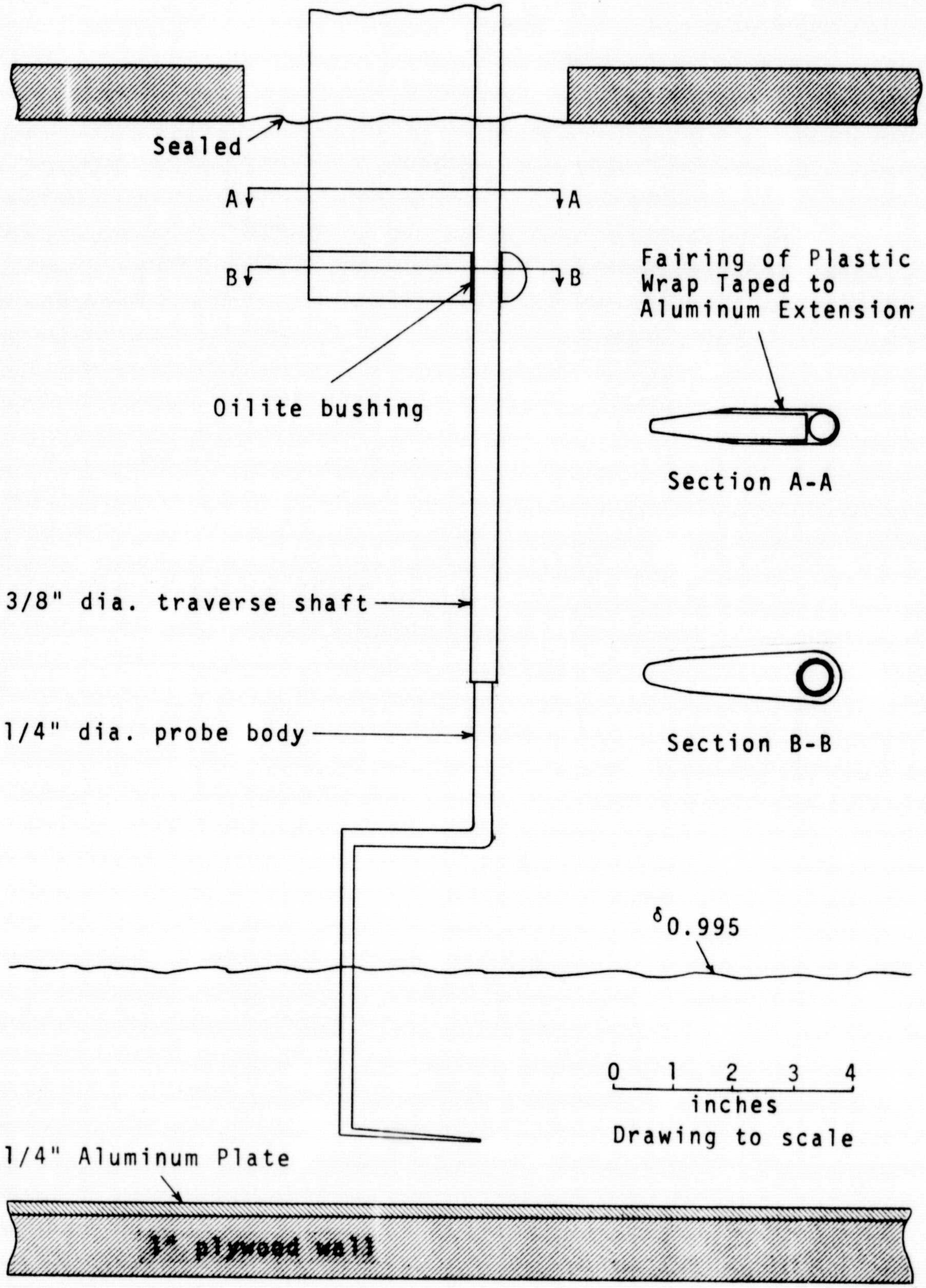

Fig. 9 Mounting of a B.L. Probe In Tunnel

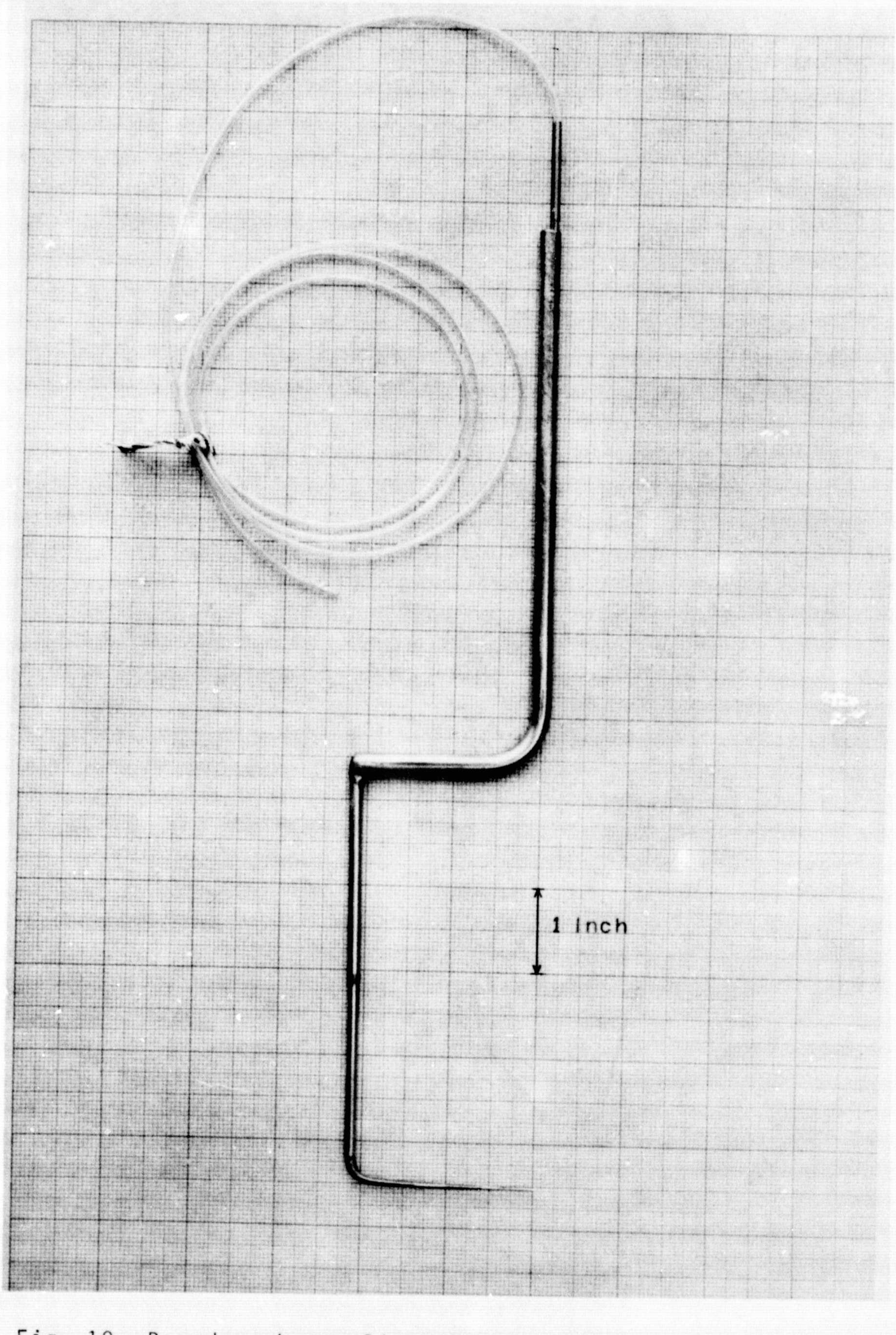

Fig. 10 Boundary Layer Pitot Probe

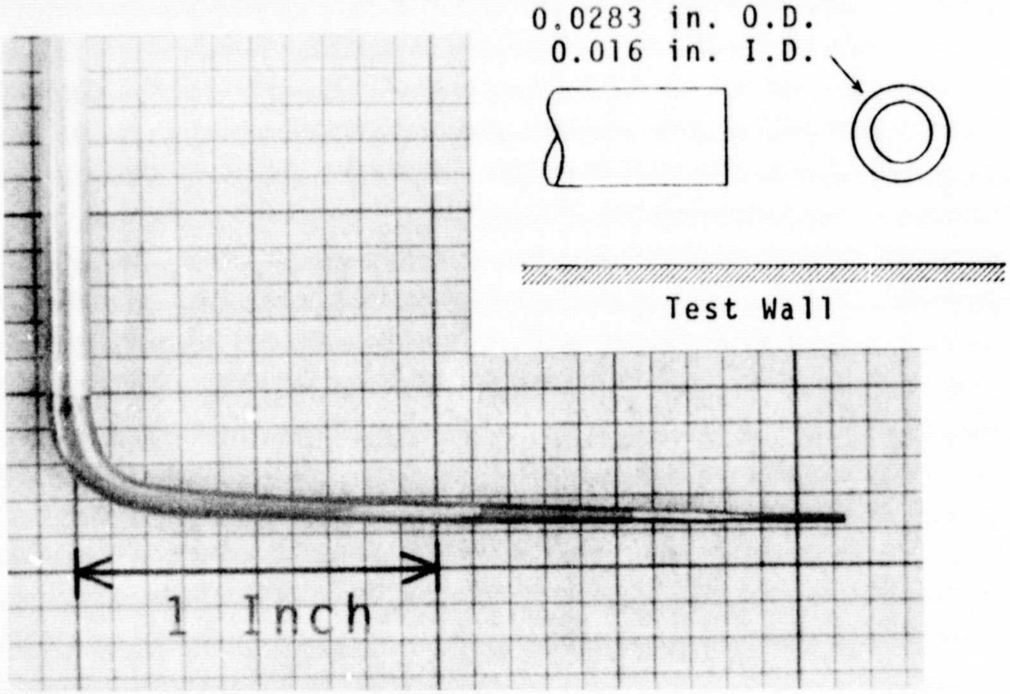

a.) Circular Pitot Probe

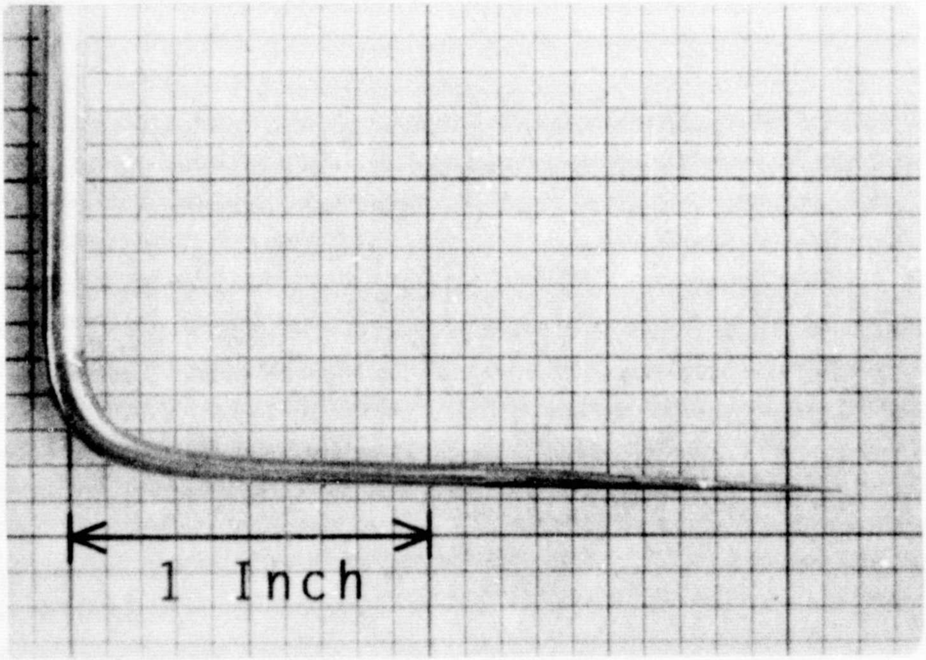

b.) Rectangular Pitot Probe

Fig. 11 Bottom Portion of B.L. Probes

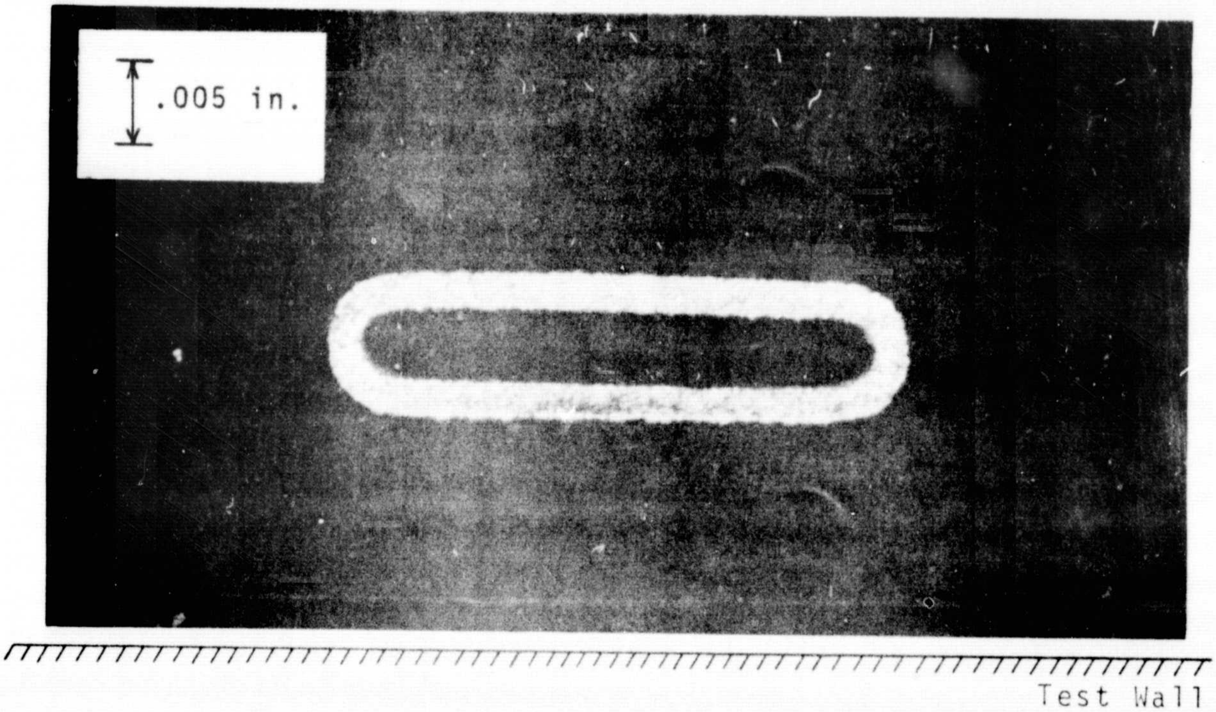

c.) Microphoto of Rectangular Pitot Probe Tip

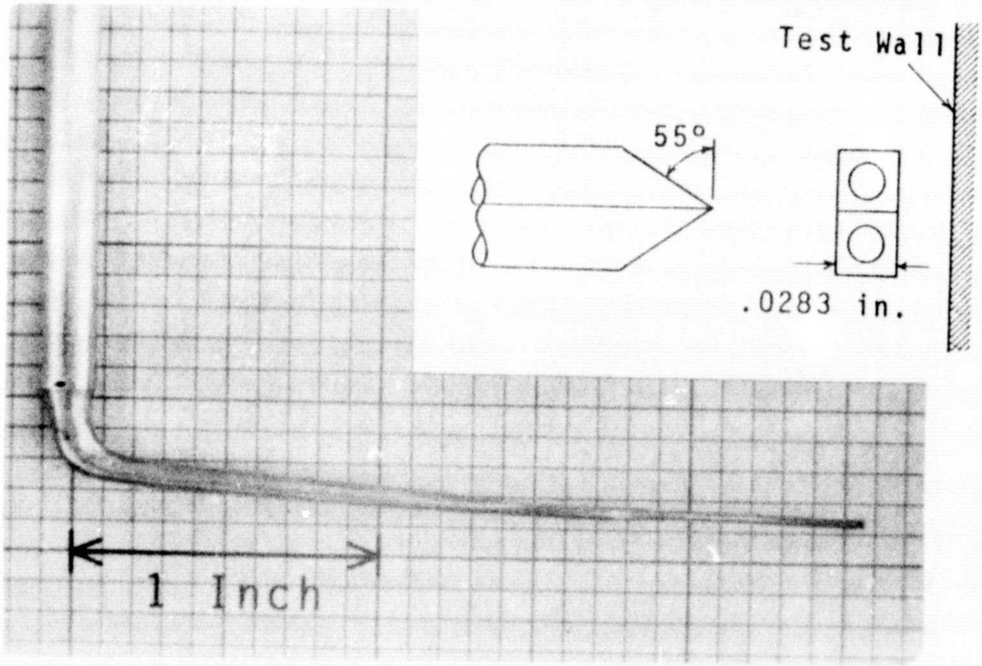

d.) Conrad Probe

Fig. 11 Bottom Portion of B.L. Probes (Cont'd)

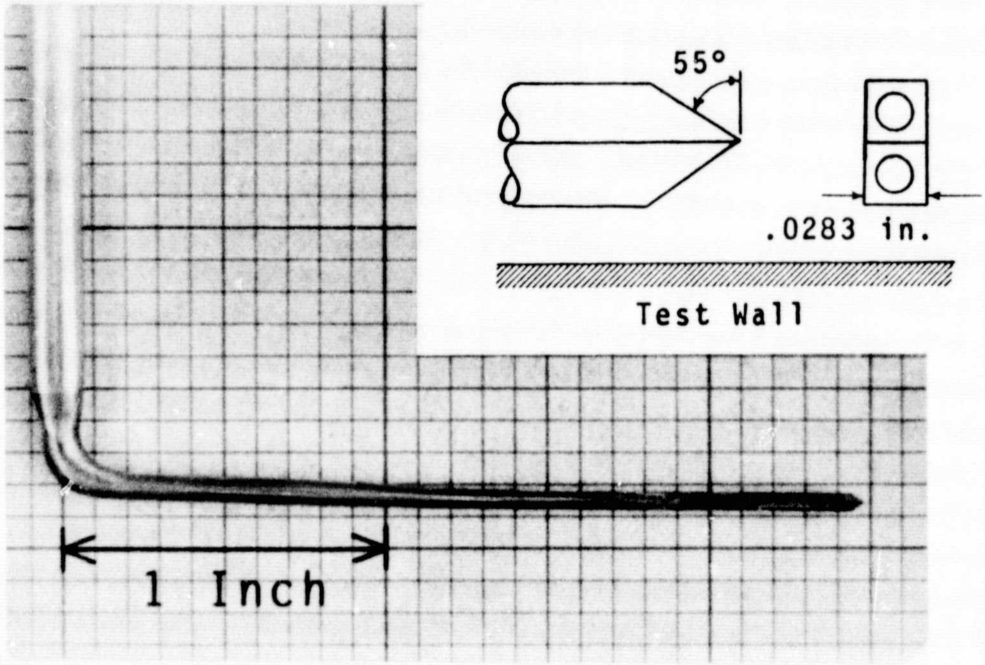

e.) Pitch Probe

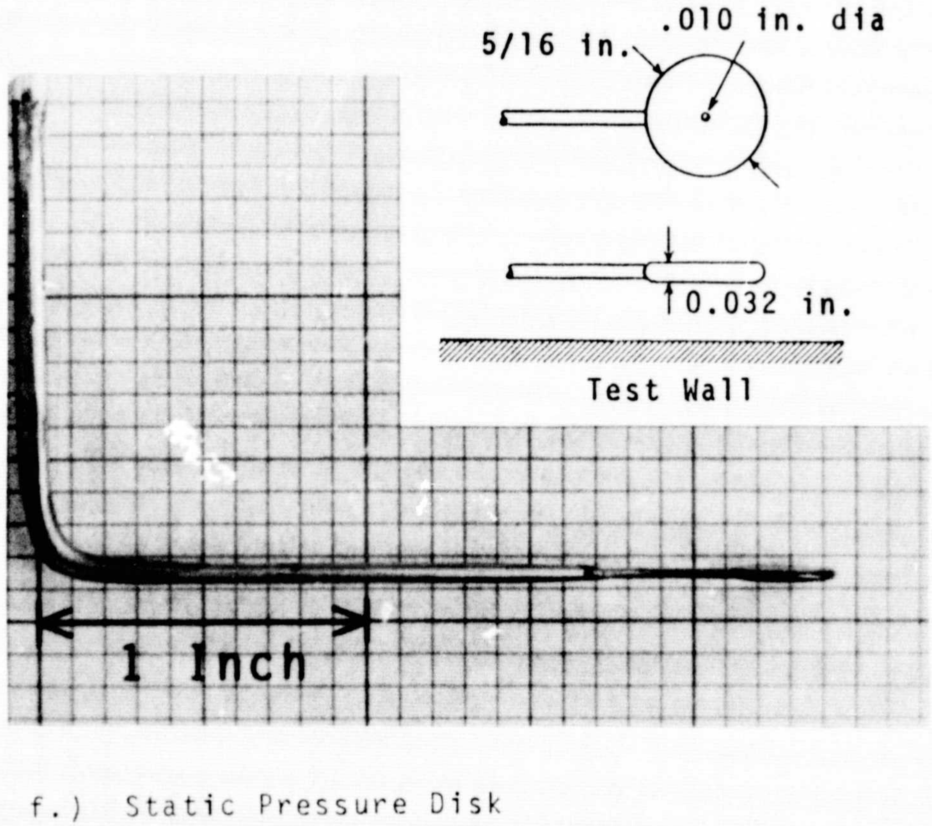

f.) Static Pressure Disk

Fig. 11 Bottom Portion of B.L. Probes (Cont'd)

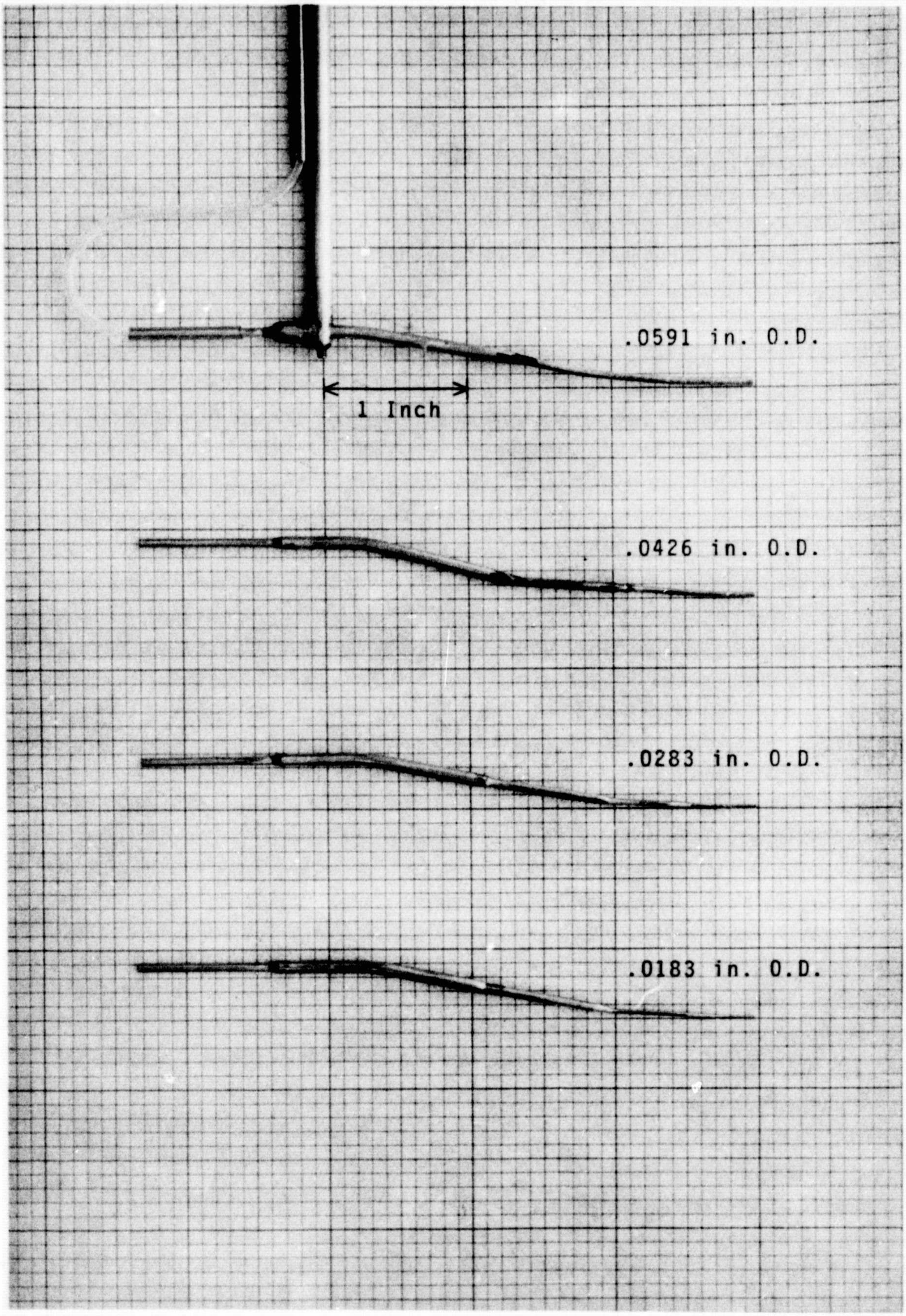

g.) Preston Probes
Fig. 11 Bottom Portion of B.L. Probes (Cont'd)

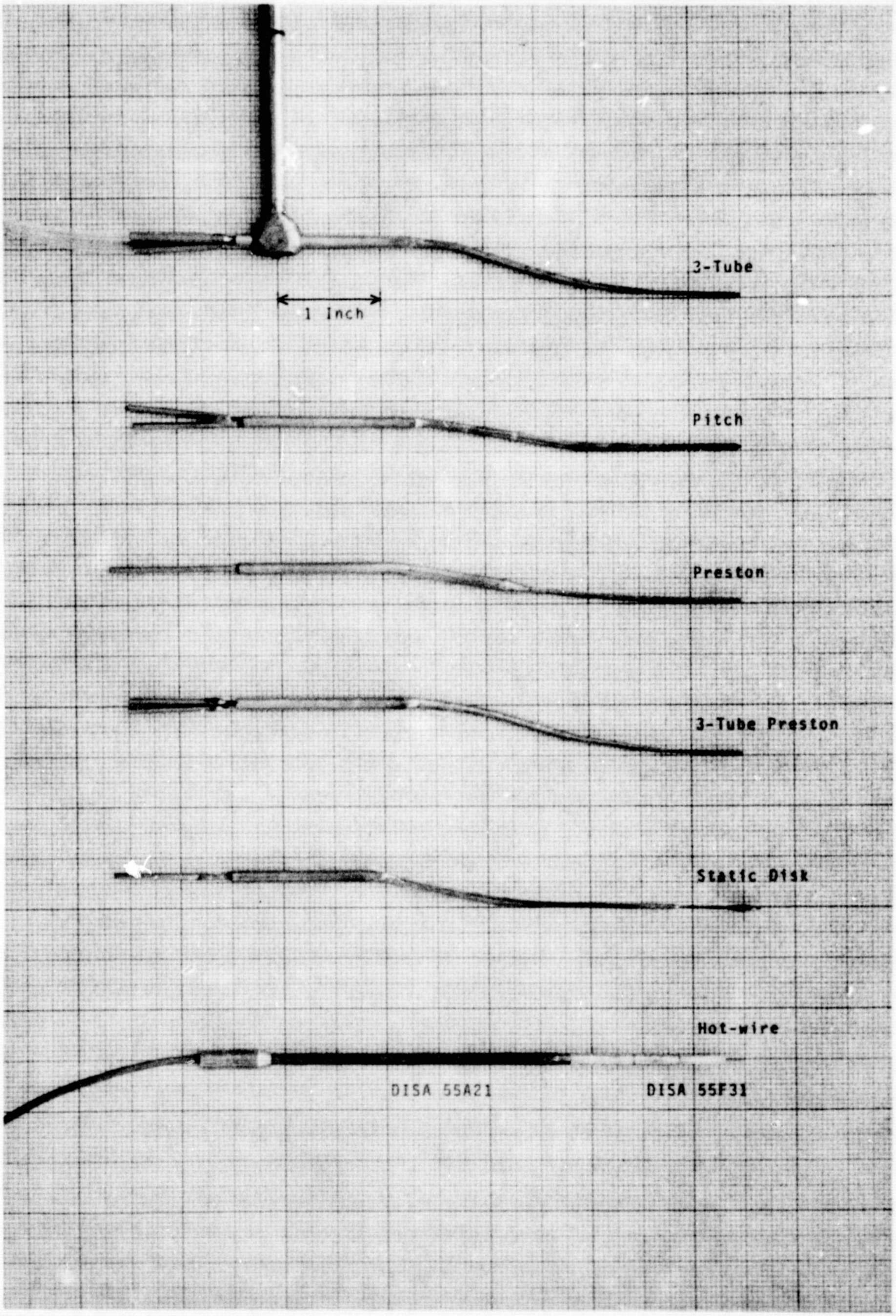

Fig. 12 Transverse Traverse Probes

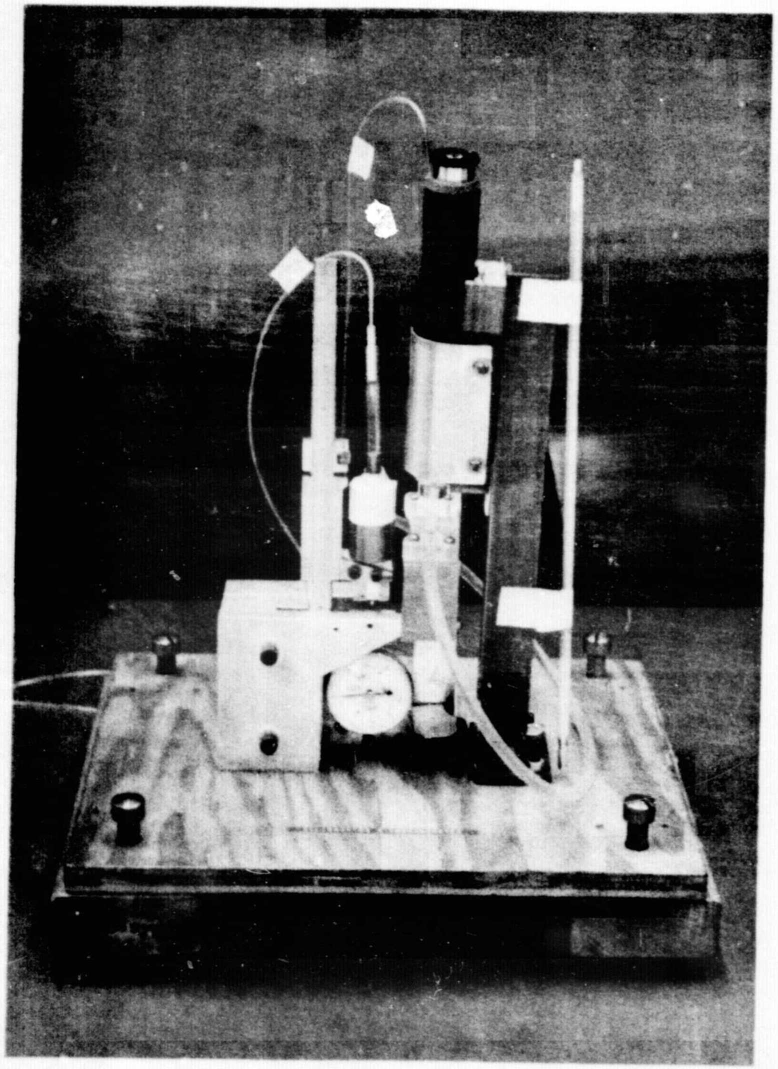

a.) Calibration Micromanometer

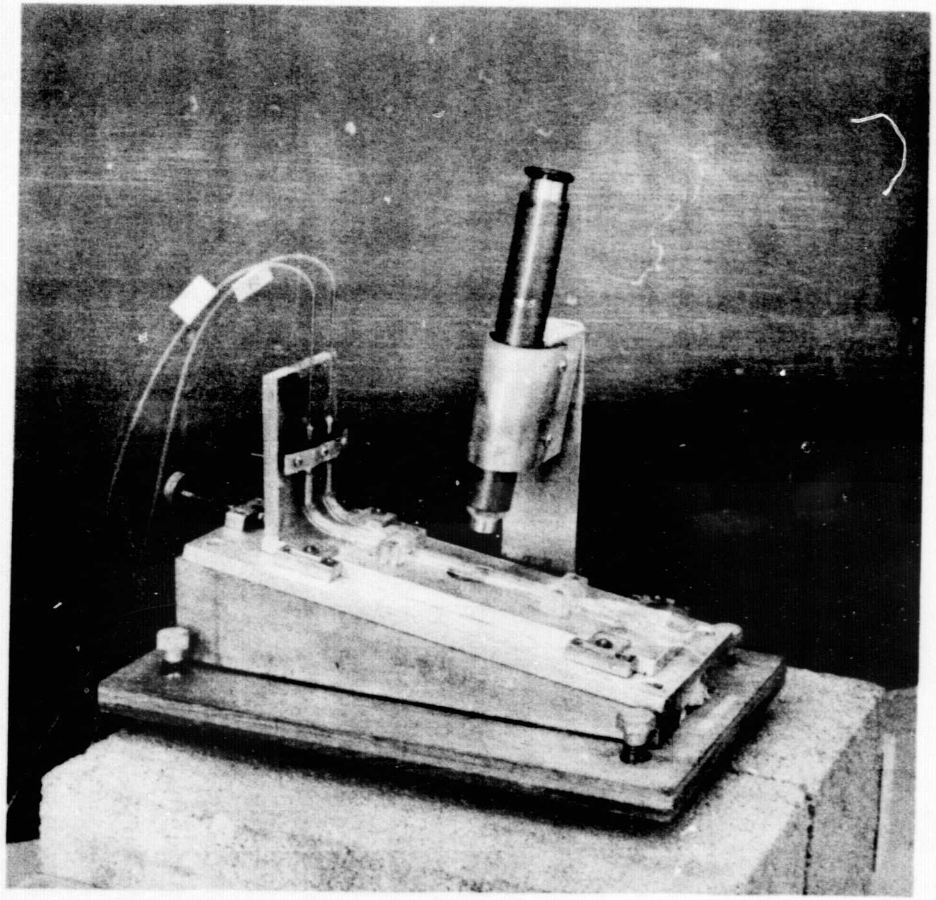

b.) Nulling Micromanometer

Fig. 13 Micromanometers

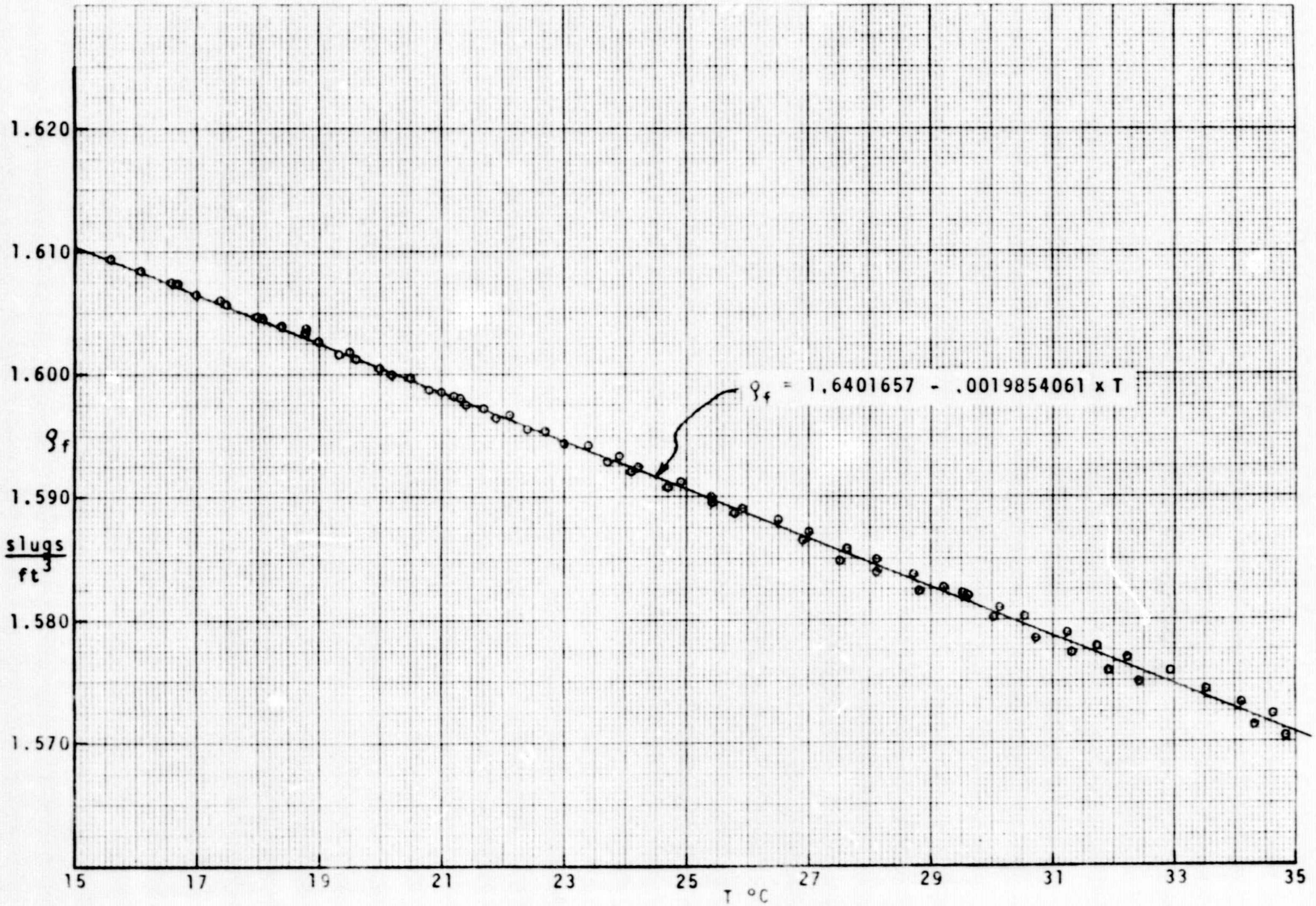

Fig. 14 Calibration of DC-200 Silicon Oil For Micromanometers

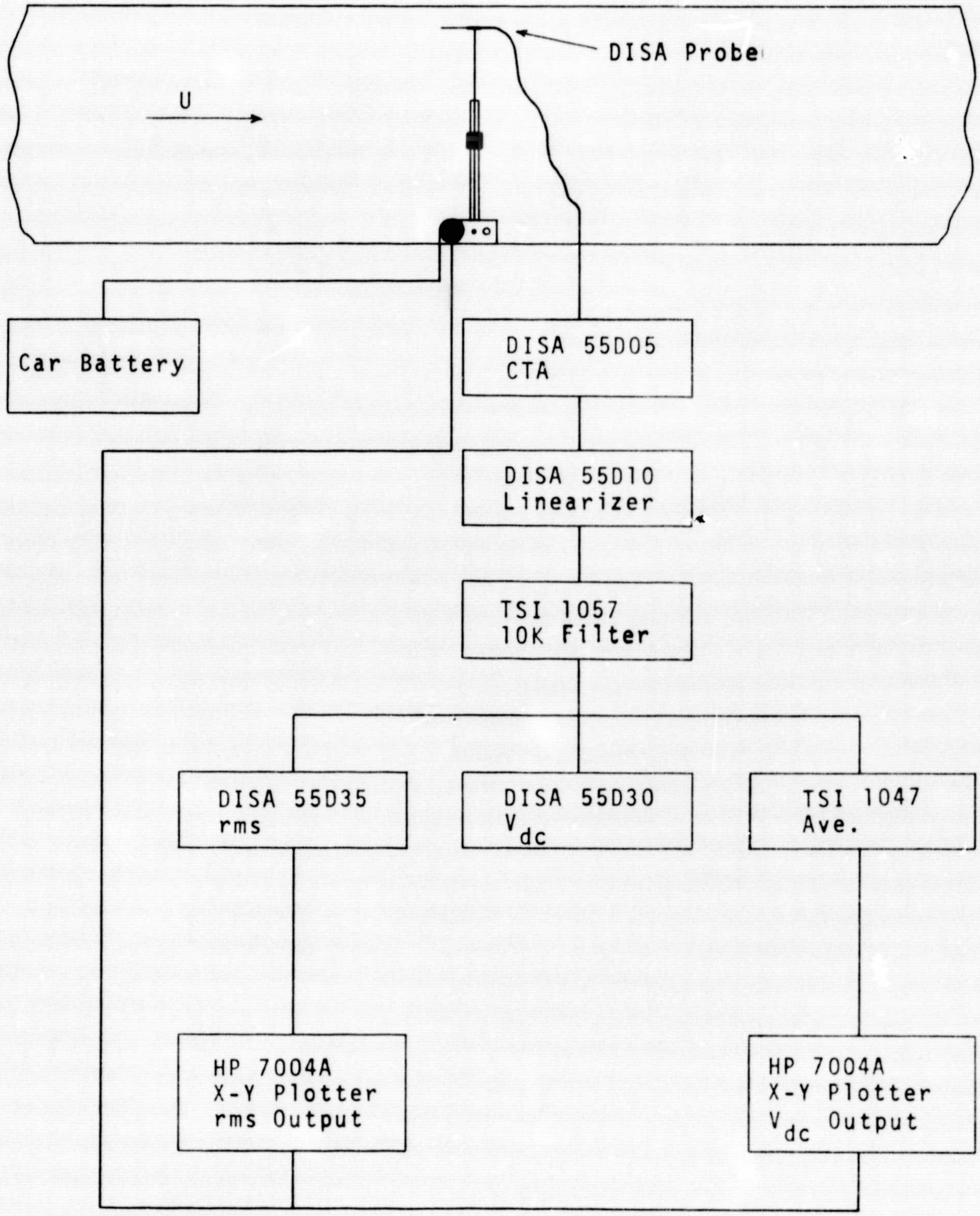

Fig. 15 Hot-Wire Anemometer Circuit

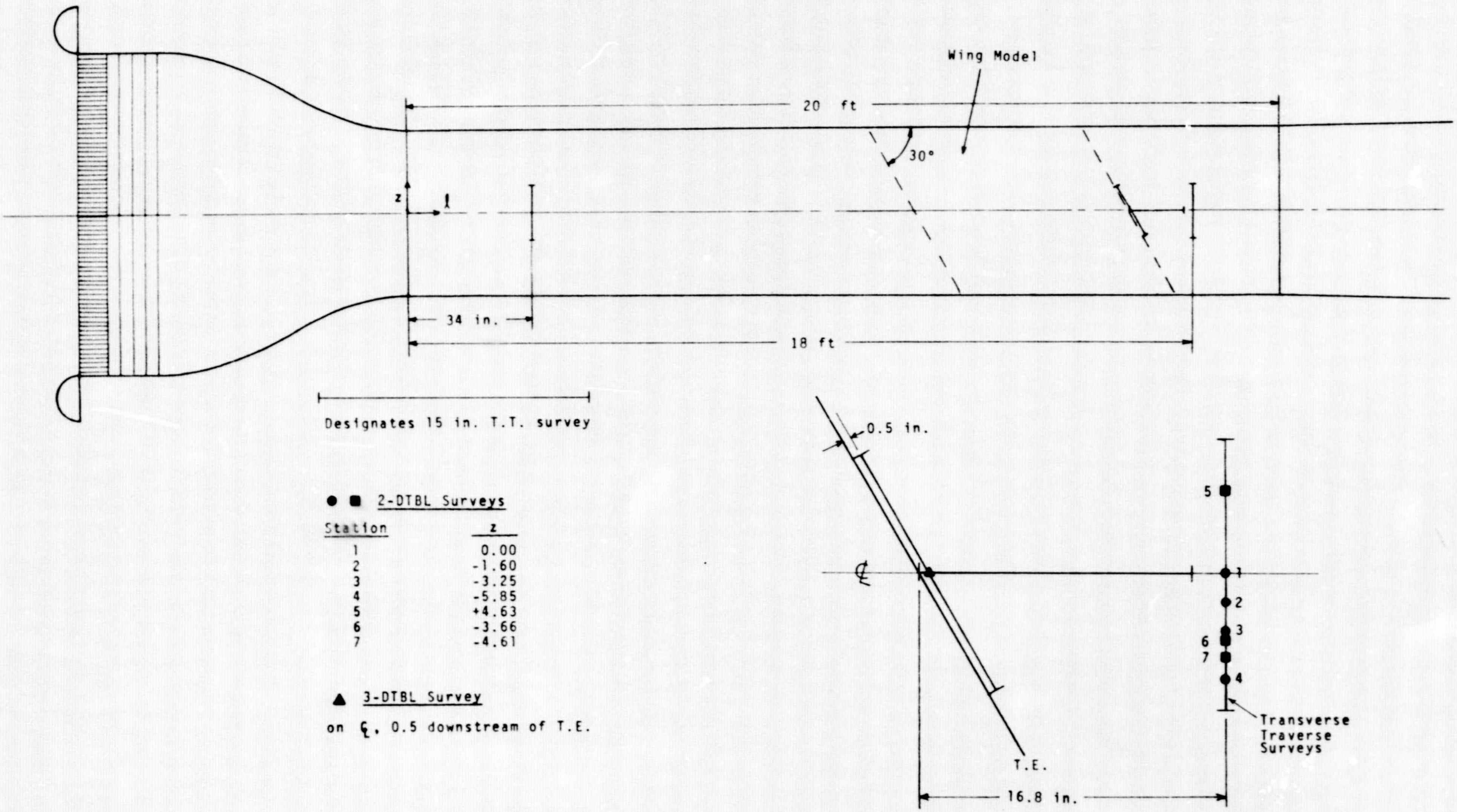

Fig. 16 Location of Transverse Traverse and Boundary Layer Surveys

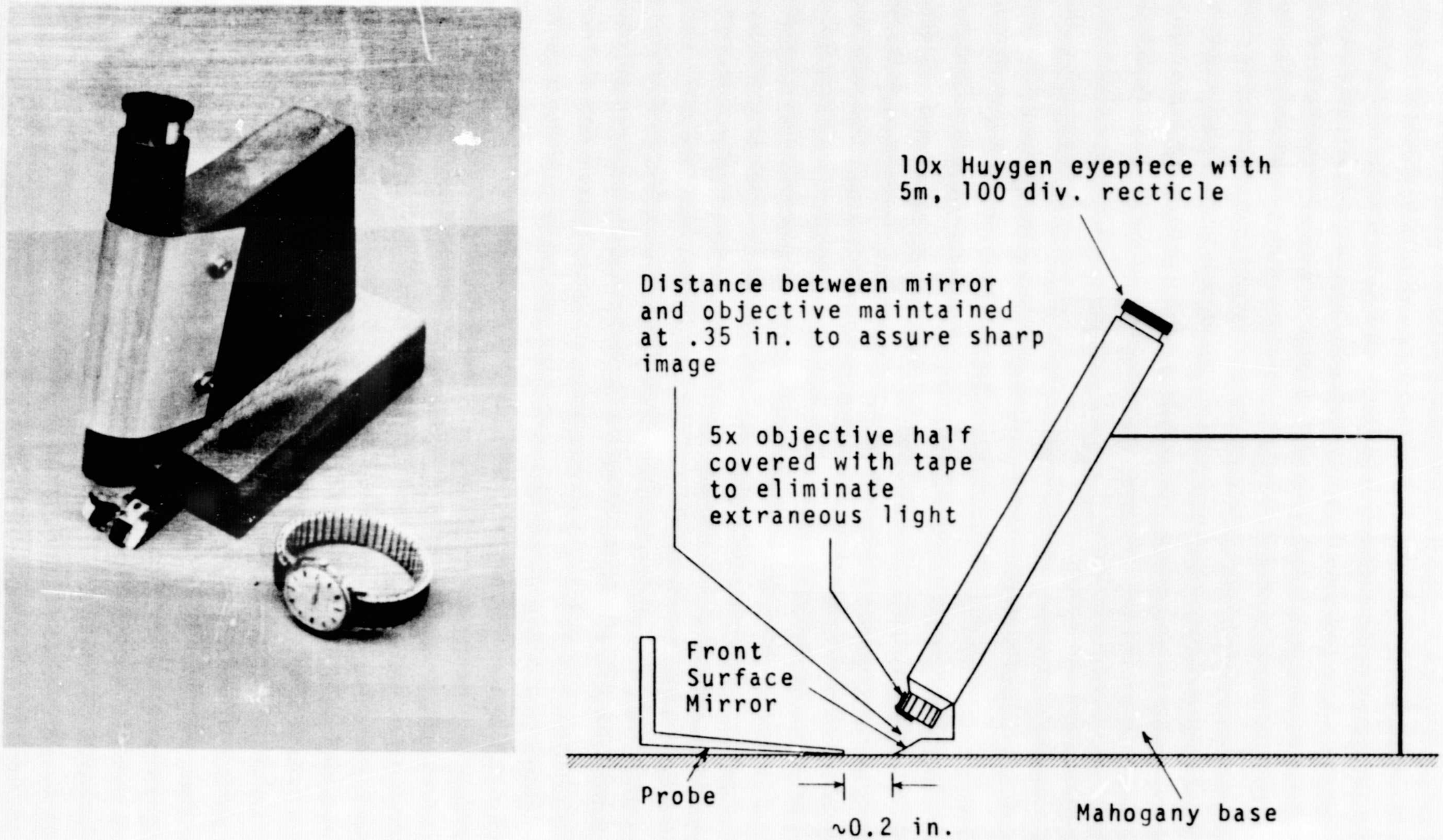

Fig. 17 Probe Sighting Device

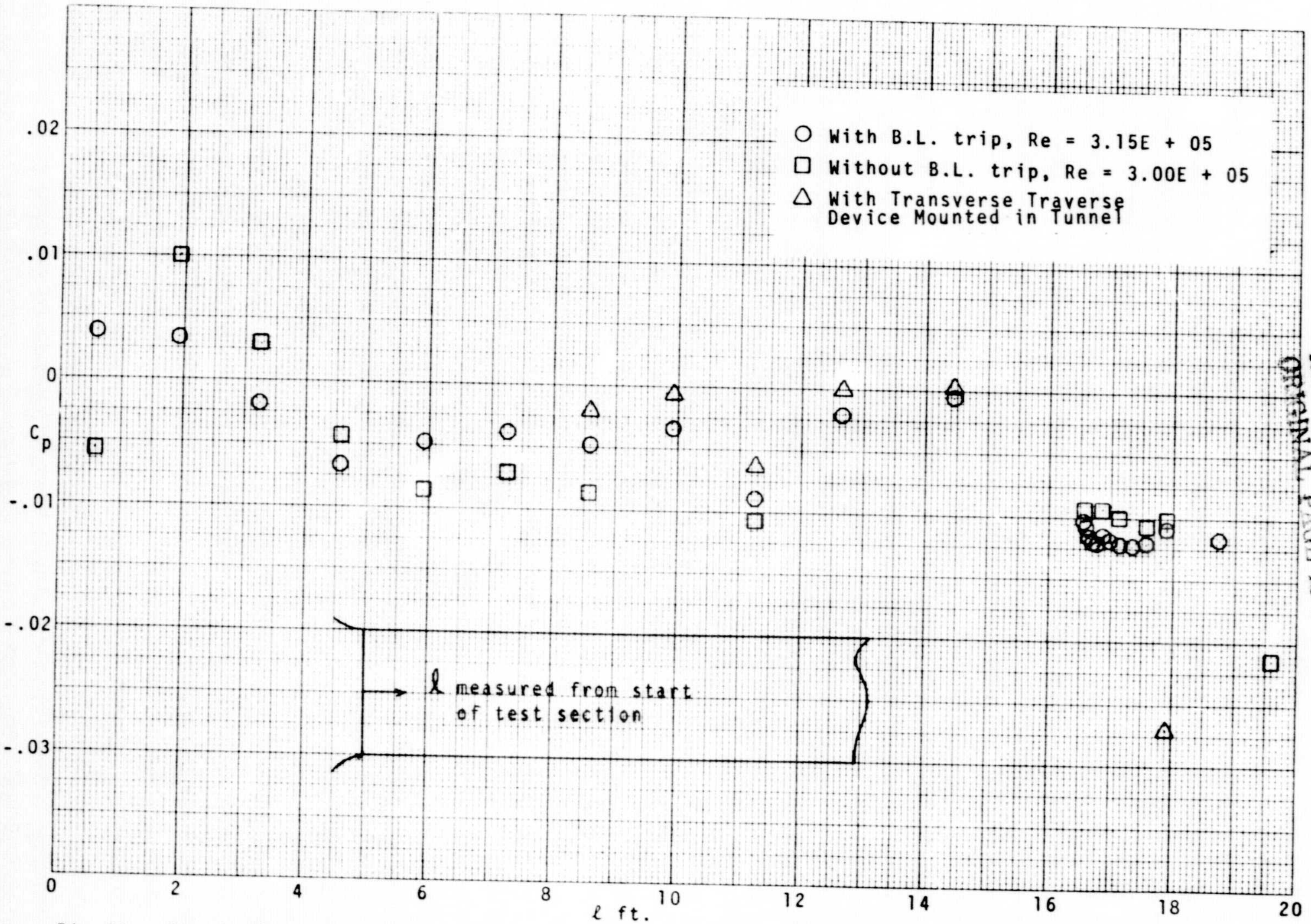

Fig.18 Static Pressure Distribution in the 2-D Test Section

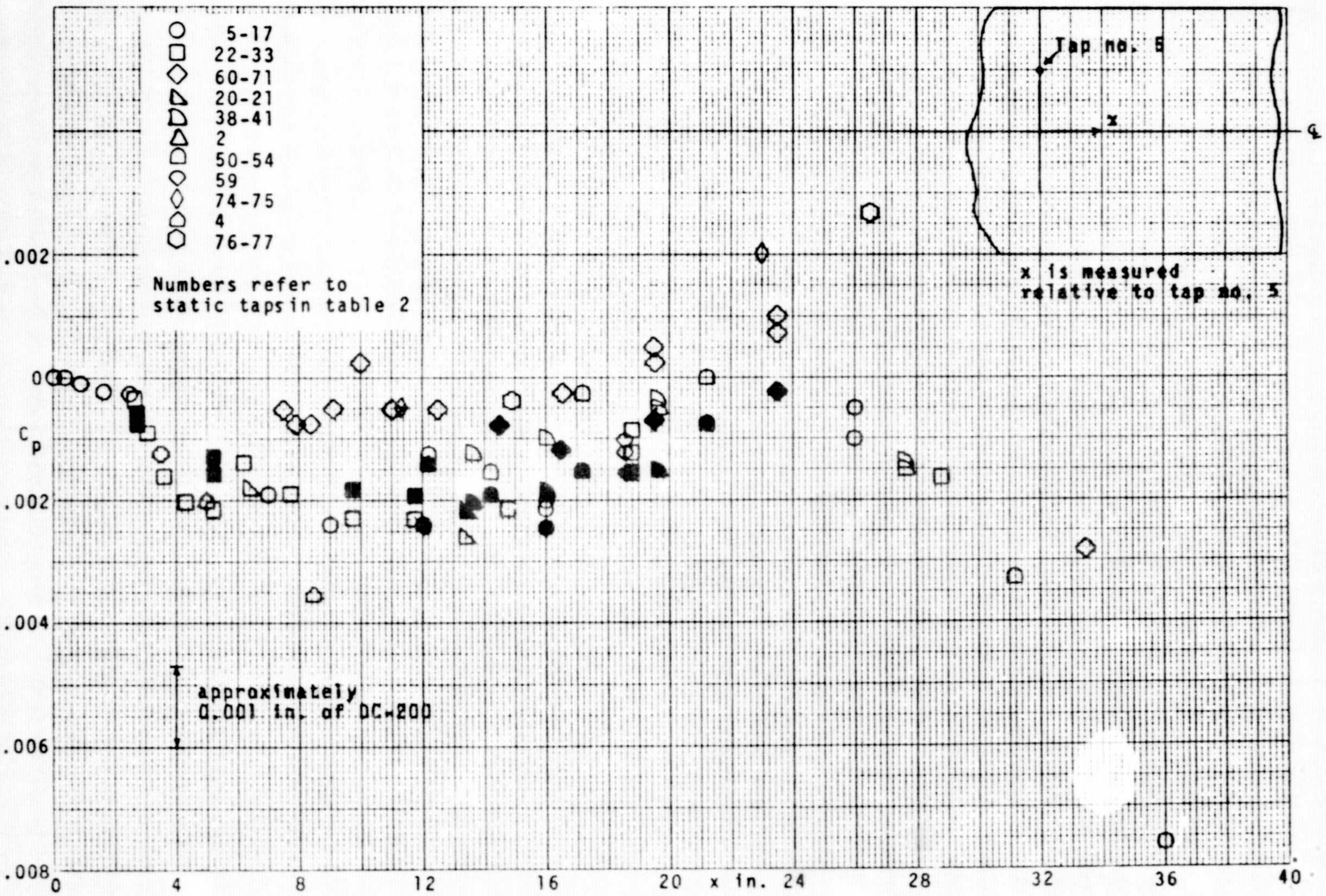

Fig.19 Static Pressure Distribution on Aluminum Insert (2-D)

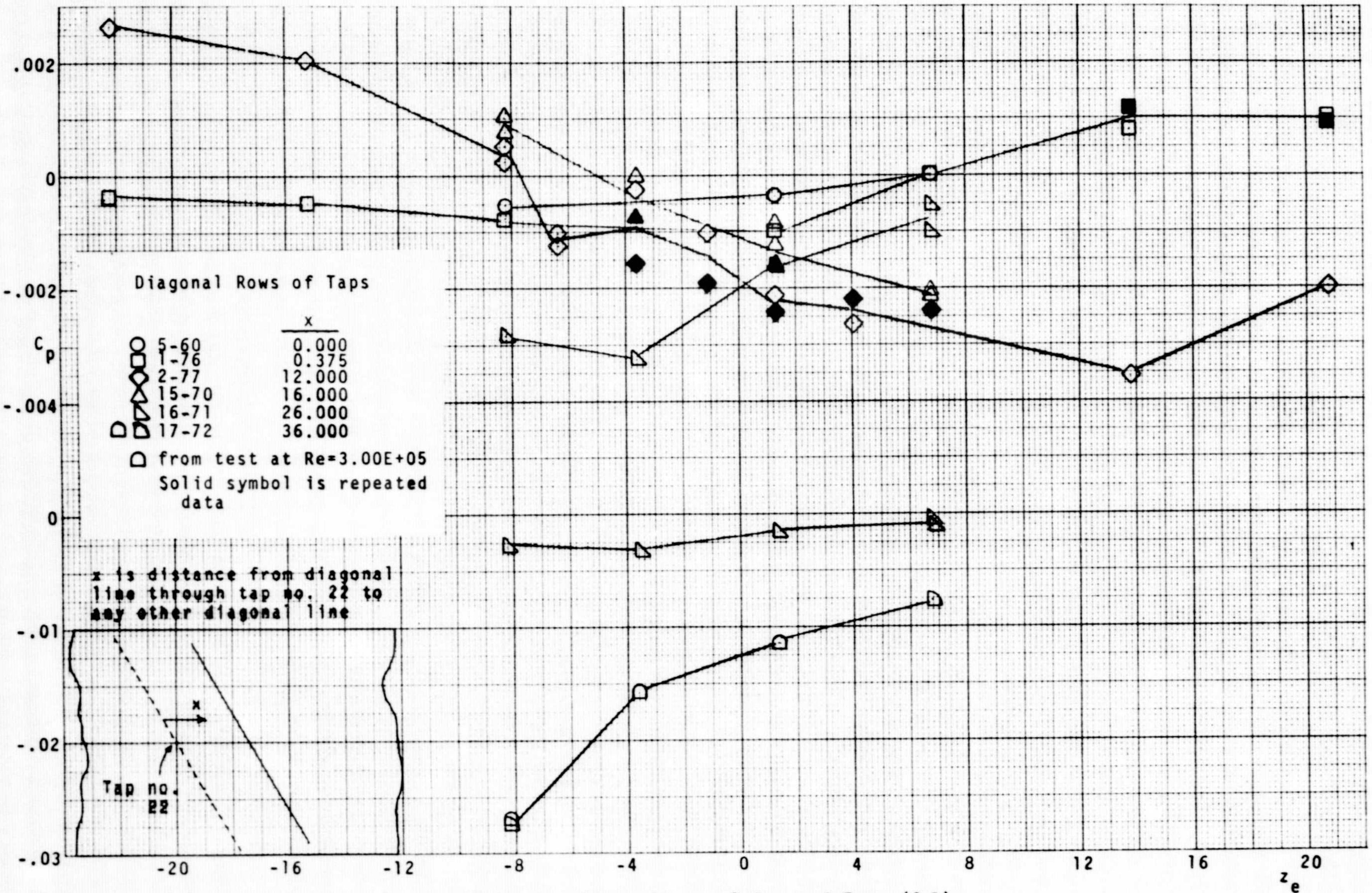

Fig. 20 Static Pressure on Aluminum Insert - Along Diagonal Rows of Taps (2-D)

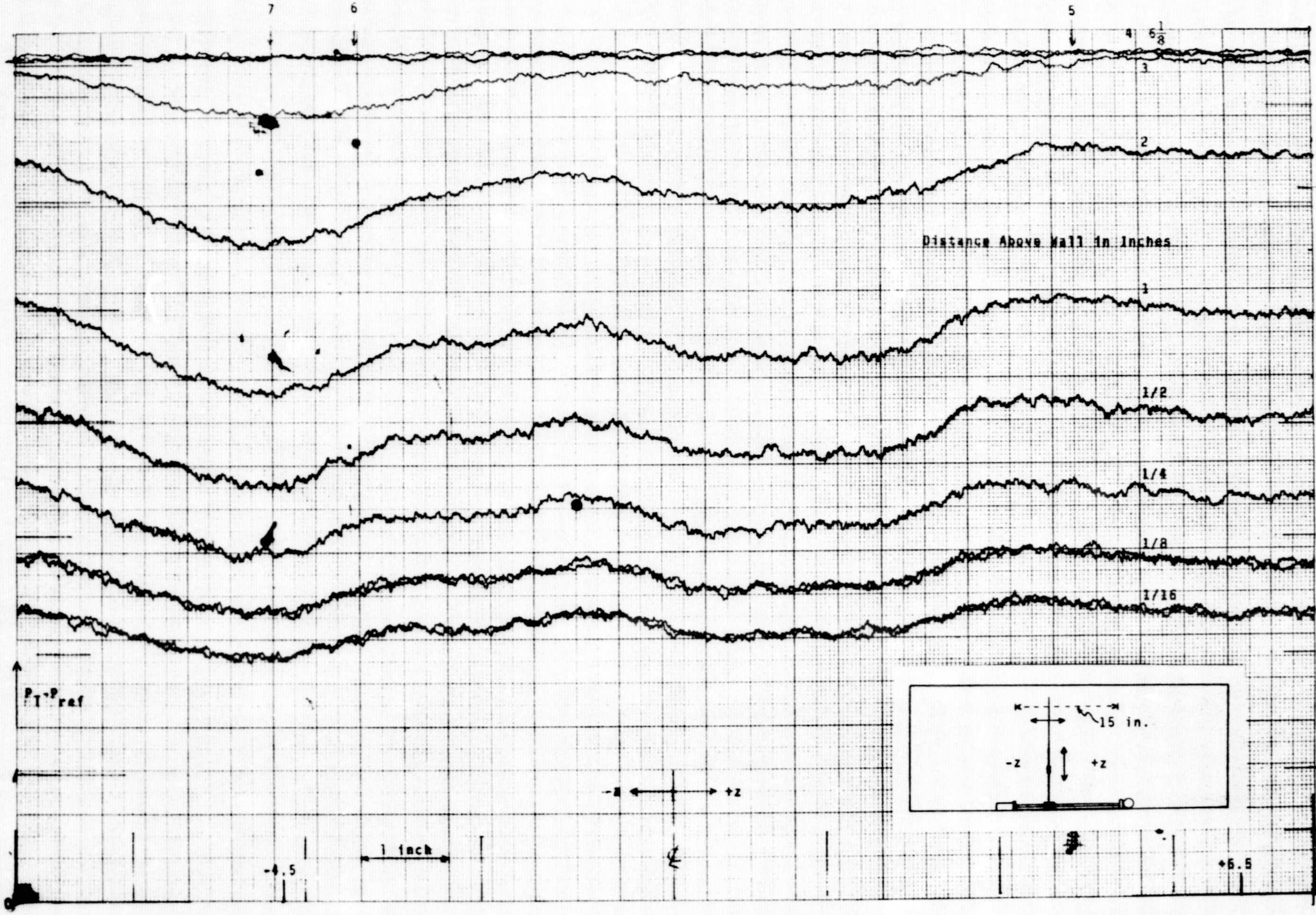

Fig. 21a   3-Tube Probe (Total) Surveys at ℓ = 18 ft

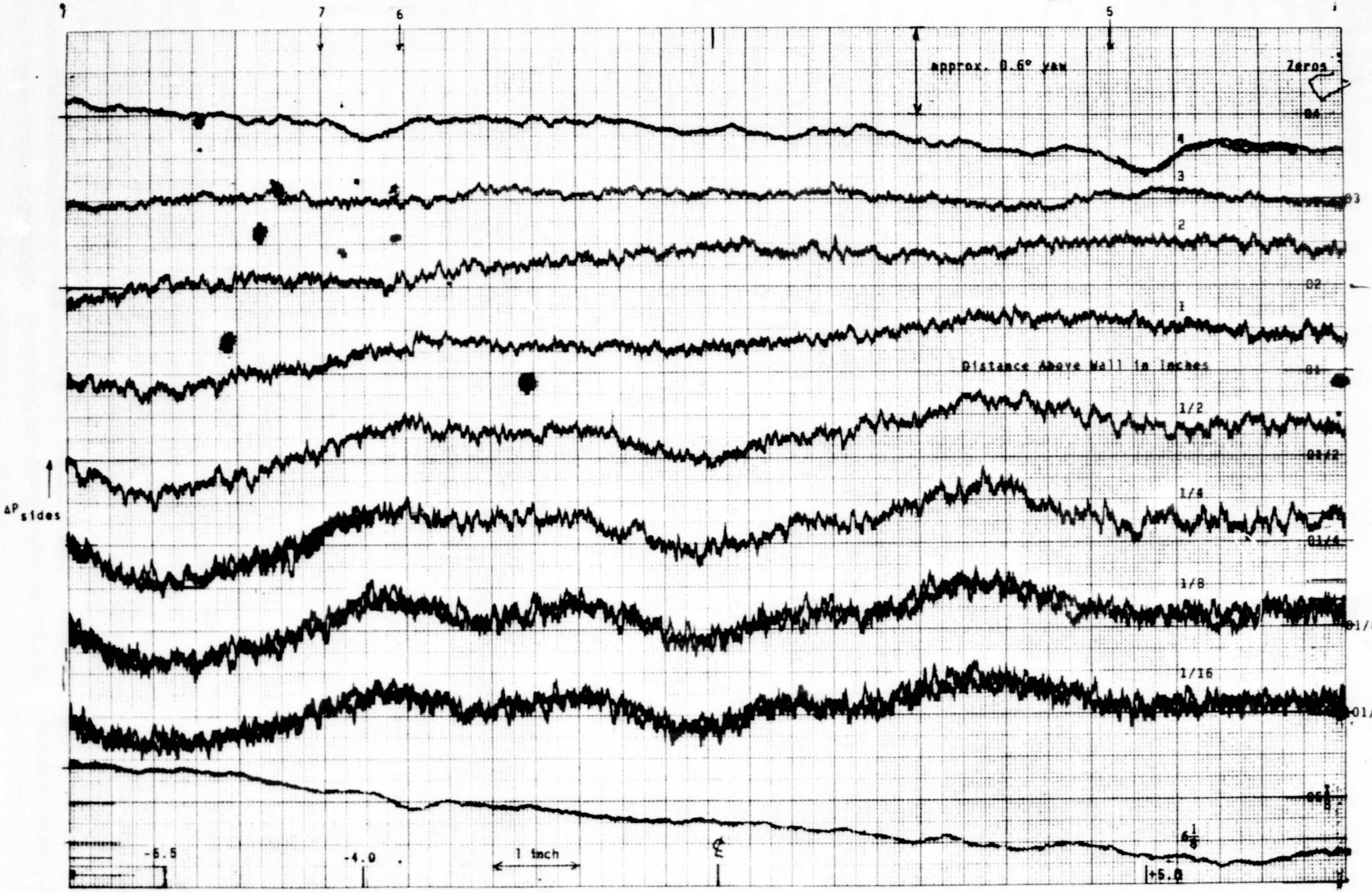

Fig. 21b 3-Tube Probe (Yaw) Surveys at λ = 18 ft

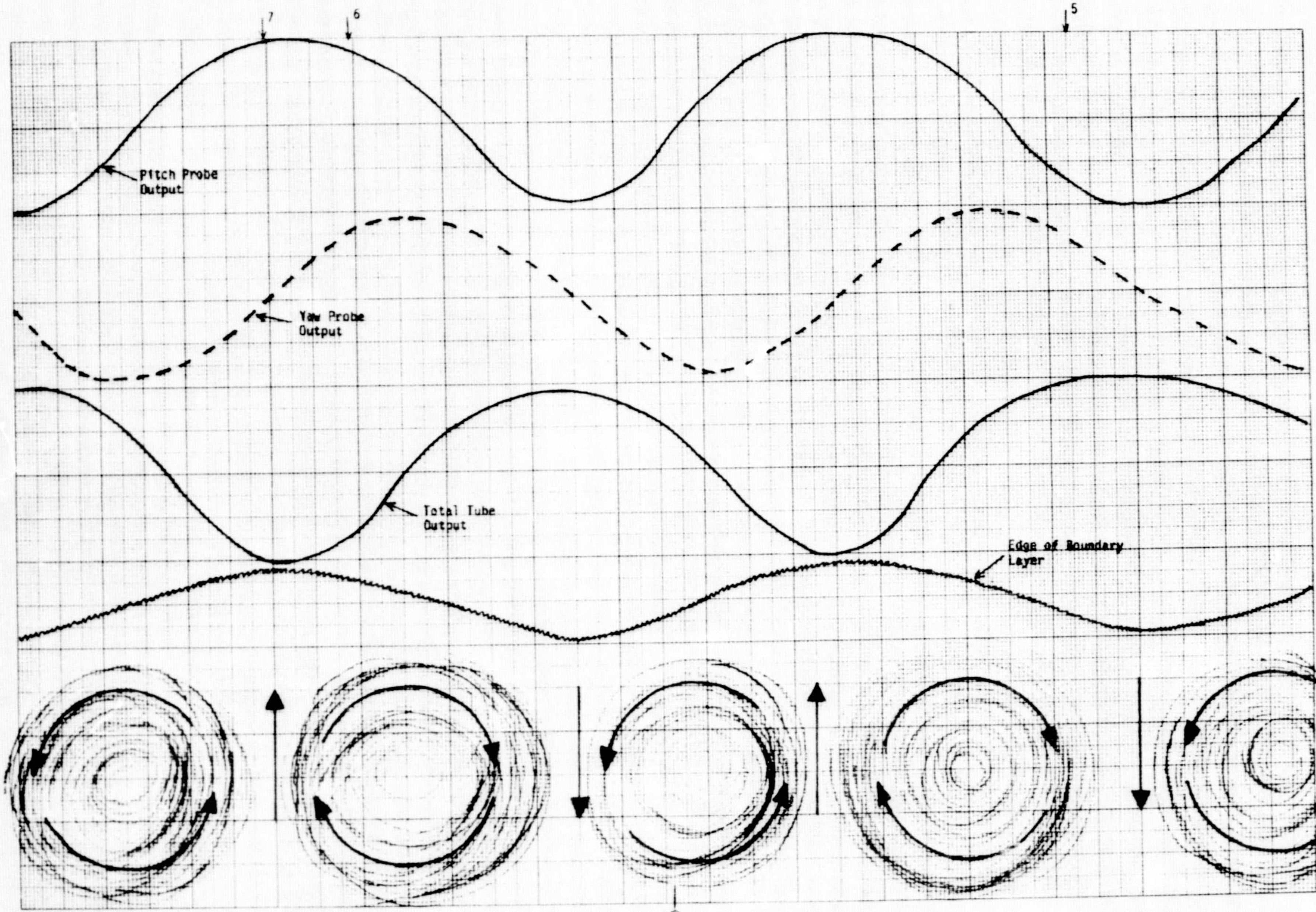

Fig.22 Possible Vortex Flow In The Nonuniform Turbulent Boundary Layer (based on ref. 43)

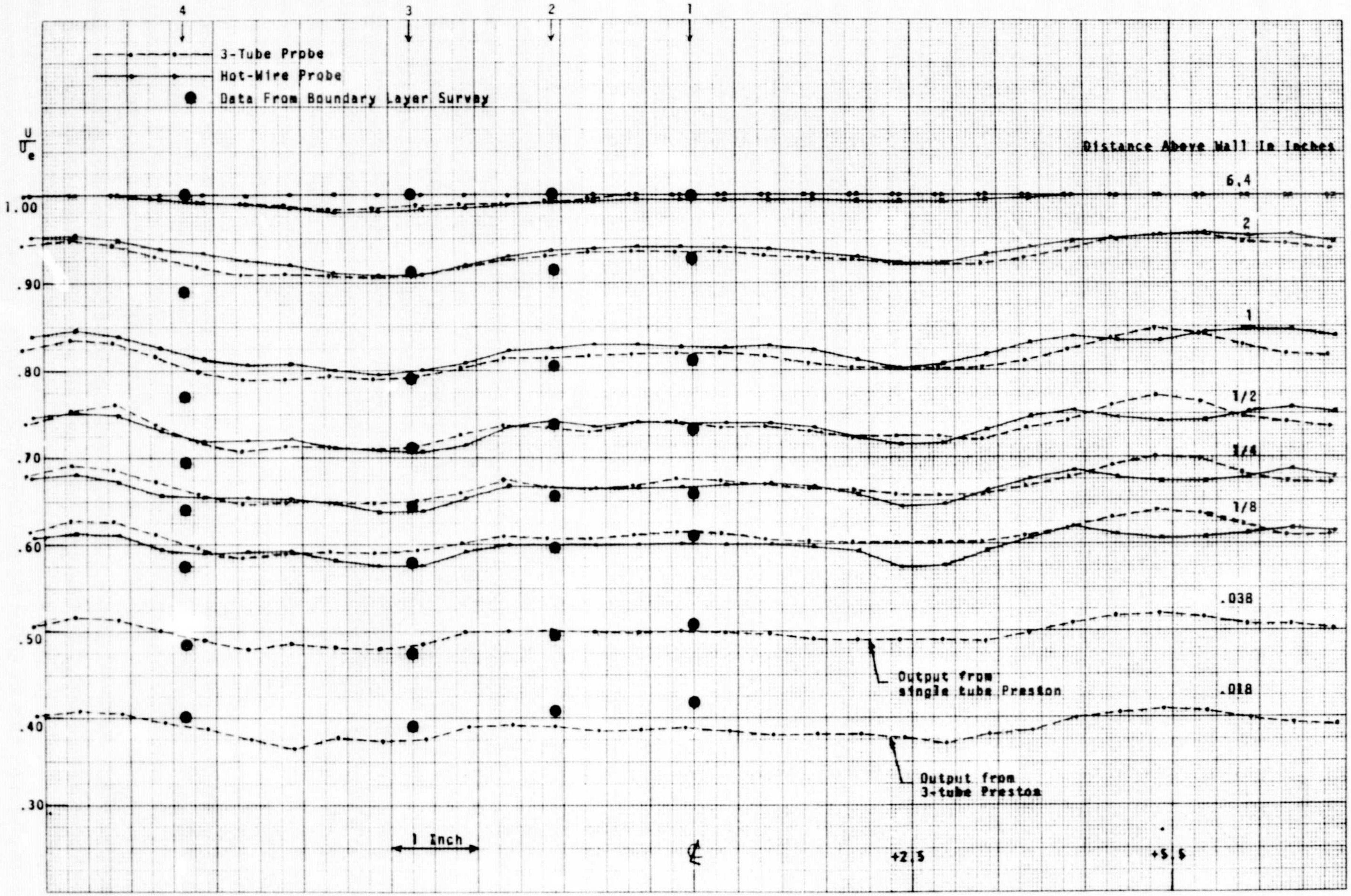

Fig. 23a 3-Tube Probe (Total) and Hot-Wire Probe Surveys at ℓ = 18 ft, Re = 3.00E+05 ft^{-1}

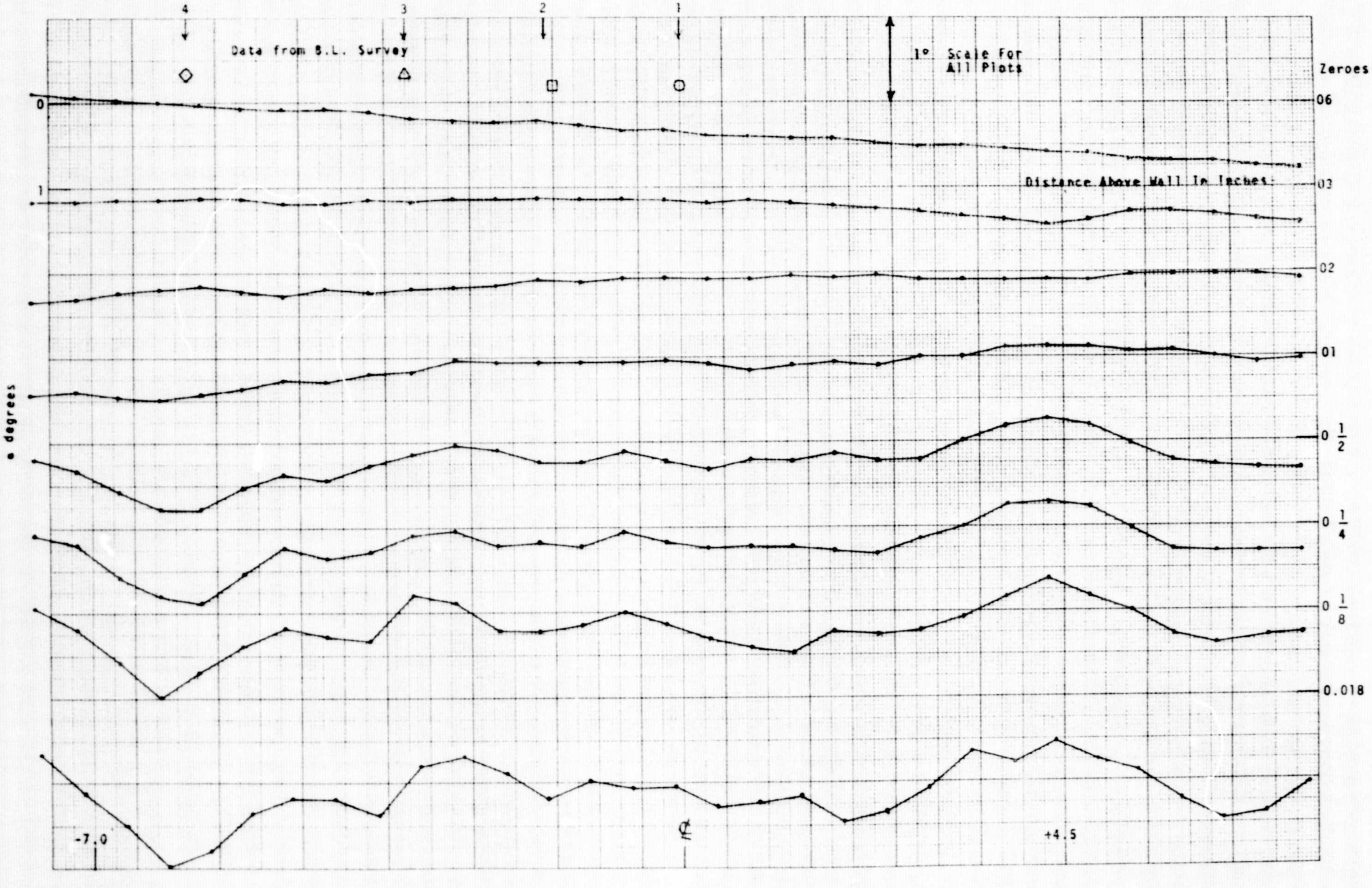

Fig.23b 3-Tube Probe (Yaw) Surveys at ℓ = 18 ft, Re = 3.00E+05 ft^{-1}

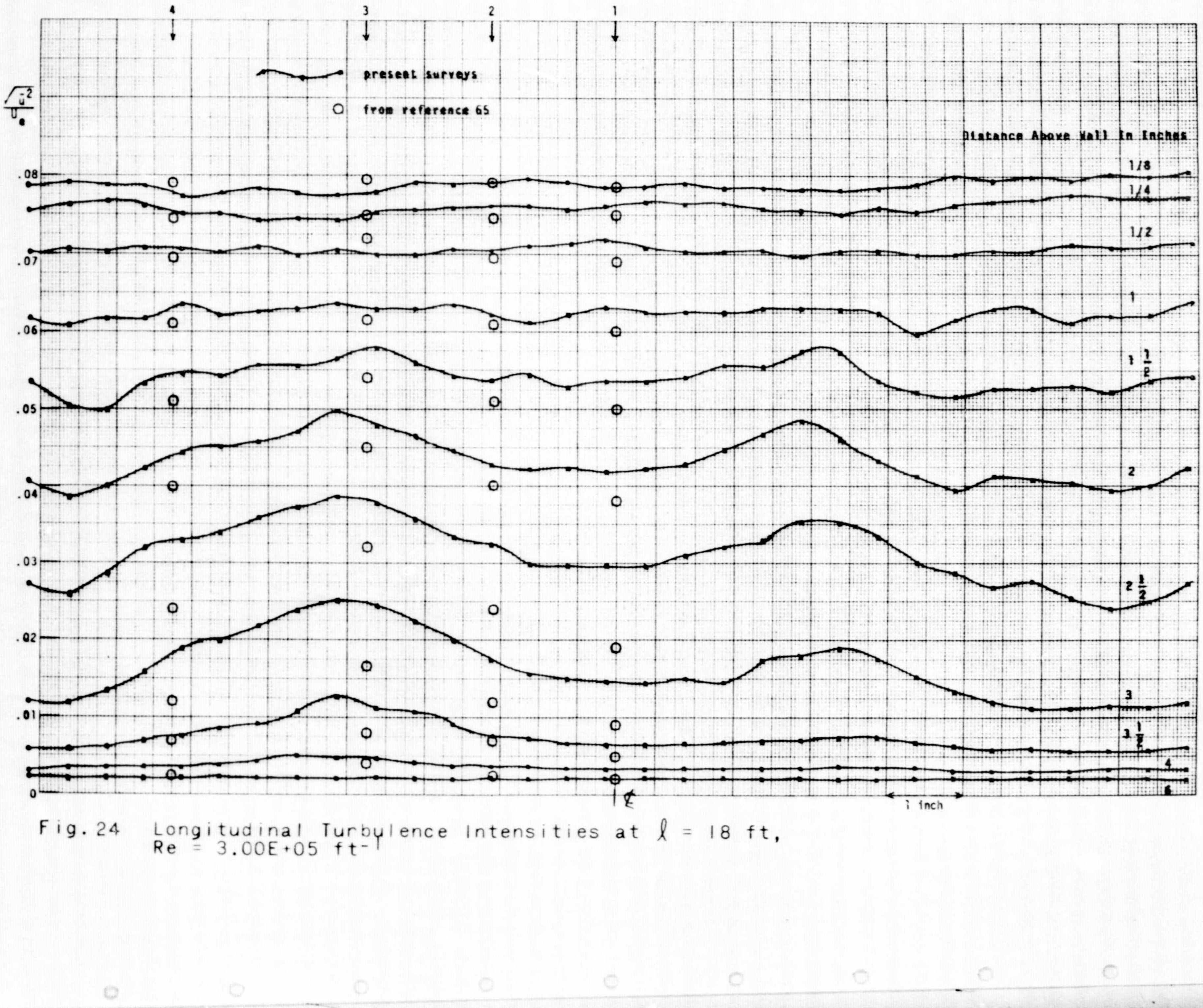

Fig. 24 Longitudinal Turbulence Intensities at ℓ = 18 ft, Re = 3.00E+05 ft^{-1}

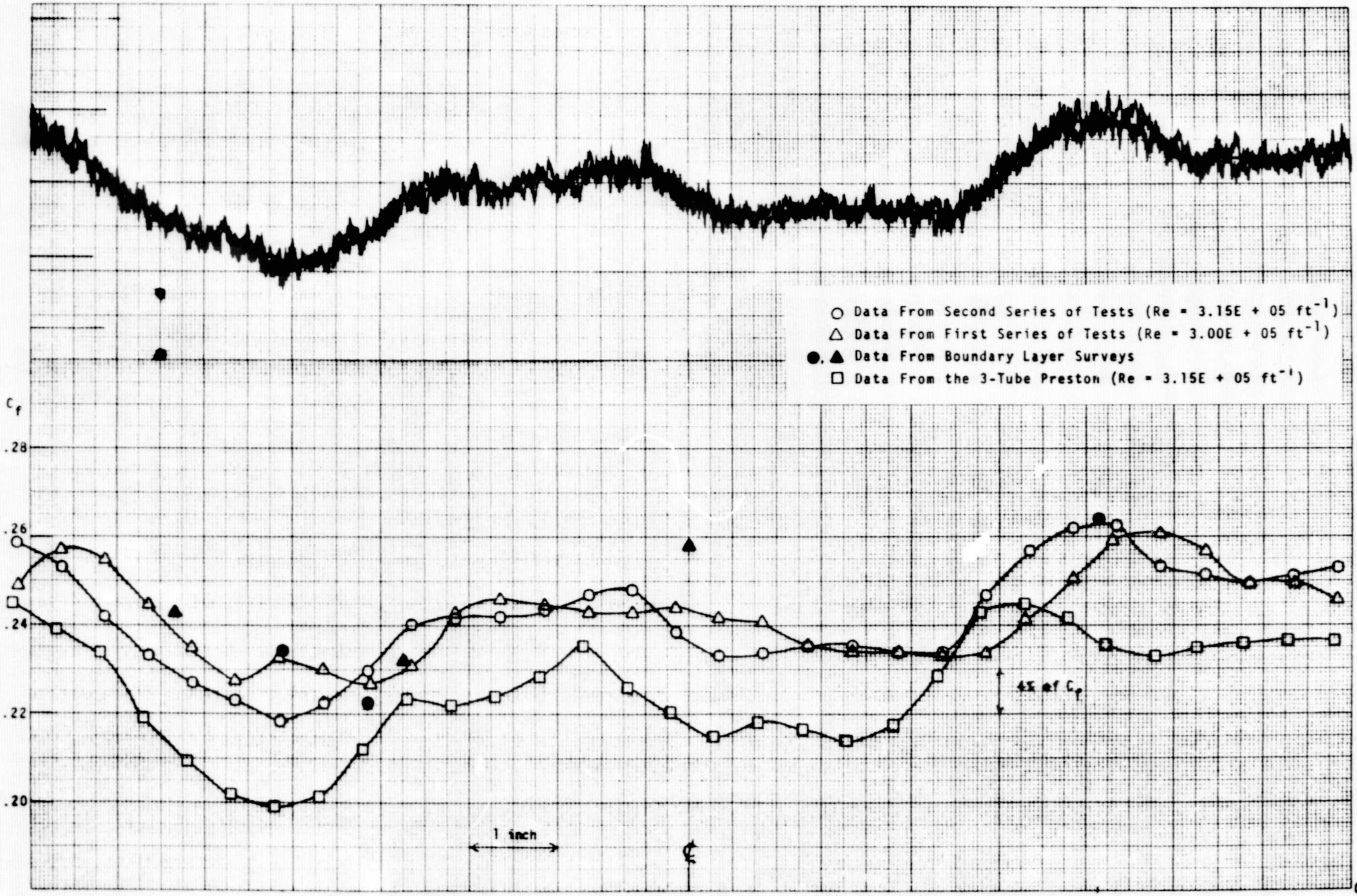

Fig.25 Transverse Variations of C_f at ℓ = 18 ft

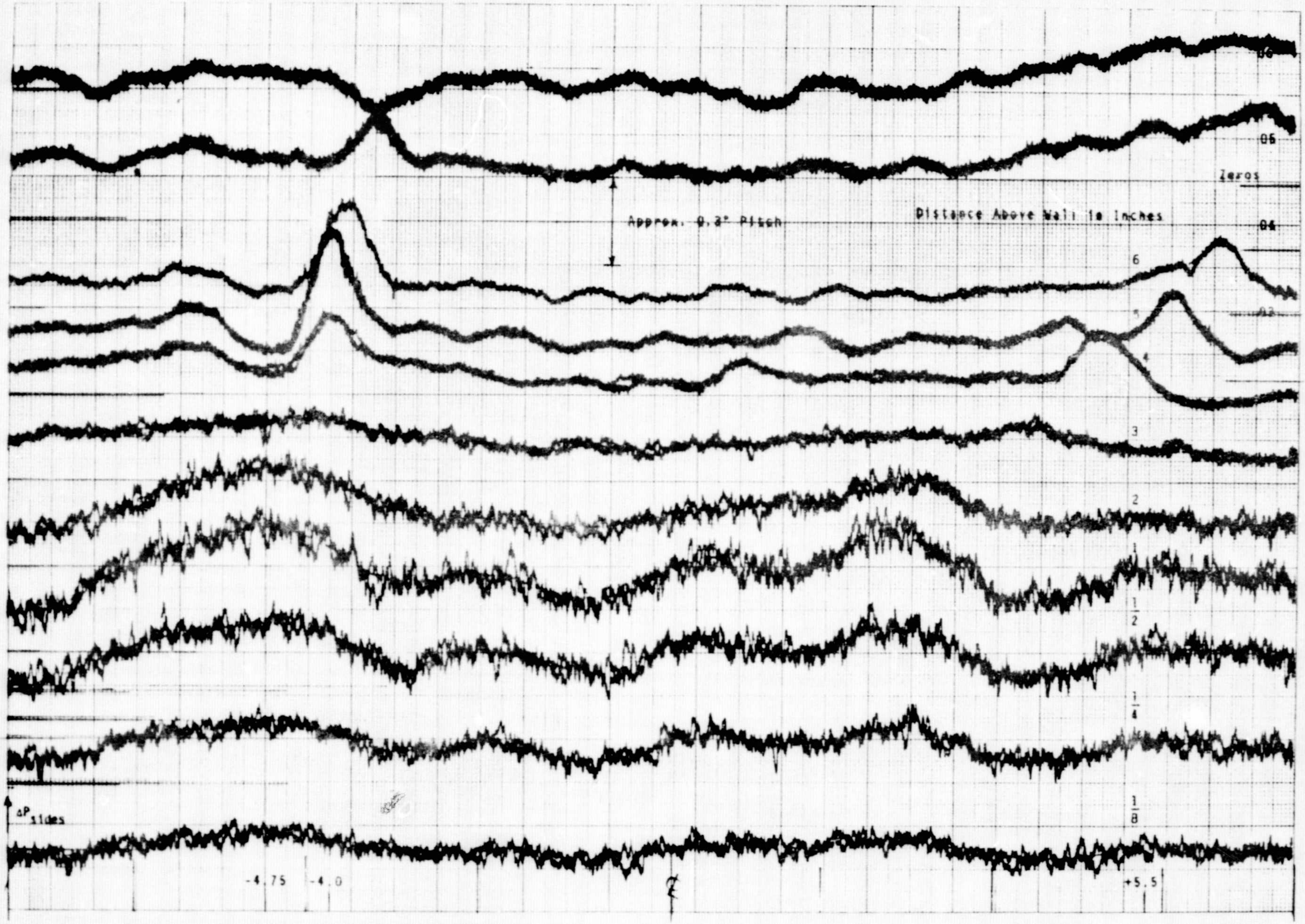

Fig. 26 Pitch Probe Surveys at ℓ = 18 ft

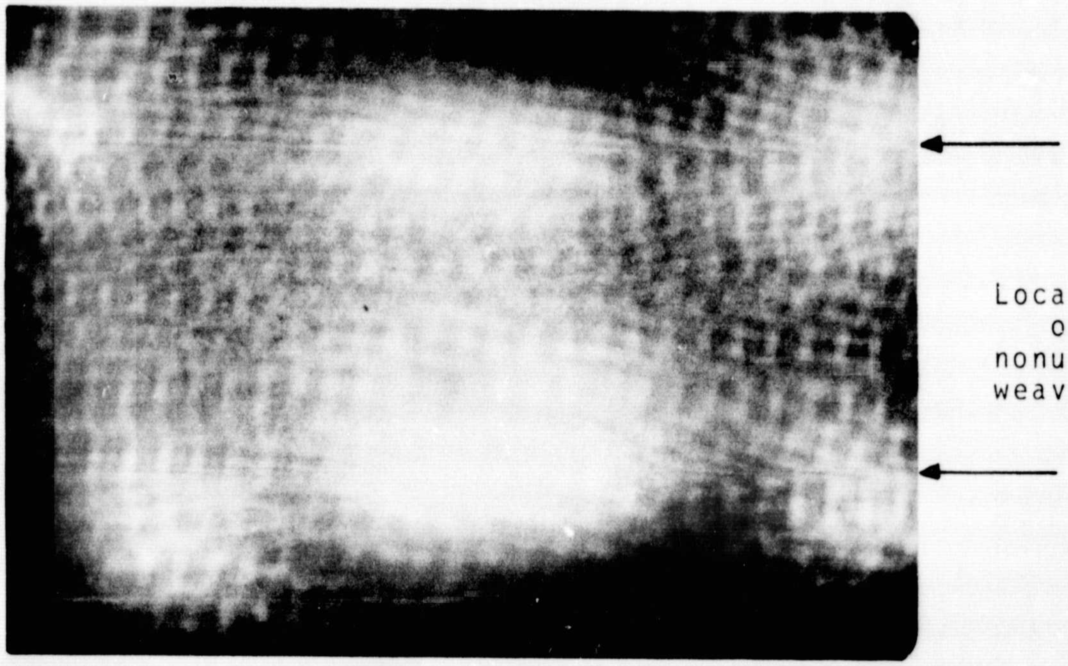

a.) Full View of screen from inside contraction inlet

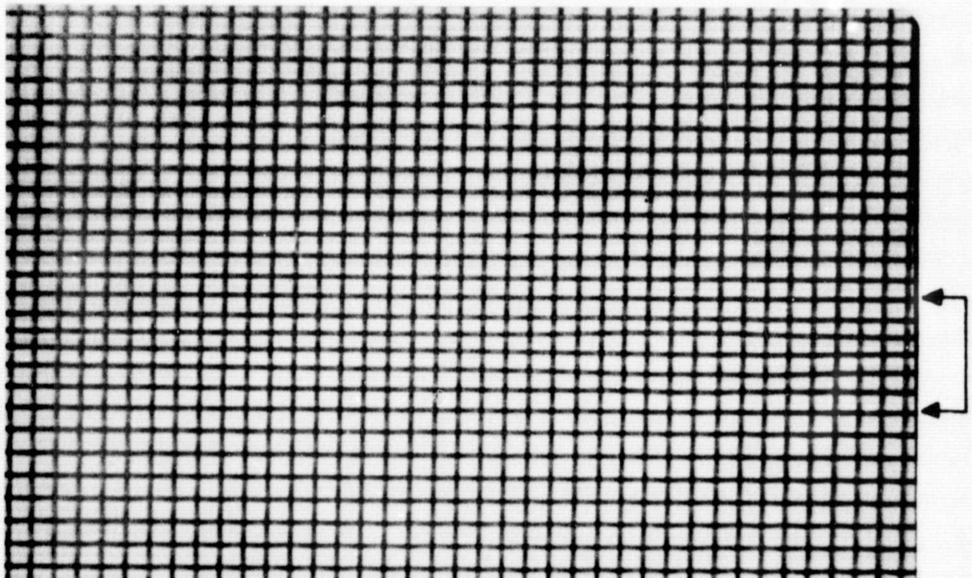

b.) Close-up of nonuniform weave

Fig. 27 Nonuniformities In The Inlet Damping Screen

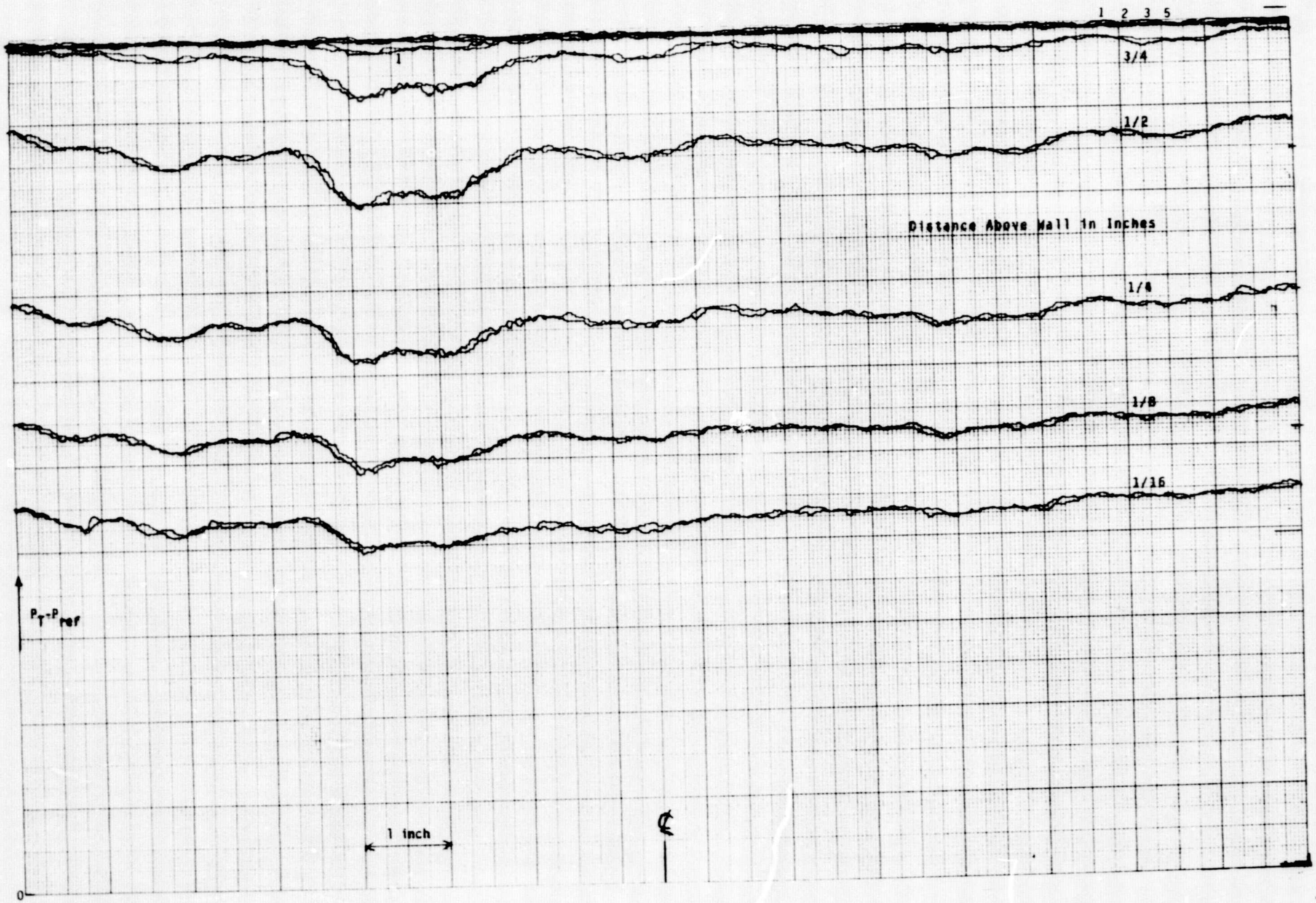

Fig.28a 3-Tube (Total) Surveys at $\ell = 34$ in.

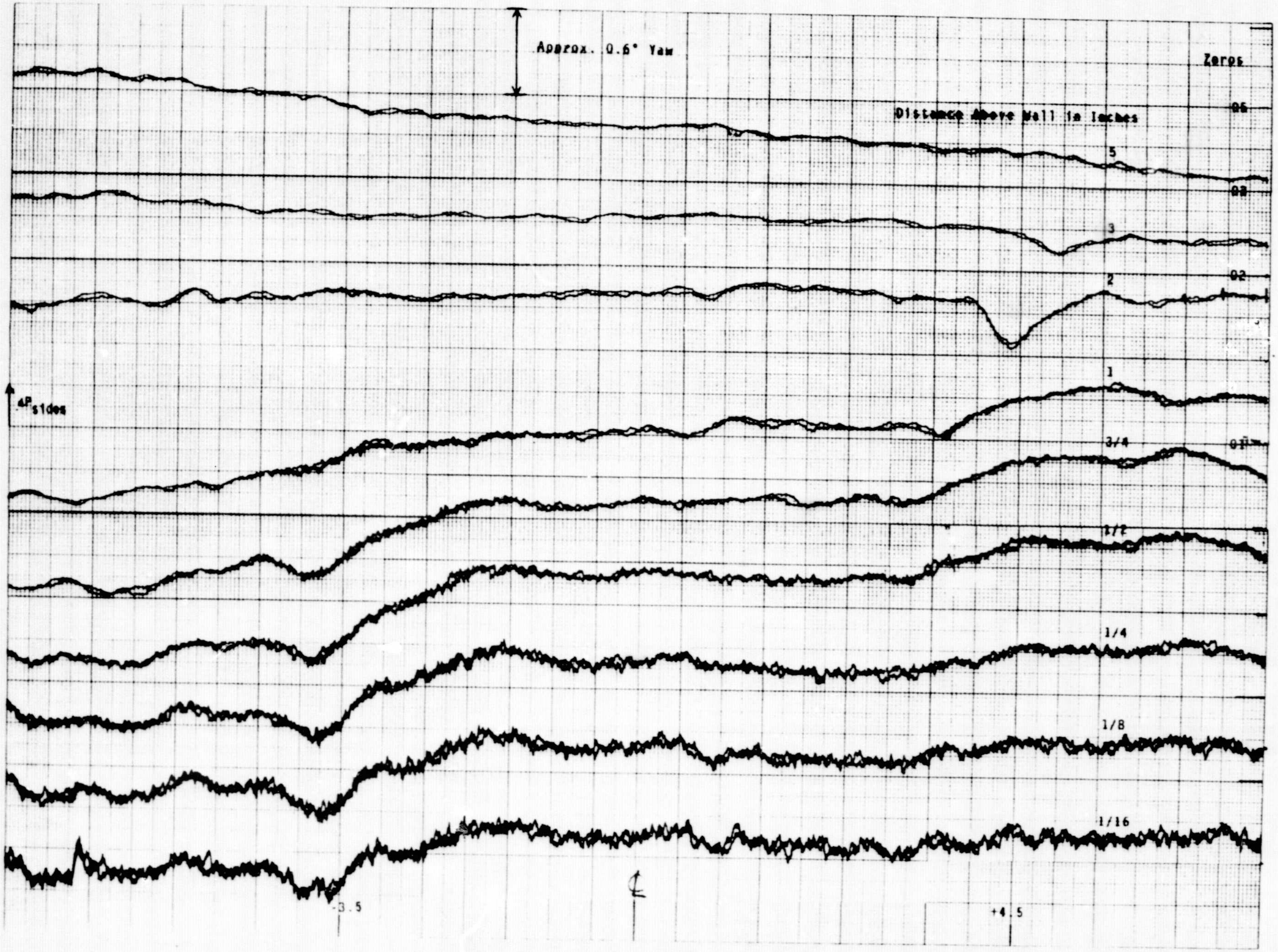

Fig. 28b 3-Tube (Yaw) Surveys at ℓ = 34 in.

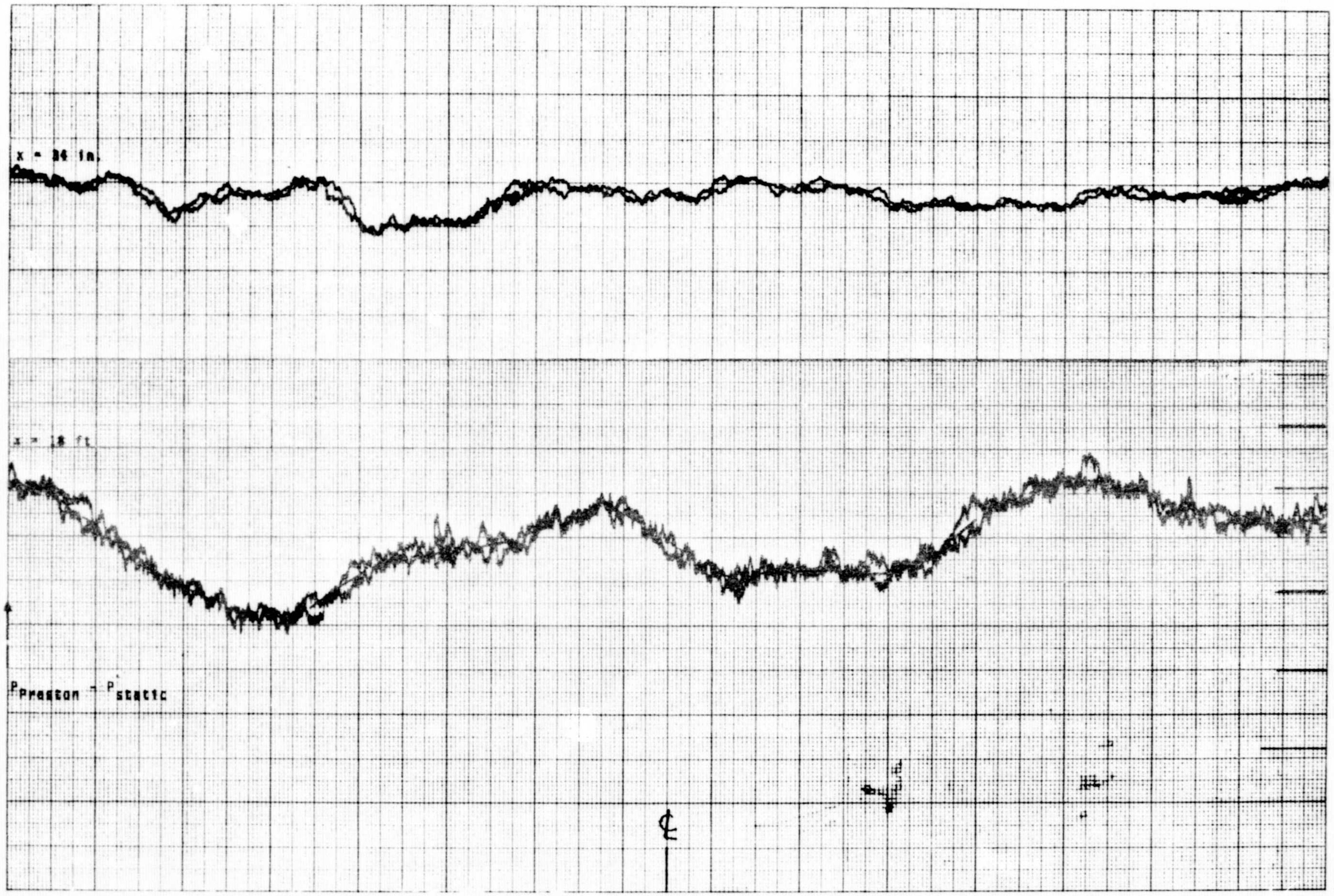

Fig.29 A Comparison of Preston Tube Surveys at ℓ = 34 in. and ℓ = 18 ft

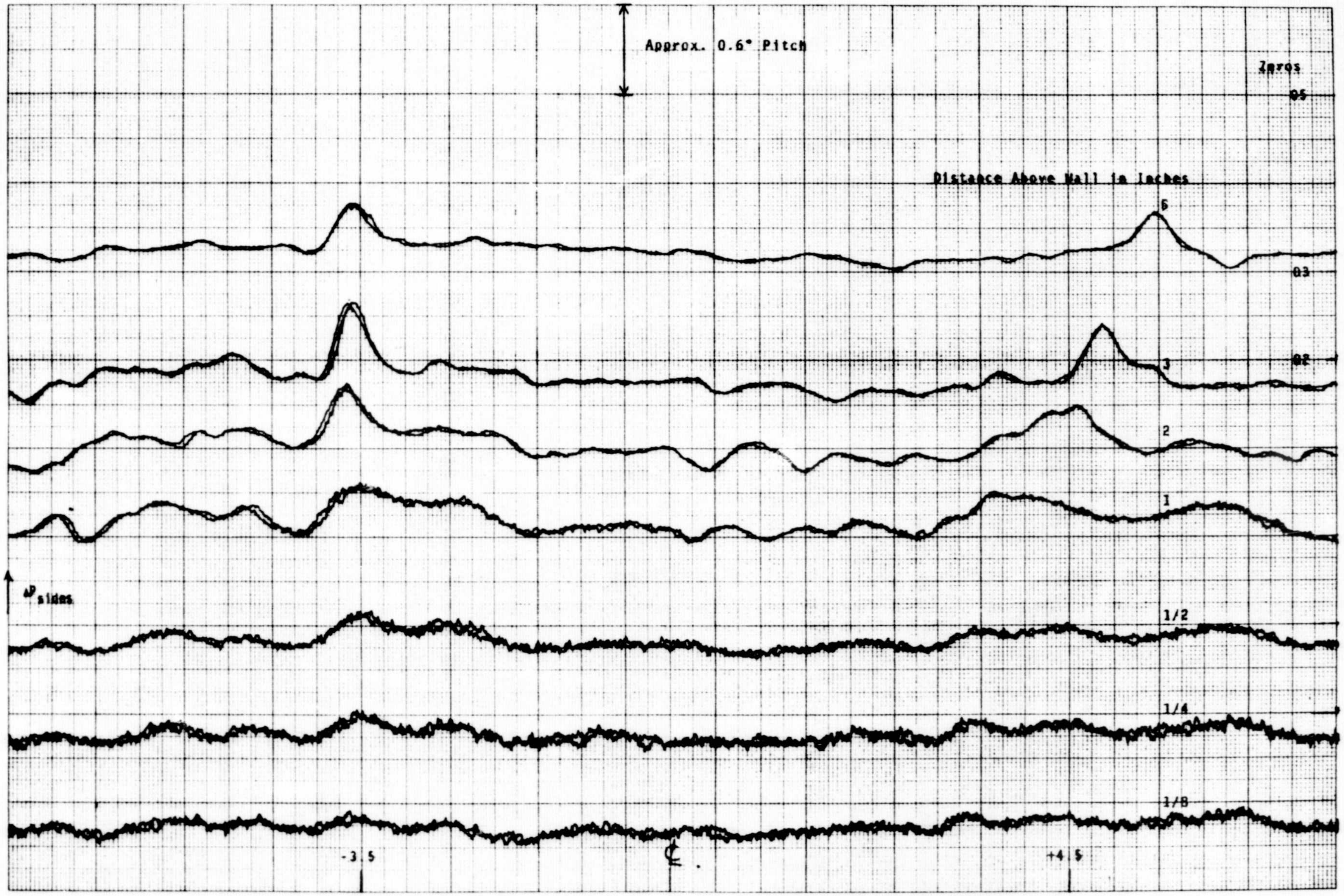

Fig.30 Pitch Probe Surveys at l = 34 in.

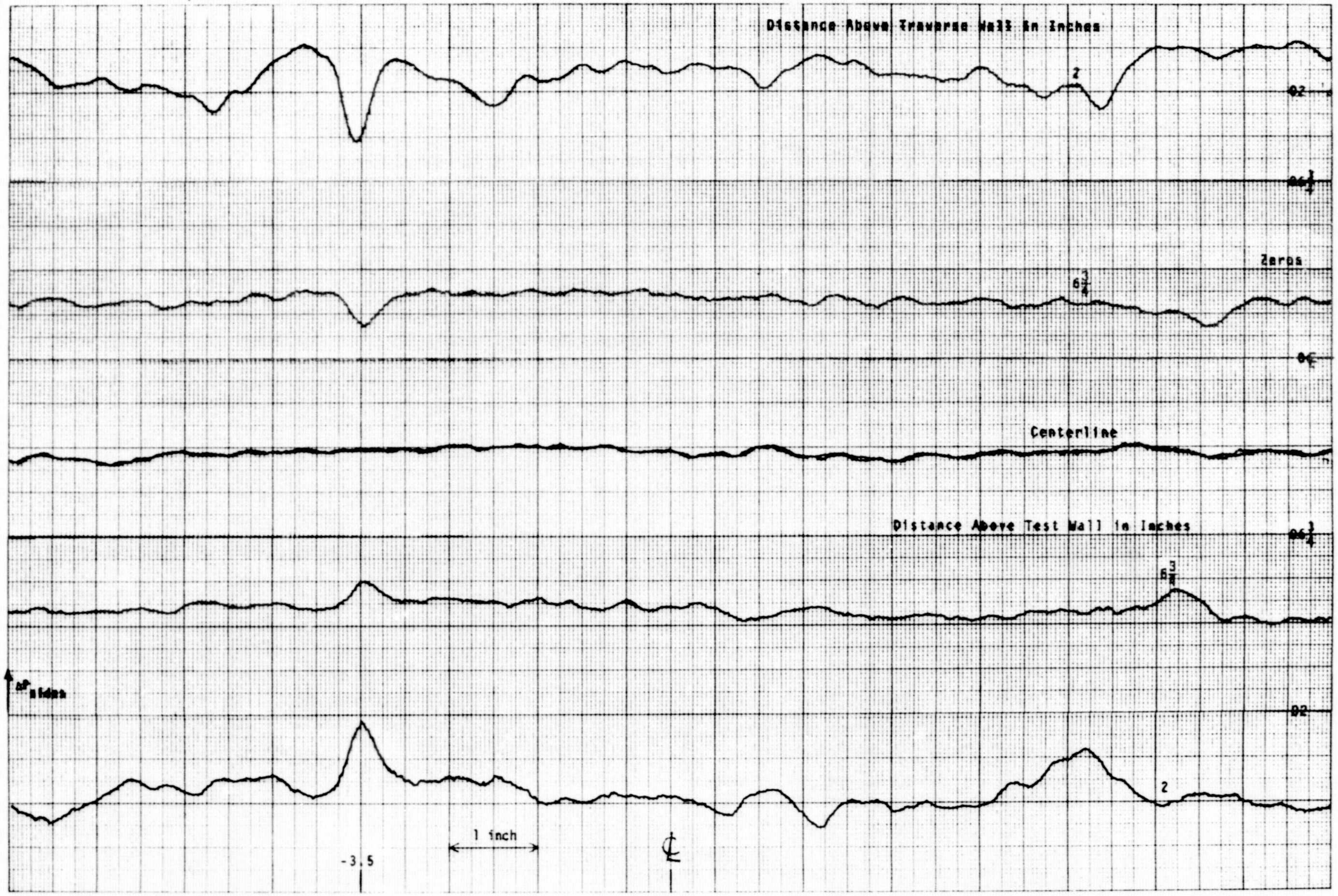

Fig. 31 Pitch Probe Surveys on Both Sides of Test Section at ℓ = 24 in.

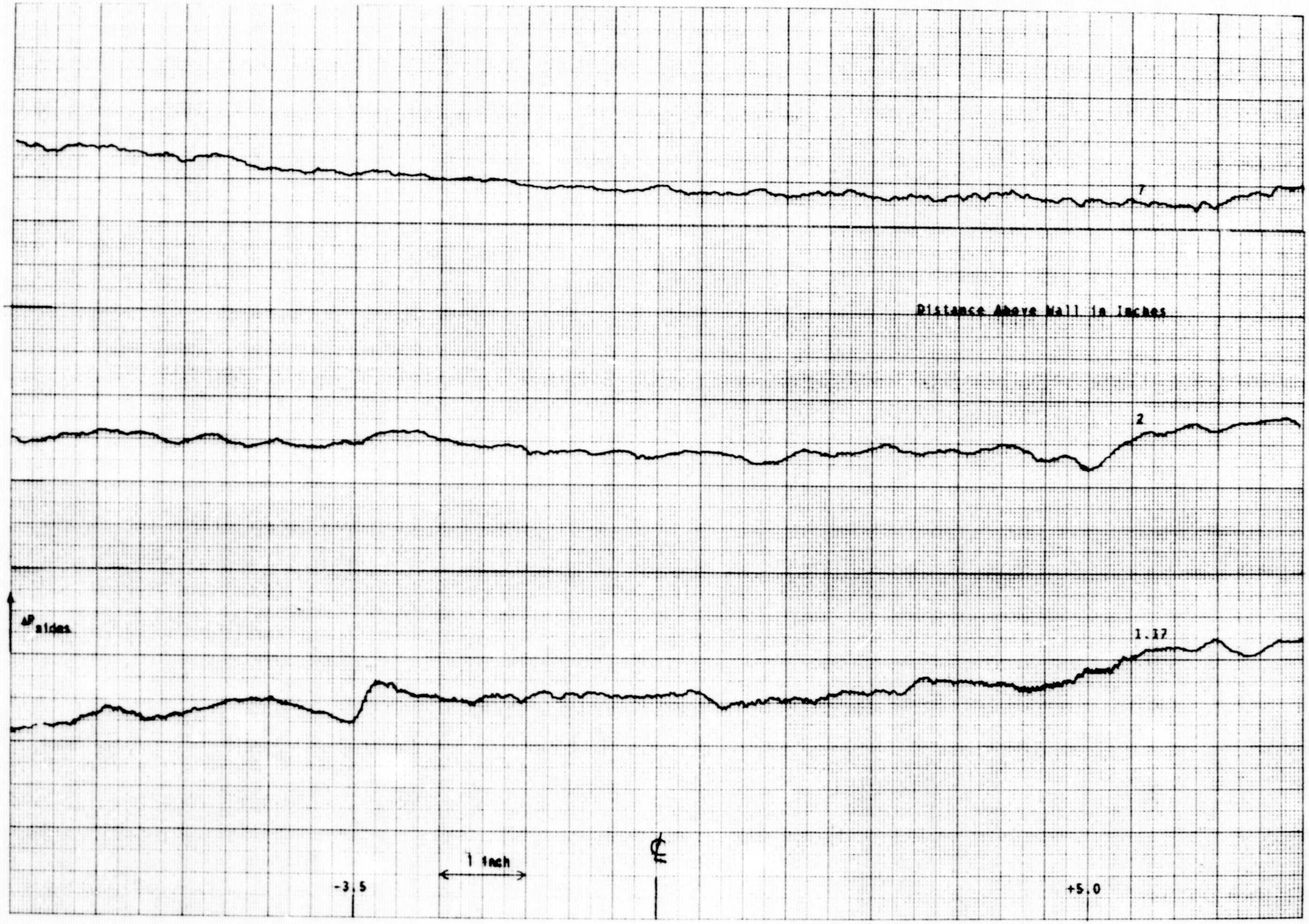

Fig.32 3-Tube Probe (Yaw) Surveys Above the Traverse Wall at ℓ = 24 in.

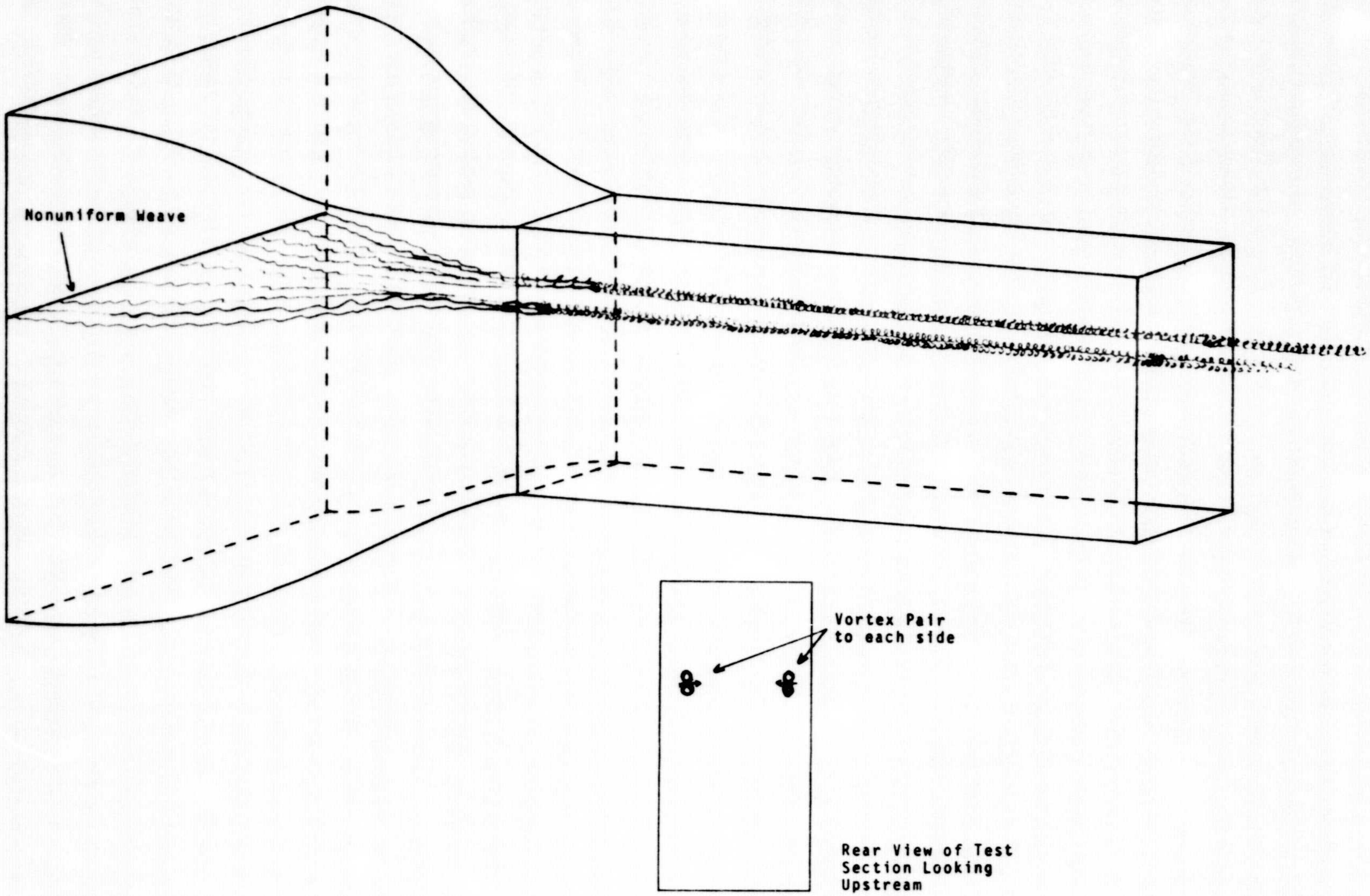

Fig. 33 Possible Vortex Flow Produced By the Nonuniform Weave In the Inlet Damping Screens

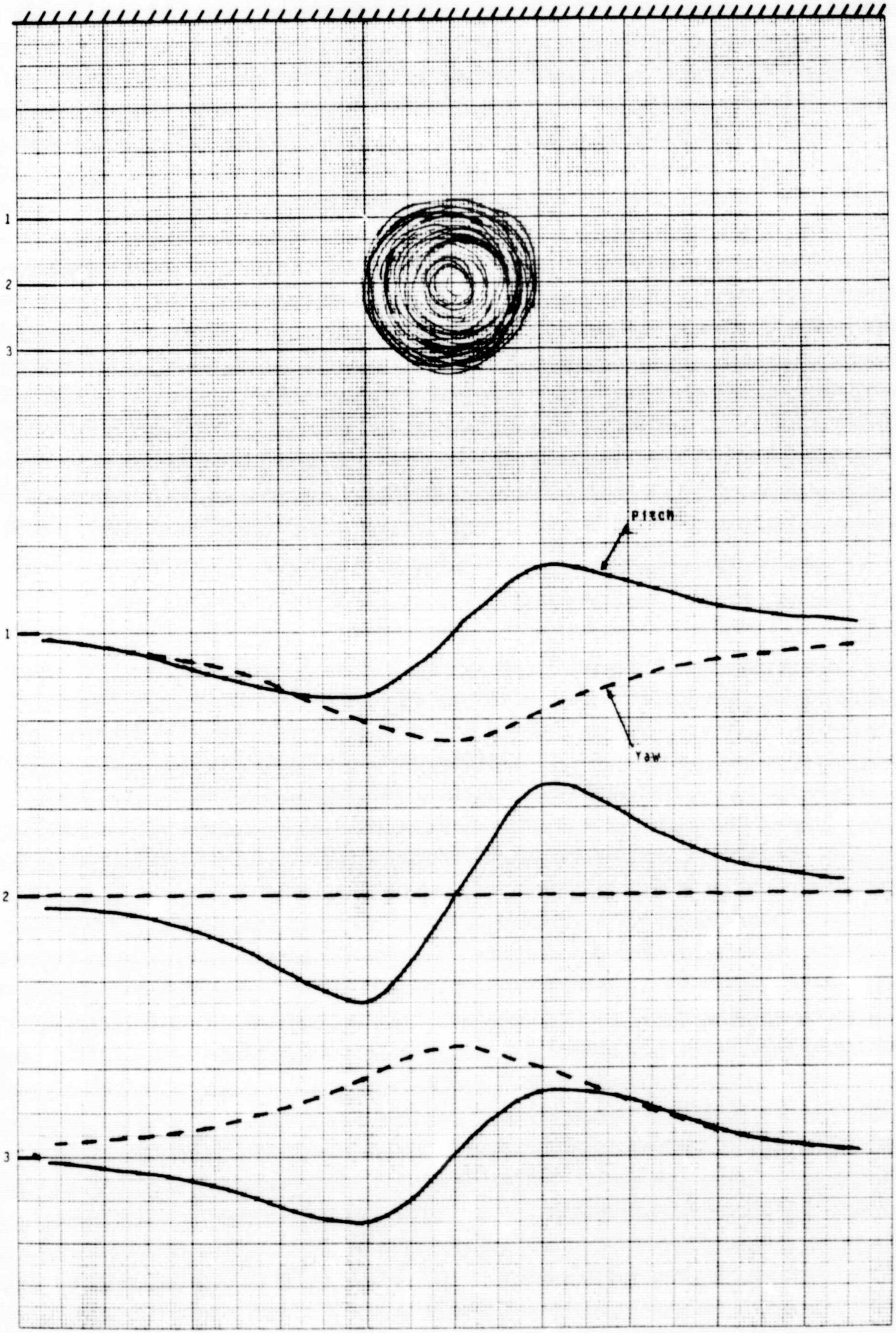

Fig.34a Possible Vortex Flow Model - Single Vortex Above Each Wall

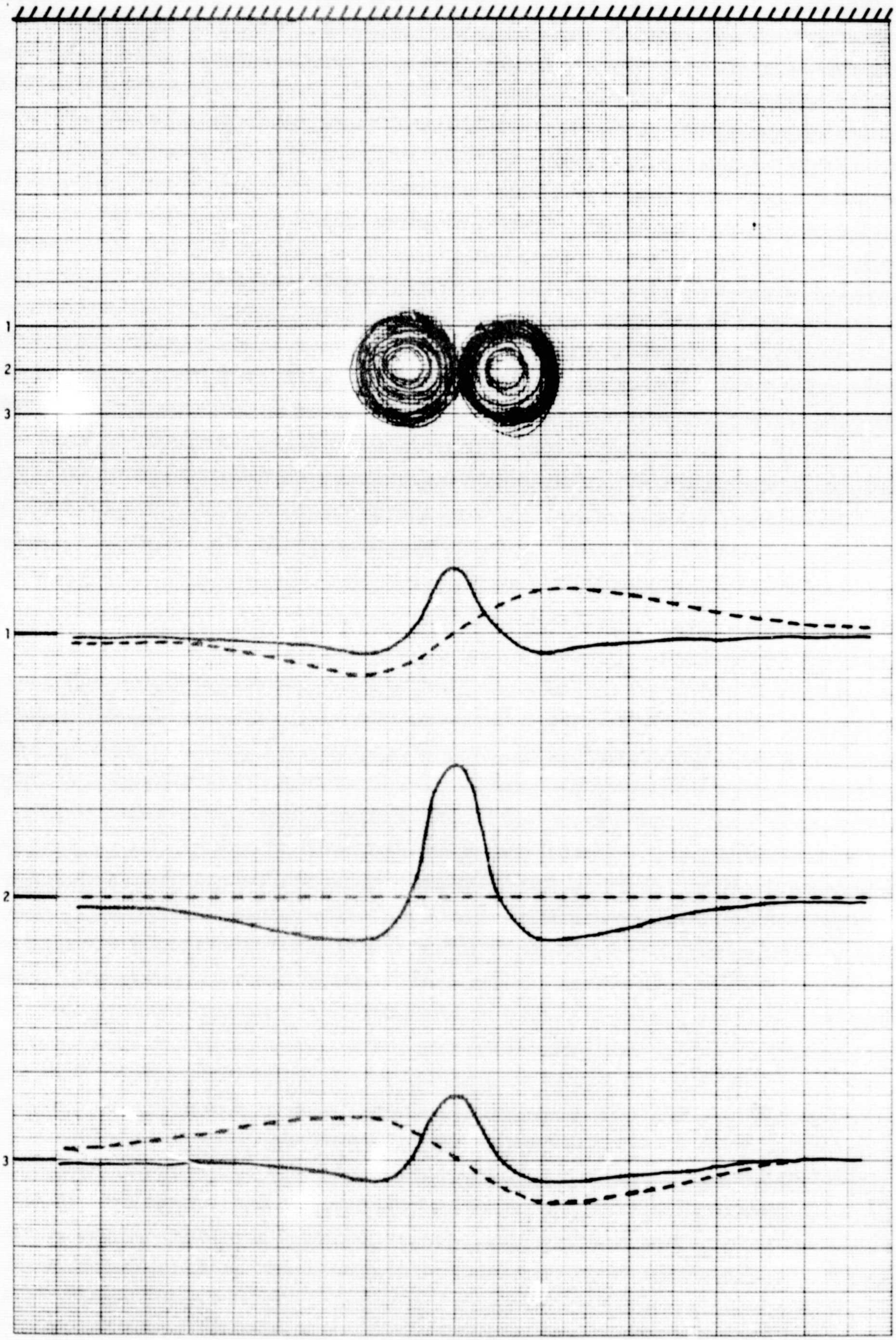

Fig. 34b Possible Vortex Flow Model - Vortex Pair Above Each Wall

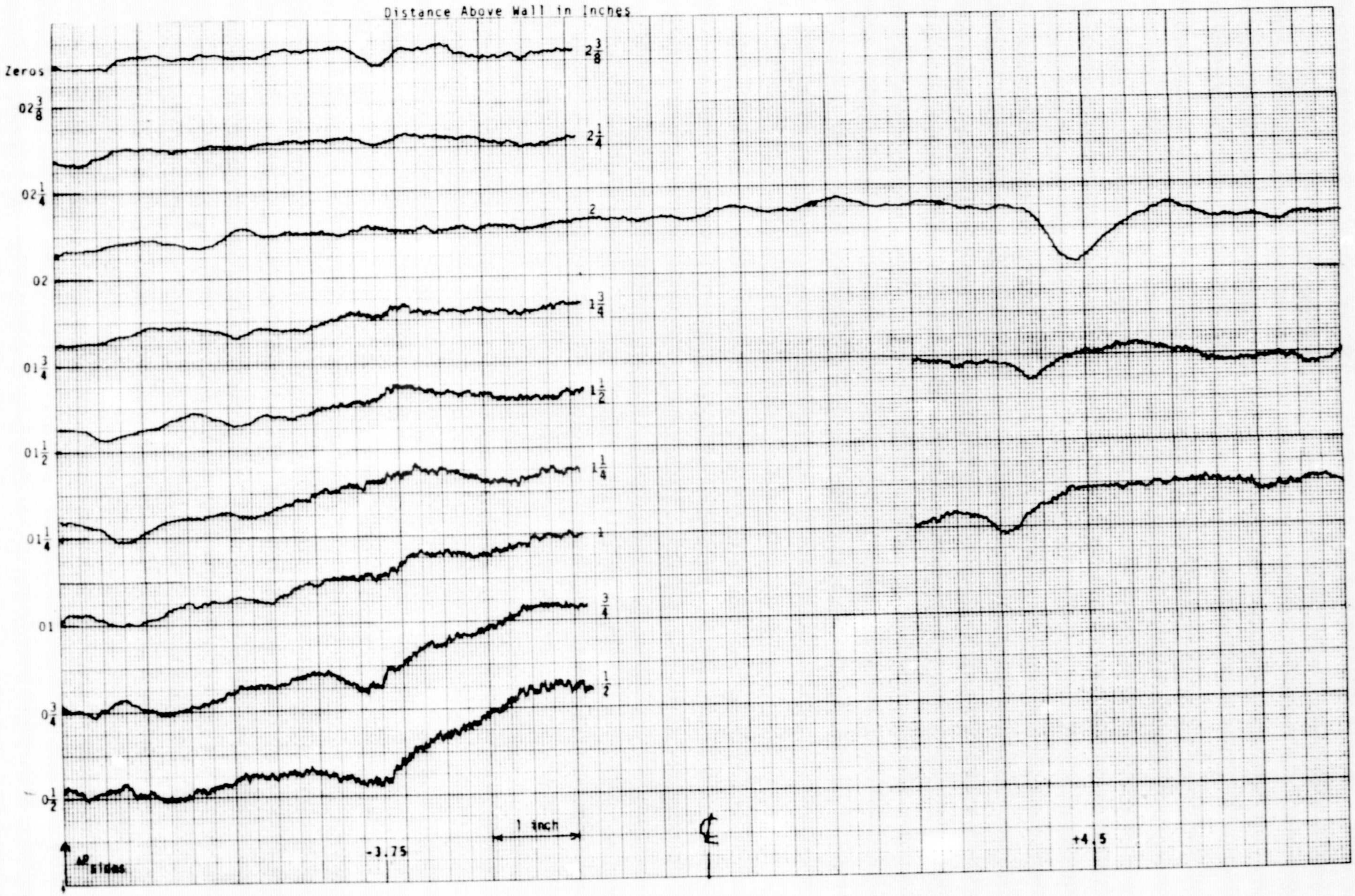

Fig. 35 3-Tube Probe (Yaw) Surveys in Search of Vortex Flow

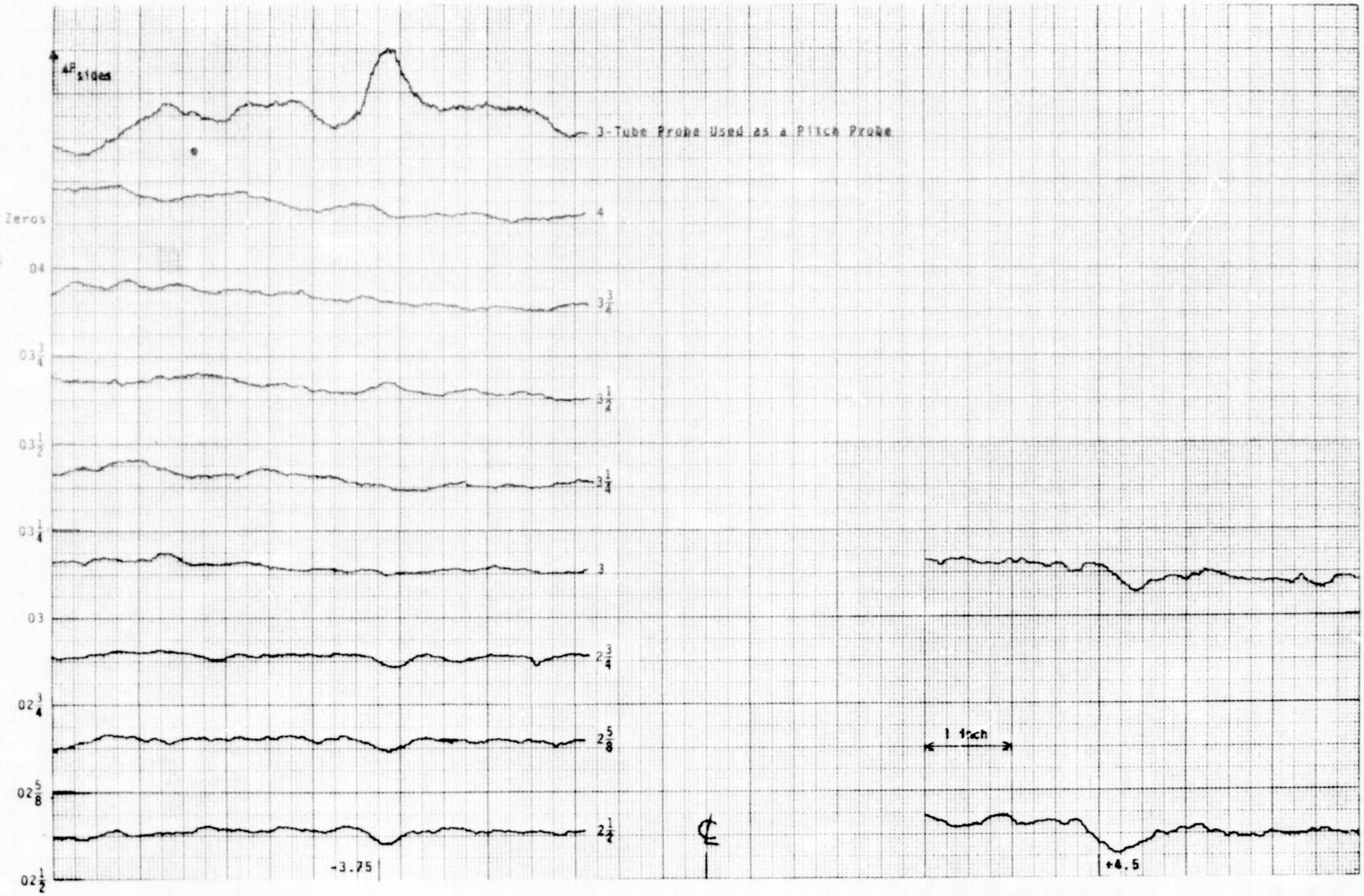

Fig.35 Continued

Fig.36 Effects of a 0.05 in. Wide Tape Placed on C of Last Inlet Damping Screen

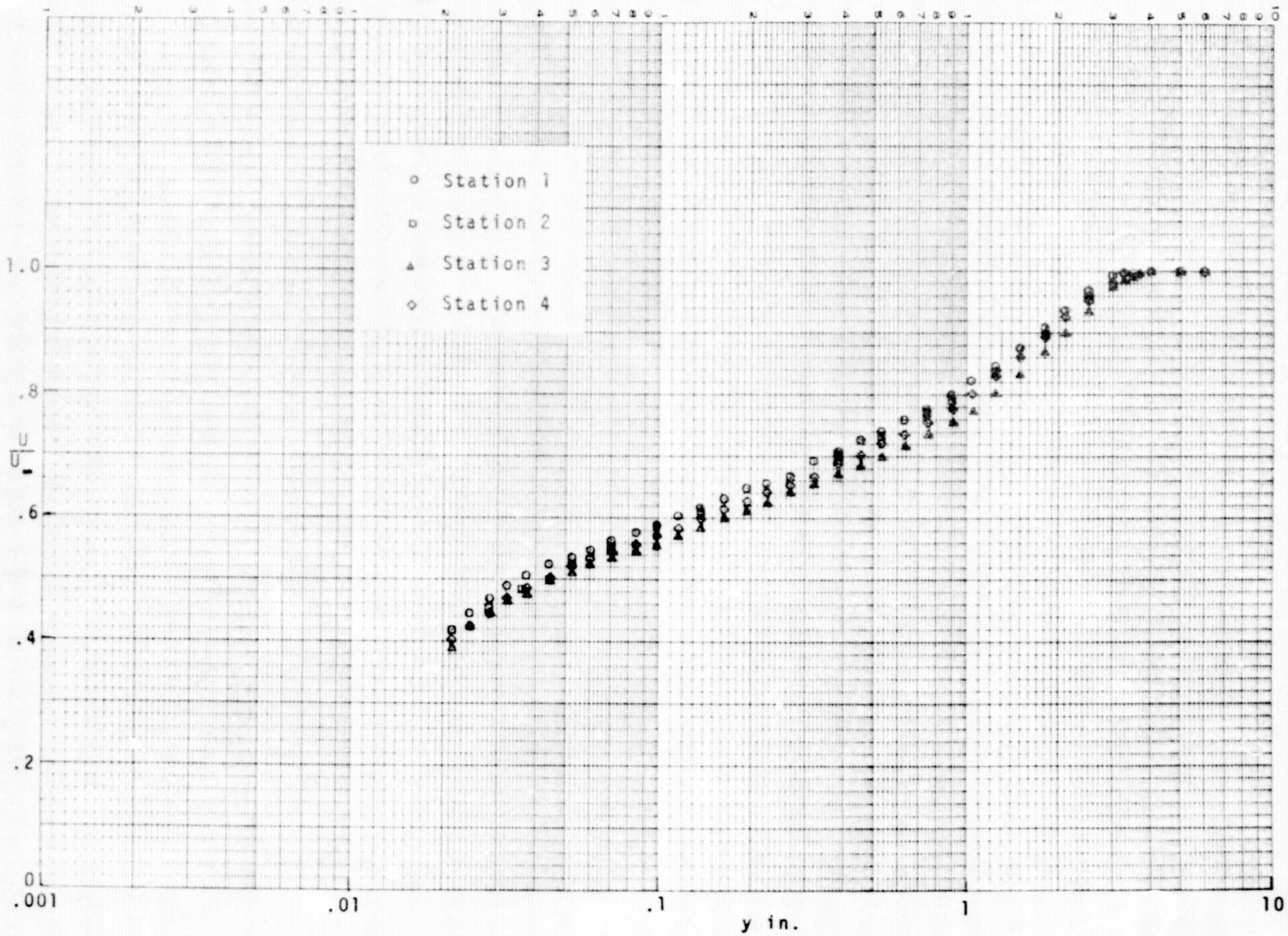

Fig. 37a Velocity Surveys in the 2-DTBL - Series 1

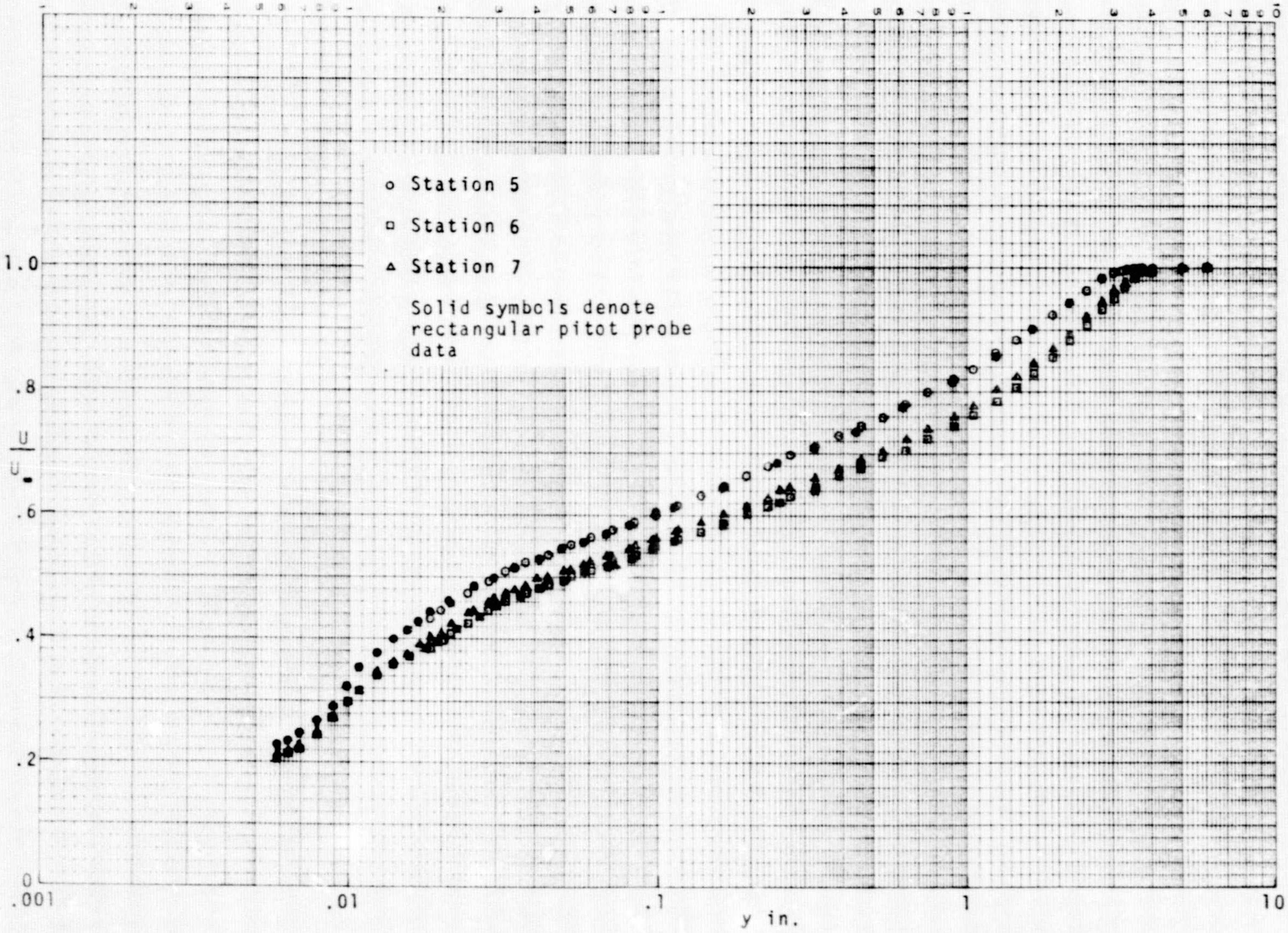

Fig.37b Velocity Surveys in the 2-DTBL - Series 2

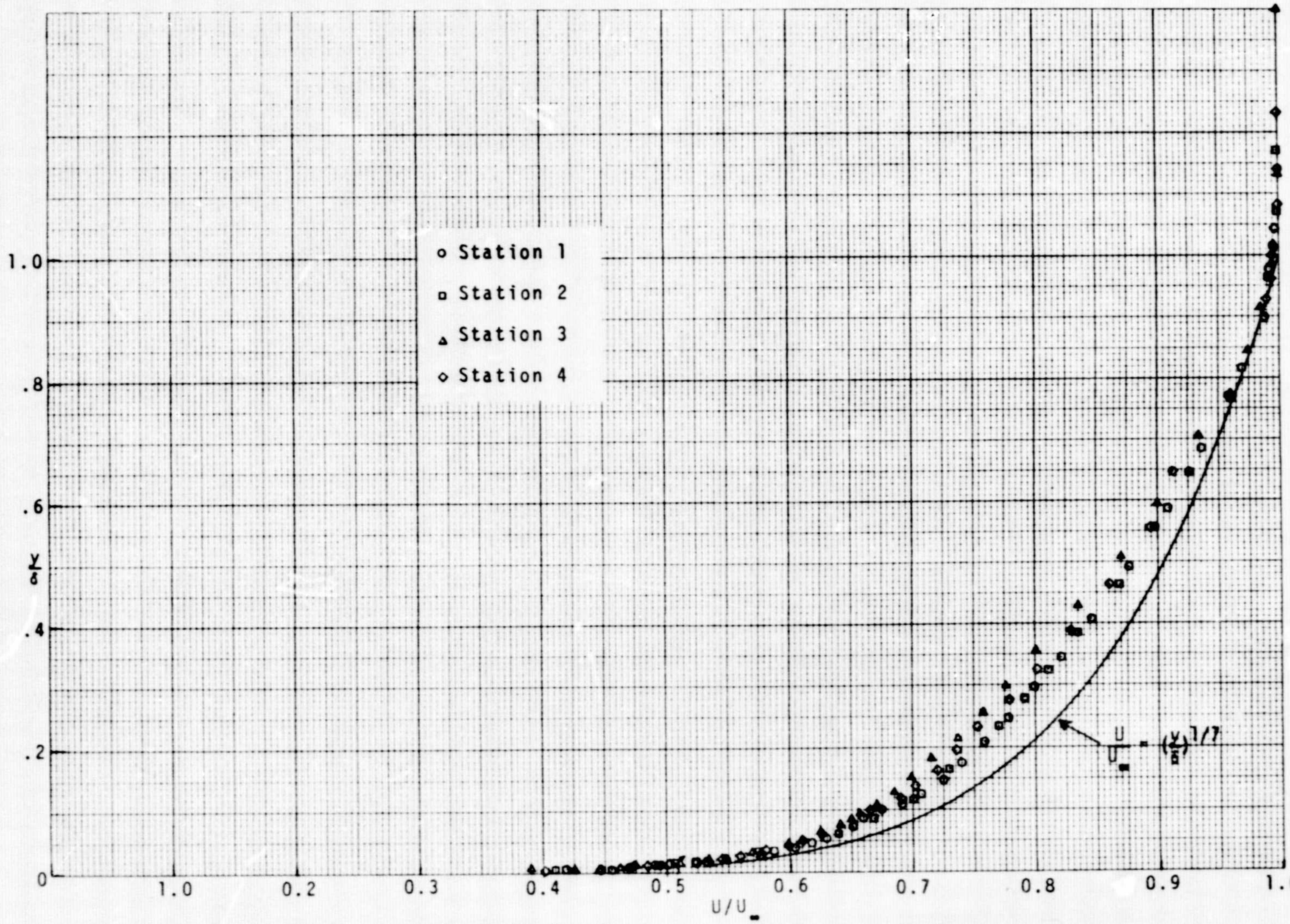

Fig. 38a 2-DTBL Velocity Profiles - Series 1

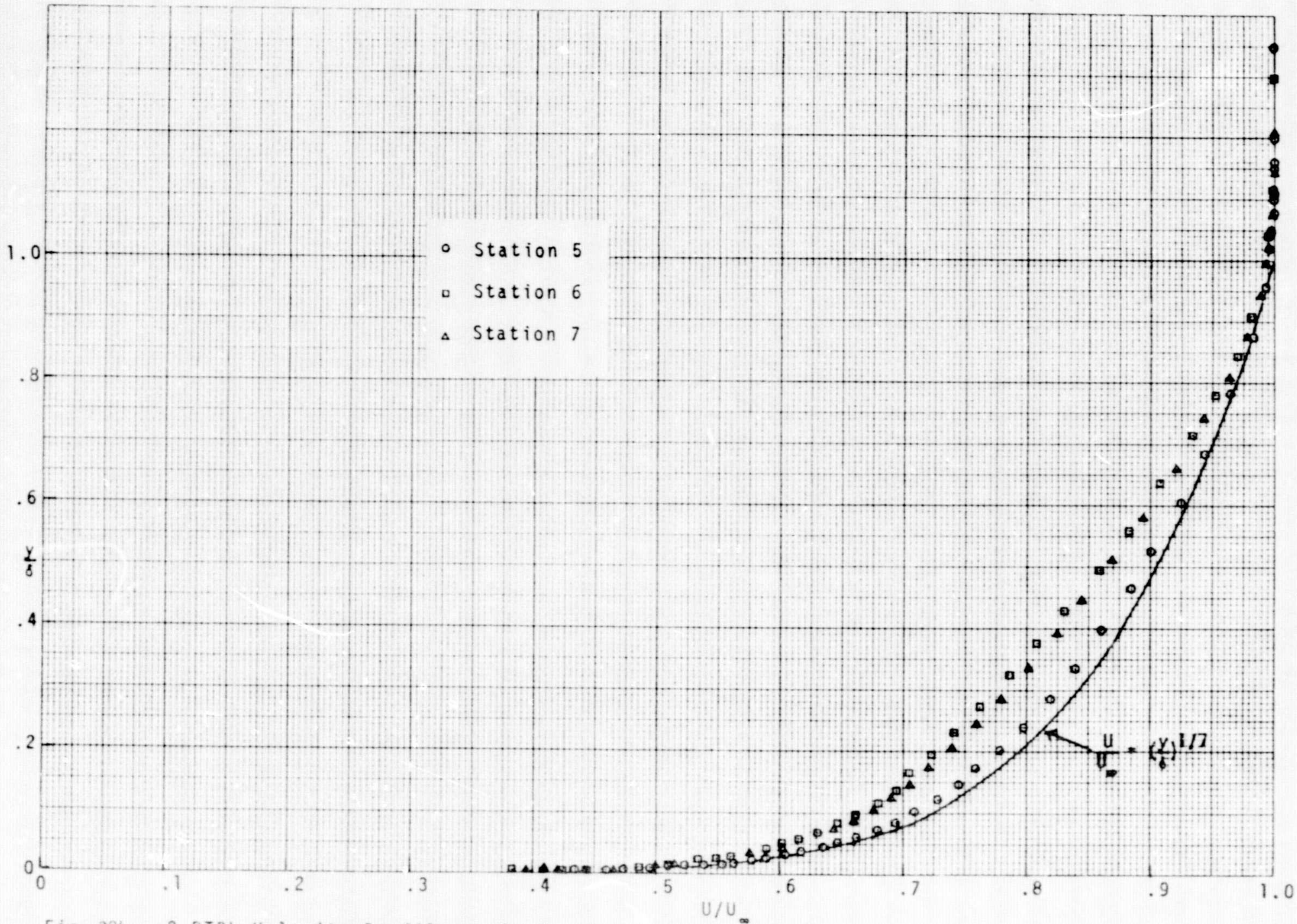

Fig. 38b 2-DTBL Velocity Profiles - Series 2

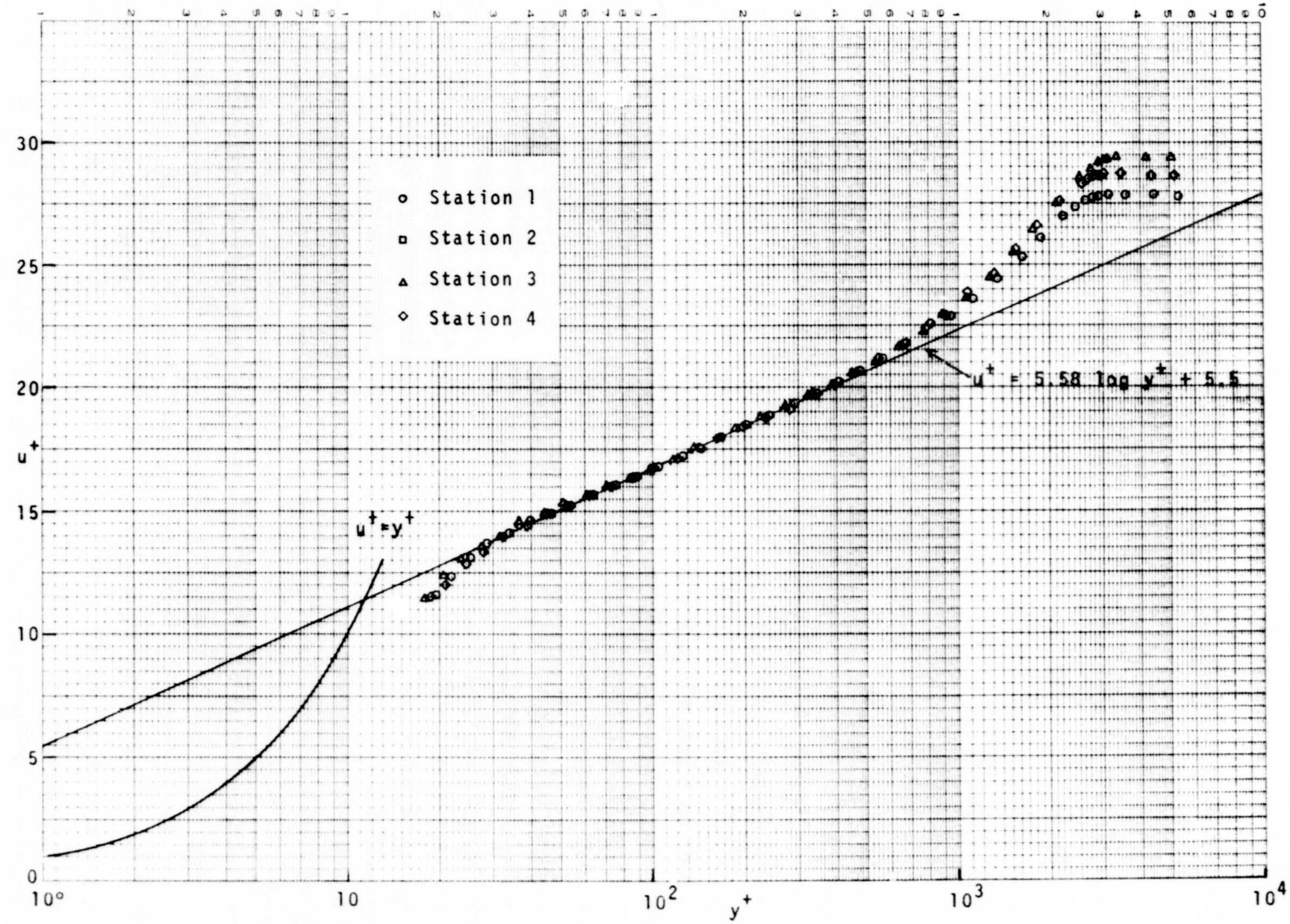

Fig. 39a 2-DTBL Velocity Profiles in Wall Coordinates - Series 1

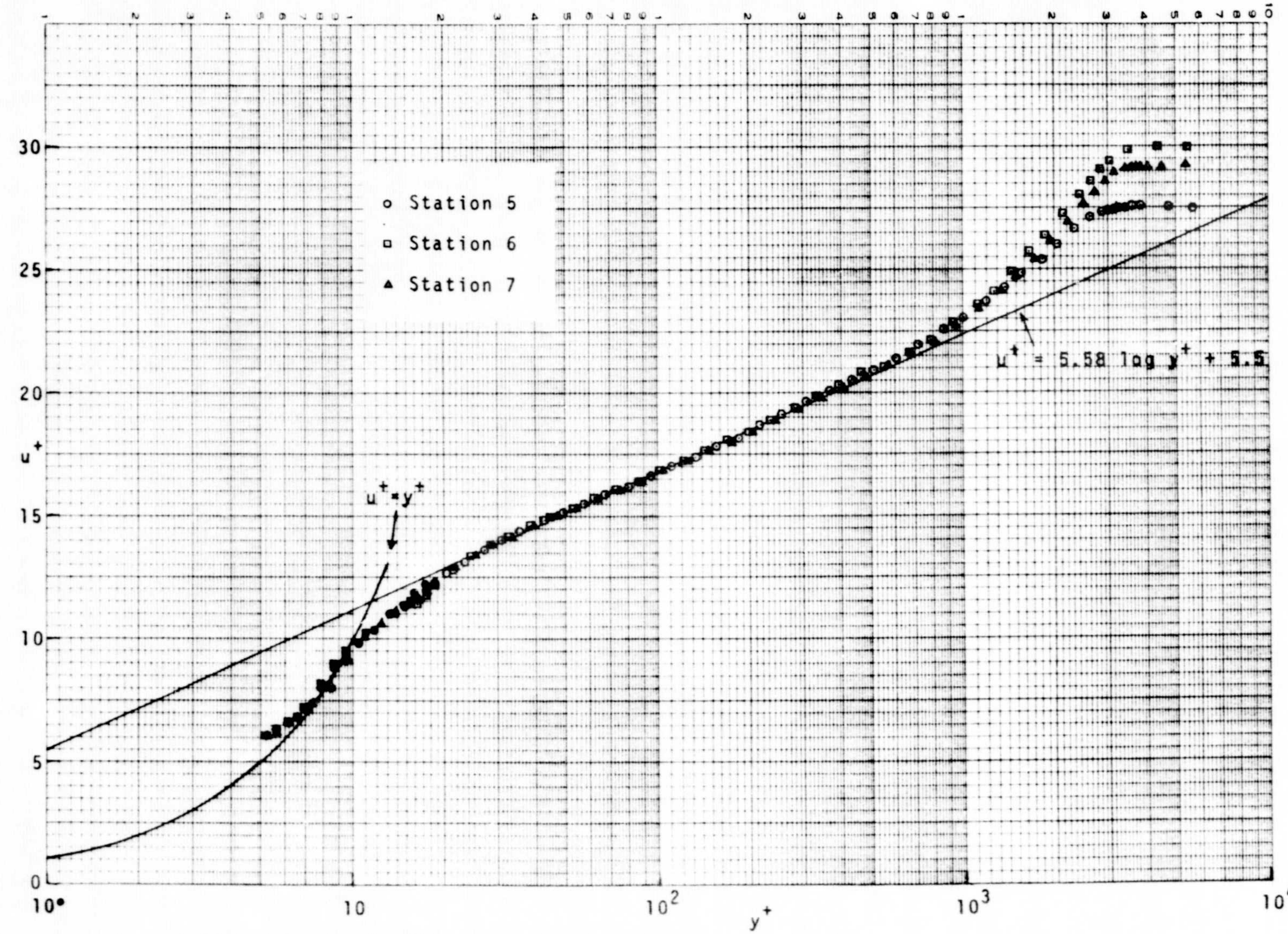

Fig.39b 2-DTBL Velocity Profiles in Wall Coordinates - Series 2

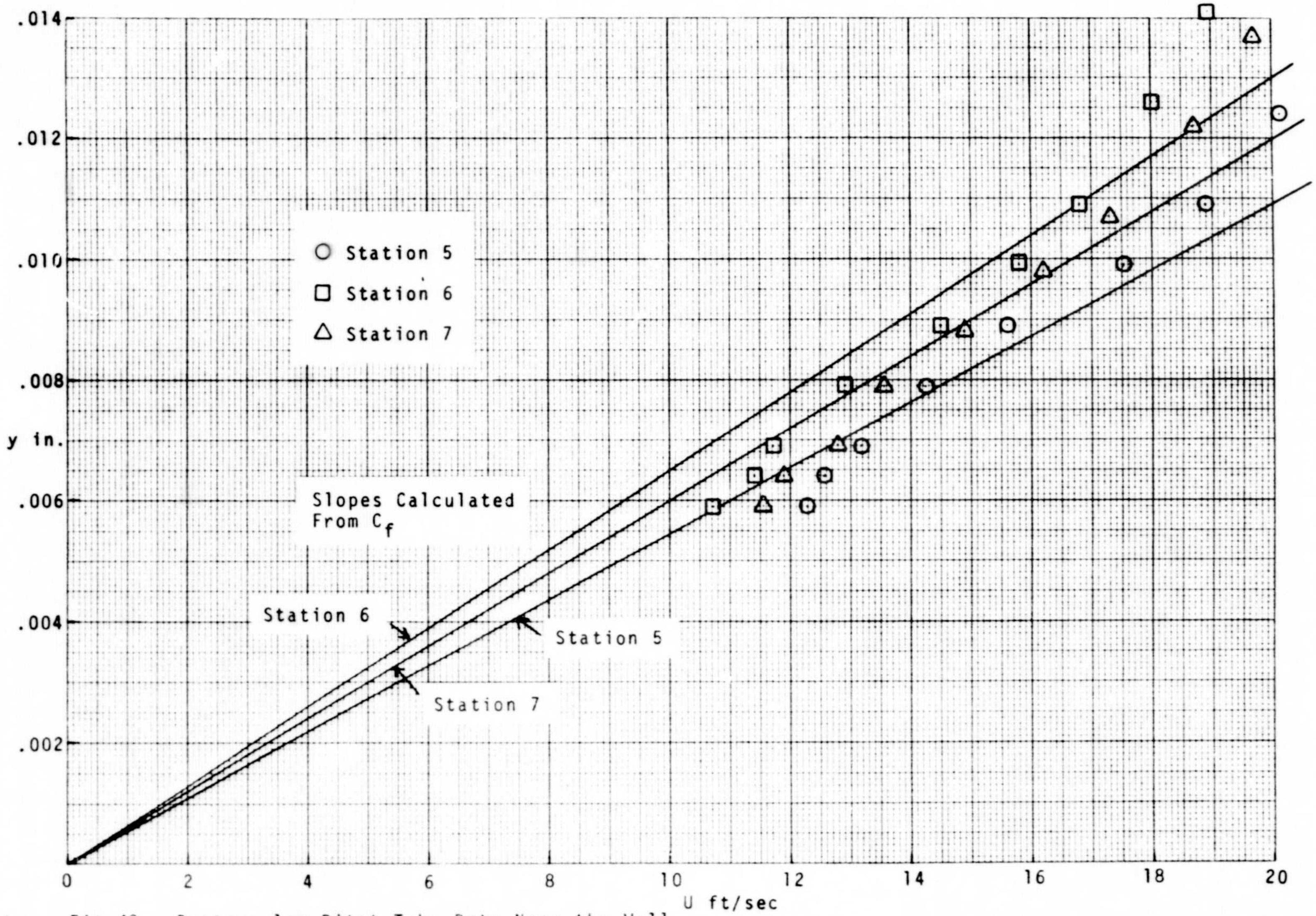

Fig. 40 Rectangular Pitot Tube Data Near the Wall

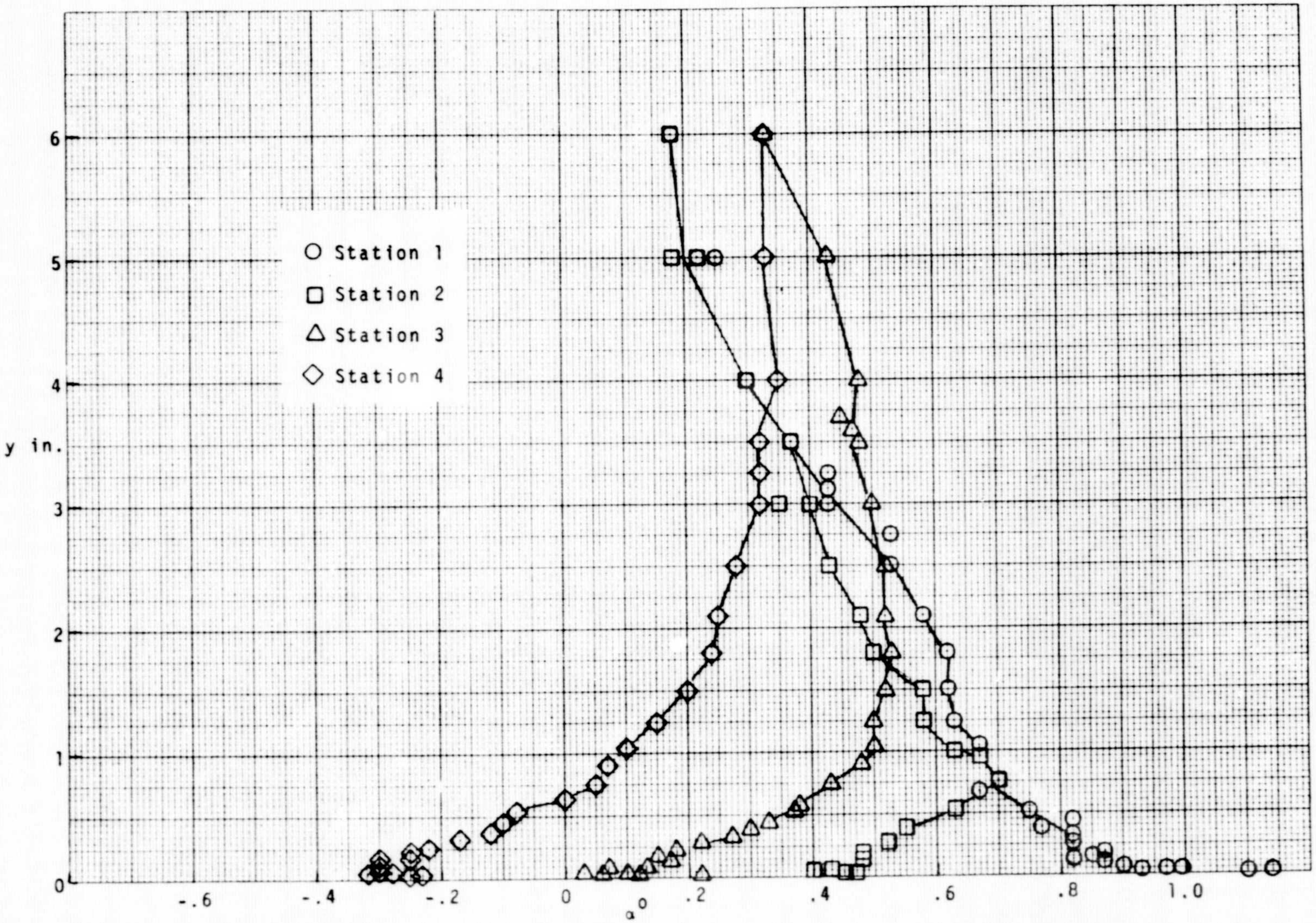

Fig.41a Yaw Probe Survey in the 2-DTBL - Series 1

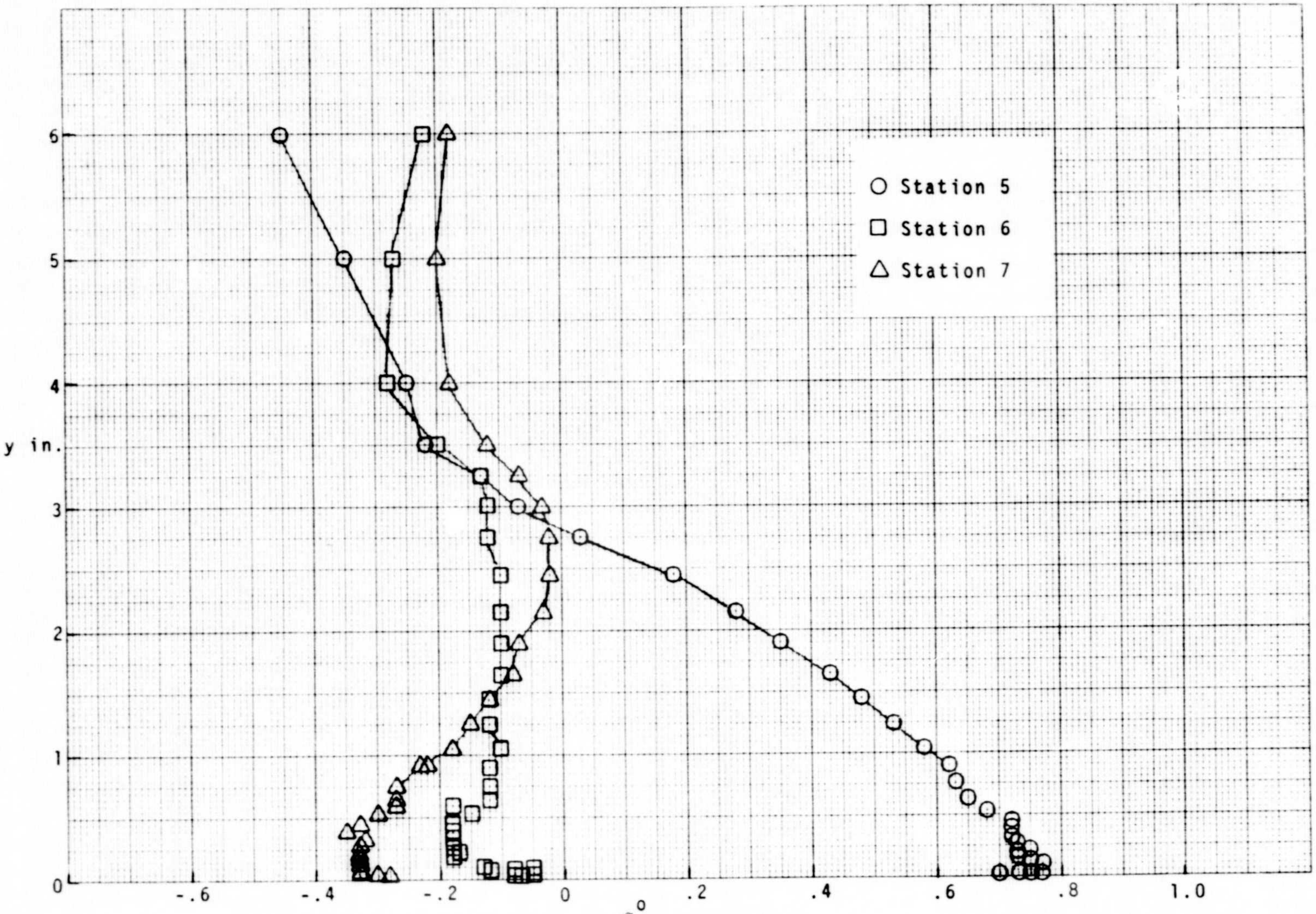

Fig. 41b Yaw Probe Survey in the 2-DTBL - Series 2

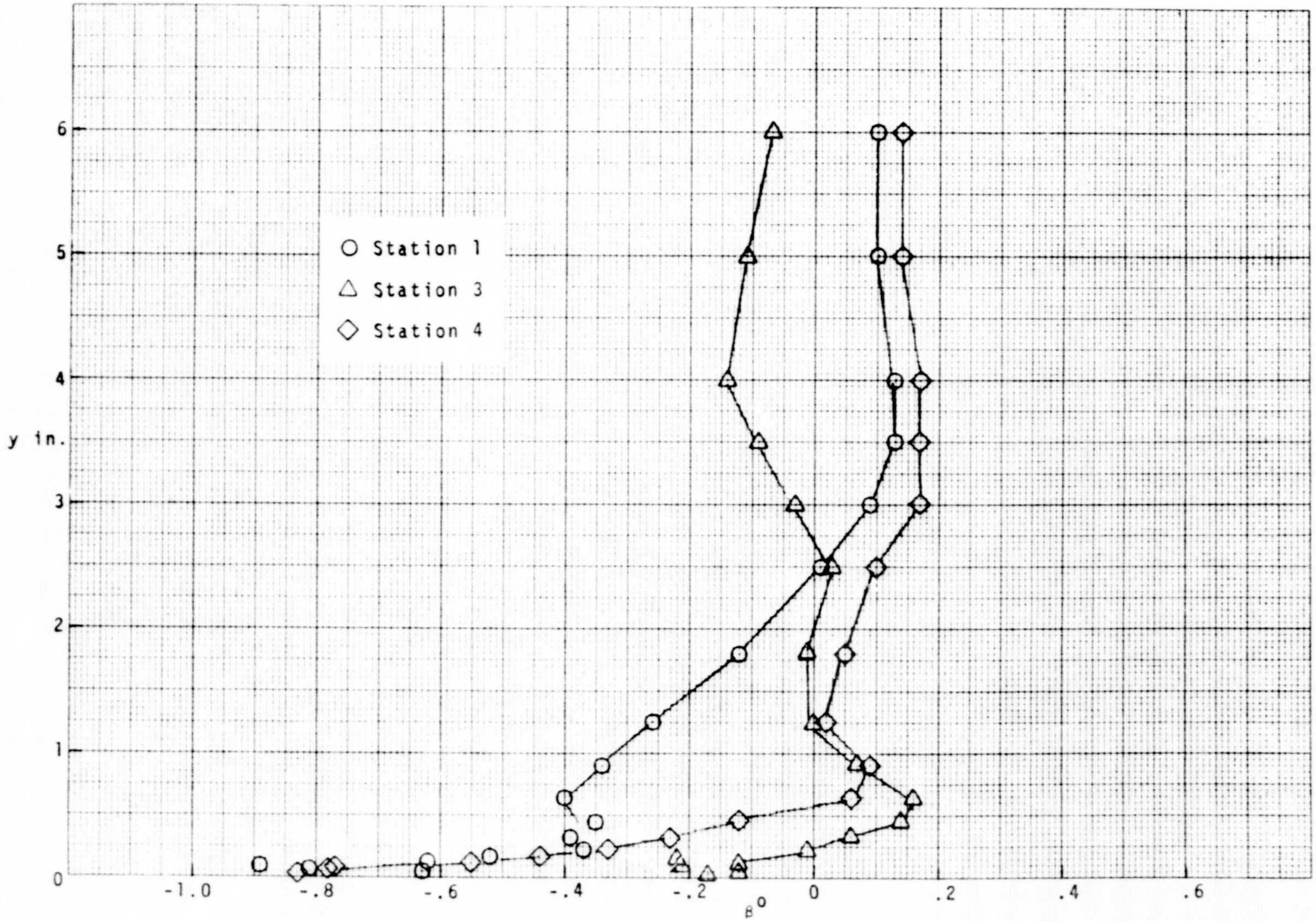

Fig.42a Pitch Probe Survey in the 2-DTBL - Series 1

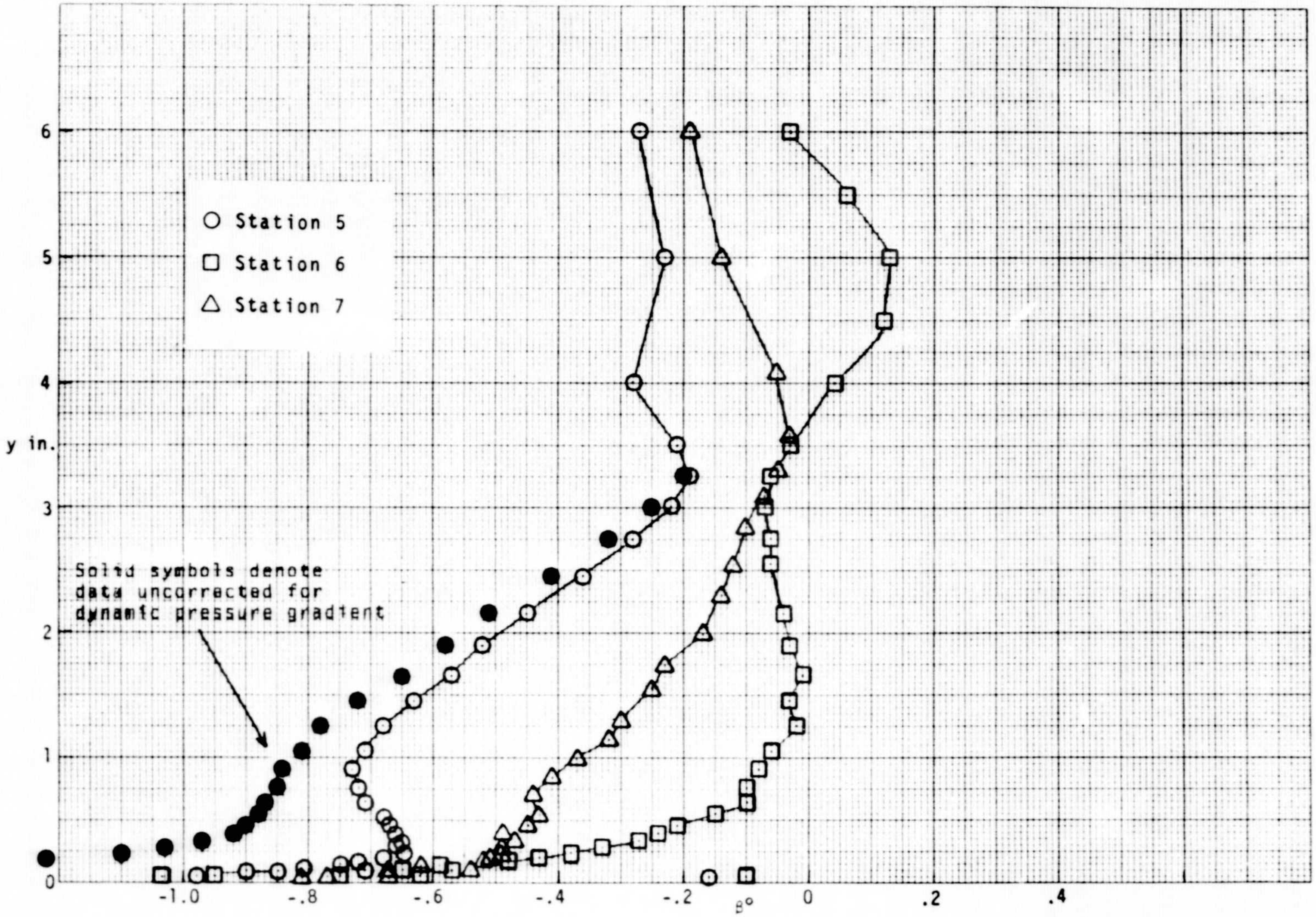

Fig.42b Pitch Probe Survey in the 2-DTBL - Series 2

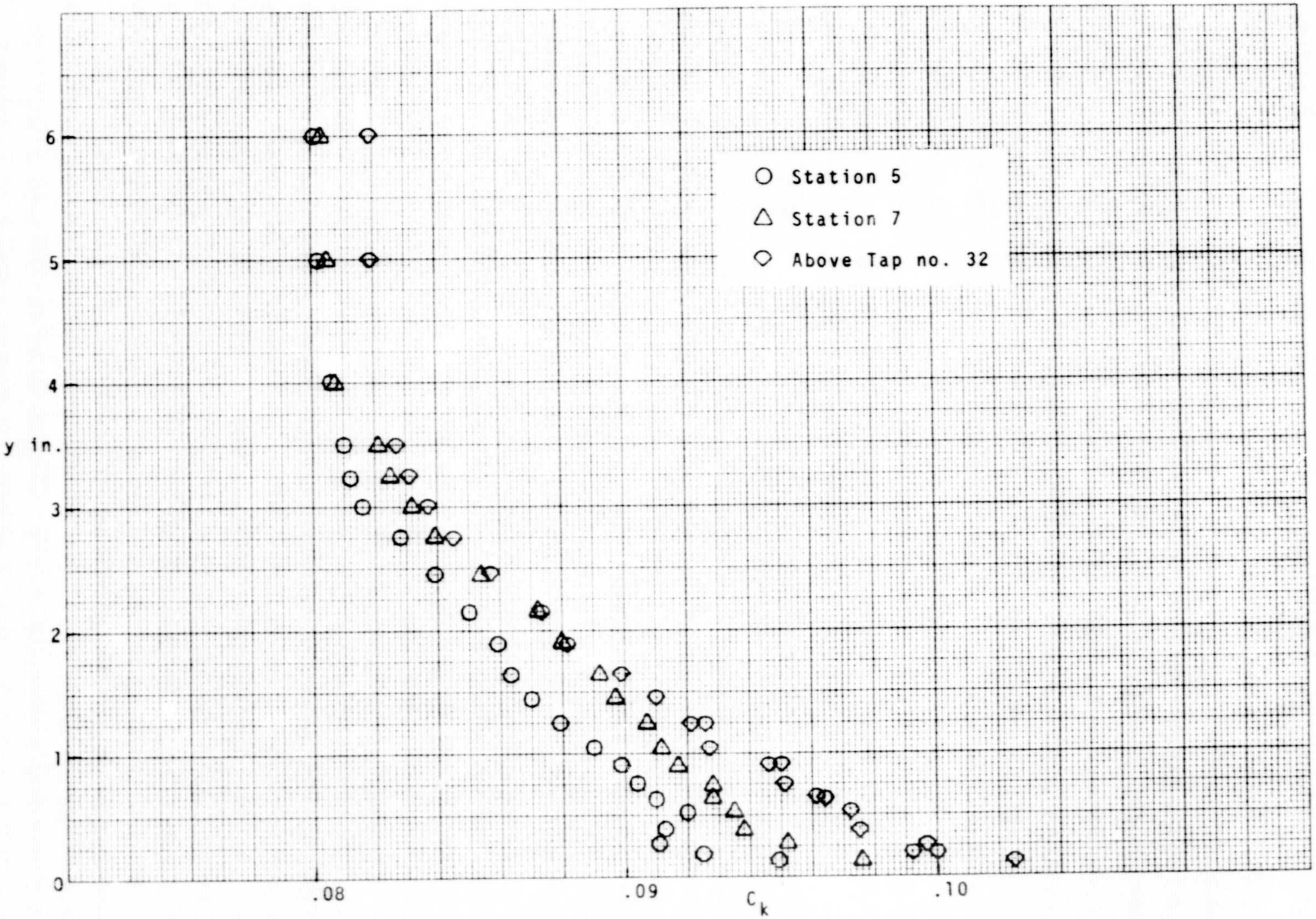

Fig.43 Static Disk Probe Surveys in the 2-DTBL

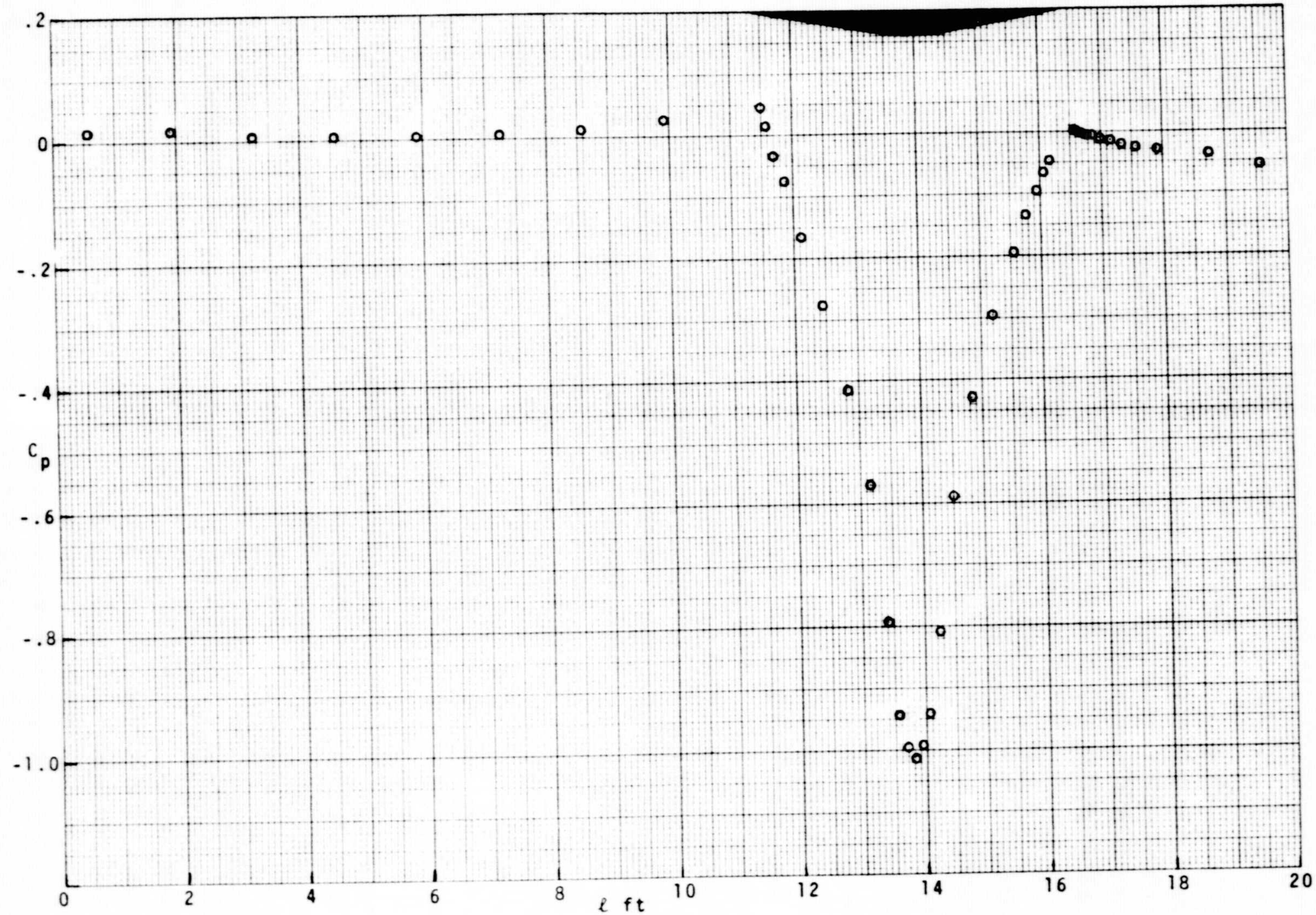

Fig. 44 Static Pressure Distribution on Test Wall With Wing Model

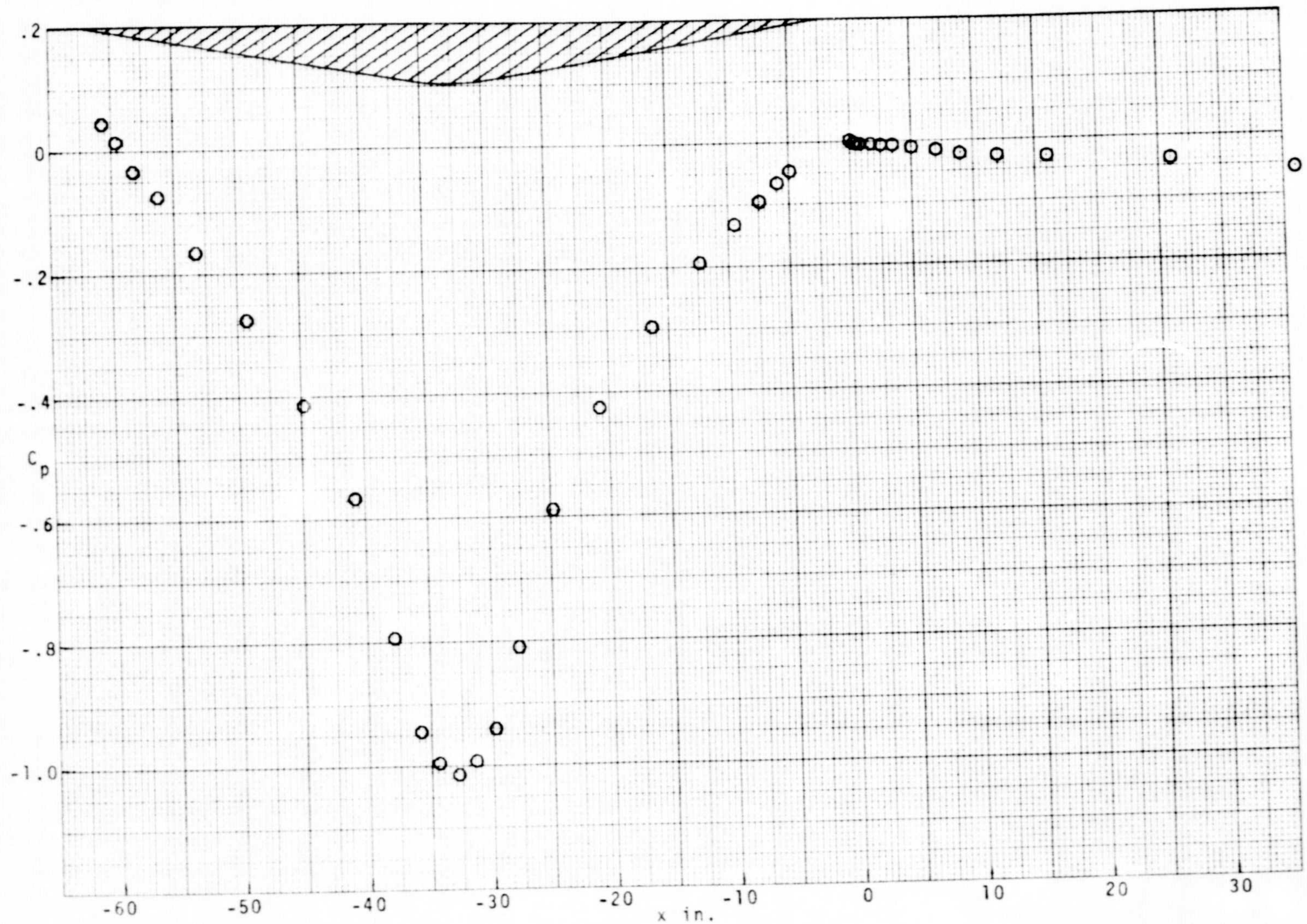

Fig.45 Static Pressure Distribution on Wing Model and Aluminum Wall

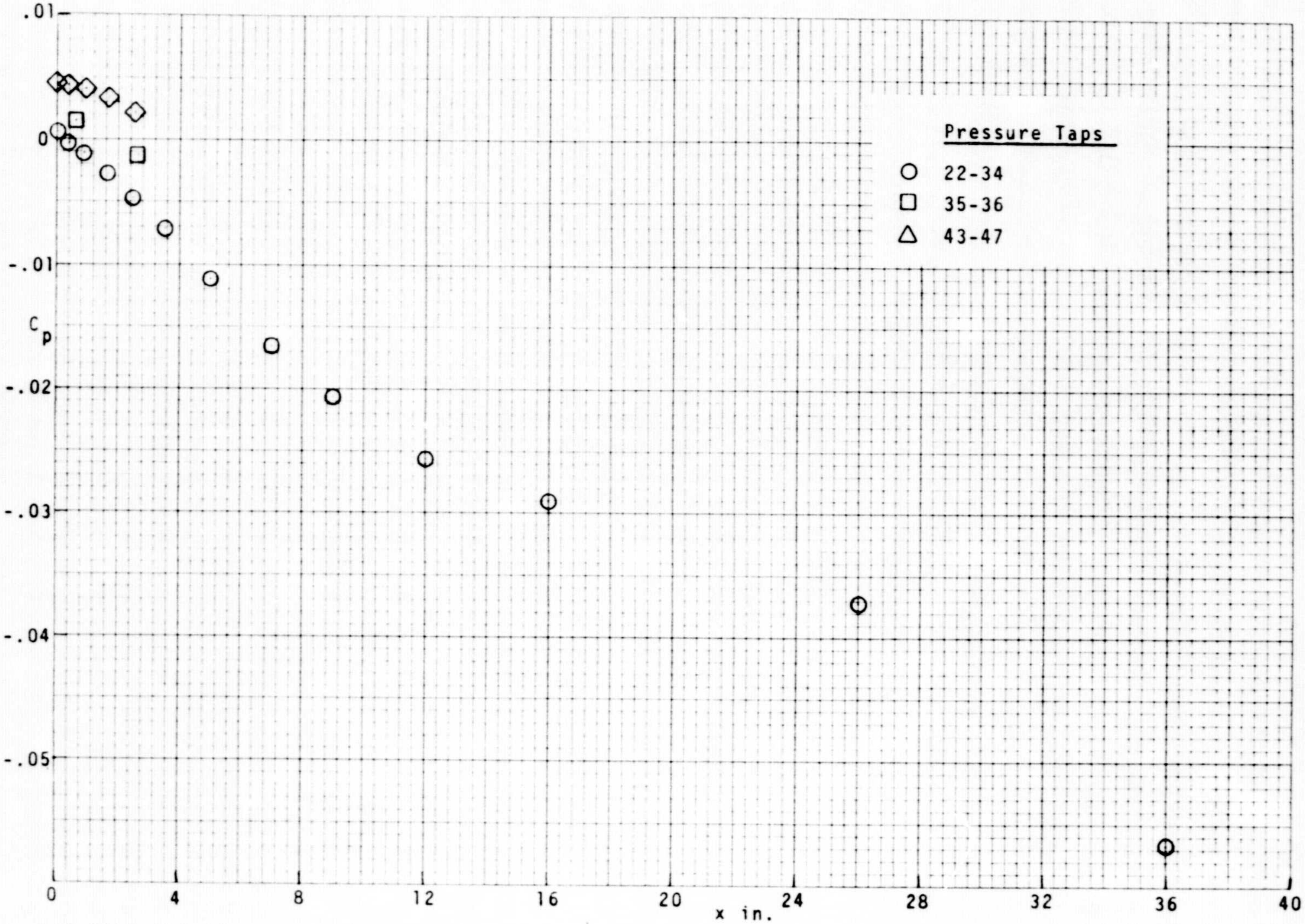

Fig.46 Static Pressure Distribution Downstream of Wing Model

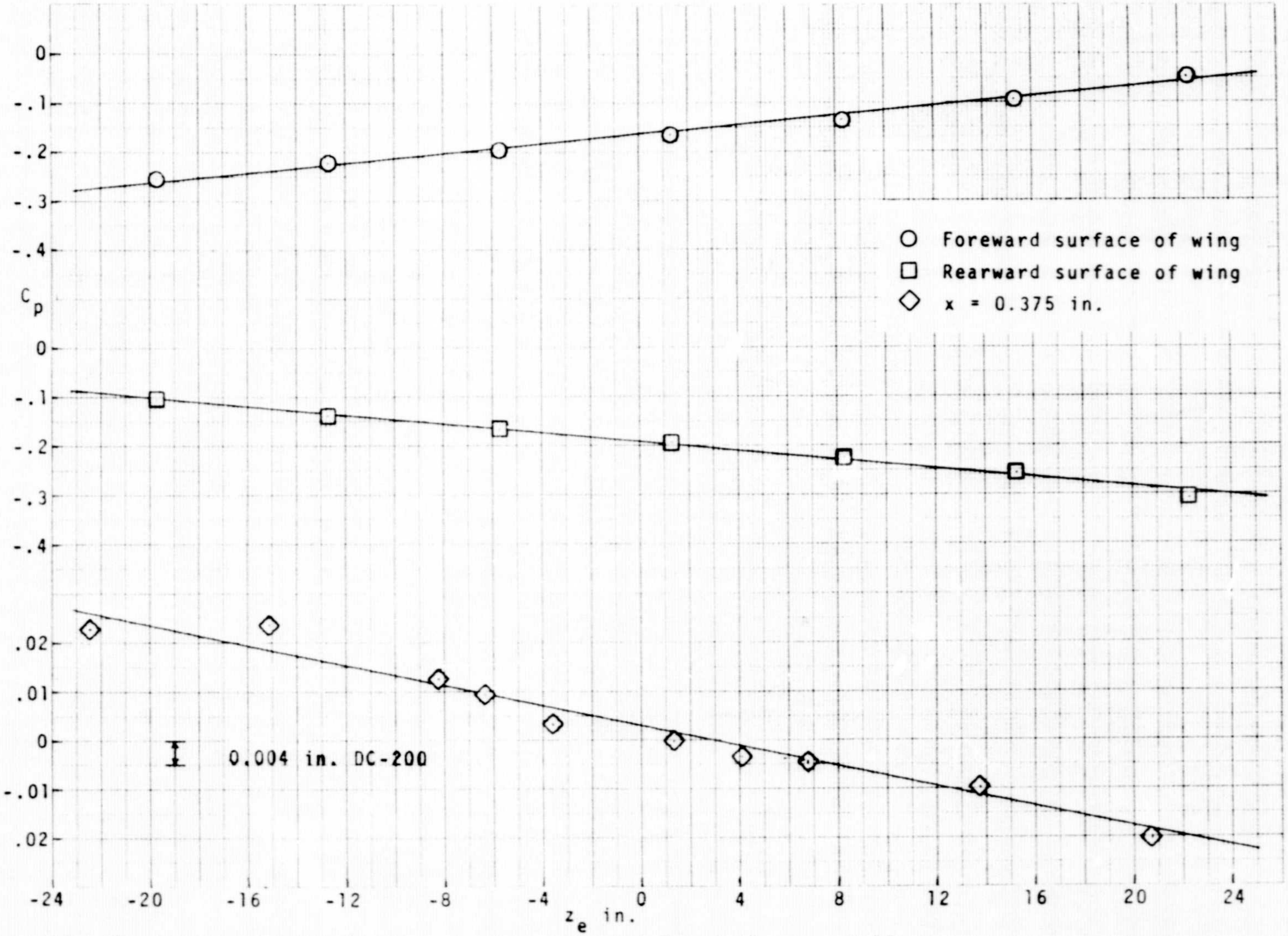

Fig. 47a Pressure Distributions on the Wing Model and Aluminum Wall Along Lines Parallel to the T.E.

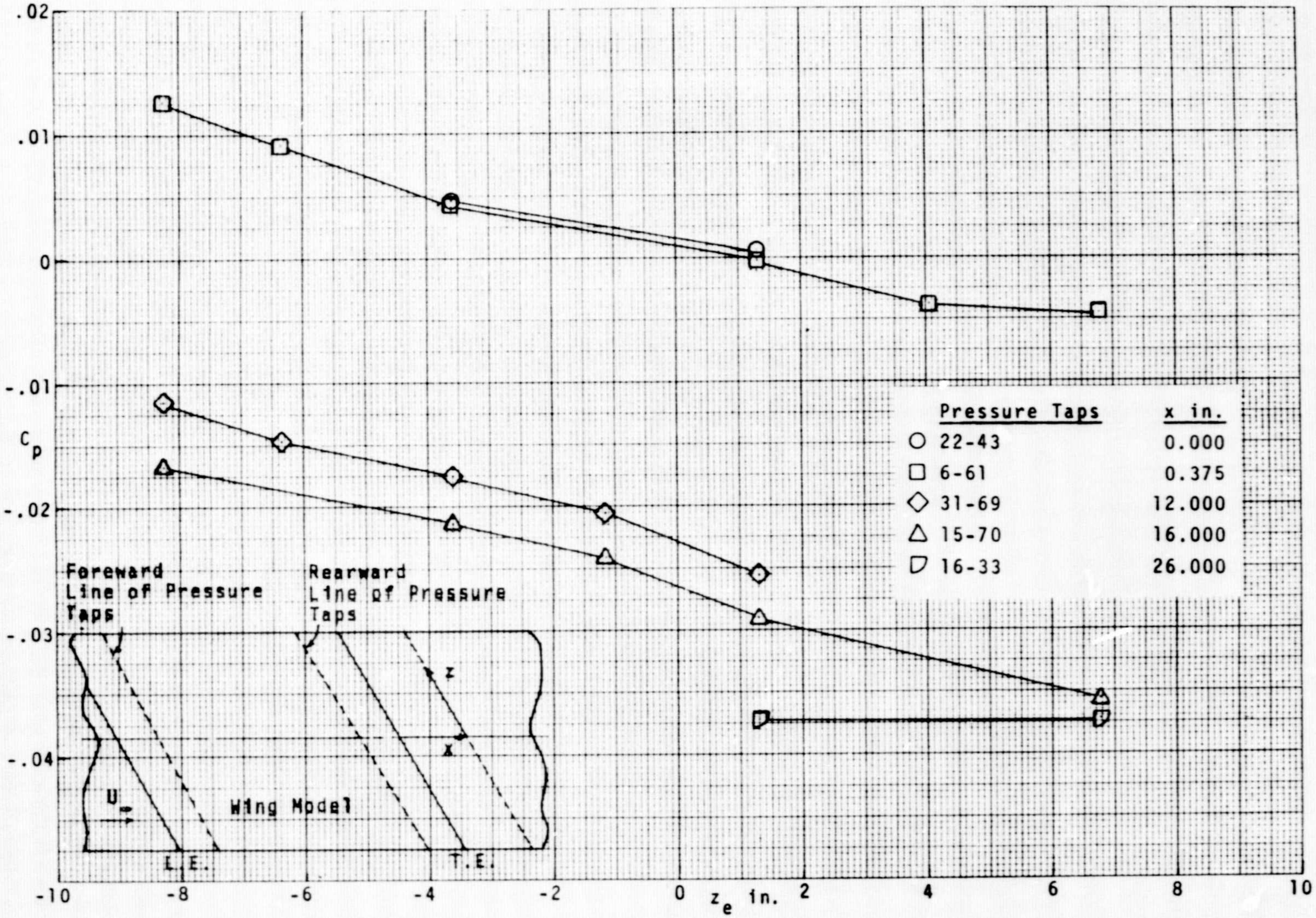

Fig.47b Pressure Distributions on the Aluminum Wall Along Lines Parallel to the T.E.

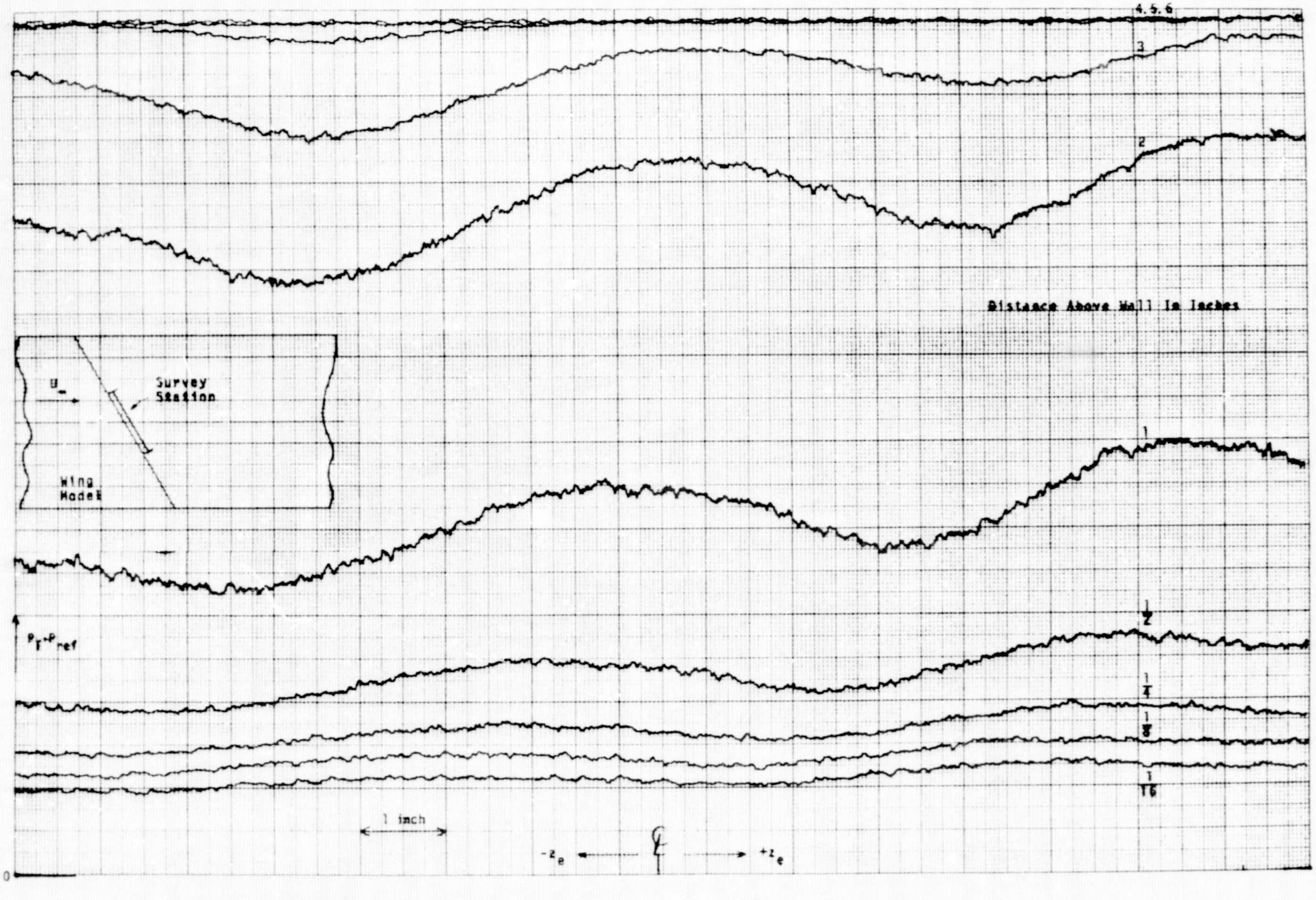

Fig.48a 3-Tube Probe (Total) Surveys Parallel to T. E. of Wing

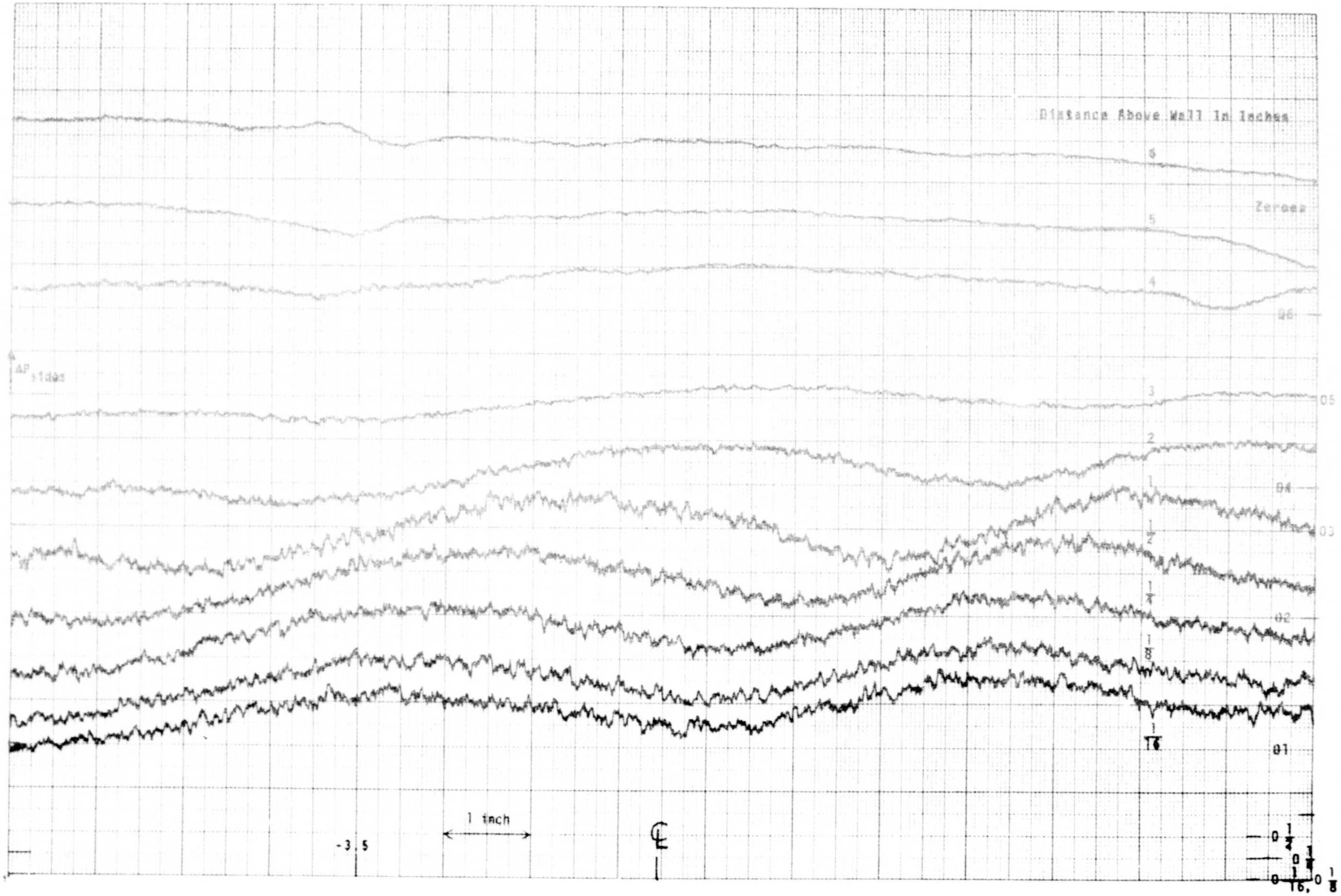

Fig.48b 3-Tube Probe (Yaw) Surveys Parallel to T. E. of Wing

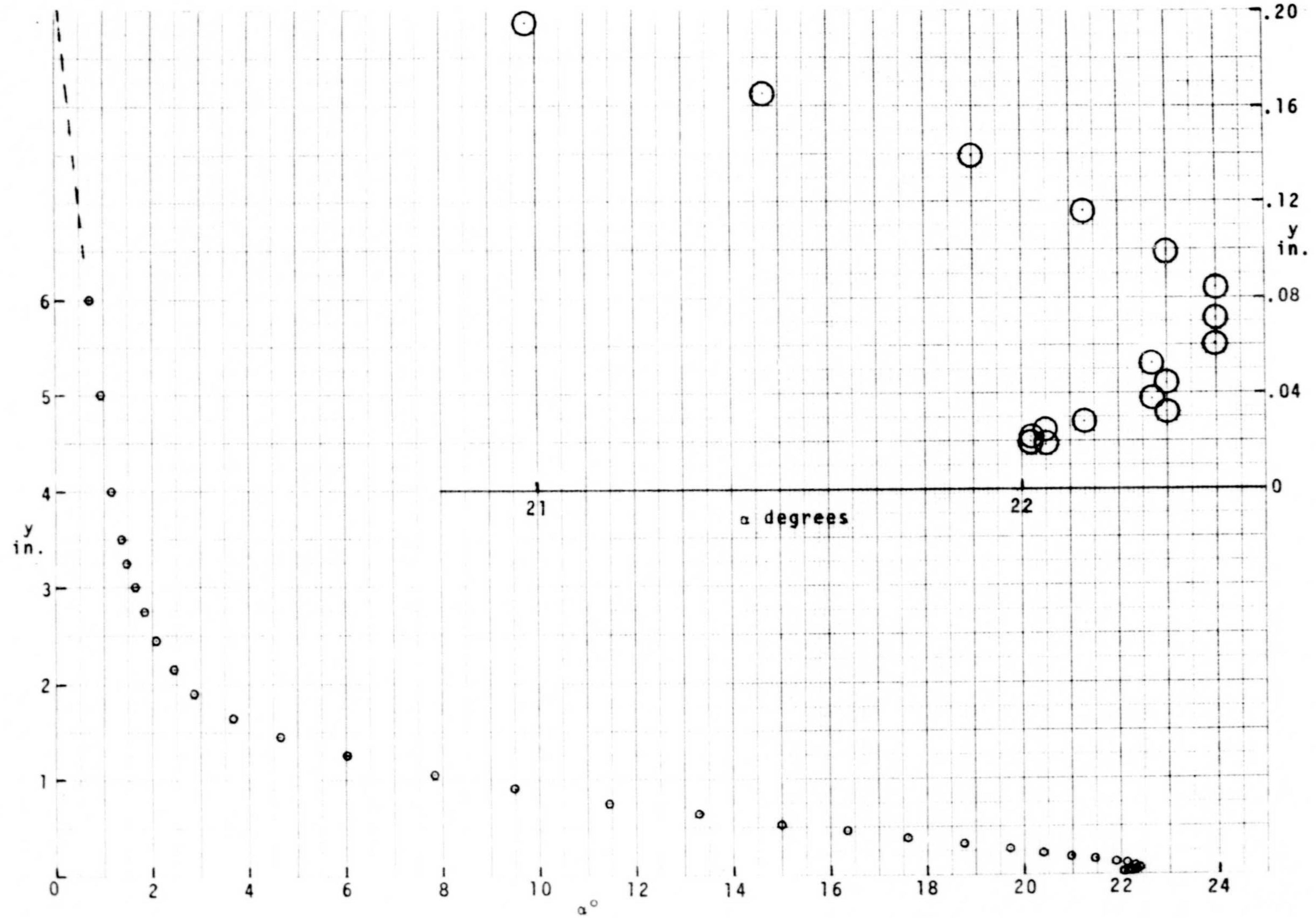

Fig.49 Variation of Cross Flow Angle Through the 3-DTBL

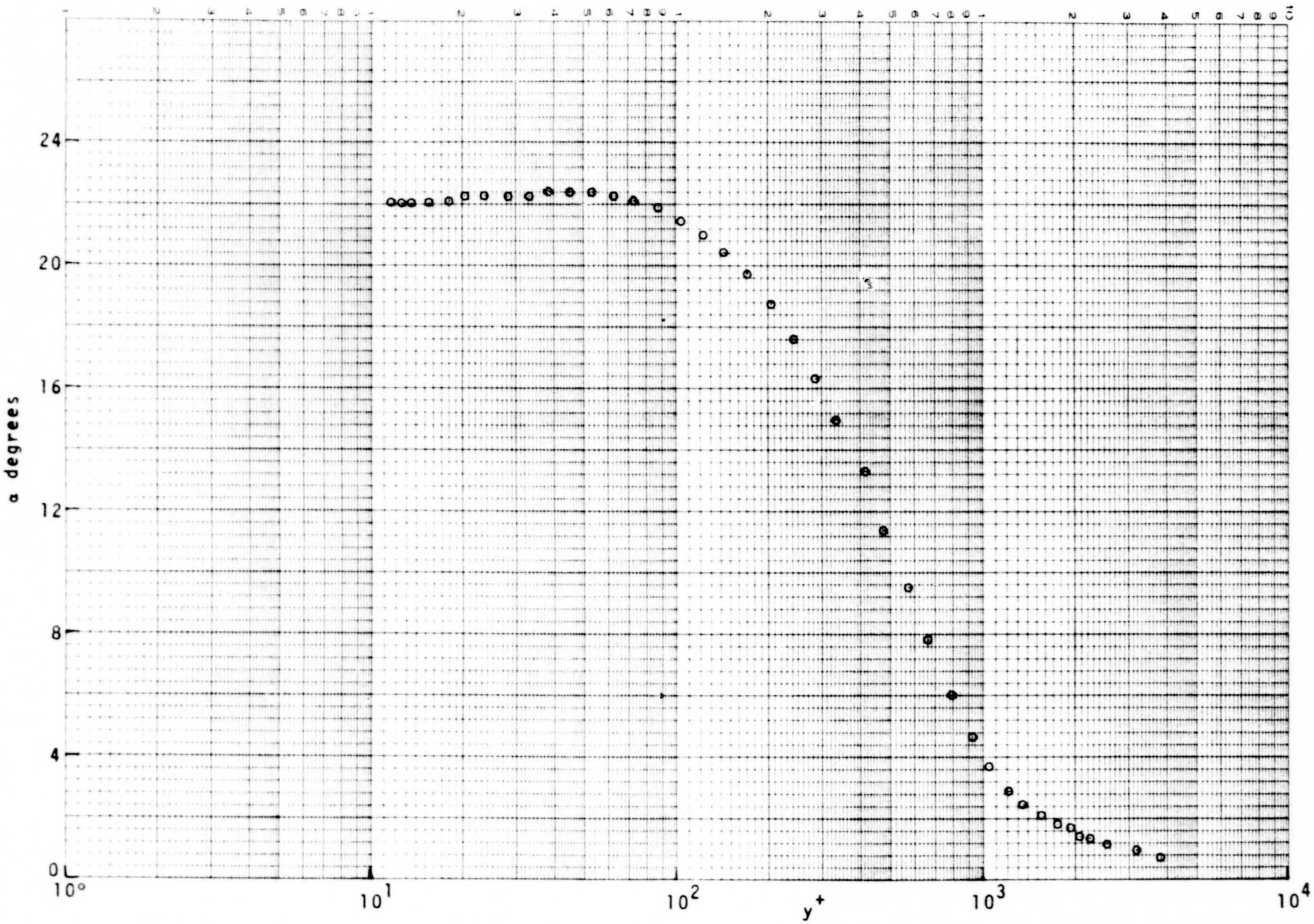

Fig. 50 Cross Flow Angle Plotted in Wall Coordinates

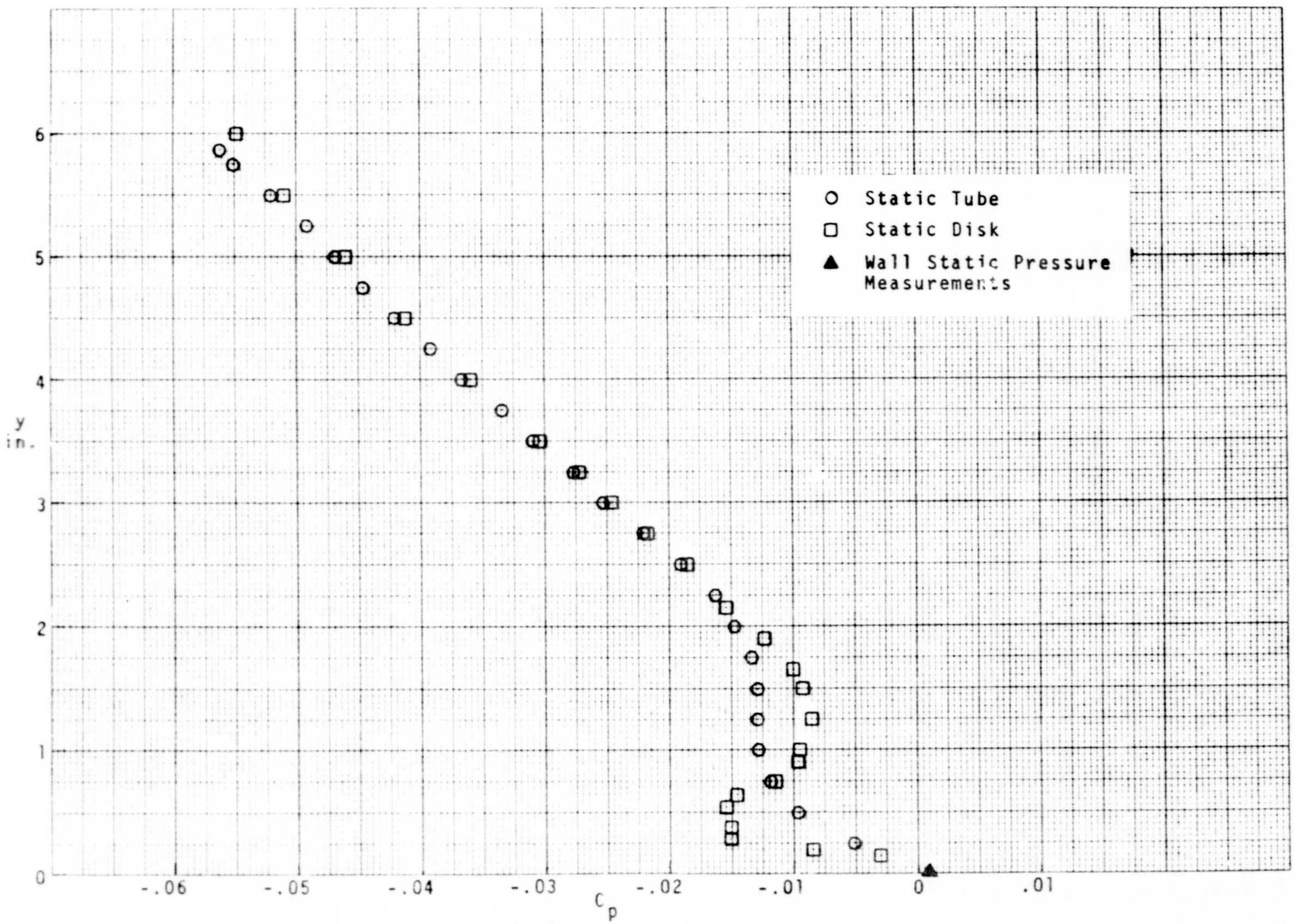

Fig.51 Variation of C_p Through the 3-DTBL

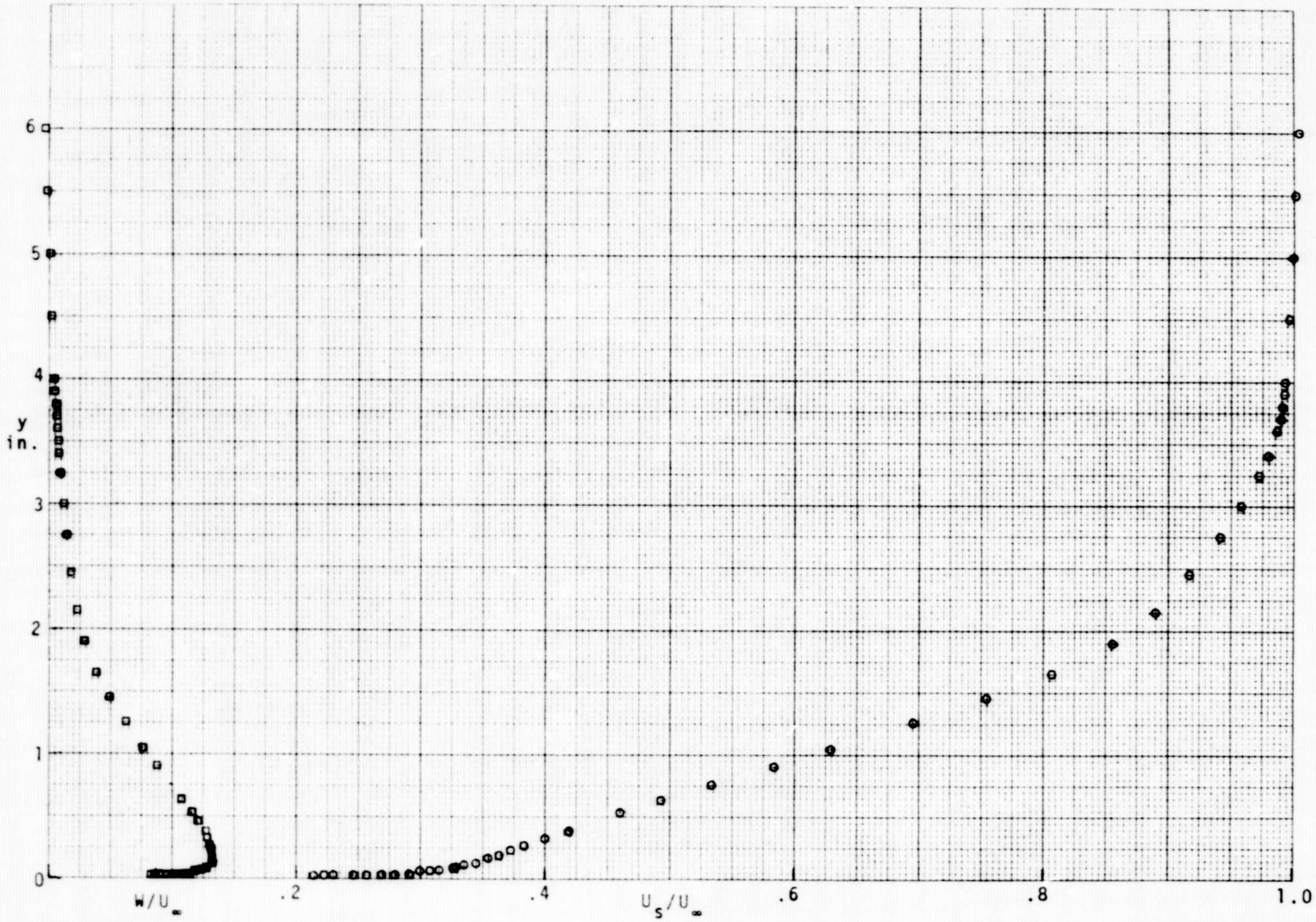

Fig. 52 Streamwise and Cross Flow Velocity Profiles

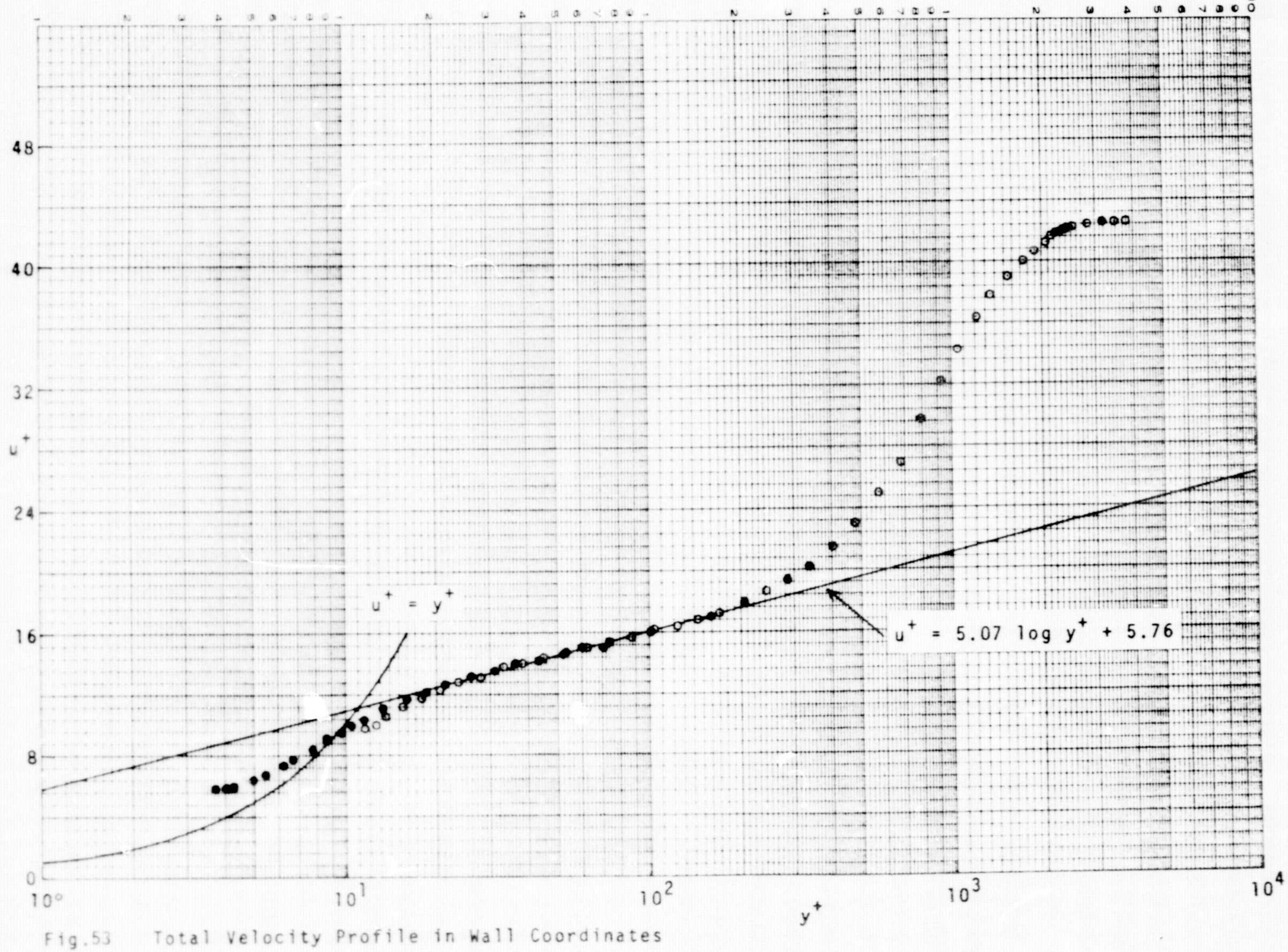

Fig.53 Total Velocity Profile in Wall Coordinates

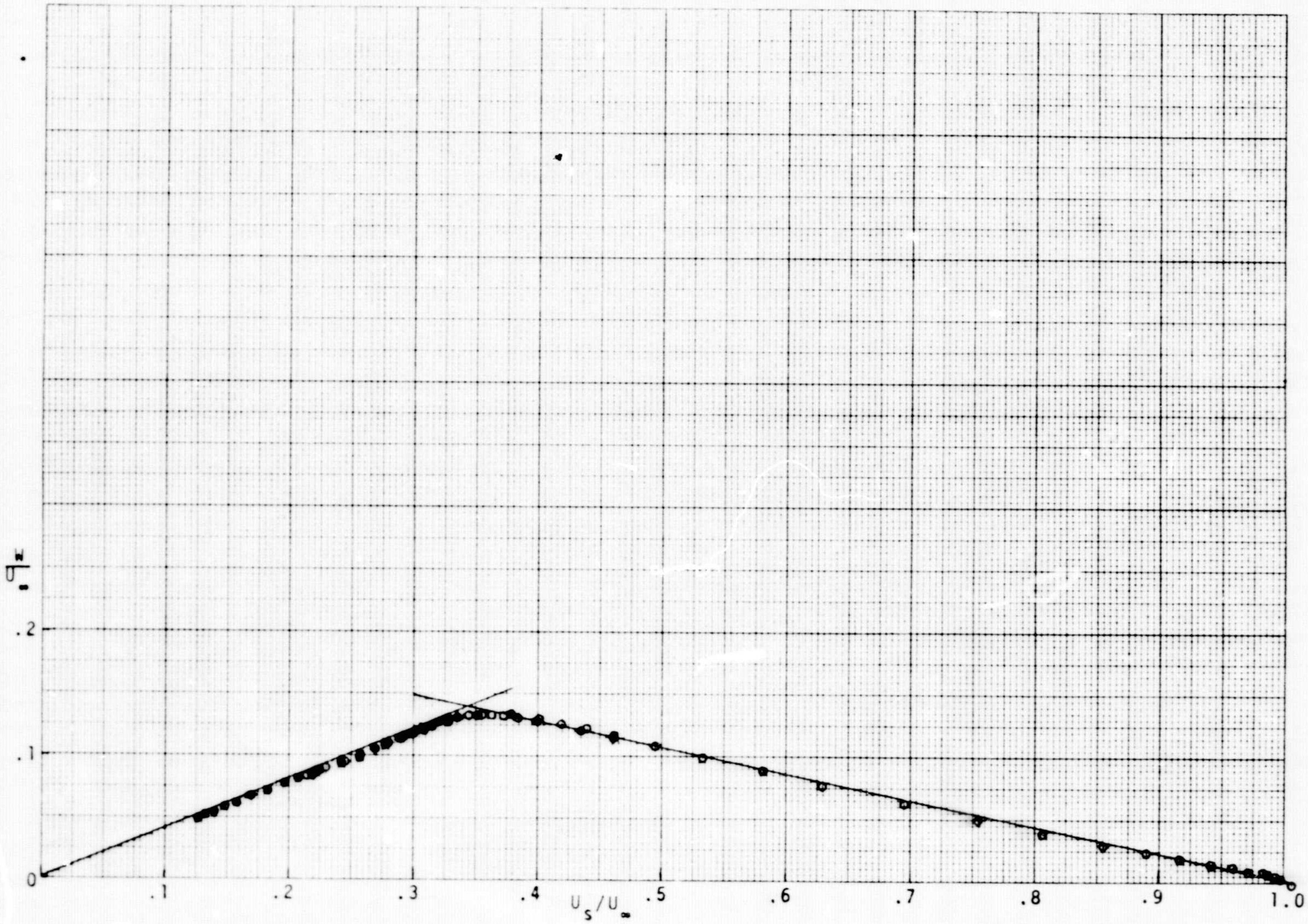

Fig. 54 Polar Plot of 3-DTBL Velocity Distribution

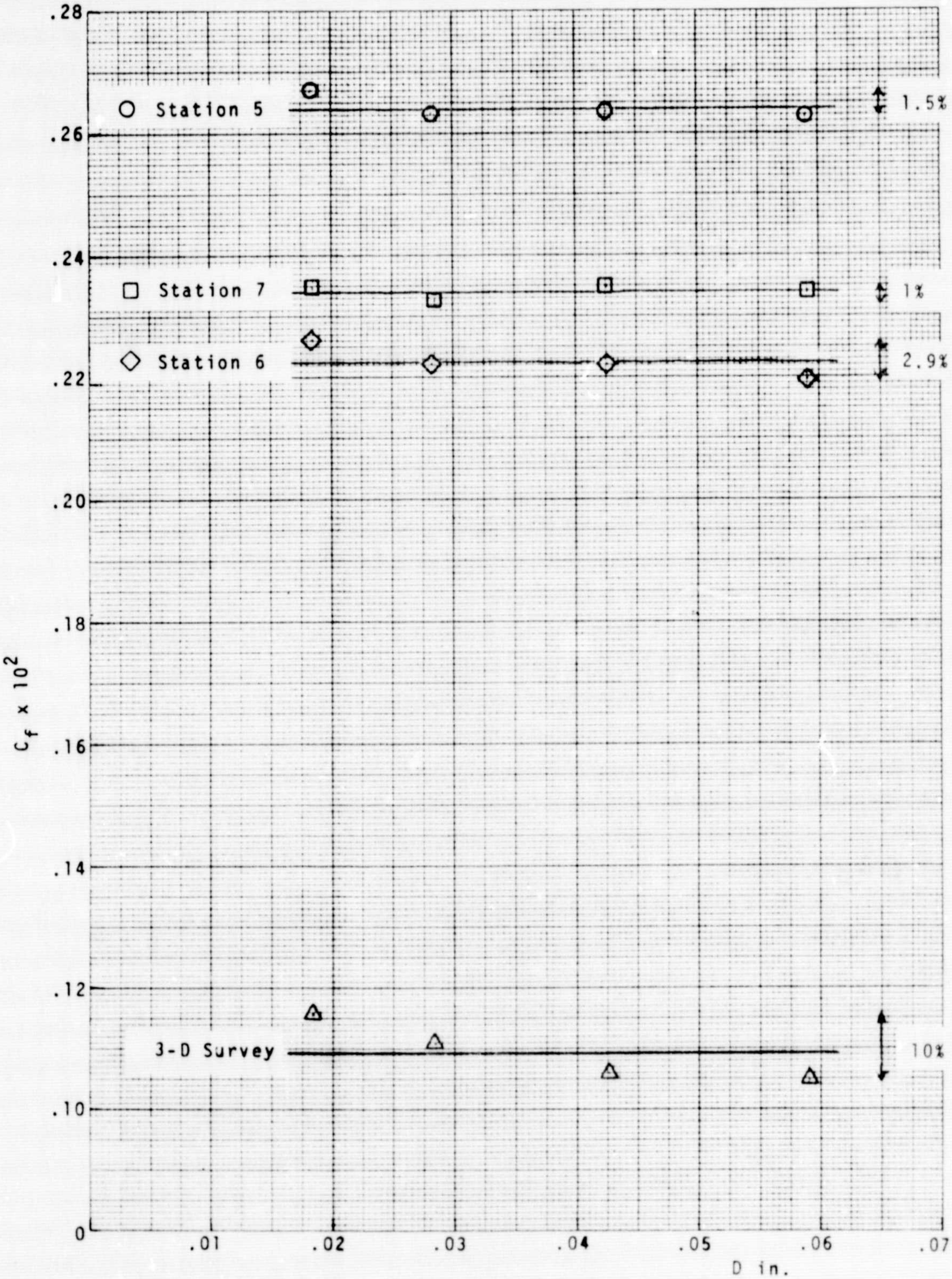

Fig.55 Variation of C_f With Preston Tube Diameter

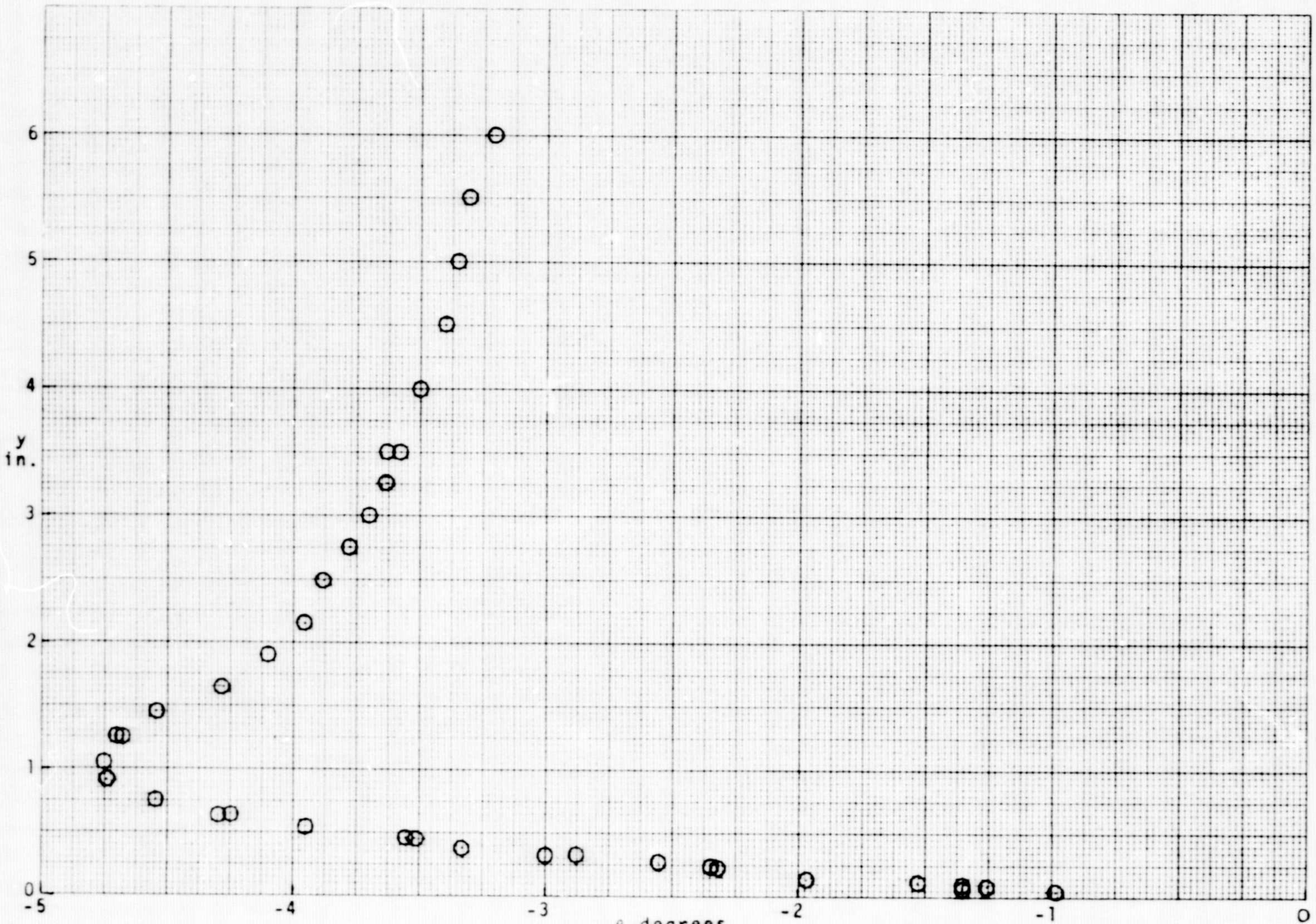

Fig. 56 Variation of Pitch Angle Through the 3-DTBL